UNIVERSIDADE D
COIMBRA

Tiago Jorge da Cruz Manco

Behaviour of Unstiffened and Stiffened Curved Steel Panels Under In-Plane and Out-of-Plane Actions

PhD thesis in Steel and Composite Construction supervised by Professor Luís Alberto Proença Simões da Silva, Professor João Pedro Simões Cândido Martins and Professor Maria Constança Simões Rigueiro and submitted to the Department of Civil Engineering, Faculty of Sciences and Technology of the University of Coimbra.

August 2018

Tiago Jorge da Cruz Manco

BEHAVIOUR OF UNSTIFFENED AND STIFFENED CURVED STEEL PANELS UNDER IN-PLANE AND OUT-OF-PLANE ACTIONS

PhD thesis in Steel and Composite Construction supervised by Professor Luís Alberto Proença Simões da Silva, Professor João Pedro Simões Cândido Martins and Professor Maria Constança Simões Rigueiro and submitted to the Department of Civil Engineering, Faculty of Sciences and Technology of the University of Coimbra

August 2018

UNIVERSIDADE D
COIMBRA

This work was financially supported by: *i)* the Portuguese Ministry of Science, Technology and Higher Education (Ministério da Ciência, Tecnologia e Ensino Superior) under the individual contract Grant SFRH/BD/99945/2014 and project contract Grant PTDC/ ECM-EST/1494/2014; *ii)* FEDER funds through the Competitivity Factors Operational Programme – COMPETE; and *iii)* by national funds through FCT – Foundation for Science and Technology within the scope of the project POCI-01-0145-FEDER-007633 and through the Regional Operational Programme CENTRO2020 within the scope of the project CENTRO-01-0145-FEDER-000006.

Preface

This thesis is the outcome of the research work developed within the research unit ISISE (Institute for Sustainability and Innovation in Structural Engineering) at the Civil Engineering Department of the University of Coimbra, under the supervision of Professor Luís Simões da Silva, Professor João Pedro Martins and Professor Constança Rigueiro.

It is hoped that this work may contribute for a better understanding of the behaviour of curved panels, which is of interest for several engineering fields.

Tiago Manco

Coimbra, August, 2018

Acknowledgments

I would like to express my gratitude to my supervisors Professor Luís Simões da Silva, Professor João Pedro Martins and Professor Constança Rigueiro for their valuable supervision which gave this work an important contribution. A very special thanks to Professor Luís Simões da Silva for his guidance, dedication and, mainly, for his teachings, which, I am sure, will be very useful throughout my professional career.

The financial support from the Portuguese Ministry of Science, Technology and Higher Education (Ministério da Ciência, Tecnologia e Ensino Superior) under the individual contract Grant SFRH/BD/99945/2014 is gratefully acknowledged.

A word of gratitude for all my colleagues who accompanied my work closely and, especially, for my office colleagues Nuno Rosa, Cláudio Martins and Filip Ljubinkovic for the good times spent together.

I am deeply grateful to you, Ana, for your support, patience and encouragement. Thank you for believing in me and always being at my side.

Resumo

Apesar de serem cada vez mais usados em vários campos da engenharia, as provisões para prever a resistência de painéis curvos são maioritariamente empíricas e com reduzida gama de aplicação. Consequentemente, o principal objetivo desta tese é prever o comportamento não-linear e carga última de painéis curvos cilíndricos não reforçados e reforçados com base numa abordagem fisicamente robusta, através de métodos semi-analíticos (MSA). A principal vantagem desta abordagem, comparativamente às abordagens usuais, como o método dos elementos finitos (MEF), é permitir identificar os parâmetros-chave que influenciam o comportamento dos painéis curvos e desenvolver expressões puramente baseadas no contexto físico do problema, as quais têm um enorme interesse prático. Contudo, o MEF é também usado por duas razões: *i)* para caracterizar detalhada e realisticamente o comportamento dos painéis curvos através de um estudo paramétrico alargado; neste caso, é desenvolvida uma forma inovadora de modelar as imperfeições, sendo esta mais desfavorável, numa grande parte dos casos, que a abordagem padrão utilizada em estruturas de casca; e *ii)* para validar a formulação semi-analítica desenvolvida para os painéis curvos.

Os parâmetros analisados mostram-se capazes de alterar drasticamente o comportamento dos painéis, os quais, em alguns casos, podem conduzir a resultados inesperados. Por exemplo, pode ser bastante inseguro dimensionar um painel curvo como se fosse uma placa plana. Contrariamente, em outros casos, são obtidos ganhos significativos da resistência com o aumento da curvatura. Isto mostra que o dimensionamento de painéis curvos deve ser realizado com um profundo conhecimento deste complexo comportamento.

Embora apenas compressão uniaxial no plano (o especto-chave na estabilidade de estruturas de parede fina) e pressão fora do plano sejam estudadas, a formulação é desenvolvida para ter em conta carregamento generalizado. É implementada uma formulação de grandes deslocamentos com uma solução de multi-graus de liberdade (MGDL) e imperfeições. Adicionalmente, o MSA tem em conta condições de fronteira simplesmente apoiadas restringidas e não restringidas no plano. Isto requer uma solução rigorosa do problema de valor de fronteira das equações diferenciais parciais não-lineares de quarta ordem.

Apesar do complexo comportamento identificado para os painéis curvos, o MSA é capaz de ter em conta, de forma precisa, todos os parâmetros geométricos, condições de fronteira e carregamento. Embora os painéis com maiores curvaturas beneficiem da solução MGDL implementada, expressões de forma fechada, baseadas numa aproximação de um único grau de liberdade (UGDL), são capazes de fornecer resultados precisos para as trajetórias de equilíbrio de painéis curvos não reforçados e reforçados com significância prática, sob carregamento no plano e fora do plano.

O MSA é seguidamente usado com um critério de cedência para prever a resistência de painéis curvos não reforçados sob compressão. São derivadas expressões para calcular a carga última destes painéis, mostrando bom acordo com o MEF.

Palavras-Chave

Painéis curvos não reforçados e reforçados | Comportamento de grandes deslocamentos | Carga última | MEF | Método semi-analítico | Expressões de forma fechada.

Abstract

Despite being increasingly used in several engineering fields, design provisions to predict the strength of steel curved panels are mostly empirical and with a small range of application. Consequently, the main aim of this thesis is to predict the nonlinear behaviour and ultimate strength of stiffened and unstiffened cylindrically curved steel panels under in-plane and out-of-plane loading based on a physically robust approach, through semi-analytical methods (SAM). The main advantage of this approach, in comparison to the usual approaches, like the Finite Element Method (FEM), is allowing to identify the key parameters that influence the behaviour of the curved panels and to develop expressions purely based on the physical background of the problem, which have a large practical interest. However, the FEM is also used for two reasons: *i)* to characterize thoroughly and realistically the behaviour of the panels through a wide parametric study; in this case, an innovative way to model imperfections is developed, being more unfavourable than the default approach in shell structures, in a large part of the cases; and *ii)* to validate the semi-analytical formulation developed for the curved panels.

The analysed parameters are found to change dramatically the behaviour of the panels,

which, in some cases, may lead to unexpected results. For example, it may be quite unsafe to design a curved panel as if it was a flat plate. In contrast, in other cases, significant gains in resistance are obtained with the increase in curvature. This shows that the design of curved panels has to be performed with a deep knowledge of this complex behaviour.

Although only uniaxial in-plane compression (the key aspect in the stability of thin walled structures) and out-of-plane pressure are studied in this thesis, the formulation is developed to account for generalized loading. A large deflection formulation with a multi degree-of-freedom (MDOF) solution and imperfections is implemented. Additionally, the SAM accounts for in-plane constrained and unconstrained simply supported boundary conditions. This requires a rigorous solution of boundary value problem of the fourth order nonlinear partial differential equations.

Despite the complex behaviour identified for the curved panels, the SAM is able to account accurately for all the geometric parameters, boundary and loading conditions. Although the panels with larger curvatures benefit from the implemented MDOF solution, closed-form expressions, based on a SDOF approximation, are able to provide accurate results for the equilibrium paths of unstiffened and stiffened curved panels with practical significance under in-plane and out-of-plane loading.

The SAM is then used, with a yield criterion, to predict the resistance of unstiffened curved panels under compression. Expressions are derived to calculate the ultimate load of these panels, showing good agreement with the FEM.

Keywords

Unstiffened and stiffened curved panels | Large deflection behaviour | Ultimate load | FEM | Semi-analytical method | Closed-form expressions.

Contents

List of figures

List of tables

Notation

Greek lowercase letters

α	Aspect ratio
α_{loc}	Local aspect ratio (between stiffeners)
ε_x, ε_y, ε_{xy}	Strain components
$\varkappa_x$, $\varkappa_y$, $\varkappa_{xy}$	Curvature components
σ_x, σ_y, σ_{xy}	Stress components
σ_{cr}	Critical stress
σ_{vM}	von Mises' stress
υ	Poisson's ratio
υ_x, υ_y, υ_{xy}	Poisson's ratio components for the orthotropic panels

GREEK UPPERCASE LETTERS

Δu	Variation of displacement in the x direction
Δv	Variation of displacement in the y direction

ROMAN LOWERCASE LETTERS

a	Width of the panel
a_{mn}	Amplitude of the out-of-plane imperfection
a_s	Width of the subpanel between stiffeners
b	Length of the panel
b_{mn}	Amplitude of the out-of-plane deflection
d_s	Height of the stiffeners
e_{0G}	Amplitude of the global imperfection in FEA
e_{0L}	Amplitude of the local imperfection in FEA
e_{0s}	Amplitude of the stiffener imperfection in FEA
f_y	Yield strength of the steel
h	Thickness of the panel
h_s	Thickness of the stiffeners
k_σ	Elastic buckling coefficient
m	Number of transversal half waves
n	Number of longitudinal half waves
n_s	Number of stiffeners
p_y	In-plane axial pressure in y direction
p_z	Out-of-plane pressure in z direction

u	In-plane displacement along x axis
v	In-plane displacement along y axis
$w(x,y)$	Out-of-plane displacement (along z axis)
$w_0(x,y)$	Initial out-of-plane imperfection
x, y, z	Coordinate system
z_0	The distance from the middle surface of the panel to the neutral axis (*N.A.*) of the stiffener with the associated part of the panel

Roman uppercase letters

C	Extensional stiffness
D	Flexural stiffness
D_x, D_y	Flexural stiffness components for the orthotropic panels
D_s	Orthotropic parameter
E	Modulus of elasticity
E_x, E_y	Modulus of elasticity components for the orthotropic panels
F	Airy's stress function
F_0	Homogeneous solution of the differential equation
F_1	Particular solution of the differential equation
G	Shear modulus
G_{xy}	Shear modulus for the orthotropic panels
H	Orthotropic parameter
I_s	Inertia of a single stiffener
M_x, M_y, M_{xy}	Bending moment component
N_x, N_y, N_{xy}	Membrane force components

R	Radius of curvature
T_p	Potential energy of the external in-plane load
T_{lp}	Potential energy of the external out-of-plane pressure load
U_b	Bending strain energy
U_m	Membrane strain energy
U_{tot}	Total potential energy
Z	Parameter of curvature
$Z_{Batdorf}$	Batdorf's parameter of curvature
Z_{loc}	Parameter of local curvature (between stiffeners)

Mathematical operators

∇^2	Harmonic operator
∇^4	Biharmonic operator

Abbreviations

BC	Boundary conditions
BUU	Boundary conditions with transversal and longitudinal edges in-plane unrestrained
BCU	Boundary conditions with transversal and longitudinal edges in-plane restrained and unrestrained, respectively
BCC	Boundary conditions with transversal and longitudinal edges in-plane restrained
DMV	Donnell-Mushtari-Vlassov
DOF	Degree of freedom
FEA	Finite element analysis

FEM	Finite element method
FGM	Functionally graded material
FSDT	First order shear deformation theory
GMNIA	Geometrically and materially nonlinear analysis with imperfections
GNIA	Geometrically nonlinear analysis with imperfections
HSDT	High order shear deformation theory
LBA	Linear buckling analysis
MDOF	Multi degree of freedom
NLFEM	Non-linear finite element method
SAM	Semi-analytical method
SDOF	Single degree of freedom
SDT	Shear deformation theory

1 Introduction

1.1 Problem description and motivation

The interest in curved panels, both unstiffened and stiffened, has recently increased in several engineering fields (*e.g.* civil, naval, offshore and aeronautics). While in aeronautics the application of curved panels is not particularly new due to the intrinsic need to use them, other fields such as civil engineering have progressively adopted this type of structural elements. The main reasons for this are: *i)* its geometry – the curvature brings not only aesthetical but also functional advantages; for example, curved panels allow the design of bridge decks which are better integrated on the landscape and with improved aerodynamics behaviour; *ii)* besides performing a structural function, curved panels provide complete enclosure, particularly important in naval, offshore and aeronautics; and *iii)* the structural efficiency of these elements leads to improved load bearing capacity to weight ratios. However, like all thin structures, curved panels are very susceptible to local and global instabilities because they are much stiffer in-plane than out-of-plane. This implies the need for a deep knowledge of their behaviour. With this in mind, these

elements if properly designed can present good overall structural efficiency.

To obviate the potential instability issues, curved panels are, in many cases, fitted with stiffeners which allow them to improve substantially their bearing capacity. Naturally, this aspect increases the complexity of the analysis and the influence of these additional elements must be understood.

Compared to the more classical case of flat plates, curved panels have the particularity of its curvature, which leads to dramatic changes in behaviour. Significant gains in resistance can be obtained with the introduction of curvature. However, as shown in this thesis and perhaps in contrast to common belief, curvature does not always lead to an increase in resistance. In particular conditions, a curved panel may withstand a lower load than the corresponding flat plate. Consequently, it may not be safe to design a curved panel as a flat plate.

In contrast to flat plates, robust and physically consistent design formulations able to deal with all the specific features inherent to curved panels are generally not available in various engineering fields. For example, in the construction sector, these elements fall clearly outside the scope of EN 1993-1-5 [1], which gives provisions for plates (and panels with very low curvatures, *i.e.* $Z=a^2/(Rh)<1$, where a is the width, R is the radius and h is the thickness of the panel), and EN 1993-1-6 [2], which deals with shells of revolution. As it will be shown later, neither of the two standards is able to provide adequate provisions for the ultimate load of curved panels.

On the other hand, offshore standards like DNVGL-RP-C202 [3], DNVGL-CG-0128 [4] and ABS – Guide for Buckling and Ultimate Strength Assessment for Offshore Structures [5] account for cylindrical curved panels but for very specific conditions. They do not provide a holistic and adequate alternative to deal with the whole range of parameters relevant to curved panels, and, consequently, they provide unsafe provisions for some situations, as recently shown by Martins *et al.* [6].

The solution currently carried out by engineers to obviate this lack of design provisions for curved panels is the use of the Finite Element Method (FEM). Despite this tool is able to address the problem correctly, it requires experienced users and it is time-consuming; consequently, simpler provisions in the form of design equations provided in standards are preferable. However, in order to derive reliable and robust design equations, the use

of physical models and analytical methods are the desirable approach. The reasons to develop an analytical model and design equations based on it are twofold: *i)* analytical models have the advantage of identifying the key parameters that influence the non-linear behaviour of curved steel panels and clearly establishing the range of validity of the developed formulation. Advanced FEM models are not able to do this and require skilled users and large parametric studies in order to cover a specific range of geometries, load cases and boundary conditions. Design equations based on advanced FEM results will necessarily involve more empirical coefficients based on statistical assessment, leading to worse adjustment to reality; secondly, *ii)* design equations based on analytical methods have the potential of leading to closed-form equations that will significantly improve productivity by allowing designers to perform their work faster and more reliably. This is the main motivation for this thesis.

The application of curved panels in offshore structures is usual. In general, these elements are reinforced by longitudinal stiffeners and associated to longitudinal and transversal girders. While the stiffeners rigidly connected to the panel provide resistance to local buckling (if the buckling of the stiffener is prevented), the girders at the boundaries of the panel provide support and consequently they prescribe the boundary conditions of the panels.

In Figure 1.1 *a)* is possible to see the construction of one of these panels to be applied in a Spar offshore structure. These panels are then connected to other adjacent similar

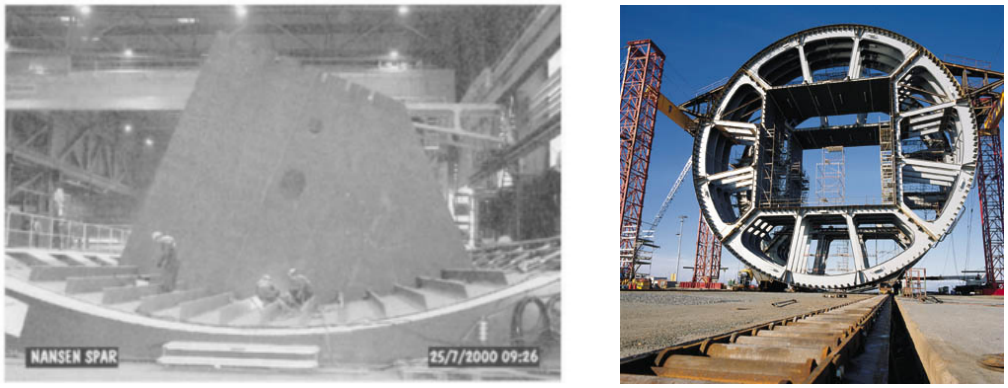

a) *b)*

Figure 1.1: Spar offshore platform: *a)* construction of a stiffened curved panel [7]; *b)* final cross-section composed by adjacent stiffened curved panels [8]

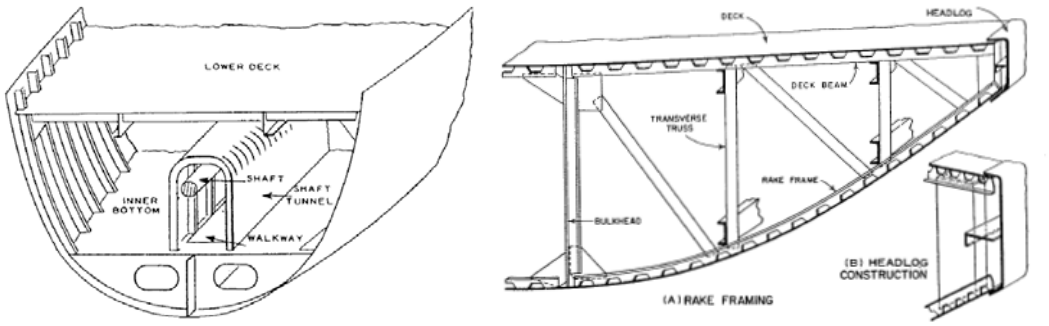

Figure 1.2: Examples of curved panels in naval construction [9]

panels to compose a cylindrical section of the Spar offshore platform as the one shown in Figure 1.1 *b)*.

The use of curved panels is also usual in naval construction. In Figure 1.2, examples of a ship hull are presented. Similarly to offshore construction, these elements are generally longitudinally stiffened and supported by longitudinal and transversal girders.

The classical application of curved panels in aeronautics is in the fuselage of airplanes. Although they are, nowadays, often composed by more innovative materials due to the need for lighter materials (*e.g.* high performance alloys and composites), the behaviour of these elements follows the same principles. In Figure 1.3, the stiffened curved panels for the fuselage of a Boeing 777 are presented.

More recently, the application of curved panels in bridges has gained momentum. These elements, besides greater resistance due to curvature, provide aesthetical advantages not

Figure 1.3: Fuselage stiffened curved panel of a Boeing 777 [10]

a) *b)*

Figure 1.4: Curved cross-section of: *a)* Renault bridge (Boulogne-Billancourt) [11]; and *b)* bridge over the river Deba in Guipúzcoa [12]

possible to reach with the more conventional flat plates. Among many examples, the Renault bridge in Boulogne-Billancourt , France (Figure 1.4 *a)*) and the bridge over the river Deba in Guipúzcoa, Spain (Figure 1.4 *b)*) may be highlighted. In Figure 1.4 it is possible to verify that the bottom flange of the cross-section of both bridges is mainly composed by a single stiffened curved panel transversely.

Besides in-plane loads acting on the curved panels, in most cases of offshore and naval structures, these elements are generally also subject to out-of-plane loads (*e.g.* hydrostatic pressure).

Taking into account the way curved panels are connected to the adjacent structure, the boundary conditions may be considerably distinct. For example, in offshore and naval construction, the panels are generally supported by stiff girders in the longitudinal and transverse directions, and the panels may be considered with the edges remaining straight. The consideration of this condition provides additional strength which is useful in practical design. On the other hand, in bridges, the curved panels are often isolated, without adjacent panels in the transverse direction. This means that the panels do not have much restraint in the transverse direction, and consequently, it is safer to consider the longitudinal edges as free to wave.

Similarly, the way as the edges of the panels are supported influences the kind of supports to consider. If the longitudinal supports are vertically oriented, they restrain vertical displacements, however if radially oriented they restrain radial displacements.

These particularities have practical significance and are also addressed in this thesis.

1.2 Objectives and approach

In practical terms, the current available design formulations are insufficient if a robust and physically consistent description of the structural behaviour is intended. Consequently, this thesis is focused on the analytical derivation of a large deflection formulation for unstiffened and stiffened curved panels subjected to different loading conditions and the implementation of a semi-analytical solution procedure. Special emphasis is given to compressive stresses which represent the key aspect in the stability of thin walled structures and also out-of-plane pressure. Other loading conditions are not the object of study in this thesis; however, the semi-analytical method is formulated to cover wider load situations, namely biaxial compression and shear forces. So, if intended, the proposed semi-analytical procedure should be able to account properly for a generic combination of loading cases.

The prediction of the nonlinear behaviour and ultimate strength of stiffened and unstiffened curved steel panels based on a physically robust approach is one of the main ambitions of this thesis. The objective is not only to formulate a semi-analytical method to predict the behaviour and ultimate strength of curved panels but also to propose closed-form design expressions for practical use. In order to accomplish this objective, others contributions are also produced in this work, namely:

i) The proposed semi-analytical formulation is based on nonlinear stability models with large deflection theory incorporating initial imperfections and geometric nonlinearity. The equilibrium paths are obtained using the Rayleigh-Ritz method with a multi degree-of-freedom (MDOF) displacement field. The ability to deal with a MDOF solution is shown to be crucial for a good agreement with Finite Element results;

ii) The appropriate treatment of simply supported boundary conditions for curved panels. Three distinct boundary conditions are distinguished taking into account the way the edges are constrained. Two of them are assessed with the semi-analytical formulation: with edges free to deflect or forced to remain

straight. The semi-analytical procedure addresses this by only assuming displacement function for the out-of-plane displacements and initial imperfections, while the remainder of the solution is obtained by solving directly the differential compatibility equation for the respective boundary conditions, *i.e.* the displacement are not assumed for the in-plane directions;

iii) The derivation of a consistent energy formulation for the elastic post-buckling behaviour of cylindrically-curved isotropic and orthotropic panels compatible with a semi-analytical method. Due to the presence of stiffeners, the problem exhibits structural anisotropy. Noting that the stiffeners are asymmetrically placed (towards the concave side of the panel) an equivalent orthotropic approach is applied following available results in the literature for stiffened flat plates. The proposed formulation is thus able to incorporate the elastic properties of the equivalent orthotropic curved panel;

iv) The behaviour of unstiffened and stiffened curved panels is deeply characterized based on numerical parametric studies. The key parameters are identified and important conclusions are drawn about the non-linear behaviour and ultimate load of the panels;

v) An extensive study on the influence of initial imperfections is performed and important conclusions on the subject are drawn. For example, it is shown that the default approach of assuming an imperfection pattern given by the eigenmodes of linear buckling analyses, usually the default approach in Finite Element Analyses, is compared with other other perfectly reasonable imperfection patterns;

vi) The validity of the developed formulation is assessed with the results of advanced finite element analyses for unstiffened and stiffened panels for a wide range of curvatures, aspect ratios and configurations of stiffeners for different boundary conditions under different loading conditions, yielding good results;

vii) Analytical closed-form equations are derived for the non-linear load-deflection paths of both unstiffened and stiffened curved panels under in-plane compression and out-of-plane pressure;

viii) Strength criteria are employed in the semi-analytical model to predict the ultimate load of unstiffened curved panels. Good predictions are obtained in comparison with numerical results. Expressions to predict the ultimate load of these panels are provided;

1.3 THESIS LAYOUT

The thesis is organized as follows.

In this Chapter 1, *Introduction*, a brief presentation of the subject was presented. The motivation and the scope of the work were described and objectives of the research were identified.

Chapter 2, *State of the art*, is intended to provide a detailed state of the art of curved panels, presenting the most important literature regarding semi-analytical and numerical studies. The most important advances in flat plates and cylindrical shells are presented. Despite having characteristics that distinguish them from the curved panels, the knowledge of flat plates is currently much more detailed and its background is useful. The studies about curved panels are separated into critical and large deflection behaviours. Some advances in laminated, sandwich and functionally graded curved panels are referred. Despite similar in geometry these elements have characteristics that require distinct approaches. The main differences are identified. The validity and limitations of the existing standards dealing with curved panels will be discussed and framed in the present research.

Some important concepts indispensable to understand the next chapters are briefly described in Chapter 3, *Fundamentals of curved panels*. The differences between the several existing shell theories are identified. Justification is given to the choice of the theory used in this thesis. The geometry, the boundary and loading conditions are described. Some basic concepts of stability are presented and the differentiation of the behaviour of flat and curved panels is discussed. The theoretical aspects of the different methods of analysis of shells are briefly described with particular attention for the Rayleigh-Ritz method and finite element method.

Chapter 4, *Formulation of large deflection theory for curved panels*, is devoted to the

formulation of a large deflection theory for isotropic and orthotropic curved panels. This is the core of the proposed semi-analytical method. The energy formulation is derived for the potential energy components and the Rayleigh-Ritz method is employed as the method of solution for a MDOF solution.

All assumptions used to model the panels in finite element analyses are explained in Chapter 5, *Modelling curved panels by the Finite Element Method*. Here, the types of analysis, the boundary and loading conditions, material and modelling of the imperfections used in the ABAQUS software are described.

In Chapter 6, *Characterization of the behaviour and ultimate load of unstiffened and stiffened curved panels under compression and out-of-plane loading*, a detailed characterization of the behaviour of the curved panels is presented. A discussion is first presented about the critical behaviour of the panels, which is fundamental to explain some aspects in the following sections. A preliminary analysis is carried out to define the importance of some parameters and assess the need for its consideration in the further analyses. A thorough parametric study is carried out with the Finite Element Method, to characterize the non-linear behaviour and ultimate load of unstiffened and stiffened panels, both under in-plane and out-of-plane load.

In Chapter 7, *Validation of the Semi-Analytical Model for curved panels under in-plane compression and out-of-plane pressure*, the objective is to validate the semi-analytical formulation with the results of Finite Element analyses. For validation purposes, the critical load of the panels is calculated with the semi-analytical method for some cases. Then, the nonlinear load-deflection behaviour is presented and discussed in more detail. Here the results of the semi-analytical behaviour are compared with the ones from FE analyses in terms of the equilibrium paths through a wide parametric range.

Chapter 8, *Design oriented closed-form equations for the elastic large displacement behaviour and ultimate resistance of curved panels,* presents proposals to calculate the elastic large deflection behaviour and the ultimate load of curved panels, based on the semi-analytical method. Firstly, expressions for the non-linear equilibrium paths of unstiffened and stiffened curved panels under combined in-plane and out-of-plane loading are presented. Then, the ultimate load of unstiffened curved panels is calculated

by the semi-analytical method using a strength criterion and compared with the results from Finite Element analyses. For validation purposes, besides the geometry, the influence of aspects like initial imperfections are also assessed. Based on this, expressions are then proposed to predict the ultimate strength of the unstiffened curved panels.

Finally, Chapter 9, *Conclusions and outlook*, concludes about the main findings of the thesis and summarizes the main contributions. Recommendations for further works are proposed.

2 State of the art

2.1 Introduction

The interest in structural curved panels is not new. In 1934, Redshaw [13] published a paper about the elastic stability of curved panels under compression. Although the study of curved panels was never forgotten by the scientific community, curved panels were never so scrutinized as flat plates. With the appearance of new applications, the study of curved panels seems to have gained a new enthusiasm, as shown in recent research and PhD theses on the topic (*e.g.* Tran [14] and Martins [15]).

The objective of this chapter is to present an outlook of the studies carried out by the scientific community about thin curved panels in structural applications. Because of the scarcity of studies of curved panels in some areas, it is relevant to present some studies on the more classical cases of flat plates and shells of revolution (closed tubes/cylinders). In these cases, the amount of existing studies is much larger and some advances found in the literature are also useful for the study of curved panels and therefore they deserve to be mentioned.

Consequently, the advances in flat plates, where the knowledge level is, currently, at a more advanced stage, are described next and, in comparison, the main limitations found on the current knowledge of curved panels are identified. For this, the latest research on both areas is useful to set the starting point of the work.

However, despite the approaches for the analysis of flat plates and shells of revolution being established on similar general principles, both for analytical or numerical formulations, they have particularities that distinguish them very markedly and not all conclusions for one type of element may necessarily be valid for the other, reason why their studies have to be performed independently. In this particular topic, the original contributions of the work will be defined in next sections.

The literature review in section 2.2 is organized as follows: *i)* firstly, some historical references on the early analytical studies and the most recent advances in flat plates and cylindrical tubes are identified; *ii)* secondly, the most important studies about the critical and large deflection of both unstiffened and stiffened curved panels under in-plane and out-of-plane loading are presented; *iii)* thirdly, laminated, sandwich and functionally graded panels are briefly introduced. The associated differences are identified and explained why they are of limited relevance for the present study; and *iv)* finally, the references dealing with the ultimate resistance of both unstiffened and stiffened curved panels are presented. In section 2.3, the standards applicable to the design of curved panels are addressed and their applications and limitations are discussed.

Although all references are considered important, they are either analytical, numerical or experimental, larger emphasis is given on analytical references due to the main focus of the thesis. Some relevant studies excluding analytical procedures are also relevant especially for the ultimate load, where most results were exclusively achieved with numerical methodologies.

2.2 LITERATURE REVIEW

2.2.1 Flat plates

The critical stress of a flat plate was first obtained by Bryan [16], still before the 20th century. From the geometry of the plate, the elastic properties of the material and the

number of half waves of the buckling modes, it was then possible to estimate the critical stress, σ_{cr}, of a simply supported flat plate under in-plane compression as follows:

$$\sigma_{cr} = k_{\sigma} \frac{\pi^2 E}{12\left(1-\upsilon^2\right)}\left(\frac{h}{a}\right)^2 \tag{2.1}$$

where a is the width of the panel, h is the thickness, E is the modulus of elasticity of the material, υ is the Poisson's ratio and k_{σ} is the elastic buckling coefficient, which for plates is given by $k_{\sigma,plate}$ as follows:

$$k_{\sigma,\,plate} = \left(\frac{n}{\alpha} + \frac{m^2}{n}\alpha\right)^2 \tag{2.2}$$

where m and n are the number of transversal and longitudinal half waves, respectively, and α is the plate aspect ratio which is given by the ratio between the length and width, b/a. The minimum value of $k_{\sigma,plate}$ is 4.0.

Since then, many developments were proposed by several authors on the critical behaviour of flat plates, accounting for different boundary and loading conditions, stiffeners, etc., a thorough review being found in Allen and Bulson [17].

Of greater practical interest is the study of the large deflection behaviour, which is able to account for the postbuckling resistance, characteristic of flat plates. The historical references are very extensive, so only key contributions are mentioned, complemented by developments of larger practical significance for this work, especially when related to the use of semi-analytical methods.

Since the classical contributions of *e.g.* von Kármán [18], Marguerre [19] and Levy [20] on the large deflection theory of plates, many developments were made using semi-analytical methods, with more sophisticated implementations with regard to the incorporation of different boundary conditions, loading conditions, imperfections and methods of resolution, both for unstiffened and stiffened plates.

Yamaki [21] studied the postbuckling behaviour of imperfect unstiffened plates under compression for a wide range of combinations of simply supported and clamped boundary conditions. The author solved the differential equations under the assumed boundary conditions, applying the Galerkin's method to solve the differential equations.

The author also studied the ultimate load of those plates based on the Tresca's criterion. Maquoi and Massonnet [22] studied the postbuckling resistance of stiffened box girders using the non-linear theory of orthotropic plates. The authors replaced a stiffened plate by an equivalent orthotropic plate using the von Kármán equations with imperfections. The authors used the method of Bubnov-Galerkin to integrate the equilibrium equation. Prabhakara and Chia [23] were among the first to study the post-buckling behaviour of perfect orthotropic plates subjected to edge loading. The authors used von Kármán large deflection theory using a double Fourier series for the displacement field. Jetteur [24], based on the study of Maquoi and Massonnet, proposed a design method for stiffened plates under longitudinal compression. The author's approach substitutes a stiffened plate by an isotropic plate and an orthotropic plate idealizing the stiffeners. The solutions are derived using a variational formulation and an assumed stress and displacement field. The results of this approach were adopted by Eurocode 3, part 1-5 [1] to assess the resistance of flat stiffened compressed plates.

Paik *et al.* [25] presented a semi-analytical method to deal with the post-buckling behaviour and ultimate strength of unstiffened plates under in-plane and out-of-plane loading. The Galerkin's method was used to solve the system of the governing differential equations. As usual, in structures with naval and offshore applications, simply supported boundary conditions with all edges considered to remain straight were assumed. An incremental version of the governing differential equations was applied to obviate the difficulty to solve the resulting set of third order simultaneous equations when the non-incremental differential equations are used, especially when the number of variables becomes large. This approach leads to a simpler set of linearized simultaneous equations which results in computational advantages. Besides that, in this way, the three admissible solutions for the displacements unknowns are reduced to single solutions. However, with this incremental approach, the possibility to obtain analytical closed-form solutions is lost. A strength formulation was developed numerically, assuming that the plate is subdivided in several regions, their contributions being progressively removed once yield is reached for the von Mises' stresses in those regions.

Later, Paik *et al.* [26] extended the previous study to stiffened plates under combined biaxial loading and lateral pressure, developing a procedure to account properly for the elastic orthotropic properties of asymmetrically placed stiffened plates. Thus, the authors

were able to study the post-buckling behaviour of stiffened plates exhibiting a global buckling failure. Contrarily to their previous study, the incremental Galerkin approach was abandoned and the governing equations were solved analytically assuming a single degree of freedom for the displacement function. Additionally, the ultimate load is assumed to be reached when first yield occurs, leading to the possibility to obtain closed-forms expressions.

Paik and Lee [27] re-implemented their incremental approach with the Galerkin's method to stiffened plates (with local buckling of stiffeners prevented) under generalised loading. Plasticity was dealt numerically by subdividing the plate in a meshed region. When the average membrane stress in each region meets the yield criterion, the membrane action at that region is removed, as before.

Paik *et al.* [28] extended the previous formulation to account for non-uniform lateral pressure in unstiffened plates. It was concluded that the simplified consideration of an average uniform pressure may underestimate the lateral deflection in comparison with the real non-uniform pressure.

Also in the context of flat stiffened plates, Byklum and Amdahl [29] used energy principles with the Rayleigh-Ritz's method and perturbation theory to develop an incremental arc-length scheme able to deal with snap-through and snap-back problems. The interaction between global and local buckling of the stiffened plate was accounted for through the coupling between plate and stiffener components. The ultimate load was estimated through the implementation of a first yield criterion. Comparison with FE analyses were provided. However, closed-form expressions were not proposed.

Ferreira and Virtuoso [30] studied the influence of distinct simply supported boundary conditions with regard to in-plane restraints on the post-buckling behaviour and ultimate strength of orthotropic flat plates. The authors extended the original work of Coan [31] to orthotropic plates, where the exact solution for isotropic plates with in-plane displacements had been derived considering the loaded and unloaded edges remaining straight and free to deflect, respectively.

Further details of the implementation of strength prediction techniques in semi-analytical methods will be given in section 8.3.3.

Although it can be considered that the implementation of semi-analytical methods is at an advanced stage for flat plates and little innovation can be incorporated, for example with respect to non-linearity, imperfections, methods of analysis, etc., the same is not true regarding curved panels that exhibit particularities which do not appear in flat plates. These differences, mainly due to the curvature, are found to differentiate flat and curved panels very markedly, and distinct outcomes are achieved.

2.2.2 Cylindrical tubes

In parallel to the study of flat plates, an extensive amount of work has been performed in thin tubes (closed cylindrical shells). Similarly to the case of flat plates, cylindrical tubes have particularities that distinguish their behaviour from curved panels. However, some developments carried out on these elements are useful for the study of curved panels and some of the main advancements deserve to be presented.

The study of a large-displacement theory for cylindrical shells started with Donnell [32] and von Kármán and Tsien [33]. The authors concluded that the classical theory of thin shells of perfect elements (*e.g.* Southwell [34]) is inadequate to explain the intricate behaviour of cylindrical shells (the calculated buckling load can be several times higher than the maximum load found by experiments). Various authors, as Leggett [35], Michielsen [36] and Almroth [37], extended those studies by incorporating more terms in the displacement function to improve the agreement of the theoretical solutions with experimental results. Donnell and Wan [38] addressed the problem of initial imperfections of thin cylinders under compression, and later Hutchinson [39], for pressurized cylindrical shells under axial compression, explicitly incorporated initial imperfections, which were found to have an important influence.

The first studies regarding stiffened curved elements started with circular cylindrical shells. In this context, Jones [40] studied the buckling of circular cylindrical shells with multiple orthotropic layers and eccentric stiffeners. Sheinman and Simitses [41] analysed the buckling of imperfect stiffened cylinders under compression incorporating the effect of the stiffeners based on the "smearing" technique.

Regarding the study of out-of-plane pressure on stiffened shells, the study of Yamada and Croll [42] may be highlighted. The elastic buckling and post-buckling behaviour of

pressure loaded cylinders was tackled. Analysing the energy of the system, the authors were able to use a reduced stiffness model which is claimed to provide a safer extension to the classical analysis of pressure loaded cylinders.

2.2.3 Critical behaviour of curved panels

Only after the critical behaviour of flat plates had been understood, the study of the critical behaviour of curved panels was initiated. To account for the non-negligible effect of the curvature on the buckling resistance of these elements, expression (2.1) was modified by adjusting the buckling coefficient, $k_{\sigma,Z}$, as a function of curvature. Among various authors, Redshaw [13], Timoshenko [43], Stowell [44] and Batdorf [45] are highlighted. One of the most known is Stowell's formula, given by:

$$k_{\sigma,Z} = \frac{k_{\sigma,plate}}{2}\left(1+\sqrt{1+\frac{48\left(1-\upsilon^2\right)}{k_{\sigma,plate}{}^2\pi^4}Z^2}\right) \tag{2.3}$$

where Z is the parameter of curvature given by:

$$Z = \frac{a^2}{R\,h} \tag{2.4}$$

and R is the radius of curvature.

The parameter defined in equation (2.4) is based on the simplification of a similar parameter first defined by Batdorf, $Z_{Batdorf}$, as:

$$Z_{Batdorf} = \frac{a^2}{R\,h}\sqrt{1-\upsilon^2} \tag{2.5}$$

Nowadays, the parameter of curvature exclusively defined with the geometrical properties, Z, is usually preferred and it is the one used throughout this work.

Equation (2.3) for Z=0 converges to the theory of flat plates, $k_{\sigma,Z}$=4.0, the minimum elastic buckling coefficient for simply supported plates. However, it has been shown by more recent studies that the expression present non-negligible errors, as it will be posteriorly discussed.

Based on a modified form of Donnell's equations, Batdorf [45] studied the buckling

stresses of simply supported and clamped perfect cylindrically curved panels using trigonometric series to approximate the displacements. The author claimed that these modified equations were better adapted to solutions by Fourier series for both boundary conditions.

Batdorf and Schildrout [46] carried out one of the first studies on stiffened curved panels. They derived the theoretical critical stress of a simply supported curved rectangular panel with one middle transverse stiffener under axial compression. Later, Schildrout and Stein [47] carried out a similar study with one longitudinal stiffener.

Already during the 1950's, the differences between the theoretical critical load and experimental data of curved panels under compression had been identified. Gerard and Becker [48] verified the disagreement between theory and experimental data for curved panels under compression. This discrepancy was found to be much more evident than for flat plates. It was identified that the theoretical critical buckling load may not be reached by a curved element and large deflection theory should be used. Imperfections were also identified as much more important for curved panels than for flat plates. This is due to the fact that while flat plates have a stable post-buckling path, curved panels have an unstable one. This will be explained in further detail in Section 3.6. Becker [49] continued the work, this time for stiffened curved panels, comparing existing experimental data with empirical solutions.

Despite the fact that the critical buckling load is unable to provide a reliable estimate of the resistance of curved panels and, consequently, possesses less practical importance, the critical load has still some interest to be studied because it can be used indirectly in design methodologies to calculate the slenderness as a step to estimate the ultimate load of the element. With this in mind, some authors continued to study the critical buckling of curved panels.

Many years later, Domb and Leigh [50] proposed improvements to earlier expressions for the unstiffened cases using Finite Element analyses. Wilde *et al.* [51] studied the buckling stresses of cylindrical curved panels with three edges simply supported and one free subjected to axial compression.

Eipakchi and Shariati [52] compared with FE analyses the critical stresses of curved panels obtained by a perturbation technique in Donnell's linear theory. The authors

applied a correction factor as a function of the curvature to the formula for the critical stress of cylindrical shells. Recently, Martins *et al.* [53] showed that the formulas of Stowell and Domb and Leigh present non-negligible errors. The author, based on Finite Element analyses, proposed expressions to calculate the critical stress of simply supported cylindrical curved panels with edge constraints. Trying to improve the fact that previous solutions had been derived only through calibration of numerical results, and they lacked mechanical meaning, Martins *et al.* [54] addressed the same problem with energy methods, proposing expressions to predict the critical buckling stresses of unstiffened curved panels under in-plane stresses. Simply supported panels considering the non-loaded longitudinal edges restrained and free to wave were considered. Displacement functions were assumed for each direction obviating the resolution of the differential equations. The number of degrees of freedom (DOFs) was found to be important for the accuracy of the results. For long panels a larger number of DOFs would have been required and a numerically calibrated correction was applied to the results of shorter panels. A thorough review of the critical behaviour of cylindrically curved panels is presented in Martins *et al.* [6] with larger emphasis on numerical studies.

2.2.4 Large deflection behaviour of curved panels with semi-analytical methods

2.2.4.1 Unstiffened curved panels under compression

Only after being applied to cylindrical tubes, the large deflection theory was extended to curved panels (a part of a cylindrical shell). The interest in these panels was driven by the application to the fuselage of airplanes. Around the 1940's, the study of a large deflection theory of curved panels was started by Levy [55] by adapting the large-deflection theory of flat plates for panels with an initial curvature. Through a simplified consideration of the curvature, the author assumed a curved strip plate with an initial sinusoidal displacement in one direction only. The panels were considered free from imperfections and simply supported along the edges parallel to the generator. The author concluded that curvature may cause an important increase in the buckling load. A nonnegligible effect on the effective width due to the curvature was also found. Volmir [56], adopting the Galerkin's method, proposed an approximate solution for the post-buckling behaviour of perfect thin curved panels. However, the boundary conditions were not

fully satisfied and good accuracy could not be achieved. To deal with this problem, Tamate and Sekine [57] proposed an improved solution for the post-buckling behaviour of simply supported perfect thin curved panels with all edges simply supported and free to wave. Recognizing that imperfections might not be the only reason for discrepancy with experimental tests, some authors also started including the effect of edge restraints in compressed curved panels. One of the first studies dealing with this aspect in curved panels is by Chia [58]. Although he was mostly interested in aspects like vibration and applications to laminated panels, the author investigated the post-buckling behaviour of imperfect curved shallow panels with edges elastically restrained against rotation.

Breivik [59] investigated the post-buckling behaviour of unstiffened curved composite panels subjected to combinations of thermal and mechanical end-shortening loading. The author used the Rayleigh-Ritz method assuming the displacement functions for all directions, avoiding to solve the fourth-order von Kármán-Donnell differential equations.

Magnucka-Blandzi and Magnucki [60] studied the buckling and post-buckling of cylindrical curved panels under compression using the Galerkin method. The imperfections were not considered and the boundary conditions were assumed as simply supported but once again the in-plane restraints at the edges were not taken into account.

A larger number of studies are found for laminated, sandwich and functionally graded composite curved panels. As will be discussed posteriorly in section 2.2.5, these type of materials introduce particularities which in some cases have to be tackled with specific theories (*e.g.* shear deformation theory). This signifies that in these cases the applicability to the panels studied in this thesis is reduced.

2.2.4.2 Stiffened curved panels under compression

The analytical study of stiffened elements started with flat plates and a large number of studies has been carried out on that topic since then.

Very few contributions about the large deflection of curved panels were identified in the literature. For orthotropic curved panels, it is possible to highlight the following study. White *et al.* [61], based on Koiter's [62] original theory and using the differential quadrature method, investigated the initial post-buckling behaviour of variable-stiffness

curved panels and compared the results with FE analyses in the vicinity of the buckling load.

2.2.4.3 Unstiffened and stiffened panels under combined uniaxial compression and out-of-plane pressure

In several engineering fields, like aeronautics, naval and offshore engineering, in some of their applications, besides in-plane loading, curved panels are also subjected to out-of-plane pressure. Examples of structures with these applications are airplanes, silos, tanks, ships and offshore structures. However, classically the problem of flat plates and closed cylindrical shells under out-plane loading has received greater attention by researchers and engineers.

The study of curved panels under lateral pressure was tackled by Singer *et al.* [63] studying the structural stability of cylindrical panels using linear theory. The authors concluded that cylindrical panels may buckle at lower pressure than the corresponding cylindrical tubes. Yamada and Croll [64] performed a classical bifurcation analysis and applied a non-linear Ritz procedure to study pressure loaded isotropic cylindrical panels. In this study it was shown that curved panels present a very complex behaviour and it was concluded that the classical linear theory is not able to provide reliable estimates for the buckling of pressure loaded imperfect curved panels. To obviate this problem, the same authors suggested an extension of the classical theory by using a reduced stiffness occurring in the post-buckling phase to provide a lower bound to the imperfection sensitivity of the elastic buckling pressure. Dennis *et al.* [65] studied the bifurcation and the non-linear behaviour of clamped cylindrical panels under normal pressure applying a finite element solution.

van Campen *et al.* [66], using the Partitioned Solution Method (PSM), studied the post-buckling solutions of perfect doubly-curved orthotropic shallow panels under lateral pressure. The authors also compared the bifurcations loads with the PSM and the Adjacent Equilibrium Method (AEM).

Some studies are found regarding the large deflection of curved panels for composite materials, particularly relevant in aeronautics. However, these panels have some particularities that hinder somewhat its applicability to the present case, as discussed in

section 2.2.5.

2.2.5 Laminated, sandwich and functionally graded panels

In parallel to the study of homogeneous panels, substantial work has been performed on laminated (or multi-layered) and sandwich panels widely used in aeronautics, for example. However, these panels have particularities that distinguish them from the previous elements and, consequently, with few exceptions, their approaches of analysis are, generally, difficult to be directly applicable to the study of homogeneous panels, like the ones considered in this thesis. Taking this into account, they will be only briefly described.

Laminated panels, being generally composed by several layers of different materials, either isotropic or orthotropic, or composed by the same orthotropic material arranged in different directions, have their global properties calculated by the contribution of each individual layer. However, several simplifications are usually assumed to allow an easier implementation of the problem, for example, that the relative displacement between layers is null. Simplifications of this type allow to deal with the problem in a more similar way to homogeneous materials. As an example of this implementation, the study of Shen and Williams [67] may be highlighted. The authors used a perturbation technique to study the buckling and post-buckling behaviour of laminated stiffened plates in compression. Effect of stiffeners was considered "smeared out" and the classical laminated theory was employed with some refinements for better accounting of the effect of the stiffeners on the plate.

Zhang and Matthews [68] studied the behaviour of shallow cylindrical curved panels of layered composite materials under compression using the principle of virtual displacements. The results of their approach were compared with available data for flat plates but imperfections were not considered. Sheinman and Yeoshua [69] presented an analytical solution with a modified Galerkin's method to deal with the postbuckling of stiffened laminated curved panels. Positive and negative signs were considered for the curvature of the panels and comparisons with Finite Element analyses were provided. In a series of studies on laminated curved panels by Kasuya and Watamori [70], Watamori and Kasuya [71] and Kasuya *et al.* [72] the post-buckling behaviour of laminated perfect and imperfect unstiffened curved panels under uniaxial and biaxial compression was

assessed. The equivalent laminated properties were used and the behaviour under axial compression was assessed with the second variation of the potential energy.

Sandwich panels are generally composed by two thin layers of higher resistance separated by a thicker intermediate layer with lower stiffness and resistance [73]. In the case of sandwich panels, it is generally assumed that only the exterior layers contribute to the bending and twisting resistance. However, in this case, neglecting the transverse shear stiffness of the intermediate layer is not acceptable, contrary to the homogeneous cases. This led to the need to employ shear deformation theories (SDT). This theory is relevant for thick and composite structures where the effect of transverse shear deformation is non-negligible. So, contrarily to the classical theory based on the Kirchhoff's hypotheses (see section 3.2) one must resorts to the Reddy's theory [74] which is a high order shear deformation theory (HSDT). This theory, contrary to the first order shear deformation theory (FSDT), *e.g.* Mindlin [75], is able to account for null shear stresses at the faces of the panel obviating the use of a shear correction factor used on the FSDT.

The panels studied in this thesis are outside the scope of the SDT and, consequently, the relevance of this theory is reduced. However, an example of the application of this theory to curved panels is given by Chang and Librescu [76]. The authors studied the post-buckling of imperfect shear deformable doubly curved shallow panels under compressive and lateral pressure using a shear deformation theory (SDT). The Galerkin's method was used. However, the solution was restricted to a single degree of freedom (SDOF) with a half-wave in each direction and validation with the FEM was not performed. Shen [77] used a higher order shear deformation theory (HSDT) for the governing equations with a von Kármán-Donnell type of kinematic non-linearity for axially loaded shear-deformable laminated curved panels. In order to obtain the post-buckling solutions a perturbation technique was employed. Martins *et al.* [78] developed an energy formulation for cylindrically curved sandwich panels subjected to uniaxial compression using the Rayleigh-Ritz method and characterized the elastic critical stress behaviour.

Another relevant class of materials used in composites are Functionally Graded Materials (FGMs) which have changes in properties along its volume. For example, the properties may change along the thickness and each surface of the element exhibit different properties. Duc and Tung [79] investigated functionally graded imperfect curved panels

under axial compression using the Galerkin method. All edges were considered simply supported but in-plane restraints were not considered. Later, the same authors [80] extended the study to account for lateral pressure and temperature effects. The authors sought to introduce the effect of a FGM in a simplified way in the von Kármán-Donnell theory defining the modulus of elasticity varying along the thickness by a simple expression. The authors limited the study to a single global buckling deformation mode (with a half-wave in each direction) and despite all edges were considered simply supported, in-plane restraints were not considered again.

The methods reviewed in this section are of special relevance for laminated and composite materials, and not so much for homogeneous isotropic materials like steel structures, and consequently the applicability of most of these approaches is somewhat limited for the present thesis.

2.2.6 Ultimate load of curved panels

In section 2.2.1 the ultimate load for flat panels was already discussed. Some of the semi-analytical formulation presented in that section led to the development of specific software to predict the ultimate strength of stiffened flat plates. The work of Paik and his co-authors culminated in the development of the ALPS/ULSAP software, while the work of Byklum and his co-authors was implemented in the DNV/PULS software. At the same time, the use of nonlinear FEM has gained force and it is particularly advantageous, for example, in cases with complex geometries, loading conditions and localized analyses of structures. However, contrarily to flat plates, methodologies to predict the ultimate strength of curved panels based on semi-analytical were not found. The existing proposals found in the bibliography for the ultimate load of curved panels are based exclusively on FEM, which are presented in next paragraphs.

Featherson [81] assessed numerically the effect of imperfections in curved panels under combined compression and shear loads. Boundary conditions were modelled to match an experimental scenario and clamping was considered for some edges. The author employed the eigenmodes of Linear Buckling Analyses (LBAs) as initial imperfections. It was concluded that the initial pattern influences both the equilibrium paths and the ultimate load. Besides that, the first eigenmode did not lead in all cases to the lowest resistance.

Tran [14] developed expressions to assess the ultimate strength of unstiffened curved panels subjected to uniform axial compression based on an Ayrton-Perry methodology calibrated, exclusively based on numerical results. The panels with curvatures up to Z=100 were considered square and simply supported with the displacement along the loaded edges forced to be remain constant. The author verified, as expected, that for $Z \leq 1$ the curve from EN 1993-1-5 [1] fits accurately the numerical results. In a different range, for larger curvature parameters, $Z \geq 40$ and small values of normalized slenderness parameter ($\bar{\lambda} \leq 1.0$), the curve from EN 1993-1-6 [2] was the one which more accurately fitted numerical results. Finally, for large values of the normalized slenderness parameter ($\bar{\lambda} \geq 3.0$) the author concluded that numerical results could be adjusted to $1/\bar{\lambda}$ curve with a proportionality factor accounting for curvature. The author proposed equation (2.6) for the reduction factor ρ applied to the plastic resistance based on the design methodology of EN 1993-1-5 [1].

$$\rho = \begin{cases} 1 & \text{, for} \quad \bar{\lambda} \leq \bar{\lambda}_0 \\ \dfrac{2\beta}{\beta + \bar{\lambda} + \sqrt{\left(\beta + \bar{\lambda}\right)^2 - 4\beta\left[\bar{\lambda} - \alpha_Z\left(\bar{\lambda} - \bar{\lambda}_0\right)\right]}} & \text{, for} \quad \bar{\lambda} > \bar{\lambda}_0 \end{cases} \tag{2.6}$$

with

$$\bar{\lambda}_0 = 0.2 + 0.473\, e^{-\frac{Z}{20}} \tag{2.7}$$

$$\beta = \frac{1 + e^{-\frac{Z}{33}}}{2} \tag{2.8}$$

and α_Z is a parameter calibrated for different values of curvature. It should be noted that this methodology uses Stowell's formula (equation (2.3)) to calculate the elastic critical stress. This approach presents the shortcoming of being valid only for square curved panels.

In the same work, the author extended the study to curved stiffened panels proposing two equivalent approaches to calculate the reduction factor due to plate type buckling. The first is given by equation (2.6)-(2.8) now with Z replaced by Z_i which corresponds to the curvature of the curved subpanel (between stiffeners). The second is based on the formulation of EN 1993-1-6 [2]. The author claims that the accuracy of both approaches

is equivalent. The relative slenderness $\bar{\lambda}$ of the curved panel is calculated in function of the elastic critical stress by Stowell's equation in function of the global curvature (Z) of the panel. The authors assumed a fixed width and thickness of a=4.8 m and h=0.012 m, respectively. A total of 8 stiffeners regularly spaced by a distance of 0.6 m was considered.

The reduction factor for column type behaviour χ_C is obtained from EN 1993-1-1 [82] using the imperfection factor α=0.49. The corresponding equivalent column is composed by the gross cross-section of the panel (shell and stiffeners).

The final reduction factor for global buckling, ρ_C, relating the interaction of plate buckling and column buckling is obtained as follows:

$$\rho_c = \chi_c + (\rho - \chi_c)\frac{1}{0.95 + \frac{0.04}{\xi} + \frac{0.01}{\xi^2}} \tag{2.9}$$

with

$$\xi = \frac{\sigma_{cr,p}}{\sigma_{cr,c}} - 1 \tag{2.10}$$

where $\sigma_{cr,p}$ is the critical plate buckling stress and $\sigma_{cr,c}$ is the critical column buckling stress.

The author found that the influence of the geometric imperfections on the ultimate strength of curved stiffened panels is very important and verified the difficulty to identify the most critical mode of imperfection without an exhaustive analysis of all eigenmodes. Based on the observation that the global modes are dominant (despite admitting it is not always the one leading to the minimum value for the ultimate strength) the author used the first global pattern from eigenmodes for initial imperfections.

Later, Tran *et al.* [83], in sequence of the previous work, presented the same formulation for unstiffened curved with minor modifications for the parameters of equations (2.7) and (2.8):

$$\bar{\lambda}_0 = 0.2 + 0.473 \times 0.95^Z \tag{2.11}$$

$$\beta = \frac{1 + 0.97^Z}{2} \tag{2.12}$$

Tran *et al.* [84] studied a preliminary design formula to assess the ultimate strength of

unstiffened and stiffened cylindrical steel panels using the design of experiment method, consisting in the statistical calibration of the variables of the problem. The authors proposed a second-order polynomial function of the most relevant parameters of the problem. This formula, unlike the previous proposals, has the advantage of incorporating different values of aspect ratios. However, the parametric range is considerably limited for some variables. For example, the range of the aspect ratio ($0.67 \leq \alpha \leq 1.5$) and the inverse of the radius ($0 \leq 1/R \leq 0.1$) can be considered relatively narrow and this is valid only for high number of stiffeners ($5 \leq n_s \leq 20$). Furthermore, this approach is based purely on numerical calibration and follows a rather distinct concept of most design guidelines which hinders its application in conventional design.

Tran *et al.* [85] studied the behaviour of stiffened curved panels under longitudinal compression and proposed a conservative design methodology based on the column-like behaviour and on the adopted by EN 1993-1-1 [82]. The scope of this approach is considered to be up to aspect ratios of $\alpha=1.25$, once for larger values the method becomes considerably conservative. The authors studied numerically the geometrical parameters influencing the response of these elements. However, the parametric variation can be considered relatively narrow which may limit some conclusions. Moreover, these results were drawn based on numerical models with the same fixed geometry as the one used in Tran [14].

Martins *et al.* [86] studied the ultimate load resistance of unstiffened curved panels subjected to biaxial loading and in-plane bending relying exclusively on finite element analyses. The proposed formulation for short panels, $\alpha \leq 1.0$ can be summarised as follows:

$$\rho = \begin{cases} 1 & \text{, for} \quad \lambda \leq \lambda_{0,Z} \\ \dfrac{\lambda_{0,p} - \lambda + \rho_{0,Z}\left(\lambda - \lambda_{0,Z}\right)}{\lambda_{0,p} - \lambda_{0,Z}} & \text{, for} \quad \lambda_{0,Z} < \lambda < \lambda_{0,p} \\ \dfrac{\lambda - 0.055\alpha_Z\left(3+\psi\right)}{c_Z \lambda^2} + S_Z & \text{, for} \quad \lambda \geq \lambda_{0,p} \end{cases} \tag{2.13}$$

In Martins [15], a correction was proposed for long panels ($\alpha>1$). The reduction factor should be multiplied by a correction factor C_{long} as shown in (2.14). This correction is

calibrated in function of curvature, Z, assuming values of 1.0, 0.782 and 0.912 for Z=1, Z=30 and Z from 70 to 100, respectively (intermediate values are obtained by interpolation).

$$\rho_{long} = C_{long}\rho \tag{2.14}$$

Martins *et al.* [87] carried out a numerical parametric study on the imperfection sensitivity of unstiffened cylindrically curved panels. The authors assessed the influence of the shape of geometric imperfections, based on the first eigenmodes of the panels and the respective amplitudes, on the ultimate load. It was concluded that the first eigenmode does not lead always to the lowest value for the ultimate load. However, the authors did not study imperfections other than those given by the eigenmodes of linear buckling analysis, like, for example, perfect semi-waves. As will be concluded later, a semi-wave in each direction leads in some cases to ultimate loads much lower those given by eigenmodes.

Park *et al.* [88] performed numerical analyses to assess the ultimate strength of curved panels. The influence of the curvature on the resistance of the panels was studied. The authors drew attention to the existence of curvatures leading to lower resistances than the corresponding flat plates. Empirical formulae based on the numerical analyses were calibrated for the ultimate strength. The generic form of the expression is presented in (2.15). β is the slenderness and χ=(β-d). The remaining variables are written as a function of geometric parameters and calibrated constants.

$$\frac{\sigma_u}{\sigma_y} = \begin{cases} A\chi^2 + B\chi + 1 & \text{, for } d < \beta \\ A_1 e^{A_2\chi} & \text{, for } d \geq \beta \end{cases} \tag{2.15}$$

Later, the same authors [89] deepened the previous work for unstiffened and stiffened panels, again through FEM. The influence of the aspect ratio was assessed in more detail both for the critical stresses and the ultimate strength. It was found that for unstiffened panels, the critical stress increases with curvature and for aspect ratios larger than 1.0 the critical stress increases as the aspect ratio increases. The same is not true for the ultimate load, where a very intricate behaviour with ups and downs was verified with the increase in aspect ratio. The influence of the shape of stiffeners was assessed for stiffened panels. It was found that angle and T stiffeners are more effective than flat stiffeners increasing

the strength of the stiffened panels due to the buckling of the stiffeners.

Seo *et al.* [90] studied through the FEM the behaviour of stiffened curved panels under compression. The post-buckling behaviour and ultimate strength was analysed and the effect of parameters like curvature, slenderness and shape and dimensions of the stiffeners was investigated. The type of stiffeners was found to affect the collapse pattern, despite the influence on the resistance being less notorious. Flat stiffeners led generally to failure induced by stiffeners. An intricate behaviour of the system panel-stiffeners was verified. It was found that the increase in curvature did not lead always to an increase in strength. An empirical design formula for predicting the ultimate load of curved panels with T stiffeners was calibrated. Two distinct expressions were provided for central angles of the panels: $\theta \leq 5^{o}$ and $\theta > 5^{o}$, where it was found that the ultimate load could be better represented if two domains were considered, see equation (2.16). For application of this formula, the calculation of the elastic buckling strength of the curved panel and of the corresponding flat plate are required for the calculation of the slenderness parameter, β'. However, despite providing numerically calibrated expressions for the elastic buckling strength of the curved panels, the authors did not provide expressions for the corresponding flat plate.

$$\frac{\sigma_u}{\sigma_{Yeq}} = \begin{cases} \dfrac{1}{\sqrt{0.0683 + 0.994\beta' + 0.0065\beta'^2}} & \text{, for } \theta \leq 5^{o} \\ \dfrac{1}{\sqrt{1.1339 - 0.1291\beta' + 0.0392\beta'^2}} & \text{, for } \theta > 5^{o} \end{cases} \tag{2.16}$$

Regarding experimental tests, many references may be found in literature since 1930's especially related with the advent of aviation. Consequently, many of them were performed on materials other than mild steel usually used in the construction sector. Some relevant references deserving be mentioned are given next as example. By topic: *i)* axial compression of unstiffened panels: Ljubinkovic *et al.* [91] compared the experimental behaviour of two unstiffened curved panels under compression with FEA and a Digital Image Correlation (DIC) system. Good agreement was obtained between experimental and DIC. The initial imperfections considered on numerical models were found to influence significantly the comparison with the experimental results; *ii)* axial compression of stiffened panels*:* Cho *et al.* [92] performed experimental tests on a series

of curved stiffened panels and comparisons with FEA were given. The authors compared the differences obtained with flat elements and concluded that the effect of curvature cannot be neglected; *iii)* circumferential compression: Guo *et al.* [93] the authors compared the resistance of two curved panels under circumferential compression. Through numerical analyses the authors extended the range of curvatures of the experimental specimens and found a linear reduction of the ultimate strength with curvature; out-of-plane pressure: Yang and Guralnick [94] carried out experimental investigations on curved panels under out-of-plane pressure. Comparisons of the buckling loads with analytical predictions based on the linear theory were done.

An extensive list of experimental research carried out about curved panels may be found in Christian [95] and in a recent review paper by Martins [6]. The latter includes also references on numerical studies also for circumferential compression and shear loads.

From the previous literature review it was found that the existing expressions to predict the ultimate load of curved panels cover only partially the presented parametric variation in this study. Additionally, all the proposed formulae are based only on calibrated numerical results and robust provisions with mechanical meaning to predict the ultimate strength of curved stiffened panels are inexistent. The objective of this work is to fill this gap covering simultaneously a broad range of aspects like the geometry, boundary conditions, imperfections and load situations.

Further details about the methodologies to predict the ultimate strength in semi-analytical methods will be given in section 8.3.3, when they will be applied in the current formulation.

2.3 Applicable standards

Nowadays, even when the FEM is in vogue, the advantages of simplified design formulae are unquestionable. They give to the engineers the possibility to know easily the resistance of an element, obviating the implementation of complex and time-consuming FEA.

Construction standards, like the Eurocode 3, lack provisions for curved panels. These elements fall clearly outside the scope of EN 1993-1-5 [1], which is devoted to flat plates (and panels with very low curvatures, $Z<1.0$), and EN 1993-1-6 [2], which deals with

shells of revolution. Consequently, none of the two standards is able to provide adequate provisions for the panels in study.

On the other hand, recent offshore standards already provide simplified design formulae for curved panels. In this case standards like DNVGL-RP-C202 – Buckling strength of shells [3], DNVGL-CG-0128 - Buckling [4] and ABS – Guide for buckling and Ultimate strength Assessment for Offshore Structures [5] are identified. However, besides applied only to specific conditions their validity has been called in question (*e.g.* Martins *et al.* [6]).

DNVGL-RP-C202 [3] provides formulae to calculate the critical stresses for axial, circumferential and shear loading of unstiffened curved panels considered between stiffeners of a cylindrical shell. The critical stress is calculated through equation (2.1) with the buckling coefficient, k_σ, for axial in-plane stresses given by:

$$k_\sigma = 4\sqrt{1+\left(\frac{0.5\left(1+\frac{R}{150\,h}\right)^{-0.5}\,0.702\,Z_{Batdorf}}{4}\right)^2} \tag{2.17}$$

with $Z_{Batdorf}$ given by equation (2.5).

Similar formulae are provided for circumferential compression and shear stresses. These critical stresses are then used to calculate the corresponding slenderness which is introduced in the following expression to calculate the normalized strength, χ:

$$\chi = \frac{1}{\sqrt{1+\lambda^4}} \tag{2.18}$$

where, λ, is the slenderness calculated based on the critical stress. If other loads exist the buckling coefficient for those loads should be calculated and introduced in λ which is formulated to account for other loads.

DNVGL-CG-0128 [4] makes use of an interaction formula to deal with curved panels with $R/h \leq 2500$ (*i.e.* $Z \geq (a/h)^2/2500$) under in-plane longitudinal loading stresses, in-plane circumferential loading, out-of-plane loading and shear stresses. For each case buckling coefficients are proposed. For axial compression the buckling coefficient, k_σ, is

given by:

$$k_\sigma = \begin{cases} 1+\dfrac{2}{3}\dfrac{b^3}{Rh} & \text{, for} \quad \dfrac{b}{R} \le 0.5\sqrt{\dfrac{R}{h}} \\ 0.267\dfrac{b^3}{Rh}\left(3-\dfrac{b}{R}\sqrt{\dfrac{h}{R}}\right) \ge 0.4\dfrac{b^2}{Rh} & \text{, for} \quad \dfrac{b}{R} > 0.5\sqrt{\dfrac{R}{h}} \end{cases} \tag{2.19}$$

The accuracy of DNVGL-RP-C202 and DNVGL-CG-0128 was assessed with numerical results by Martins *et al.* [6] for curvatures up to Z=100 and different aspect ratios, α=1.0, 1.5 and 3.0 for the buckling coefficient and ultimate strength. The authors verified that: *i)* for the buckling coefficients, DNVGL-RP-C202 provides more accurate results than DNVGL-CG-0128. In fact, the latter fails to give valid results in most cases providing estimates for the buckling coefficient much larger than the numerical results; *ii)* both standards are unable to provide, for all cases, safe estimates for the ultimate load, especially for larger curvatures. Additionally, in the cases were safe values are given they may be too conservative, even for small curvatures.

ABS [5] provides specifications to assess the local buckling of curved panels composing cylindrical shells between stiffeners. The standard refers the limit for cylindrical shells of diameter to thickness up to 1000, meaning a limit for the curved panels composing the shells of $R/h \le 500$, *i.e.* $Z \ge (a/h)^2/500$. The buckling coefficient, k_σ for a curved panel under axial compression is calculated by:

$$k_\sigma = \begin{cases} 4+\dfrac{3Z_{Batdorf}^{\ 2}}{\pi^4} & \text{, for} \quad Z_{Batdorf} \le 11.4 \\ k_\sigma = 0.702\, Z_{Batdorf} & \text{, for} \quad Z_{Batdorf} > 11.4 \end{cases} \tag{2.20}$$

The corresponding critical stress calculated by equation (2.1) is then reduced by the application of knock-down factors to account, for example, for imperfections and then applied on an interaction formula.

2.4 SUMMARY

In this chapter, a state-of-the-art on curved panels for structural applications was presented. The most important studies regarding flat plates and cylindrical shells were highlighted. Despite presenting characteristics that differentiate these elements from

curved panels in study, some of the advances are useful for application in the present thesis.

Despite larger attention being, historically, given to flat plates and cylindrical shells, there has been, recently, a growing interest in curved panels due to the appearance of new applications in several engineering fields. In fact, the studies about some aspects of curved panels, *e.g.* regarding semi-analytical methods, are rather scarce as identified in this chapter. The objective of this thesis is to fill the main gaps identified in the state-of-the-art.

Some historical references on the critical behaviour of curved panels were presented and recent development about the topic were identified. Regarding the large deflection behaviour of curved panels, the studies found on unstiffened and stiffened curved panels under compression and out-of-plane pressure were described with main focus on semi-analytical methods. Very few contributions about the large deflection of curved panels were identified in the literature.

A distinct class of studies were identified in respect to composite materials namely laminated, sandwich and FG materials. This type of materials is mainly used in the aeronautics industry, which has been employing these materials in curved panels for quite some time. However, as shown these materials have particularities that require usually different theories, like the SDT, which hinders the applicability to the current study.

Construction standards, like Eurocode 3, do not provide design guidelines for curved panels maybe due to the only recent application of these panels in civil engineering. On the contrary, offshore standards, due to the older use of these panels already provide simplified formulae for curved panels. However, these empirical expressions show a poor accuracy and in some cases, as documented in the literature, they were proved to provide unsafe estimates for the resistance. Consequently, an urgent need for more robust standards was identified in this chapter, and, in this regard, the objective of this thesis is to deepen the work of curved panels based on numerical and, mainly, on semi-analytical methods. With this it is expected to contribute to the development of design provisions with more mechanical meaning.

To the best of the author's knowledge, the approach of the problem as presented in this thesis is not available in the literature.

3 Fundamentals of curved panels

3.1 Introduction

Some important concepts indispensable to understand the approach followed in this thesis are described in this chapter.

In section 3.2 the concepts and assumptions underlying the various shell theories are presented and the implications are discussed. Special attention is given to Donnell's work and the corresponding DMV theory, which is of particular interest in this study. Comments are made about the interaction between the membrane and the bending components. The accuracy and the limits of validity of the theory are discussed and verified for the curvatures studied in this thesis.

The following sections (3.3 to 3.6) are devoted to describe aspects like the geometry, boundary and loading conditions. These aspects are found to play an important role on the behaviour of the panels and, consequently, they will be object of study in the

following stages of the thesis.

Finally, in section 3.7, the existing analytical and numerical methods of analysis of shells are described, with special emphasis for the Rayleigh-Ritz and Finite Element Method, respectively, which will be extensively used in the following chapters.

3.2 SHELL THEORIES

3.2.1 Development of shell theories

The number of different theories in the study of shells is high. Several considerations have been assumed and specialised theories have been developed for diverse cases. The differences between most of these theories are related with the level of simplification introduced.

Kirchhoff [96] introduced some important assumptions to the analysis of plates and Love [97] later applied them to curved shells, which are commonly known as the Kirchhoff-Love assumptions [98]:

i) Hypothesis of straight normals: a straight line normal to the middle surface before deformation continues straight and normal after deformation and having the same length, *i.e.* the cross-section remains plane and normal to the middle surface after deformation;

ii) Stresses normal to the middle surface (σ_z) may be neglected in comparison with the ones acting in the direction of the surface.

Love [97], based on these assumptions and simplified constitutive relations, developed the linear theory of shells, which is only applicable to very small deformations. Subsequent authors, like Reissner, Sanders and Flügge sought to solve some inconsistencies found in the original Love's theory [99]. In particular, Flügge [100], through less restrictive simplifications, developed one of the most general theories that is usually used to assess more simplified formulations.

The accurate treatment of shells becomes, at some point, very complex (*e.g.* Flügge's theory [100]) and simplifications must be introduced to allow the viable treatment of a given problem.

Donnell [101[97] started the study of the buckling of cylindrical shells. His theory makes use of some approximations, namely the consideration of the shells as shallow. Shallow shells assumptions are established based on the fact that the rise of the arc meets certain limits in comparison with the dimensions of the shell, and may be stipulated as [98]:

i) In-plane displacements, u and v, are smaller in comparison with the out-of-plane displacement, w, which is of the same order as the thickness, h;

ii) The squares and products of the derivatives of w are considered as the same order of strains. The derivatives are considered small;

iii) Curvature changes may be represented by a linear function of w. The contributions of u and v may be neglected. The curvatures of the bending component may be regarded as the ones from shallow shells, equations (3.11)-(3.13).

In the linear theory, rotations are not considered for the strains and in the equilibrium equations. However, for many shell problems, the linear theory is not sufficient and large deflection shell theory is required to accurately deal with the observed behaviour. Besides the nonlinearity in the strain-displacement relations, when a shell undergoes large deflections its deformed shape has to be considered. Consequently, the consideration of the non-deformed configuration of the shell in the equilibrium equations has to be abandoned and the deformed configuration has to be taken into account.

Marguerre [19] developed a nonlinear theory for plates. von Kármán and Tsien [102] extended the Donnell's theory for nonlinear large deflection behaviour. Mushtari [103] and Vlassov [104] generalised the original theory of Donnell (based on the same assumptions) for arbitrary curvature and nonlinear behaviour. The Donnell-Mushtari-Vlassov (DMV) theory, as it is known, is a simplified theory based on the general theory of thin shells, especially applicable to shallow shells. It considers the Kirchhoff-Love and the shallow shells assumptions, plus some additional assumptions [99][105]:

i) The geometry of the shell is cylindrical or almost cylindrical;

ii) The interaction between the membrane and bending surfaces of Figure 3.1 is done at the expense of the normal force p_B, *i.e.* the tangential forces q_{xB} and q_{yB} may be neglected;

iii) There is no tangential surface traction on the shell (allowing the use of the Airy

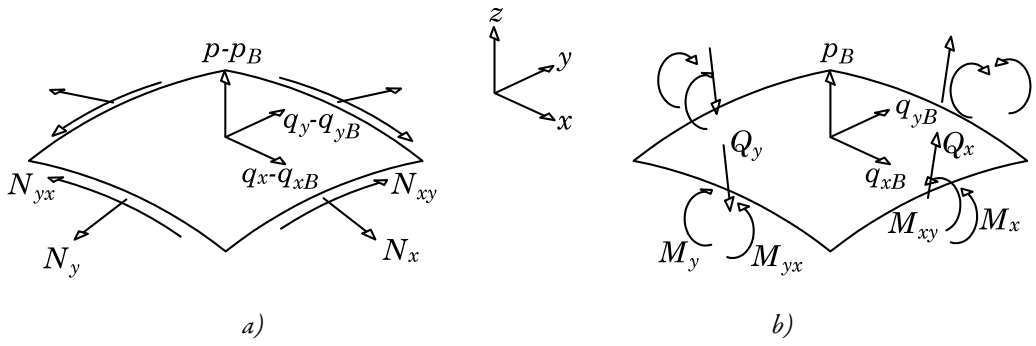

Figure 3.1: Stress resultants on a thin shell: *a)* stretching and *b)* bending components (adapted from Calladine [105])

stress function);

These assumptions are particularly valid for: *i)* shallow shells and *ii)* non-shallow shells with stresses varying rapidly along the shell [99].

Further developments were introduced by Sanders [106] using tensor form and Koiter [107] which developed the study of nonlinear general thin shell theories.

In nonlinear theory the limitation to small displacements is not required and rotations $\partial w/\partial x$, $\partial w/\partial y$ are not neglected. Contrarily to linear theory, in nonlinear theory more than one equilibrium configuration (stable and unstable) exists in the same conditions.

Lamé's [108] work on curvilinear coordinates led to the development of the Lamé's coefficients which are useful to deal with the geometry of shells. The Lamé's coefficients provide a convenient way to deal with the transformation from a cartesian coordinate system to a curvilinear coordinate system and vice-versa. They are recurrently used to define shells theories in their more general forms.

Imperfections were found to be responsible for the differences between theoretical and experimental loads verified at the beginning of the study of shell buckling. Because it has been shown that imperfections can affect considerably the resistance of shells, their study is still nowadays an area of intense research. The usual approach, as proposed by Koiter [62], is to apply an equivalent initial geometric imperfection. These equivalent imperfections should account for the remaining imperfections, like residual stresses, for example. This approach has advantages in terms of ease of application, because it obviates the introduction of the "real" geometric imperfection and residual stresses explicitly. In

FEM, eigenmodes from linear buckling analyses (LBAs) are usually used for the sake of convenience. However, this approach shows limitations when a more detailed modelling of imperfections is required, as happens in stiffened panels. A solution for this will be presented later.

Both geometric nonlinearity and imperfections aspects will be introduced in the semi-analytical formulation and they will be discussed in further detail in Chapter 4.

Contrarily to the classical theory based on the Kirchhoff's hypotheses, the shear deformation theory (SDT) was developed to include the effect of transverse shear deformation, which, as previously identified in section 2.2.5, is indispensable to study laminated and composite materials. This group of theories is subdivided in first order shear deformation theory (FSDT) and higher order shear deformation theories (HSDT). The latter, developed by Reddy [74], corrects some gaps and extends the application of the FSDT. Consequently, it is the more accurate theory to tackle problems with these materials. Despite the fact that extensive work has been carried out in light of SDT for more innovative materials, the relevance for thin steel panels is reduced and consequently is not followed here.

When nonlinearity is of geometric origin the problem is said to be geometric nonlinear. In cases when the material also contributes to the nonlinearity, the problem is said to be geometrically and material nonlinear. Despite not being impossible to account for material nonlinearities analytically, this turns out to be a very difficult task from the mathematical point of view. Consequently, the problem is tackled analytically with simplified methods or with numerical methods, like the finite element method.

3.2.2 Shallow shells

For cases with constant thickness, h, the geometry of a thin shell may be represented by its middle surface. A shell may be classified according the type of curvature (*e.g.* cylindrical, ellipsoidal, spherical, etc.) which leads to specific behaviour in each case [99].

In a simplified way, according to Novozhilov [109], a shell may be considered, in a simplified way, as thin if the following condition is verified for the thickness, h, to radius, R, ratio, h/R:

$$\frac{h}{R} \leq \frac{1}{20} \tag{3.1}$$

Most shells in practice meet this criterion.

For exemplification, using this condition and considering that h/R may be written as a function of the curvature parameter, $Z=a^2/(Rh)$ - considering the curvature along the width of the panel, a,- and the width to thickness ratio, a/h, by equation (3.2), the maximum values of Z to fulfil the classification of a shell as thin are calculated for different values of a/h in Table 3.1. The values of the ratio a/h cover very stocky to very slender panels. Despite the lowest value presented for a/h being used in very rare occasions in practice, it is useful to conclude that even for that case curvatures of 31.25 allow to cover many cases of curvatures in real structures. For the remaining cases of a/h, the limiting curvatures to fulfil the thin shell criterion reach high values which cover almost all cases in practice.

$$\frac{h}{R} = Z\left(\frac{1}{a/h}\right)^2 \tag{3.2}$$

In problems with thin shells there are situations where membrane action is the main responsible for carrying the load, and the bending action may be neglected. In these situations, shells may be characterised by the membrane hypothesis with sufficient accuracy (*e.g.* a closed cylindrical shell under uniform pressure). In other cases, bending contributes significantly, carrying the load and the contribution of the interaction between membrane and bending components should the accounted for to characterize properly the behaviour of the shell. This relative contribution depends on the geometry of the shell.

To better understand the influence of each component on the behaviour of a shell and to assess the contributions resisting the loads applied to a shell, Calladine [105] developed

Table 3.1: Maximum values of the parameter of curvature, Z, according the condition of Novozhilov [109] for classification of a shell as thin

a/h	25	50	100	200	300
Z_{max}	31.25	125	500	2000	4500

the concept of two surfaces in the shell, one rendering the effect of stretching (*i.e.* membrane) and the other the bending of the shell. The effect of each component may be accounted for separately, provided that proper interaction forces are taken into account. The author decomposed the stress components for the stretching and bending components[1], as shown in Figure 3.1 *a)* and *b)*, respectively. In order to account for the interaction between the surfaces, the author considered that a part of the out-of-plane force per unit area p, is carried by the bending surface, p_B, and the remaining part p-p_B is carried by the stretching surface. The same happens for the tangential forces q_{xB} and q_{yB}, which arise from the unbalanced forces Q due to curvature of the element. However, using the approximation established in the shallow shell theory the tangential interaction forces may be neglected.

Thin shells that satisfy the conditions in equations (3.3)-(3.4) may be considered as shallow shells, according to Novozhilov [109]:

$$\left(\frac{\partial z}{\partial x}\right)^2 < \frac{1}{20} \tag{3.3}$$

$$\left(\frac{\partial z}{\partial y}\right)^2 < \frac{1}{20} \tag{3.4}$$

These conditions lead to a maximum admissible angle of $\tan^{-1}(\sqrt{(1/20)})=12.6^{o}$. They arise from the simplification of considering the surface of a shell with curvilinear coordinates α and β, represented by the projection of the coordinate system Oxy, according to Figure 3.2. In the figure, ds_1 and ds_2 are the sides of an element defined on the shell's middle surface and the corresponding rectangle formed by its projection on the plane Oxy has sides dx and dy. The radii of curvature are represented by R_1 and R_2, respectively, for coordinates α and β.

If the arc lengths d_{s1} and d_{s2} are defined by the change in the coordinate line d_α and d_β, as follows:

$$\mathrm{d}s_1 = A\mathrm{d}\alpha \tag{3.5}$$

[1] For convenience, the stretching and bending components are, here exceptionally, written by their resultants on the respective infinitesimal face, *i.e.* they have, respectively, dimensions of force/length and bending/length.

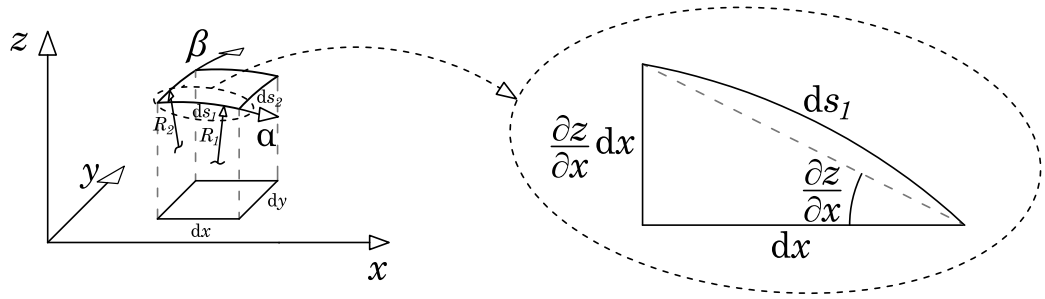

Figure 3.2: Correspondence between the curvilinear coordinate system and the projection coordinate system *Oxy* (adapted from Ventsel and Kauthammer [99])

$$ds_2 = B d\beta \tag{3.6}$$

A and *B* are called the Lamé's coefficients which depend on the chosen coordinate system.

According to Figure 3.2, the value of sides ds_1 and ds_2 are approximately given by the hypotenuse of the triangle formed with the projection plane *Oxy*:

$$ds_1 = \sqrt{1+\left(\frac{\partial z}{\partial x}\right)^2}\,dx \tag{3.7}$$

$$ds_2 = \sqrt{1+\left(\frac{\partial z}{\partial y}\right)^2}\,dy \tag{3.8}$$

However, if the angle is relatively small as defined in equations (3.3)-(3.4), and the shell may be considered a shallow shell, one may assume the following simplification:

$$ds_1 \approx dx \tag{3.9}$$

$$ds_2 \approx dy \tag{3.10}$$

and considering the system *x, y* as orthogonal, one can assume the Lamé parameters as *A*=*B*=1. Consequently, the curvatures for a shallow shell may be written as follows:

$$\kappa_1 = \frac{1}{R_1} \approx \frac{\partial^2 z}{\partial x^2} \tag{3.11}$$

$$\kappa_2 = \frac{1}{R_2} \approx \frac{\partial^2 z}{\partial y^2} \tag{3.12}$$

$$\kappa_{12} \approx \frac{\partial^2 z}{\partial x \partial y} \tag{3.13}$$

Through kinematics and using the simplification in equations (3.11)-(3.13) with the displacement w in the coordinate z, taking into account that the sign of the second derivative $\partial^2 w/\partial x^2$ is negative (and similarly for the y direction), *i.e.* convex side point in the direction of the z axis, one may write:

$$\kappa_1 = -\frac{\partial^2 w}{\partial x^2} \tag{3.14}$$

$$\kappa_2 = -\frac{\partial^2 w}{\partial y^2} \tag{3.15}$$

$$\kappa_{12} = -\frac{\partial^2 w}{\partial x \partial y} \tag{3.16}$$

Introducing Hooke's law leads to the classical equation for an isotropic plate. In fact, this surface is equivalent to a nearly flat plate in bending and shear [105].

$$D\nabla^4 w = p_B \tag{3.17}$$

where $D=Eh^3/(12(1-\upsilon^2))$ is the flexural stiffness and ∇^4 is the biharmonic operator.

3.2.3 Membrane and bending components

To better understand the interaction between membrane and bending action, Calladine [105] proposed to analyse a long cylindrical shell under doubly-sinusoidal pressure. In this case we can obtain a series of connected panels, of width, a, and length, b, with null out-of-plane displacements along their edges. In this way, a doubly sinusoidal displacement field may be considered for both the membrane and bending components. Additionally, this theoretical case avoids conveniently the explicit consideration of the boundary conditions allowing to draw more easily important conclusions.

Assuming a sinusoidal function both for the pressure load, p_B, and for displacements, w, with maximum amplitudes, p_{nB} and b_{nB}, respectively, in equation (3.17) a value of b_{nB} is found to be:

$$b_{nB} = \frac{p_{nB}}{\pi^4 D} \frac{a^4 b^4}{\left(a^2 + b^2\right)^2} \tag{3.18}$$

Similarly applying again a sinusoidal pressure with a maximum amplitude p_{nS} ($=p_n$-p_{nB}) in equations of equilibrium and Hooke's law and solving for w, the maximum amplitude for the displacement b_{nS} is:

$$b_{nS} = \frac{p_{nS}}{Eh} \frac{R^2}{a^4} \left(a^2 + b^2\right)^2 \tag{3.19}$$

Making equal b_{nB} and b_{nS} from equations (3.18) and (3.19) and solving for $\xi=p_{nS}/p_{nB}$, the ratio between the membrane and bending stiffness components, one obtains the ratio between stretching and bending stiffnesses of the shell:

$$\xi = \frac{12 a^8 b^4}{\pi^4 R^2 h^2 \left(a^2 + b^2\right)^2} \tag{3.20}$$

Based on this equation, one can plot the graph of Figure 3.3 for several values of ξ. Assuming, according to Calladine [105], that a shell is dominated by membrane when ξ>10 and contrarily a shells is dominated by bending when ξ<0.1, two different zones may be defined as shown in the graph. At the zone between both limits, interaction between membrane and bending has to be considered, and neglecting one or other component is not realistic. The value of ξ=1.0 is also plotted for comparative purposes.

The graph is plotted for $b/\sqrt{(Rh)}$, in function of the parameter of curvature of the subpanels, Z. Along with the curves of ξ, curves representing different aspect ratios of the subpanels, $\alpha=b/a$ are also presented. In this case, values of 0.5, 1.0 and 2.0 are presented.

According with the same figure it is verified that as the aspect ratio, α, increases, a smaller change on b is required to pass from bending to membrane zone, or vice-versa. Consequently, for large aspect ratios (α>2) the resistance from the bending component comes mainly from the bending action on the smaller direction, the width, a. For short aspect ratios (α<0.5) the contours are practically constant, *i.e.* the change in width, a, has no influence on the curve and consequently the influence in this zone of the graph comes mainly from the change on the length, b. In the case of the membrane action for short panels it is possible to conclude that the practically constant values are mainly due to the

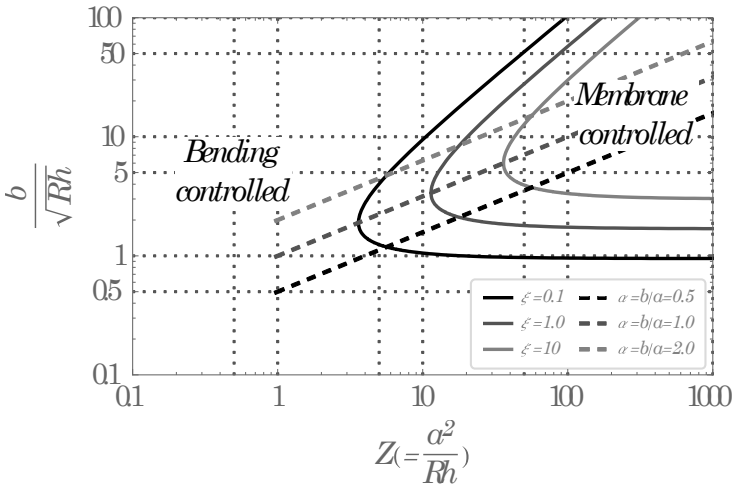

Figure 3.3: Membrane and bending contributions of a cylindrical shell subjected to sinusoidal loading applied on curved subpanels with width, *a*, length, *b*, radius, *R* and thickness, *h*.

stretching in the circumferential direction. For short panels ($\alpha \leq 0.5$), ξ is relatively independent of the value of Z. In fact, its value is practically constant whatever it is the value of Z. In this case, maintaining all the variables the shell passes from bending to membrane controlled if the length, b, is increased.

3.2.4 Derivation of the Donnell's equations

The approach of separating the shell in membrane and bending surfaces proves to be convenient also to derive the Donnell's equations for cylindrical shells, imposing that the change of the Gaussian curvature is the same in both surfaces.

Along with the equation for the bending component in equation (3.17), doing the equilibrium for the membrane component (Figure 3.1 *a)*) and introducing the Airy's stress function, F, leads to[2]:

$$\frac{1}{R_2}\frac{\partial^2 F}{\partial x^2}+\frac{1}{R_1}\frac{\partial^2 F}{\partial y^2}=p-p_B \tag{3.21}$$

Putting together (3.17) and (3.21) one obtains the Donnell's *equilibrium equation* as

[2] The Airy's stress function means that $N_x=\partial^2 F/\partial y^2$ and $N_y=\partial^2 F/\partial x^2$.

follows:

$$D\nabla^4 w + \left(\frac{1}{R_2}\frac{\partial^2 F}{\partial x^2} + \frac{1}{R_1}\frac{\partial^2 F}{\partial y^2} \right) = p \tag{3.22}$$

According to the approach of Calladine, to obtain the Donnell's compatibility equation one must make use of the change in Gaussian curvature, g, to make compatible the membrane and bending surfaces [105].

$$g = \frac{\kappa_1}{R_2} + \frac{\kappa_2}{R_1} \tag{3.23}$$

Based on equation (3.23) and making use of the curvatures in equations (3.14)-(3.16) one may write the change in Gaussian curvature for the bending surface, g_B, as:

$$-\frac{1}{R_2}\frac{\partial^2 w}{\partial x^2} - \frac{1}{R_1}\frac{\partial^2 w}{\partial y^2} = p \tag{3.24}$$

Analogously, to derive the change in Gaussian curvature for the stretching surface, g_S, equation (3.23), the Hooke's law and Airy's function must be used leading to:

$$g_S = -\frac{1}{Eh}\nabla^4 F \tag{3.25}$$

Since the Calladine's approach [105] stipulates that the change in Gaussian curvature must be equal in both surfaces, we obtain the *compatibility equation* of the problem:

$$\left(-\frac{1}{R_2}\frac{\partial^2 w}{\partial x^2} - \frac{1}{R_1}\frac{\partial^2 w}{\partial y^2} \right) + \frac{1}{Eh}\nabla^4 F = 0 \tag{3.26}$$

Equations (3.22) and (3.26) constitute the Donnell's equations, also known as the DMV equations for small displacement behaviour and free of imperfections. They are nonlinear fourth order differential equations coupled in w and F. Further developments to account for the effect of nonlinearity and imperfections will be introduced in Chapter 4.

The accuracy of the existing shell theories, namely the one from Donnell, is related with the different level of simplifications introduced, *i.e.* with the terms neglected in the most general expressions. The objective of these theories is to neglect terms that may facilitate dealing with the problem but, at the same time, the associated error should be controlled within limits considered tolerable. Obviously, simplifications considered valid for certain type of problems may not be to other cases, and consequently the implications introduced

with certain simplifications should be understood.

3.2.5 Accuracy of the Donnell's equations

Despite the simplifications of shallow shells, introduced in equations (3.11)-(3.13), they are accurate enough for a very large cases of thin shells in practice, and particularly the panels studied in this thesis. This simplification may be eliminated if more complete expressions are used for the curvatures. If the simplifications of shallow shells were not considered, the exact equations for the curvatures would be:

$$\kappa_1 = -\frac{\partial^2 w}{\partial x^2} - \frac{w}{R_1^{\,2}} \tag{3.27}$$

$$\kappa_2 = -\frac{\partial^2 w}{\partial y^2} - \frac{w}{R_2^{\,2}} \tag{3.28}$$

$$\kappa_{12} = -\frac{\partial^2 w}{\partial x \partial y} + \frac{1}{R_2}\frac{\partial v}{\partial x} + \frac{1}{R_1}\frac{\partial u}{\partial y} \tag{3.29}$$

i.e. the simplification in (3.11)-(3.13) occurs on the assumption that the radii, R_1 and R_2, are sufficiently large to assume that the respective terms where R appears in the denominator can be neglected.

Hoff [110] and Kempner [111] assessed the accuracy of Donnell's equations compared with the more general Flügge's theory. The first author, comparing the characteristic roots of Donnell's equation, provided a range of parameters where both theories are comparable and where discrepancies become important. It was found that the error of the Donnell's equations increases as the circumferential wavelength increases, *i.e.* when the length is much greater than the radius.

With the objective of maintaining the same simplicity of the Donnell's equations, Morley [112] modified the original equations with an additional term accounting for the radius of cylindrical shells on the bending curvatures. In this way, equation (3.17) becomes affected by the radius as follows:

$$D\left(\nabla^2 + \frac{1}{R_2^{\,2}}\right)^2 w = p_B \tag{3.30}$$

Morley compared the roots of this equation with the ones of Donnell and the more

general theory of Flügge, which is usually used as reference for comparison purposes. The author showed that some differences may appear for long shells in Donnell's theory when the number of circumferential waves is reduced. However, according the author, the proposed improvement is able to provide closer results with the ones from Flügge, even for long shells with a reduced number of circumferential waves, where the Donnell's theory fails.

Houghton and Johns [113] compared the characteristic roots from several theories, including the one from Donnell and less approximate theories. The authors concluded than when the number of circumferential waves, m, is less than 4, non-negligible errors may arise for long cylinders. In these cases, the magnitude of in-plane displacements is of the same order than the out-of-plane displacements and Donnell's theory starts to provide non-negligible errors. However, the authors highlight application advantages in using the Donnell's equations in comparison with more less approximate theories. Yamaki [98] reached the same conclusion about the accuracy of Donnell's equations.

In order to assess the error of the Donnell's assumption the previous example of a cylindrical shell under a sinusoidal pressure is used next [105]. Following a similar procedure to obtain the maximum displacement by the equation of Morley, $b_{nB,M}$, instead of equation (3.18) the following expression is obtained:

$$b_{nB,M} = \frac{p_{nB,M}}{\pi^4 D} \frac{a^4 b^4 m^4}{\left(a^2 m^2 + b^2\left(-1+m^2\right)\right)^2} \tag{3.31}$$

where $m=\pi R/a$ is the integer number of circumferential waves, if a corresponds to half wavelength.

Rewriting the previous equation in a more convenient form, in terms of $p_{nB,M}$, one obtains the following relation between the amplitude of the pressure and the amplitude of the displacement:

$$p_{nB,M} = b_{nB,M}\pi^4 D\left(\frac{1}{b^2} + \frac{1-\frac{1}{m^2}}{a^2}\right)^2 \tag{3.32}$$

where taking $m\to\infty$ leads to the original Donnell's solution. Consequently, the differences

between both theories increase as m decreases.

The magnitude of this error was assessed by Calladine [105]. He found that the influence of the correction introduced in the circumferential bending is negligible when: *i)* the behaviour is controlled by bending in the longitudinal direction and stretching in the circumferential direction; *ii)* when the stretching effects are negligible. The correction has only relevance for cases dominated by stretching in the longitudinal direction and bending in the circumferential direction. In this case the error is non-negligible and the previous correction should be applied when $m<4.5$ (calculated for a difference of 10%), or more conveniently:

$$Z > 0.49\frac{R}{h} \tag{3.33}$$

Calculating the ratio R/h for different values of curvatures and assuming different a/h ratios one obtains the limiting values for curvature, Z, in Table 3.2 for which inequality (3.33) is verified. These values show that for the values of Z and a/h considered in the analytical study of this work there is no need for the correction for long shells in Donnell's equation. Even, for uncommonly small values of $a/h=50$, it is necessary to account for the correction, only if $Z>35$. For a typical value of $a/h=100$ the correction should be applied only for $Z>70$.

Table 3.2: Values of Z for various a/h ratios from which correction must be considered

a/h	50	75	100	125	150	175	200
$Z>$	35	52.5	70	87.5	105	122.5	140

A more in-depth analysis of the analytical approach employed in this work will be presented posteriorly for the specific boundary and loading conditions. The nonlinear behaviour of the panels with imperfections included will be studied in detail and the influence of every parameter will be properly analysed.

3.3 GEOMETRY OF THE CURVED PANELS

3.3.1 Unstiffened panels

Given a thin unstiffened cylindrical curved panel with uniform thickness (h), radius (R), width (a) and length (b), one can define the non-dimensional curvature parameter, Z, as:

$$Z = \frac{a^2}{R\,h} \tag{3.34}$$

and the aspect ratio, α, as:

$$\alpha = \frac{b}{a} \tag{3.35}$$

The y axis is considered parallel to the generator of the cylindrical panel and the x axis is perpendicular. The z axis is orthogonal and radially inward. The origin of the coordinate system is at the centre of the surface. The components of the displacements in each axis are respectively u, v and w for x, y and z (see Figure 3.4).

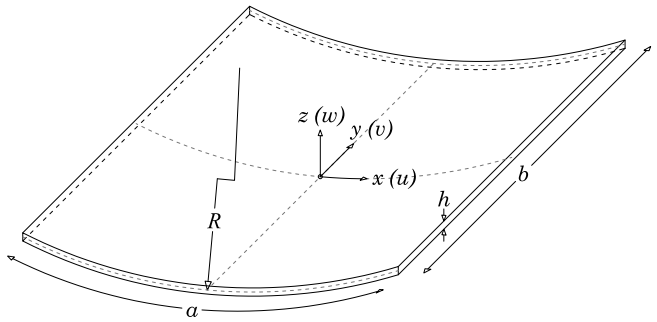

Figure 3.4: Geometry and coordinate system of a curved panel

3.3.2 Stiffened panels

In addition to the geometric variables defined for unstiffened panels, a thin asymmetrical stiffened cylindrical curved panel may have the geometry of its flat eccentric stiffeners represented by the thickness (h_s) and depth (d_s) (see Figure 3.5). Assuming that the panel is composed by n_s number of stiffeners, the width of the n_s+1 sub-panels is represented by a_s. The distance from the middle surface of the panel to the neutral axis (*N.A.)* of the stiffener with the associated part of the panel with width a_s is z_0 (see Figure 3.5 c)).

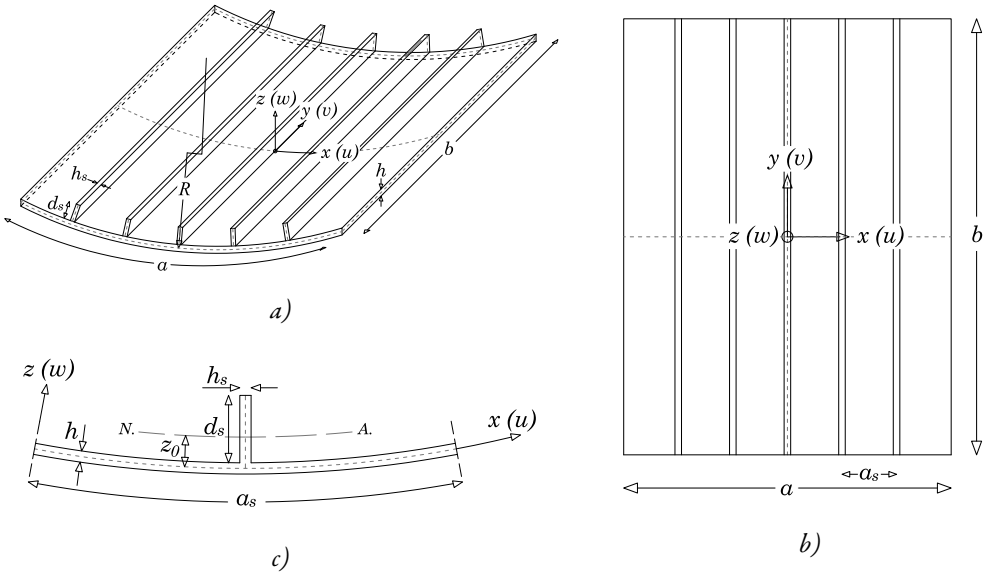

Figure 3.5: Geometry and coordinate system of a stiffened curved panel: *a)* Perspective view; *b)* top view; and *c)* geometry of a stiffener

Besides the non-dimensional global curvature parameter Z and aspect ratio α of the full stiffened panel, given by equations (3.34) and (3.35), respectively, one can define the effective properties of the subpanels between stiffeners. Thus, the geometrical properties of the subpanels namely the local curvature (Z_{loc}) and the local aspect ratio (α_{loc}) are given, respectively, by equations (3.36) and (3.37).

$$Z_{loc} = \frac{{a_s}^2}{R\,h} = \frac{\left(a/\left(n_s+1\right)\right)^2}{R\,h} = \frac{Z}{\left(n_s+1\right)^2} \tag{3.36}$$

$$\alpha_{loc} = \frac{b}{a_s} = \alpha\left(n_s+1\right) \tag{3.37}$$

3.4 BOUNDARY CONDITIONS

In all cases, the panels are considered as simply supported at all edges. These boundary conditions reproduce better the boundary conditions of the panels in real scenarios. Besides that, these boundary conditions provide results on the safe side where a certain degree of rotational restrain exists (partially or totally clamped).

However, depending on how the supports are oriented and how the edges are restrained

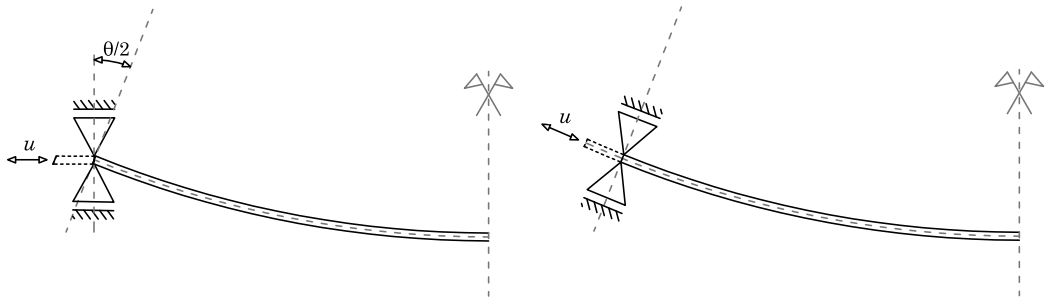

Figure 3.6: Supports at longitudinal edges for: *a)* rectangular coordinate system; and *b)* rectangular coordinate system

in-plane, different cases of simply supported boundary conditions may be distinguished. Firstly, the supports may follow a rectangular or a cylindrical coordinate system (CS). For a curved panel, a rectangular coordinate system means that at the longitudinal edges the supports are vertically oriented and, consequently, they restrain vertical displacements, see Figure 3.6 *a)*. On the other hand, supports following a cylindrical coordinate system restrain radial displacements at the longitudinal edges, see Figure 3.6 *b)*. The angle between the z axis of the rectangular and the cylindrical coordinate system is given by $\theta/2$, where θ is the central angle given by a/R.

$$\theta = \frac{a}{R} \tag{3.38}$$

Additionally, for each of these coordinate systems, it is possible to distinguish distinct simply supported boundary conditions depending on how the edges are restrained in-plane. These boundary conditions are named as follows. If an edge is considered to be constrained and, consequently, to remain straight, the edge is represented by the letter C. If on the other hand, an edge is considered to be unconstrained and, consequently, free to wave, the edge is represented by the letter U. Thus it is possible to assume a nomenclature for boundary conditions with 3 letters being the first "B" from boundary, the second "C" or "U" for the transversal edges ($y=\pm b/2$) and the third "C" or "U" for the longitudinal edges ($x=\pm a/2$). For example, a boundary condition BCU has its transversal edges forced to remain straight while its longitudinal edges are free to wave. Three types of these boundary conditions are considered from now on: BUU, BCU and BCC, which are schematically represented from Figure 3.7 to Figure 3.9, respectively.

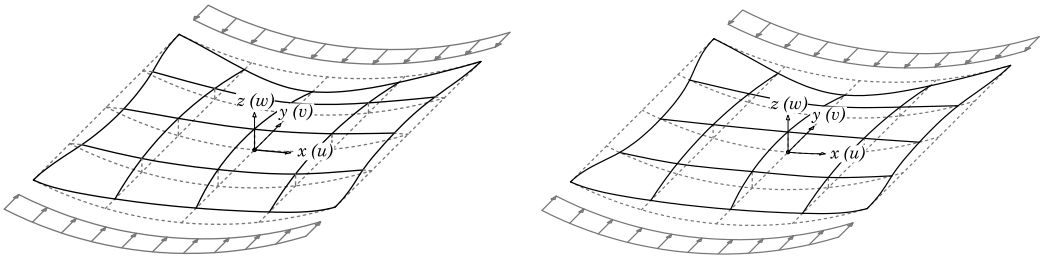

a) *b)*

Figure 3.7: Boundary conditions for BUU for: *a)* rectangular; and *b)* cylindrical coordinate system

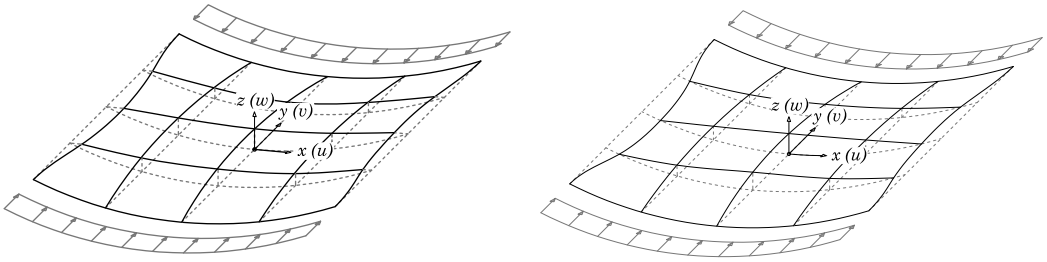

a) *b)*

Figure 3.8: Boundary conditions for BCU for: *a)* rectangular; and *b)* cylindrical coordinate system

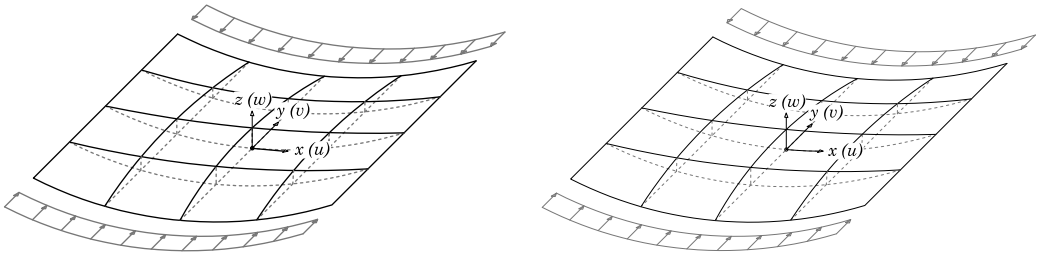

a) *b)*

Figure 3.9: Boundary conditions for BCC for: *a)* rectangular and *b)* cylindrical coordinate system

The objective of this distinction is to simulate the cases of straight and stress-free edges which represent the limits of real situations. In the same figures both rectangular and cylindrical CS are considered in *a)* and *b)*, respectively.

Despite being idealized boundary conditions, they seek to represent real scenarios. BCU

and BCC have clearly more practical applicability. While BCU corresponds to cases where the panel is supported by rigid supports (*e.g.* stiff girders) only in the longitudinal direction, BCC corresponds to cases in which the panel is supported by rigid supports in both the longitudinal and transversal directions. For example, a box-girder bridge with a curve bottom flange with two vertical webs bordering the longitudinal edges may be represented by BCU using a rectangular coordinate system. In this case, the in-plane restraint at the longitudinal edges is very small and the panel should be considered as unconstrained in-plane along these edges. On the other hand, a series of contiguous curved panels with radial transversal and longitudinal girders in an offshore structure may be represented by BCC using a cylindrical coordinate system. BUU conditions may have less applicability in real cases but it can represent an isolated panel or a panel with reduced constraints and, consequently, it is useful to compare it with the more restrained cases, assessing the differences in its behaviour.

The impact of the constraint of boundary conditions and the coordinate system for the supports on the behaviour of the curved panels will be discussed posteriorly.

3.5 LOADING CONDITIONS

Although the formulation developed in this thesis is able to account for several loading conditions (*e.g.* biaxial compression, out-of-plane pressure and shear) only the most relevant ones are deeply studied: *i)* longitudinal uniform in-plane load distributed along the sides $y=\pm b/2$ (Figure 3.10 *a)*); and *ii)* uniform out-of-plane pressure p_z normal to the curved surface ($z=0$) (Figure 3.10 *b)*).

Depending on the location considered for the load application, in stiffened panels, two situations may be distinguished: *i)* the load is applied on the total cross-sectional area (stiffeners and panel); or *ii)* the load is applied only on the panel. The differences between both situations are assessed posteriorly in section 6.3.7 but unless otherwise stated the load is assumed acting on the total cross-sectional area (stiffeners included). This situation reproduces better real cases and, furthermore, it is better described by the orthotropic model.

In the same way, unless otherwise stated, the out-of-plane pressure is considered as

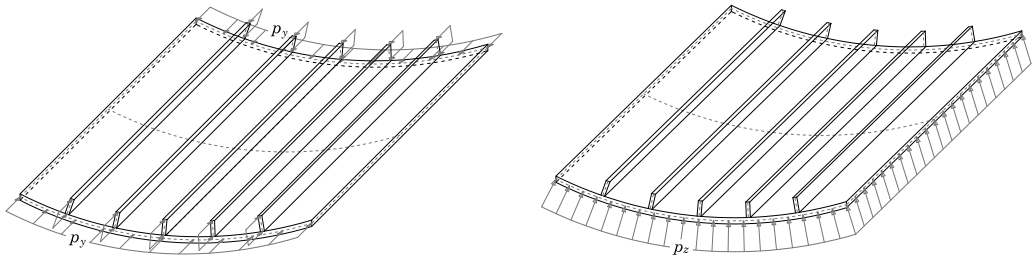

a) *b)*

Figure 3.10: Load application: a) in-plane compression and b) out-of-plane pressure

centripetal, which corresponds to most real situations (*e.g.* hydrostatic pressure). However, in order to assess the applicability of the semi-analytical procedure for centrifugal pressures this load is also considered for some cases.

The in-plane load is defined positive in compression and out-of-plane pressure is defined positive when centripetal.

3.6 STABILITY BEHAVIOUR OF CURVED PANELS

For an ideally perfect panel, the critical buckling stress, σ_{cr}, corresponds to the point of intersection between the fundamental path and the post-critical path. More than one point of intersection exists on the fundamental path corresponding to different load levels (and buckling modes). The most relevant one is, naturally, the minimum. As the out-of-plane displacements, w, begin to develop, second order effects take place and secondary stresses grow. For the flat plate, the load increases as the displacement increases and consequently the postbuckling path is stable. The same is not necessarily true for a curved panel. In this case the load can decrease as w increases, which means an unstable postbuckling path. This depends considerably of the boundary conditions and its effect is more evident the larger the curvature. Consequently, the effect of curvature on the post-buckling behaviour of thin panels is very important. As will be discussed in Chapter 6, curvature is not the only influencing factor, the boundary conditions can also affect substantially the postbuckling paths.

In real panels out-of-plane imperfections, w_0, are always present. These imperfections force the panel to deform right from the beginning of the loading. Generally, the first

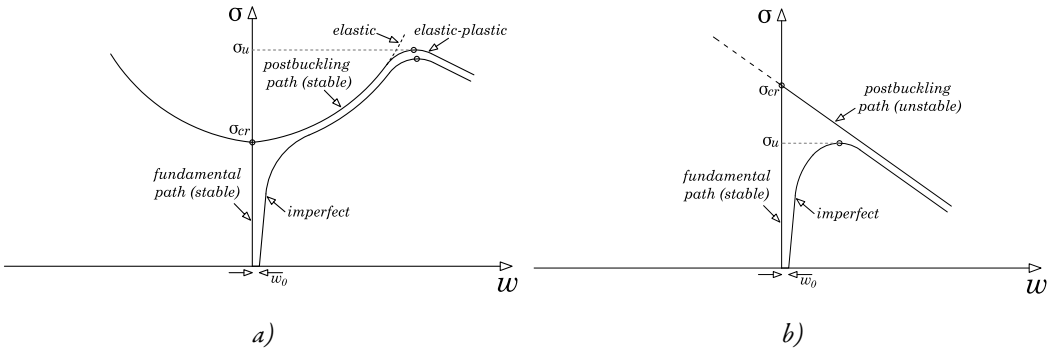

Figure 3.11: Schematic post-buckling behaviour of *a)* a flat plate and *b)* a curved panel

deformation follows the initial shape of imperfections; however, the deformation pattern can change with the development of the displacements.

Even if the panel does not fail by instability (the value of this maximum corresponds to the ultimate stress, σ_u) and larger loads are able to developed, for large displacements plastification takes place and the panel can fail by excessive deformation or fracture.

In order to illustrate what has been said, the equilibrium paths of perfect and imperfect flat and curved panels are schematically plotted in Figure 3.11 *a)* and *b)*, respectively. It is easily seen that the critical buckling stress is clearly conservative for flat panels but non-conservative for curved panels, as explained by Koiter in 1945 [62]. In the first case, the critical buckling stress does not take into account the stable post-buckling resistance while in the second case it does not account for the high imperfection-sensitivity of curved panels, which may be on the unsafe side ($\sigma_{cr}>\sigma_u$). This justifies the importance of studying the post-buckling behaviour of such elements through its large deflection range.

When the deformation "jumps" suddenly from one unstable equilibrium to a stable one, an instability phenomenon called "snap-through" takes place. This phenomenon can imply a substantial decrease in load which may be detrimental for the structural capacity of the panel.

Because it has been found that imperfections affect drastically the stability of shells, the assessment of the imperfections is still nowadays one of the most studied subjects in this area. The application of "real" imperfections in the finite element analysis is difficult to implement and they are hardly available for practical design. Thus, the usual alternative, following studies of authors such as Koiter [62], is to applying a pattern of equivalent

imperfections in the form of initial deflections perpendicular to the middle surface of the shell. These imperfections, being "equivalent", must cover the effects of other imperfections like load eccentricities, residual stresses, etc. One hypothesis recurrently used in thin-walled elements for these equivalent patterns is to use the eigenmodes of a perfect element obtained by a linear buckling analysis (LBA). However, as will be shown in Chapter 6 the initial imperfection from eigenmodes may lead to overestimation of the ultimate load for curved panels.

In this research, for comparison purposes of the results between the semi-analytical formulation and the FE analyses, a geometric equivalent imperfection is adopted. For the study of the ultimate load, besides an initial geometric imperfection the effect of the residual stresses will be assessed (section 6.5).

3.7 METHODS OF ANALYSIS OF SHELLS

3.7.1 Exact solutions and approximate methods

Exact solutions for shell problems are practically non-existent, exception for some very simple cases, boundary and loading conditions. For example, for circular plates with symmetric lateral load and rotationally symmetric boundary conditions. Therefore, exact analytical solutions do not cover most cases of practical significance. Consequently, approximate analytical solutions are required and they are the only possible solution for more complex problems. Even so, it is commonly assumed that the accurate calculation of the post buckling behaviour of shells is complicated hindering generally the obtainment of closed-form expression [114]. The complexity of the problem derives from the difficulties to obtain analytical solutions for the differential equations, for which only in some cases approximate solutions can be obtained. This is because the verification of the boundary conditions leads in most cases to mathematical difficulties.

3.7.2 Equilibrium methods and energy methods

The equilibrium method is formulated through Newton's law of equilibrium of forces from which one can derive the differential equations for shells. This is the Newtonian approach of the problem. The solution is then sought in terms of the displacements, w, which must satisfy the differential equations and the boundary conditions. However, the

exact solution may be obtained only for some rare cases, for example for circular plates and rectangular plates under specific conditions. For other cases, this approach is found to be less effective.

However, a more adequate approach to the problem is through energy methods using Bernoulli's principles of virtual work, the problem is approached in terms of its potential energy and work. This is the Lagrangian approach of the problem. When a deformable body is subjected to external loads, deformation occurs. The corresponding internal forces produce internal work which allow the application of energy methods to study the response of the element. One of the advantages of energy methods is the potential to get approximate analytical solutions. Two of the main methods are the Rayleigh-Ritz and the Galerkin.

3.7.3 Variational methods

The variational methods deal with the stationary values of functionals (definite integrals). If assumed solutions with variable parameters are substituted into the functional, the determination of the stationary (or the extreme) conditions for these parameters constitute the direct methods for variational calculus. In this case, the assumed solution is substituted into the energy principle equivalent to the governing equations.

These methods are considered as approximated because in this case a field of displacements in a form of a finite linear combination of coefficients and functions has to be assumed. Consequently, the accuracy of the methods depends on this selection. It should be noted that, if the assumed field of displacements coincides with the exact one, the solution will be the correct. It is also because of this assumption that approaches based on these methods are generally described as "semi-"analytical.

3.7.4 Rayleigh-Ritz method

Rayleigh's method is based on the principle of energy conservation. However, only one term for the displacements may be used with this method, implying the use of sufficiently accurate function. The Ritz method based on the principle of the minimum potential energy overcomes this limitation allowing to write the deformed shape of the shell as a sum of functions, preferably orthogonal ones. The basic principle of both method is the

same and consequently the Ritz method is usually called as Rayleigh-Ritz method.

The Rayleigh-Ritz method can be generally formulated as follows. Given a set of n of linearly independent functions Φ_i with i=1,2,...,n, one can define the approximate function w_n as a sum given by:

$$w_n(x,y) = C_1\Phi_1(x,y) + C_2\Phi_2(x,y) + \ldots + C_n\Phi_{n1}(x,y) \tag{3.39}$$

where C_i are the undetermined coefficients and each of the functions Φ_i has to satisfy the geometric boundary conditions of the problem. The functions Φ_i are chosen in advance.

The quantity which is to be extremised $I(w)$ becomes a function of a finite number of coefficients C_i. Consequently:

$$\frac{\partial I}{\partial C_i} = 0 \quad , i = 1, 2, \ldots n \tag{3.40}$$

This condition leads to a set of n simultaneous algebraic equations where the constants C_i are the unknowns to be determined.

The Rayleigh-Ritz method will be the method employed in the present semi-analytical formulation.

3.7.5 Alternative methods

Although only the Rayleigh-Ritz will be used in this thesis, there are other viable alternative methods which could be employed and, consequently, they deserve to be mentioned for reference. The most reasonable alternative is the Galerkin method.

The Galerkin method uses the differential equation directly without the need to use a functional. The Galerkin method, instead of formulating the problem directly in terms of the energy components of the system, uses the equilibrium equation to consider total potential energy.

Given a linear differential equation containing a linear operator, for example, the harmonic (∇^2) or the biharmonic operator (∇^4), with homogeneous boundary conditions, one may write:

$$L\left[w(x,y)\right] = f(x,y) \tag{3.41}$$

or more conveniently:

$$L\left[w(x,y)\right] - f(x,y) = 0 \tag{3.42}$$

If we write *w(x,y)* as a set of independent continuous functions:

$$w(x,y) = \sum_{k=1}^{\infty} C_k \Phi_k (x,y) \tag{3.43}$$

we may formulate, considering the orthogonality of the left side of equation (3.42) with every term of equation (3.43):

$$\iint_A \left\{ L\left[w(x,y)\right] - f(x,y) \right\} \Phi_k (x,y)\, dx\, dy = 0 \quad , k = 1,2,\ldots \tag{3.44}$$

If we truncate equation (3.43), to a finite number of terms *n*, equation (3.44) becomes:

$$\iint_A \left\{ L\left[\sum_{k=1}^{n} C_k \Phi_k (x,y) \right] - f(x,y) \right\} \Phi_i (x,y)\, dx\, dy = 0 \quad , i = 1,2,\ldots,n \tag{3.45}$$

which provides a set of *n* algebraic equations in the unknowns C_k.

The method belongs with other techniques to a broader method named as Method of Weighted Residuals (MWR).

While the Rayleigh-Ritz method needs only to satisfy the geometric boundary conditions, the Galerkin needs to satisfy geometric and forced boundary conditions. Additionally, while the approximation functions must be differentiable in Rayleigh-Ritz, in Galerkin method they must have the same differentiability as the differential equation.

3.7.6 Numerical methods and Finite Element Method (FEM)

To overcome the mathematical difficulties of analytical approaches, numerical methods were developed like the Finite Difference Method (FDM) and the Finite Element Method (FEM) that are based on the discretization of the shell, avoiding to solve the partial differential equations for the continuous element.

Numerical methods are more flexible since they allow the application to more complex problems than the analytical approaches. To achieve this, the surface is discretised, and a mesh of points is created on the surface of the shell. Based on these points, simultaneous algebraic equations are obtained and solved.

The FEM was developed in the 1960s and it has become an essential tool in several engineering fields. In this method the surface is divided in a number of smaller adjacent finite elements connected at their nodes and along their boundaries, where equilibrium and compatibility must be satisfied.

This method is easily automatized which facilitates its implementation in computational methods.

The considerations assumed in the implementation of the Finite Element Method will be the subject of Chapter 5.

3.8 SUMMARY

In this chapter, the basic concepts to understand the theory supporting the study of curved panels were presented. A brief review of the different shells theories available to tackle the problem was carried out. The DMV theory based on the Donnell's theory and derived for shallow shells was shown to be the most adequate theory for application to the curved panels studied in this work. This theory combines simplicity and accuracy if certain limits are fulfilled. The hypotheses on the basis of the theory and the consequences on the simplifications underlying the shallow shells assumption were discussed.

Besides some basic concepts related with the geometry, boundary and loading conditions of curved panels, the general differences in the stability of curved panels was discussed in comparison with the classical case of flat plates. The curvature was found to influence considerably the post-buckling behaviour of the panels.

The methods of analysis of shells were presented and the advantages and drawbacks of each approach are discussed. The approaches employed in this work, namely, the Rayleigh-Ritz and the FEM for the analytical and numerical approach, respectively, are described and compared with concurrent procedures.

4 Formulation of large deflection theory for curved panels

4.1 Introduction

Comparatively to a flat plate, a curved panel presents curvature in the unloaded state. Despite curvature does not affecting significantly the response of the element in bending, it changes significantly the behaviour of the element under membrane actions due to in-plane forces. The in-plane forces are divided in primary effects from edge loads, and secondary effects from flexural deformations. For an initial flat plate, the effect of secondary forces may be neglected for small displacements (in comparison with its thickness) without a substantial error, and one may analyse the panel with small deflection theory. However, when large deflections are present, the secondary forces become important and they should also be considered through the large deflection

theory. In the case of a curved panel, secondary forces should be considered whether the magnitude of the flexural deformations is large or not [115].

In order to account for this effect, the theory presented in section 3.2 is now extended in this chapter to account for large deflections. Besides the introduction of the nonlinear terms in the kinematic relations, initial imperfections are also taken into account. In this way, different patterns and amplitudes may be given to initial geometric imperfections.

In this way, in large deflection theory, the contribution of edge restraints in the plane of the panel becomes important, reason why two distinct cases of boundary conditions are considered in the semi-analytical study. Both are simply supported with the transversal loaded edges kept straight. However, in one case the longitudinal unloaded edges are kept straight (BCC) and in the other they are free to displace in-plane (BCU), as seen in section 3.4. As previously discussed these are the most common situations in real scenarios. Besides different boundary conditions, the energy formulation is derived to take in account different load conditions.

The aim of this chapter is to propose a formulation for unstiffened and stiffened panels based on the classical shell theory with large deflection theory and geometric nonlinearity (von Kármán-Donnell kinematic nonlinearity) incorporating initial imperfections. The formulation is derived for a multi degree of freedom (MDOF) displacement field.

The formulation is first developed for isotropic curved panels under uniaxial in-plane compression in section 4.2. This is the reference case. The formulation is then extended for orthotropic curved panels under generalized loading in section 4.3. Although, uniaxial in-plane compression and out-of-plane pressure are the only loads studied in this thesis, the formulation is perfectly applicable to generalized loading and, consequently, for the sake of generalization in-plane compression in the transversal direction and shear load will be also accounted for. It should be noted that the most general orthotropic formulation can be used to obtain the simpler cases by simplification.

The orthotropic model is formulated to account properly for the number and geometry of the asymmetrical stiffeners (relatively to the middle surface of the panel) in one direction. Finally, in section 4.4, the Rayleigh-Ritz method is presented as the method of solution.

4.2 FORMULATION FOR ISOTROPIC CURVED PANELS UNDER UNIAXIAL IN-PLANE COMPRESSION

4.2.1 Introduction

The analytical formulation to deal with isotropic curved panels is derived in this section. It is able to deal with unstiffened curved panels constituted by a homogenous and elastic material under uniaxial in-plane compression in the longitudinal direction. The formulation follows the assumptions of the DMV shell theory described in section 3.2.

4.2.2 Basic equations

4.2.2.1 Kinematic and constitutive relations

For a thin curved panel with radius, R, according to Figure 3.4, the normal and shear stresses in the z direction are negligible ($\sigma_z=\tau_{yz}=\tau_{zx}=0$). Therefore, taking into account the initial out-of-plane imperfections, w_0, the normal in-plane strains, ε_x, ε_y, and the shear strain, ε_{xy}, the following kinematic relations are defined:

$$\varepsilon_x = \frac{\partial u}{\partial x} - \frac{w}{R} + \frac{\partial w}{\partial x}\frac{\partial w_0}{\partial x} + \frac{1}{2}\left(\frac{\partial w}{\partial x}\right)^2 \tag{4.1}$$

$$\varepsilon_y = \frac{\partial v}{\partial y} + \frac{\partial w}{\partial y}\frac{\partial w_0}{\partial y} + \frac{1}{2}\left(\frac{\partial w}{\partial y}\right)^2 \tag{4.2}$$

$$\varepsilon_{xy} = \frac{1}{2}\left(\frac{\partial u}{\partial y} + \frac{\partial v}{\partial x} + \frac{\partial w}{\partial y}\frac{\partial w_0}{\partial x} + \frac{\partial w}{\partial x}\frac{\partial w_0}{\partial y} + \frac{\partial w}{\partial x}\frac{\partial w}{\partial y}\right) \tag{4.3}$$

The bending curvatures, $\varkappa_x$, and $\varkappa_y$, and the twisting curvature, $\varkappa_{xy}$, may be written, accounting with the simplifications of shallow shells, see section 3.2.2, as:

$$\kappa_x = -\frac{\partial^2 w}{\partial x^2} \tag{4.4}$$

$$\kappa_y = -\frac{\partial^2 w}{\partial y^2} \tag{4.5}$$

$$\kappa_{xy} = -\frac{\partial^2 w}{\partial x \partial y} \tag{4.6}$$

The material is linear isotropic and the modulus of elasticity and the Poisson's ratio are denoted by E and υ, respectively. Therefore, it is possible to define the constitutive relations using Hooke's law with the stress-strain relations written as:

$$\varepsilon_x = \frac{1}{E}\left(\sigma_x - \upsilon\,\sigma_y\right) \tag{4.7}$$

$$\varepsilon_y = \frac{1}{E}\left(\sigma_y - \upsilon\,\sigma_x\right) \tag{4.8}$$

$$\varepsilon_{xy} = \frac{\sigma_{xy}}{2\,G} = \frac{1+\upsilon}{E}\sigma_{xy} \tag{4.9}$$

with the shear modulus, G, given by:

$$G = \frac{E}{2\left(1+\upsilon\right)} \tag{4.10}$$

4.2.2.2 Equilibrium and compatibility equations

Using the Airy's stress function, F, the membrane stresses, σ, in the respective directions can be written as:

$$\sigma_x = \frac{\partial^2 F}{\partial y^2} \tag{4.11}$$

$$\sigma_y = \frac{\partial^2 F}{\partial x^2} \tag{4.12}$$

$$\sigma_{xy} = -\frac{\partial^2 F}{\partial x \partial y} \tag{4.13}$$

Through equilibrium of the membrane stresses and using equations (4.7) to (4.9) the large deflection differential *equilibrium equation* for isotropic curved panels is defined as:

$$\begin{aligned}\frac{\partial^4 w}{\partial x^4} + 2\frac{\partial^4 w}{\partial x^2 \partial y^2} + \frac{\partial^4 w}{\partial y^4} - \frac{h}{D}\Bigg[\frac{\partial^2 F}{\partial y^2}\left(\frac{1}{R} + \frac{\partial^2 w}{\partial x^2} + \frac{\partial^2 w_0}{\partial x^2}\right) - \\ 2\frac{\partial^2 F}{\partial x \partial y}\left(\frac{\partial^2 w}{\partial x \partial y} + \frac{\partial^2 w_0}{\partial x \partial y}\right) + \frac{\partial^2 F}{\partial x^2}\left(\frac{\partial^2 w}{\partial y^2} + \frac{\partial^2 w_0}{\partial y^2}\right)\Bigg] = 0\end{aligned} \tag{4.14}$$

where the flexural stiffness, D, is:

$$D = \frac{E\,h^3}{12\left(1-\upsilon^2\right)} \tag{4.15}$$

Comparing this large deflection differential equation with the corresponding equation (3.22) from linear theory, it is verified the additional inclusion of the nonlinear and imperfection terms[3].

From differentiation of equations (4.1) to (4.3) and using Airy's stress function the differential *compatibility equation* becomes:

$$\begin{aligned}&\frac{\partial^4 F}{\partial x^4}+2\frac{\partial^4 F}{\partial x^2\partial y^2}+\frac{\partial^4 F}{\partial y^4}\\&=E\left[\left(\frac{\partial^2 w}{\partial x\partial y}\right)^2+2\frac{\partial^2 w_0}{\partial x\partial y}\frac{\partial^2 w}{\partial x\partial y}-\frac{\partial^2 w}{\partial x^2}\frac{\partial^2 w}{\partial y^2}-\frac{\partial^2 w}{\partial y^2}\frac{\partial^2 w_0}{\partial x^2}-\frac{\partial^2 w}{\partial x^2}\frac{\partial^2 w_0}{\partial y^2}-\frac{1}{R}\frac{\partial^2 w}{\partial y^2}\right]\end{aligned} \tag{4.16}$$

Comparing again with the equation obtained for linear theory (equation (3.26)), this equation introduces the nonlinear and imperfection terms.

Equations (4.14) and (4.16) are fourth order nonlinear partial differential equations and constitute the so-called von Kármán-Donnell equations with imperfections. These is due to the fact that when $R\to\infty$, these equations lead to the von-Kármán equations for large deflections of flat plates.

4.2.3 Energy formulation

4.2.3.1 Potential energy due to membrane strain

Making use of the constitutive relations, the potential energy due to membrane strain U_m is given by:

$$U_m = \frac{1}{2}\int_{-b/2}^{b/2}\int_{-a/2}^{a/2}\left\{N_x\varepsilon_x + 2N_{xy}\varepsilon_{xy} + N_y\varepsilon_y\right\}\,dxdy \tag{4.17}$$

where the membrane force components N_x, N_y and N_{xy} are expressed as:

$$N_x = C\left(\varepsilon_x + \upsilon\,\varepsilon_y\right) \tag{4.18}$$

[3] The explicit appearance of h in equation (4.14) contrarily to (3.22) is due to the fact that here the Airy's stress function was defined for stresses and not for force/length units (initially used for convenience).

$$N_y = C\left(\varepsilon_y + \upsilon\,\varepsilon_x\right) \tag{4.19}$$

$$N_{xy} = C\left(1-\upsilon\right)\varepsilon_{xy} \tag{4.20}$$

with the extensional stiffness C given by:

$$C = \frac{E\,h}{1-\upsilon^2} \tag{4.21}$$

Rearranging equation (4.17) in function of F yields:

$$U_m = \frac{h}{2E}\int_{-b/2}^{b/2}\int_{-a/2}^{a/2}\left\{\left(\frac{\partial^2 F}{\partial x^2}\right)^2 - 2\,\upsilon\,\frac{\partial^2 F}{\partial x^2}\frac{\partial^2 F}{\partial y^2} + \left(\frac{\partial^2 F}{\partial y^2}\right)^2 + 2\left(1+\nu\right)\left(\frac{\partial^2 F}{\partial x \partial y}\right)^2\right\} dxdy \tag{4.22}$$

4.2.3.2 Potential energy due to bending strain

Similarly, from the bending components in equations (4.4) to (4.6) the expression for the potential energy due to bending U_b is given by:

$$U_b = \frac{1}{2}\int_{-b/2}^{b/2}\int_{-a/2}^{a/2}\left\{M_x\kappa_x + 2M_{xy}\kappa_{xy} + M_y\kappa_y\right\} dxdy \tag{4.23}$$

where the bending moment components M_x, M_y and M_{xy} are expressed by:

$$M_x = D\left(\kappa_x + \upsilon\,\kappa_y\right) \tag{4.24}$$

$$M_y = D\left(\kappa_y + \upsilon\,\kappa_x\right) \tag{4.25}$$

$$M_{xy} = D\left(1-\upsilon\right)\kappa_{xy} \tag{4.26}$$

with D given by equation (4.15).

Making the respective substitutions gives:

$$U_b = \frac{D}{2}\int_{-b/2}^{b/2}\int_{-a/2}^{a/2}\left\{\left(\frac{\partial^2 w}{\partial x^2}\right)^2 + 2\,\upsilon\,\frac{\partial^2 w}{\partial x^2}\frac{\partial^2 w}{\partial y^2} + \left(\frac{\partial^2 w}{\partial y^2}\right)^2 + 2\left(1-\nu\right)\left(\frac{\partial^2 w}{\partial x \partial y}\right)^2\right\} dxdy \tag{4.27}$$

4.2.3.3 Potential energy due to external in-plane load

The potential energy of the external in-plane load T_p is calculated as the constant compressive force multiplied with the displacement v, which means:

$$T_p = p_y\, a\, h \int_{-b/2}^{b/2} \frac{\partial v}{\partial y}\, dy \tag{4.28}$$

4.2.3.4 Total potential energy

The total potential energy U_{tot} is obtained by adding the three previous components:

$$U_{tot} = U_m + U_b + T_p \tag{4.29}$$

4.2.4 Boundary conditions

4.2.4.1 Natural boundary conditions (loading conditions)

The total force in the x direction P_x at the unloaded edges (at $x=-a/2$ and $x=a/2$) is null for boundary conditions BCC:

$$P_x = h \int_{-b/2}^{b/2} \frac{\partial^2 F}{\partial y^2}\, dy = 0 \tag{4.30}$$

while for boundary conditions BCU the stress σ_x is null in all points of those same edges, so:

$$\sigma_x = \frac{\partial^2 F}{\partial y^2} = 0 \tag{4.31}$$

The tangential stresses along all edges (at $x=-a/2$, $x=a/2$, $y=-b/2$ and $y=b/2$) are null for both BCC and BCU, so:

$$\sigma_{xy} = \frac{\partial^2 F}{\partial x \partial y} = 0 \tag{4.32}$$

At the loaded edges ($y=-b/2$ and $y=b/2$) the total force in the y direction P_y is given by, both for BCC and BCU:

$$P_y = h \int_{-a/2}^{a/2} \frac{\partial^2 F}{\partial x^2}\, dx = -a\, h\, p_y \tag{4.33}$$

For simply supported boundary conditions the bending moments M_x and M_y, for unloaded edges (at $x=-a/2$ and $x=a/2$) and loaded edges ($y=-b/2$ and $y=b/2$), respectively, are zero and must verify:

$$M_x = \frac{\partial^2 w}{\partial x^2} + \upsilon \frac{\partial^2 w}{\partial y^2} = 0$$
$$M_y = \frac{\partial^2 w}{\partial y^2} + \upsilon \frac{\partial^2 w}{\partial x^2} = 0 \tag{4.34}$$

4.2.4.2 Kinematic boundary conditions

For simply supported boundary conditions all edges have null out-of-plane displacements, so at $x=-a/2$, $x=a/2$, $y=-b/2$ and $y=b/2$ for both boundary conditions BCC and BCU, leading to:

$$w = 0 \tag{4.35}$$

To force the non-loaded edges to remain straight, the variation of displacement in the x direction (Δu) must be constant for each point along the longitudinal edges. Thus, for $x=-a/2$ and $x=a/2$, the following condition is necessary to define BCC:

$$\begin{aligned} \Delta u &= \int_{-a/2}^{a/2} \frac{\partial u}{\partial x}\, dx \\ &= \int_{-a/2}^{a/2} \frac{1}{E}\left(\frac{\partial^2 F}{\partial y^2} - \nu \frac{\partial^2 F}{\partial x^2} \right) + \frac{w}{R} - \frac{\partial w_0}{\partial x}\frac{\partial w}{\partial x} - \frac{1}{2}\left(\frac{\partial w}{\partial x} \right)^2 dx = const. \end{aligned} \tag{4.36}$$

On the other hand, for both boundary conditions (BCC and BCU) it is necessary to force the variation of displacement in the y direction (Δv) to be constant, so at $y=-b/2$ and $y=b/2$:

$$\begin{aligned} \Delta v &= \int_{-b/2}^{b/2} \frac{\partial v}{\partial y}\, dy \\ &= \int_{-b/2}^{b/2} \frac{1}{E}\left(\frac{\partial^2 F}{\partial x^2} - \nu \frac{\partial^2 F}{\partial y^2} \right) - \frac{\partial w_0}{\partial y}\frac{\partial w}{\partial y} - \frac{1}{2}\left(\frac{\partial w}{\partial y} \right)^2 dy = const. \end{aligned} \tag{4.37}$$

The in-plane edge restraints have a direct effect on the stress distribution at edges. For these boundary conditions the non-restrained edges in BCU have null σ_x stresses while for BCC their resultant is null although those stresses are not. Due to the edge restraint at the loaded edges, σ_y stresses are not null for both boundary conditions.

4.3 Formulation for orthotropic curved panels under generalized loading

4.3.1 Introduction

Due to the presence of stiffeners, a curved panel exhibits structural anisotropy. The stiffeners are usually laid down in a regular way, parallel to each other (see Figure 3.5), usually welded to one side of the plate only. Hence, despite being made of an isotropic material, stiffened panels show structural orthotropy. However, if a sufficient number of stiffeners exists, these panels can be idealized as a homogeneous orthotropic panel, where the stiffeners are "smeared" along the panel. When the stiffeners are relatively weak (do not constitute nodal lines), the stiffeners generally buckle together with the panel (overall buckling occurs) and the stiffened panel behaves as an orthotropic panel. In this case the stiffened panel can be idealized and replaced by an equivalent orthotropic panel. This is more realistic as the number of stiffeners increases.

For stiffened flat plates, Paik *et al.* [26] established the equivalence between the geometric properties of a stiffened flat plate and the elastic properties of the corresponding orthotropic differential equation. This approach is followed in this section for the curved panels.

4.3.2 Basic equations

4.3.2.1 Kinematic and constitutive relations

The kinematic relations for orthotropic panels follow the same principles and assumptions previously referred and, consequently, strains and curvatures are given, respectively, by equations (4.1)-(4.3) and (4.4)-(4.6).

Despite the material being linear isotropic, for stiffened panels, the anisotropy due to the different geometry in the perpendicular directions x and y is accounted for with the modulii of elasticity E_x and E_y in x and y direction, respectively, and with the Poisson's ratios v_x and v_y in x and y direction, respectively. Therefore, it is possible to define the constitutive relations using Hooke's law with the stress-strain relations written as:

$$\varepsilon_x = \frac{\sigma_x}{E_x} - \upsilon_y \frac{\sigma_y}{E_y} \tag{4.38}$$

$$\varepsilon_y = \frac{\sigma_y}{E_y} - \upsilon_x \frac{\sigma_x}{E_x} \tag{4.39}$$

$$\varepsilon_{xy} = \frac{\sigma_{xy}}{2\,G_{xy}} \tag{4.40}$$

with the shear modulus G_{xy} given approximately by:

$$G_{xy} \approx \frac{\sqrt{E_x E_y}}{2\left(1+\sqrt{\upsilon_x \upsilon_y}\right)} \approx \frac{E}{2\left(1+\sqrt{\upsilon_x \upsilon_y}\right)} \tag{4.41}$$

Following a procedure similar to the one of Paik *et al.* [26] for stiffened flat plates accounting explicitly with the properties of the stiffeners and determining the elastic properties of the corresponding orthotropic plate, a procedure for curved panels with eccentric stiffeners in one direction is derived next.

Taking into account the existence of stiffeners only in direction y, the moduli of elasticity of the corresponding orthotropic panel in direction x and y, are respectively E_x and E_y given by:

$$E_x = E \tag{4.42}$$

$$E_y = E\left(1+\delta\right) \tag{4.43}$$

with the relative cross sectional area, δ, relating the total area of the stiffeners (A_s is the area of a single stiffener $=d_s h_s$) and the area of the curved surface of the panel given by:

$$\delta = \frac{n_s A_s}{a\,h} \tag{4.44}$$

The flexural rigidities D_x and D_y in x and y direction for the orthotropic panel are, respectively:

$$D_x = \frac{E\,h^3}{12\left(1-\upsilon_{xy}{}^2\right)} \tag{4.45}$$

$$D_y = \frac{E\,h^3}{12\left(1-\upsilon_{xy}{}^2\right)} + \frac{E\,h\,z_0{}^2}{1-\upsilon_{xy}{}^2} + \frac{E\,I_s}{a_s} \tag{4.46}$$

with the elastic orthotropic constant υ_{xy}:

$$\upsilon_{xy} = \sqrt{\upsilon_x \upsilon_y} \tag{4.47}$$

I_s (the inertia of a single stiffener) and z_0 are given by (see Figure 3.5 *c)*):

$$I_s = \frac{h_s\, d_s^{\,3}}{12} + h_s\, d_s \left(\frac{d_s}{2} + \frac{h}{2} - z_0 \right)^2 \tag{4.48}$$

$$z_0 = \frac{h_s\, d_s \left(\frac{d_s}{2} + \frac{h}{2} \right)}{a_s\, h + h_s\, d_s} \tag{4.49}$$

The torsional rigidities components D_{xy} and D_{yx} are given by:

$$D_{xy} = \upsilon_y\, D_x \tag{4.50}$$

$$D_{yx} = \upsilon_x\, D_y \tag{4.51}$$

Based on Betti's reciprocity theorem [26] one can write:

$$\upsilon_x\, E_y = \upsilon_y\, E_x \tag{4.52}$$

$$\upsilon_x\, D_y = \upsilon_y\, D_x \tag{4.53}$$

leading to the following expression for the Poisson's ratio for the orthotropic panel in the x and y directions, respectively:

$$\upsilon_x = \frac{\upsilon}{2\sqrt{3}} \sqrt{\frac{a_s \left(E_x - E_y \right) h^3 + 12 E_x I_s + 12 a_s E_x h\, z_0^{\,2}}{E_y I_s}} \tag{4.54}$$

$$\upsilon_y = \frac{\upsilon}{2\sqrt{3}} \frac{E_y}{E_x} \sqrt{\frac{a_s \left(E_x - E_y \right) h^3 + 12 E_x I_s + 12 a_s E_x h\, z_0^{\,2}}{E_y I_s}} \tag{4.55}$$

4.3.2.2 Equilibrium and compatibility equations

Using the Airy's stress function, F, the membrane stresses σ can be written as:

$$\sigma_x = \frac{\partial^2 F}{\partial y^2} \tag{4.56}$$

$$\sigma_y = \frac{\partial^2 F}{\partial x^2} \tag{4.57}$$

$$\sigma_{xy} = -\frac{\partial^2 F}{\partial x \partial y} \tag{4.58}$$

Through equilibrium of the membrane stresses and using equations (4.7) to (4.9), the large deflection differential *equilibrium equation* for orthotropic curved panels is defined (with the incorporation of the out-of-plane pressure, p_z) as:

$$\begin{aligned} &D_x \frac{\partial^4 w}{\partial x^4} + 2H \frac{\partial^4 w}{\partial x^2 \partial y^2} + D_y \frac{\partial^4 w}{\partial y^4} - h\left[\frac{\partial^2 F}{\partial y^2}\left(\frac{1}{R} + \frac{\partial^2 w}{\partial x^2} + \frac{\partial^2 w_0}{\partial x^2} \right) - \right. \\ &\left. 2\frac{\partial^2 F}{\partial x \partial y}\left(\frac{\partial^2 w}{\partial x \partial y} + \frac{\partial^2 w_0}{\partial x \partial y} \right) + \frac{\partial^2 F}{\partial x^2}\left(\frac{\partial^2 w}{\partial y^2} + \frac{\partial^2 w_0}{\partial y^2} \right) + \frac{p_z}{h} \right] = 0 \end{aligned} \tag{4.59}$$

where H is related to the elastic orthotropic constants and can be written as follows:

$$H = \frac{1}{2}\left(\upsilon_y D_x + \upsilon_x D_y + G_{xy} \frac{h^3}{3} \right) \tag{4.60}$$

Alternatively, rearranging equation (4.60), H may be expressed as

$$H = D_{xy} + 2D_s, \tag{4.61}$$

using equations (4.50) and (4.51) and taking into account that

$$D_s = G_{xy} \frac{h^3}{12}. \tag{4.62}$$

From differentiation of equations (4.1) to (4.3) and using Airy's stress function the differential *compatibility equation* becomes:

$$\begin{aligned} &\frac{1}{E_y}\frac{\partial^4 F}{\partial x^4} + \left(\frac{1}{G_{xy}} - 2\frac{\nu_x}{E_x} \right) \frac{\partial^4 F}{\partial x^2 \partial y^2} + \frac{1}{E_x}\frac{\partial^4 F}{\partial y^4} \\ &= \left(\frac{\partial^2 w}{\partial x \partial y} \right)^2 + 2\frac{\partial^2 w_0}{\partial x \partial y}\frac{\partial^2 w}{\partial x \partial y} - \frac{\partial^2 w}{\partial x^2}\frac{\partial^2 w}{\partial y^2} - \frac{\partial^2 w}{\partial y^2}\frac{\partial^2 w_0}{\partial x^2} - \frac{\partial^2 w}{\partial x^2}\frac{\partial^2 w_0}{\partial y^2} - \frac{1}{R}\frac{\partial^2 w}{\partial y^2} \end{aligned} \tag{4.63}$$

Equations (4.14) and (4.16) are fourth order nonlinear partial differential equations and constitute the so-called von Kármán-Donnell equations with imperfections adapted for orthotropic curved panels.

4.3.3 Energy formulation

4.3.3.1 Potential energy due to membrane strain

Using the previously defined constitutive relations, the potential energy due to membrane strain U_m is given by:

$$U_m = \frac{1}{2}\int_{-b/2}^{b/2}\int_{-a/2}^{a/2}\left\{N_x\varepsilon_x + 2N_{xy}\varepsilon_{xy} + N_y\varepsilon_y\right\}\,dxdy \tag{4.64}$$

where the membrane force components N_x, N_y and N_{xy} are expressed as:

$$N_x = \frac{E_x\,h}{1-\upsilon_x\,\upsilon_y}\left(\varepsilon_x + \upsilon_y\,\varepsilon_y\right) \tag{4.65}$$

$$N_y = \frac{E_y\,h}{1-\upsilon_x\,\upsilon_y}\left(\varepsilon_y + \upsilon_x\,\varepsilon_x\right) \tag{4.66}$$

$$N_{xy} = 2\,h\,G_{xy}\,\varepsilon_{xy} \tag{4.67}$$

Rearranging equation (4.17) in function of F yields the following expression for the membrane energy component:

$$U_m = \frac{h}{2}\int_{-b/2}^{b/2}\int_{-a/2}^{a/2}\left\{\frac{1}{E_y}\left(\frac{\partial^2 F}{\partial x^2}\right)^2 + \frac{1}{E_x}\left(\frac{\partial^2 F}{\partial y^2}\right)^2 - \left(\frac{\upsilon_x}{E_x}+\frac{\upsilon_y}{E_y}\right)\frac{\partial^2 F}{\partial x^2}\frac{\partial^2 F}{\partial y^2} + \frac{1}{G_{xy}}\left(\frac{\partial^2 F}{\partial x\partial y}\right)^2\right\}dxdy \tag{4.68}$$

4.3.3.2 Potential energy due to bending strain

Similarly, from the bending components in equations (4.4) to (4.6), the expression for the potential energy due to bending U_b is given by:

$$U_b = \frac{1}{2}\int_{-b/2}^{b/2}\int_{-a/2}^{a/2}\left\{M_x\kappa_x + 2M_{xy}\kappa_{xy} + M_y\kappa_y\right\}\,dxdy \tag{4.69}$$

where the bending moment components M_x, M_y and M_{xy} are expressed by:

$$M_x = D_x\,\kappa_x + D_{xy}\,\kappa_y \tag{4.70}$$

$$M_y = D_y \kappa_y + D_{yx} \kappa_x \tag{4.71}$$

$$M_{xy} = 2 D_s \kappa_{xy} \tag{4.72}$$

with D_s given by equation (4.62).

Making the respective substitutions gives the following expression for the bending energy component:

$$U_b = \frac{1}{2} \int_{-b/2}^{b/2} \int_{-a/2}^{a/2} \left\{ D_x \left(\frac{\partial^2 w}{\partial x^2} \right)^2 + 2 D_{xy} \frac{\partial^2 w}{\partial x^2} \frac{\partial^2 w}{\partial y^2} + D_y \left(\frac{\partial^2 w}{\partial y^2} \right)^2 + 4 D_s \left(\frac{\partial^2 w}{\partial x \partial y} \right)^2 \right\} dx dy \tag{4.73}$$

4.3.3.3 Potential energy due to external in-plane loads in longitudinal and transversal direction

The potential energy of the external in-plane loads, p_y and p_x, respectively for longitudinal and transversal directions, T_p, is calculated as the constant compressive forces multiplied by the displacement v and u, which means:

$$T_p = p_y \, a \, h \int_{-b/2}^{b/2} \frac{\partial v}{\partial y} dy + p_x \, b \, h \int_{-a/2}^{a/2} \frac{\partial u}{\partial x} dx \tag{4.74}$$

In this thesis p_x is always considered as null (only the longitudinal compression is considered).

4.3.3.4 Potential energy due to external shear load

Although the applied tangential stress, p_{xy}, is not considered in the study, the potential energy of the external shear load, T_s, is calculated by:

$$T_s = p_{xy} \, h \int_{-b/2}^{b/2} \int_{-a/2}^{a/2} \left(\frac{\partial u}{\partial y} + \frac{\partial v}{\partial x} \right) dx dy \tag{4.75}$$

4.3.3.5 Potential energy due to external out-of-plane pressure

Analogously, the potential energy of the external out-of-plane pressure load T_{lp}

corresponds to a uniform pressure, p_z, multiplied by the displacement w, integrated over the surface area:

$$T_{lp} = -p_z \int_{-b/2}^{b/2} \int_{-a/2}^{a/2} w \, dxdy \tag{4.76}$$

4.3.3.6 Total potential energy

The total potential energy U_{tot} is obtained by adding the previous components:

$$U_{tot} = U_m + U_b + T_p + T_s + T_{lp} \tag{4.77}$$

4.3.4 Boundary conditions

4.3.4.1 Natural boundary conditions (loading conditions)

The boundary conditions for the orthotropic panels are defined similarly to the isotropic case, in section 4.2.4, with the respective modification for the orthotropic properties. BCC are presented next.

The total force in the x direction P_x at the unloaded edges (at $x=-a/2$ and $x=a/2$) is null because the panels are only loaded in y direction, consequently:

$$P_x = h \int_{-b/2}^{b/2} \frac{\partial^2 F}{\partial y^2} dy = 0 \tag{4.78}$$

On the other hand, at the loaded edges ($y=-b/2$ and $y=b/2$) the total force in the y direction P_y is given by:

$$P_y = h \int_{-a/2}^{a/2} \frac{\partial^2 F}{\partial x^2} dx = -a \; h \; p_y \tag{4.79}$$

The tangential stresses in all edges are null, so at $x=-a/2$, $x=a/2$, $y=-b/2$ and $y=b/2$:

$$\sigma_{xy} = \frac{\partial^2 F}{\partial x \partial y} = 0 \tag{4.80}$$

The bending moments M_x and M_y for simply supported boundary conditions are null for both unloaded edges (at $x=-a/2$ and $x=a/2$) and loaded edges ($y=-b/2$ and $y=b/2$), and,

consequently, must verify:

$$M_x = -\left[D_x \frac{\partial^2 w}{\partial x^2} + D_{xy} \frac{\partial^2 w}{\partial y^2} \right] = 0$$
$$M_y = -\left[D_y \frac{\partial^2 w}{\partial y^2} + D_{yx} \frac{\partial^2 w}{\partial x^2} \right] = 0 \tag{4.81}$$

4.3.4.2 Kinematic boundary conditions

For simply supported boundary conditions all edges have null out-of-plane displacements, so at $x=-a/2$, $x=a/2$, $y=-b/2$ and $y=b/2$:

$$w = 0 \tag{4.82}$$

In order to force the edges of the orthotropic panels to remain straight in the x direction, the variation of displacement (Δu) must be constant for each point along the longitudinal edges. Consequently, for $x=-a/2$ and $x=a/2$, it is necessary to define the following condition:

$$\Delta u = \int_{-a/2}^{a/2} \frac{\partial u}{\partial x} dx = \int_{-a/2}^{a/2} \left(\frac{1}{E_x} \frac{\partial^2 F}{\partial y^2} - \nu_y \frac{1}{E_y} \frac{\partial^2 F}{\partial x^2} \right) + \frac{w}{R} - \frac{\partial w_0}{\partial x} \frac{\partial w}{\partial x} - \frac{1}{2} \left(\frac{\partial w}{\partial x} \right)^2 dx = const. \tag{4.83}$$

Analogously, for the loaded edges, in the y direction, at $y=-b/2$ and $y=b/2$, Δv has to verify:

$$\Delta v = \int_{-b/2}^{b/2} \frac{\partial v}{\partial y} dy = \int_{-b/2}^{b/2} \left(\frac{1}{E_y} \frac{\partial^2 F}{\partial x^2} - \nu_x \frac{1}{E_x} \frac{\partial^2 F}{\partial y^2} \right) - \frac{\partial w_0}{\partial y} \frac{\partial w}{\partial y} - \frac{1}{2} \left(\frac{\partial w}{\partial y} \right)^2 dy = const. \tag{4.84}$$

4.4 METHOD OF SOLUTION

4.4.1 Procedure

The out-of-plane deflections, w, and the out-of-plane imperfections, w_0, are chosen in

advance, respectively, by the following double trigonometric series:

$$w(x,y) = h \sum_{m=1,2,3,\ldots}^{\infty} \sum_{n=1,2,3,\ldots}^{\infty} b_{mn} \operatorname{Cos}\left(\frac{m\,\pi\,x}{a}\right) \operatorname{Cos}\left(\frac{n\,\pi\,y}{b}\right) \tag{4.85}$$

$$w_0(x,y) = h \sum_{m=1,2,3,\ldots}^{\infty} \sum_{n=1,2,3,\ldots}^{\infty} a_{mn} \operatorname{Cos}\left(\frac{m\,\pi\,x}{a}\right) \operatorname{Cos}\left(\frac{n\,\pi\,y}{b}\right) \tag{4.86}$$

These deflections may be considered with as many Degrees of Freedom (DOFs) as desired. They satisfy the boundary conditions in equations (4.34) and (4.35).

The coefficients b_{mn} and a_{mn} are the amplitudes of the out-of-plane displacements and the amplitude of the out-of-plane initial imperfections, respectively, while m and n are the number of semi-waves in the transversal and longitudinal directions, respectively.

The general solution of equation (4.16) is given by the sum of the homogeneous solution (F_0) with the particular solution (F_1):

$$F = F_0 + F_1 \tag{4.87}$$

consequently, F_0 has to satisfy the biharmonic equation:

$$\nabla^4 F_0 = 0 \tag{4.88}$$

where ∇^4 is the biharmonic operator written as:

$$\nabla^4 = \frac{\partial^4}{\partial x^4} + 2\frac{\partial^4}{\partial x^2 \partial y^2} + \frac{\partial^4}{\partial y^4} \tag{4.89}$$

The homogeneous solution is in its most general form given by:

$$\begin{aligned} F_0 = & -\frac{1}{2} p_y x^2 + x\,y\,p_{xy} - \frac{1}{2} p_x y^2 + \\ & \sum_{p=1,2,\ldots} \left[\left(C_{1p} \operatorname{Cosh}\alpha x + C_{2p} \operatorname{Sinh}\alpha x\right) + x\left(C_{3p} \operatorname{Cosh}\alpha x + C_{4p} \operatorname{Sinh}\alpha x\right)\right] \operatorname{Cos}\alpha y + \\ & \sum_{q=1,2,\ldots} \left[\left(C_{5q} \operatorname{Cosh}\beta y + C_{6q} \operatorname{Sinh}\beta y\right) + y\left(C_{7q} \operatorname{Cosh}\beta y + C_{8q} \operatorname{Sinh}\beta y\right)\right] \operatorname{Cos}\beta x \end{aligned} \tag{4.90}$$

where $C_{1p}, C_{2p}, C_{3p}, C_{4p}, C_{5q}, C_{6q}, C_{7q}, C_{8q}, \alpha$ and β are unknown constants.

The particular solution F_1 is obtained substituting equations (4.85) and (4.86) in equation (4.16) and it is expressed by the following series:

$$F_1 = E\,h^2\left[\sum_{p=0,1,2\ldots}\sum_{q=0,1,2\ldots}\varphi_{pq}\,\mathrm{Cos}\frac{2\,p\,\pi\,x}{a}\mathrm{Cos}\frac{2\,q\,\pi\,y}{b}+\sum_{s=1,2\ldots}\sum_{t=1,2\ldots}\varphi_{r\,st}\,\mathrm{Cos}\frac{s\,\pi\,x}{a}\mathrm{Cos}\frac{t\,\pi\,y}{b}\right] \tag{4.91}$$

where φ_{pq} and $\varphi_{r\,st}$ are determined satisfying equation (4.16) using, *e.g.*, the method of undetermined coefficients. φ_{pq} are quadratic terms in b_{mn} and $\varphi_{r\,st}$ are linear terms in b_{mn} containing the radius R.

Imposing equation (4.87) to the respective boundary conditions, the following expression for F_0[4] is obtained for BCC and BCU:

$$F_0 = -\frac{p_y x^2}{2}+E\,h^2\sum_{p=1,2\ldots}\left[\mathrm{Cos}\frac{p\,\pi\,y}{b}\mathrm{Cosh}\frac{p\,\pi\,x}{b}\left(A_p+B_p\,x\,\mathrm{Sinh}\frac{p\,\pi\,x}{b}\right)\right]+E\,h^2\sum_{q=1,2\ldots}\left[\mathrm{Cos}\frac{q\,\pi\,x}{a}\left(C_q\,\mathrm{Cosh}\frac{q\,\pi\,y}{a}+D_q\,y\,\mathrm{Sinh}\frac{q\,\pi\,y}{a}\right)\right] \tag{4.92}$$

The expressions for A_p, B_p, C_q and D_q depend on the boundary conditions. They are relatively extensive and are not presented here for brevity reasons.

4.4.2 Solution method

As previously seen in section 3.7, a hypothesis to study the post-critical behaviour of shells is to use an approximate method with an analytical procedure such as the variational Rayleigh-Ritz method or the Galerkin method to solve the governing differential equations. Both methods are similar, working with the compatibility equation to relate the Airy's stress function, the out-of-plane displacements and the initial imperfections. However, while the Rayleigh-Ritz method uses the total potential energy of the conservative system, the Galerkin method uses the equilibrium equation (with no need of a variational function) to stablish the algebraic equations for the equilibrium path.

As previously referred, the Rayleigh-Ritz method was chosen as method of solution

[4] It should be noted that, in some cases, a mathematical solution satisfying completely all boundary conditions was not found (and it is maybe mathematically impossible for curved panels). However, the differences from the idealized cases are very small and in no way compromise the obtained results.

which was implemented through the software Mathematica [116]. In this method the total potential energy U_{tot} is a function of a finite number of parameters b_{mn}s (the unknowns of the problems), leading to an extremum problem where the objective is to find the stationary value of the function. This is the basis of the Rayleigh-Ritz method and can be mathematically stated as:

$$\frac{\partial U_{tot}}{\partial b_{mn}} = 0 \tag{4.93}$$

4.4.3 Solution of the system of algebraic equations with Newton-Raphson method

This condition results in a set of $m*n$ simultaneous non-linear third order algebraic equations in which the parameters b_{mn}'s are the unknowns of the problem. In order to solve this system of equations an iterative process is required. The Newton-Raphson method was used.

Snap-through phenomena in the analyses presented posteriorly were found to be very rare or happening for high load levels. However, it should be noted that the semi-analytical formulation should be able to account for them properly, provided that an adequate method is chosen to solve the algebraic system of equations. For this the Newton-Raphson in load-control fails to catch the equilibrium path when the tangent is zero, therefore requiring a displacement-control incrementation strategy or using an arc-length method. Due to the reasons previously presented the implementation of an arc-length resolution method was considered not justifiable.

4.5 SUMMARY

A formulation based on the large deflection theory was derived for cylindrically curved panels, which is the basis of the proposed semi-analytical method.

Provisions for isotropic panels under uniaxial compression were first presented. The formulation was then generalized for orthotropic panels under different loading conditions, namely: compression in both directions, shear loads and out-of-plane pressure. The orthotropic properties were formulated to account explicitly for the

number and geometry of stiffeners in the concave side of the panels.

The method of solution is able to deal with a Multi Degree of Freedom (MDOF) problem based on the Rayleigh-Ritz method.

Consequently, the semi-analytical model based on the presented formulation shows potential to predict the elastic post-buckling behaviour of cylindrically unstiffened and stiffened curved panels with different curvatures, aspect ratios, loading and boundary conditions.

5 Modelling curved panels by the Finite Element Method

5.1 Introduction

This chapter is devoted to the considerations assumed in the numerical modelling of the panels. The analyses were carried out using the Finite Element software ABAQUS [117].

The aim of using the Finite Element Method (FEM) is twofold: *i)* to characterize systematically the behaviour of unstiffened and stiffened curved panels in the most realist way possible (imperfections, plasticity, etc.); and *ii)* to validate the semi-analytical model through comparison of the results.

The chapter begins, in section 5.2, with a brief introduction to the type of analyses used in the current study with the FEA, namely LBA, GNIA and GMNIA. Sections 5.3 to 5.6 are devoted to explain the way boundary conditions, application of the loading, material properties and mesh were considered in the FE software. Section 5.7 addresses the

detailed modelling of imperfections. Section 5.8 shows the way residual stresses are generally incorporated in numerical models. A brief state-of-the-art about the topic is presented. The numerical models are, finally, validated in section 5.9.

The procedure and the outcomes resulting from each numerical analysis are represented in Figure 5.1. As it will be described in the following sections, several steps are carried out to analyse properly the behaviour of the panels. In generic terms the procedure is as follows: *i)* the modelling of imperfections is done defining the coordinates of each node of the panels. This provides freedom to model the imperfections as desired; *ii)* if imperfections from eigenmodes are desired, a LBA analysis is required; *iii)* with the equivalent geometric imperfections defined, they are introduced in the GNIA or GMNIA analyses; *iv)* the GNIA is performed to obtain the nonlinear equilibrium paths using an elastic material. This is useful for comparison with the SAM (Chapter 7); *v)* if the ultimate load is desired, a GMNIA has to be performed, considering the plasticity of the material. The ultimate load can be compared with the SAM when a strength criterion is employed (Chapter 8); and finally, *vi)* if the ultimate load is plotted in function of the slenderness of the panels, this has to be calculated using the eigenvalues of the LBA.

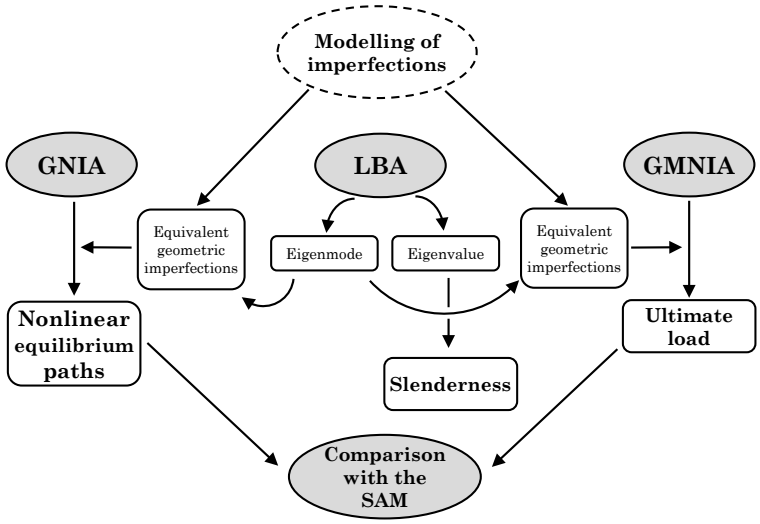

Figure 5.1: Procedure and outcomes of the different numerical analyses

5.2 TYPES OF ANALYSES

5.2.1 Introduction

The design of steel shells in general can be done using different methodologies through a single analysis or combining different types of analyses. When an element is subjected to compression, the simplest approach is to use a Linear elastic Bifurcation Analysis (or Linear Buckling Analysis) (LBA) to obtain the critical buckling load of a perfect element and applying to it a reduction coefficient, known as "knockdown factor", to take into account the imperfections of the element, either geometric or material nonlinearities [118]. This approach has important shortcomings since it does not allow introducing accurately the problem of non-linearity and imperfections found in real cases. As discussed in Chapter 2, this was the common practice in the beginnings of shell stability studies. On the other hand, to deal with the large deflection behaviour a nonlinear analysis is required. If geometric nonlinearities and imperfections are included, the analysis is named Geometrically Nonlinear Analysis with Imperfections (GNIA). Finally, if nonlinearity is considered for the material law, the analysis is called Geometrically and Materially Nonlinear Analysis with Imperfections (GMNIA), which is the most sophisticated approach.

These types of analysis are briefly discussed in the next paragraphs.

5.2.2 Linear elastic Bifurcation Analysis (LBA)

A LBA consists in the solution of a problem of eigenvalues and eigenvectors in which the loads that make the stiffness matrix, K, singular are determined. This means that:

$$\left(K + \lambda \, \Delta K\right) v = 0 \tag{5.1}$$

where ΔK is the matrix of the initial stresses due to the incremental loading, λ are the load factors (eigenvalues) and v are the nodal displacements corresponding to the buckling mode shapes (eigenvectors).

The solution of this problem was performed through the Subspace algorithm available in ABAQUS.

5.2.3 Geometrically Nonlinear elastic Analysis with Imperfections included (GNIA)

When compression is presented in geometrically nonlinear problems involving energy loss in the system (negative stiffness), characteristic of buckling problems, the equilibrium path is not monotonic and as such, solution algorithms that can efficiently follow this behaviour should be applied. For this, the Newton-Raphson in load-control fails to catch the equilibrium path when the tangent is zero. This may be overcome using the same method in displacement-control or using an arc-length method, like Riks [119]. In ABAQUS the Newton-Raphson is performed with the algorithm **Static, General* and the Riks with the algorithm **Static, Riks*. In the performed finite element analyses, preference was given to the latter.

This type of analysis is directly compared with the proposed semi-analytical procedure because a linear material is considered in both procedures.

5.2.4 Geometrically and Materially Nonlinear Analysis with Imperfections included (GMNIA)

The GMNIA in comparison with GNIA accounts additionally with a nonlinear material. This material is defined in section 5.5. The influence of the consideration of a linear or a nonlinear material is discussed posteriorly in section 6.4.

This type of analysis will be used to study the ultimate load of the panels.

5.3 Boundary conditions

As previously discussed in section 3.4, three different types of boundary conditions can be distinguished in simply supported panels which are reproduced in the numerical study. Taking into account what was previously referred, when existing, the in-plane constraints of the boundary conditions were applied defining the relative displacements between the points of a same edge as null. This condition forces the edges to remain straight. This was done through keyword **EQUATION* in ABAQUS.

5.4 LOADING CONDITIONS

As previously referred, compression is only applied in the longitudinal direction. In the stiffened panels, unless otherwise stated, the compression force was applied on the transversal edges of the panel including stiffeners through a constant linear force perpendicular to the edges as exemplified in Figure 5.2 *a)*. The effect of applying the load only on the shell as exemplified in Figure 5.2 *b),* is discussed in section 6.3.7.

The out-of-plane load was considered through a uniform distributed pressure acting perpendicularly to the surface of the shells. Furthermore, the pressure was considered to act inwards and outwards, see Figure 5.3 *a)* and *b)*, respectively.

Throughout this document, the centripetal (inward) pressure is represented with positive values and the centrifugal (outward) pressure with negative values. Preference is given to the first situation. However, for comparison purposes, some cases will be

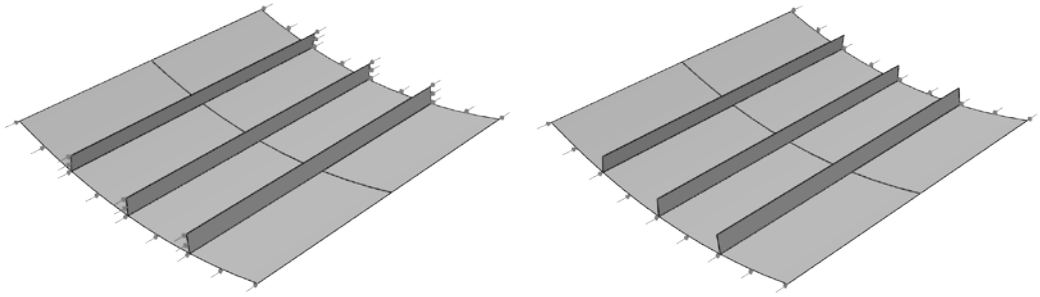

a) *b)*

Figure 5.2: Application of the in-plane compression *a)* on the panel and stiffeners *b)* only on the panel

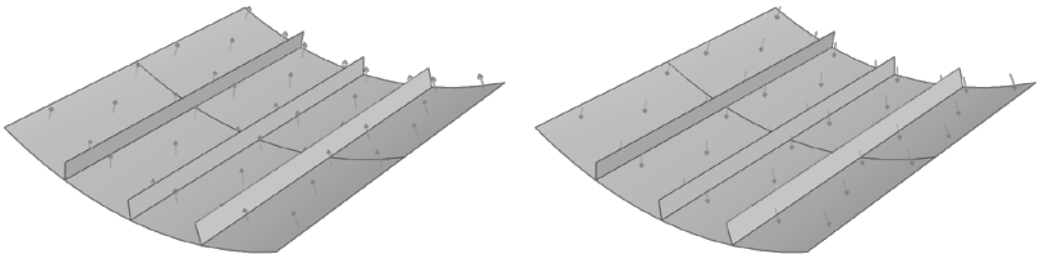

a) *b)*

Figure 5.3: Application of the out-of-plane pressure *a)* inwards *b)* outwards

considered with the latter.

5.5 MATERIAL PROPERTIES

Similarly to the semi-analytical procedure, in LBA and GNIA, the material is assumed to be elastic with a modulus of elasticity (E) of 210 GPa and a Poisson's coefficient (υ) of 0.3.

For the study of the ultimate load in GMNIA, a simplified elastic-plastic material with linear strain hardening is modelled as prescribed in EN 1993-1-5 [1]. The material is assumed with a yield stress (f_y) equal to 355 MPa (corresponding to a S355 steel). From that point, linear strain hardening is considered adopting a slope of $E/100$ and neglecting the yield plateau. Several references based on these assumptions are found in literature (*e.g.* [14], [15]). A further refinement is considered, accounting for the ultimate stress (f_u) equal to 470 MPa. This model is represented in Figure 5.4 and it is introduced in the FE software as true stress-true strain [1].

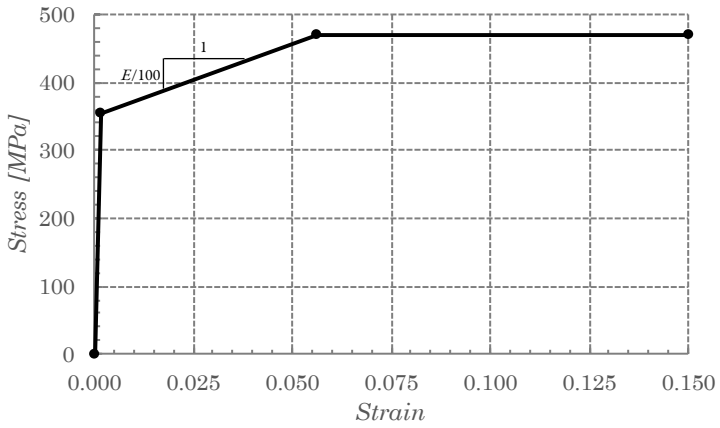

Figure 5.4: Modelling of the material behaviour for GMNIA

In some cases (properly identified), for validation purposes of the ultimate load predicted by the semi-analytical method, a different steel, corresponding to a S235, is used. In this case f_y and f_u are, respectively, assumed with 235 and 360 MPa.

5.6 Type of element and mesh convergence study

Taking into account the high value of the length/width to thickness ratios of the panels, shell elements were chosen, specifically linear four node shell with reduced integration (S4R). S4R is a robust general-purpose element suitable for shell instability problems [120], which is appropriate for the current numerical models, taking into account the mesh discretization and the relative low curvature of the panels in study, meaning that shell elements with more nodes are not justified.

The mesh size of the panels was defined following some principles for the discretization. The elements were assumed to have approximately the same dimensions in both directions, *i.e.* they are close to a square. The minimum number of elements along the stiffener was assumed to be 4. To use an approximate dimension for the surface of the panel and for geometric reasons, it was sought to maintain an integer number of elements between stiffeners, to match the node of the stiffeners with the node of the panel. 96 verifies this condition because it is common multiple of (n_s+1). The number of elements in the longitudinal direction varies respectively with the aspect ratio. This number of elements was assessed through a mesh convergence study and it was concluded that these number of elements coincides with the solution with more elements. This means that increasing the number of elements practically does not affect the results.

5.7 Modelling of imperfections

5.7.1 Introduction

Due to the particular susceptibility of these structural elements to instability phenomena and acknowledging the fact that initial geometric imperfections are of utmost importance in the behaviour of thin-walled structures, a detailed modelling of the imperfections is presented next.

The assessment of imperfections is, still nowadays, one of the most studied subjects in the area of stability analysis of shells. The application of "real" imperfections in the finite element analysis is difficult to implement and they are hardly available for practical designs. Thus the alternative, following studies of authors such as Koiter [62] consists in

applying a pattern of equivalent imperfections in the form of initial deflections perpendicular to the middle surface of the shell. One of the most used hypothesis is to assume this pattern given by the eigenmodes of a perfect element obtained by a linear buckling analysis (LBA). These imperfections, being "equivalent", must cover the effects of other imperfections like load eccentricities, residual stresses, etc. Nowadays, in order to obtain the most unfavourable situation, it is known that multiple eigenmodes and different interactions corresponding to the desired deformation for local and global panel imperfection and stiffeners imperfection should be considered. This is due to the fact that the first buckling mode is not necessarily always the most disadvantageous one [121]. However, as will be discussed throughout this thesis, it was found that eigenmodes, regardless their number, do not lead necessarily to the lowest ultimate loads in comparison with other perfectly admissible imperfections.

However, for comparison purposes, the imperfection from the eigenmodes was analysed for the unstiffened panels. This requires to perform first a LBA, from which the deformed shape of the eigenmodes (generally the first) will be used as an initial imperfection for the subsequent GNIA or GMNIA. This is done in ABAQUS through the keyword **IMPERFECTION*.

Furthermore, with respect to stiffened panels, a clear distinction is made in the standards regarding global and local imperfections of plated structures which requires to differentiate between local, global and stiffener imperfections. However, for a large number of analysis like the ones carried out in this study, the implementation of an automatic process to treat imperfections is desirable. In stiffened panels, the global mode appears sometimes only after tens of eigenmodes. Moreover, in the eigenmodes, the deformation of the stiffeners is combined, in most cases, with the deformation of the panel, which makes it impossible to define the correct amplitude for each type of imperfection separately. Consequently, in this research, imperfections were modelled defining directly the coordinates of the points composing the deformed panel. Although seeking to simulate in some cases the eigenmodes, imperfections were not set directly from LBAs.

EN 1993-1-5 [1] states that an equivalent geometric imperfection may be used and its direction should be the one leading to the lowest resistance. This standard specifies the

Table 5.1: Equivalent geometric imperfections from EN 1993-1-5 [1]

Type of imperfection	Component	Shape	Magnitude
global	longitudinal stiffener with length a	bow	min(a/400;b/400)
local	panel or subpanel with short span a or b	buckling shape	min(a/200;b/200)
local	stiffener or flange subjected to twist	bow twist	1/50

values for the equivalent geometric imperfections specified in Table 5.1. The same standard also states that when several imperfections are combined, a leading imperfection should be considered and the remaining ones may have their values reduced to 70%. This possibility was not considered in the analyses. Similar values to the ones displayed in Table 5.1 are given by DNV-RP-C208 [122] for the equivalent geometric imperfections. These values for the amplitude of imperfections were used for the stiffened panels. Besides that, both unstiffened and stiffened panels were considered in all cases with positive and negative directions for the imperfection. As will be discussed later (in section 6.7), the direction of the imperfection that induces compression on stiffeners is more detrimental in many situations. For reference, the direction of imperfections described in this section is considered as positive when they induce tension on stiffeners and the opposite direction as negative when they induce compression on stiffeners (see Figure 5.6).

Regarding unstiffened panels, besides the referred amplitude, a lower amplitude of min(a/500;b/500) was also considered[5]. The objective is to mark the variation in the ultimate load, taking into account reasonable values for the limits of local imperfections.

5.7.2 Stiffener imperfections

The amplitude for stiffener imperfections has its shape represented in Figure 5.5 and is defined by equation (5.2).

[5] Despite standards usually denominate the imperfection of unstiffened panels as local, because they are usually composing larger elements (*e.g.* a stiffened panel), in fact, if the panel is studied isolated, as posteriorly, the imperfection may be denoted as global.

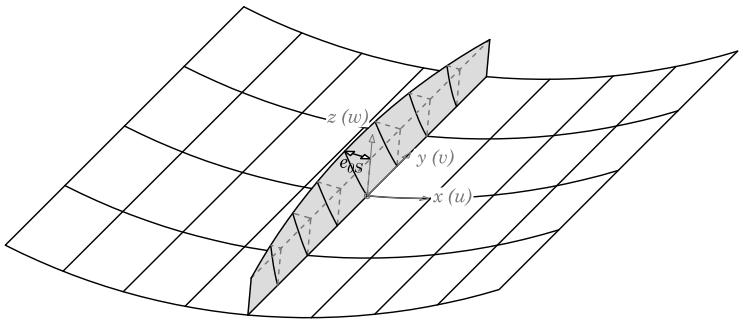

Figure 5.5: Stiffener imperfection and respective amplitude

$$x(y,z) = e_{0s} \cos\left(\frac{n\pi y}{b}\right) \tag{5.2}$$

where the amplitude of the stiffener imperfections, e_{0s}, is given by:

$$e_{0s} = z/50 \tag{5.3}$$

which corresponds to a bow twist of 1/50 and takes the maximum value at the top of the stiffener:

$$e_{0s,max} = h_s/50 \tag{5.4}$$

Conservatively and according to the indications of EN 1993-1-5 [1] a single semi-wave was considered, *i.e.* n=1 in equation (5.2).

This type of deformation is associated with the buckling of the stiffener and it occurs generally when the stiffeners are slender. This imperfection pattern facilitates de development of displacements at the stiffeners.

5.7.3 Global imperfections

The global imperfections correspond to a bow in all the extent of the panel represented in Figure 5.6.

This type of deformation occurs generally when the stiffeners have low inertia (overall buckling mode). The modelling of global imperfections is given by:

$$z(x,y) = e_{0G} \cos\left(\frac{m\pi x}{a_y}\right) \cos\left(\frac{n\pi y}{b}\right) \tag{5.5}$$

where m and n are, respectively, the number of transversal and longitudinal semi-waves,

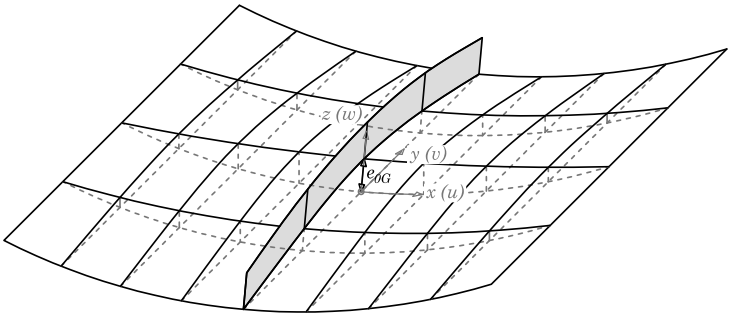

Figure 5.6: Global imperfection and respective amplitude

considered equal to 1, and a_y is the projected width on the x-axis. The amplitude of global imperfections (e_{0G}) is given by:

$$e_{0G} = \min\left(a/400; b/400\right) \tag{5.6}$$

Equation (5.5) corresponds to equation (4.86) defined for the semi-analytical model.

5.7.4 Local imperfections

A subpanel corresponds to the part of the panel between stiffeners as represented in Figure 5.7. The local dimensions which are function of the number of stiffeners are given by equations (3.36) and (3.37).

Based on this, the geometrical properties of the subpanels may be represented by the local aspect ratio, α_{loc}, (function of the local length, b_{loc}, and the local width, a_{loc}) and the local curvature, Z_{loc}, respectively, by equations (5.7) and (5.8).

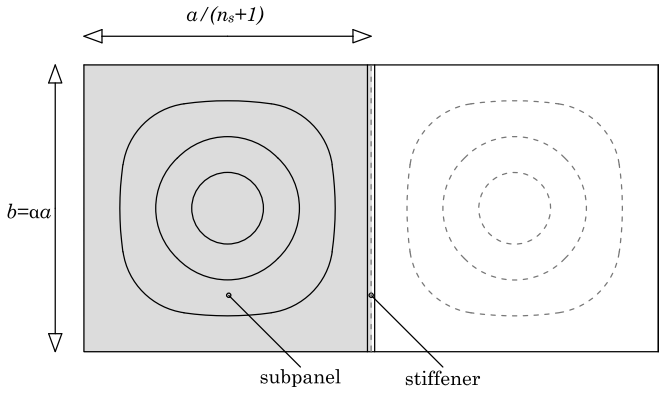

Figure 5.7: Subpanel of a stiffened panel

$$\alpha_{loc} = \frac{b_{loc}}{a_{loc}} = \frac{\alpha a}{a/(n_s+1)} = \alpha(n_s+1) \tag{5.7}$$

$$Z_{loc} = \frac{a_{loc}^{\ 2}}{Rh} = \frac{\left(a/(n_s+1)\right)^2}{Rh} = \frac{Z}{(n_s+1)^2} \tag{5.8}$$

The local imperfections may be reproduced using: *i)* perfect semi-waves; or *ii)* a sum of sines. The latter, may be justified to simulate more complex buckling shapes of the subpanels between stiffeners, for example, in stiffened panels with high curvatures and a small number of stiffeners. These imperfections can be based on the eigenmodes of the equivalent isolated subpanel and they are only possible to be simulated by a sum of sines. Both situations were implemented in the modelling of imperfections and they will be described in the next paragraphs. However, taking into account that stiffened panels present usually large values of local aspect ratio, α_{loc}, and low values of local curvature, Z_{loc}, for the subpanels between stiffeners it is possible to conclude that, in most cases, the deformation of the subpanels in the eigenmodes are very well reproduced by perfect semi-waves. Additionally, based on what was concluded for the isolated unstiffened panels, the perfect semi-waves lead, in a large part of the cases, to lower ultimate loads. Consequently, the patterns for the local imperfections are reproduced by perfect semi-waves as the default case.

This type of imperfections occurs when the stiffeners are sufficiently strong representing nodal lines, as shown in Figure 5.8.

The modelling of the imperfections based on the eigenmodes of the equivalent subpanels is described as follows. The eigenmodes depend significantly on the geometry of the

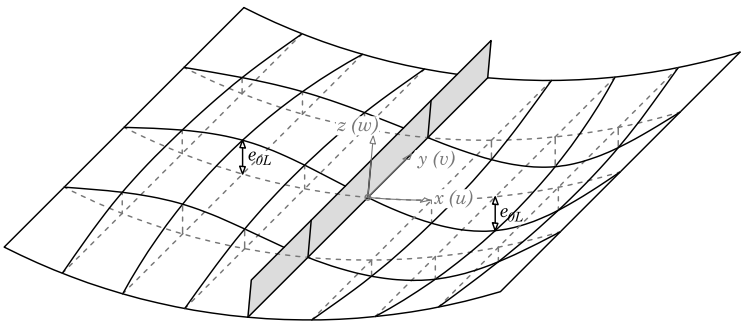

Figure 5.8: Local imperfection and respective amplitude

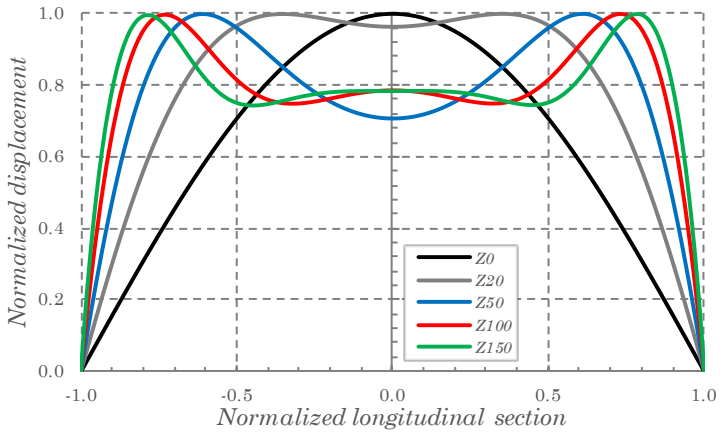

Figure 5.9: Longitudinal section of the first eigenmodes for different curvatures (α=1.0, BCC)

panels and for subpanels with high values of curvature, the eigenmodes cannot be defined by simple sinusoidal functions (see Figure 5.9). In the graph, the central longitudinal section for panel with α=1.0 and BCC is plotted for curvatures up to Z=150. It is seen that while for the flat plate the eigenmode is well represented by a single longitudinal semi-wave, as the curvature increases the maximum displacement approaches the edges and the deformation becomes more complex. The high values of curvature Z=100 and Z=150 are presented to show that for these curvatures, the eigenmodes tend to stabilize for a similar shape. In fact, it was verified that the shape for Z=100 was the one better suited to be used in the modelling of imperfections. For example, in general, for larger aspect ratios, the pattern for Z=100 fits better the deformation of the subpanels than Z=50, which leads to a depression at the centre of the panel not visible in the eigenmodes of the stiffened panels. This will better explained in section 6.2.

Moreover, the pattern of the eigenmodes depends strongly of their aspect ratio as shown in Figure 5.10, where the relative longitudinal displacements of the first eigenmodes are plotted for several aspect ratios and a curvature Z=100. It is possible to verify that as the aspect ratio increases, the deformation tends to be localized close to the edges. Except for the case with α=0.5, the displacements at the central zone of the panels are all very close. This deformation may be considered approximately representative for all boundary conditions.

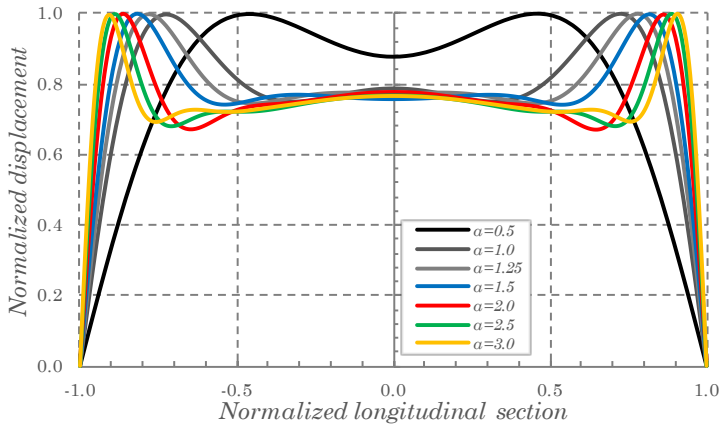

Figure 5.10: Longitudinal section of the first eigenmodes for aspect ratios (Z=100, BCC)

As shown, these complex shapes require the eigenmodes to be approximated by functions given by sum of sines. The adopted procedure uses different equations taking into account the local aspect ratio (of the subpanel between stiffeners). The expressions for these imperfection patterns are presented in Annex A.

Regarding the modelling of the local imperfections by perfect semi-waves, they are defined by:

$$z(x,y) = e_{0L} \cos\left(\frac{m\,\pi\,x}{a_y}\right) \cos\left(\frac{n\,\pi\,y}{b}\right) \tag{5.9}$$

The amplitude of local imperfections (e_{0L}) is given by:

$$e_{0L} = \min\left(a_{loc}/200; b/200\right) \tag{5.10}$$

In all the cases, the number of transversal semi-waves depends on the number of stiffeners, as follows:

$$n = n_s + 1 \tag{5.11}$$

With respect to the number of longitudinal semi-waves, they can be approximated by the number of semi-waves occurring for the eigenmodes of flat plates (equation (2.2) with the transversal semi-wave m=1). Assuming that k_τ has to be equal for n and $n+1$ (point where the curves intersect), the following expression is obtained for α at the intersection point:

$$\alpha = \sqrt{n}\sqrt{1+n} \tag{5.12}$$

or more conveniently the number of longitudinal semi-waves, n, as a function of α:

$$n = \text{Ceiling}\left[\frac{1}{2}\left(-1+\sqrt{1+4\alpha^2}\right)\right] \tag{5.13}$$

The function Ceiling gives the smallest integer greater than or equal to the argument.

The procedure of using a sum of sines was found to approximate reasonably well the eigenmodes given by the LBA. On the other hand, as it will be discussed in Chapter 6, the perfect semi-waves are fundamental because they lead, for a large part of the cases of the corresponding unstiffened panels, to lower ultimate loads, both for short panels (with a single semi-wave) and long panels (with multi semi-waves). Consequently, preference

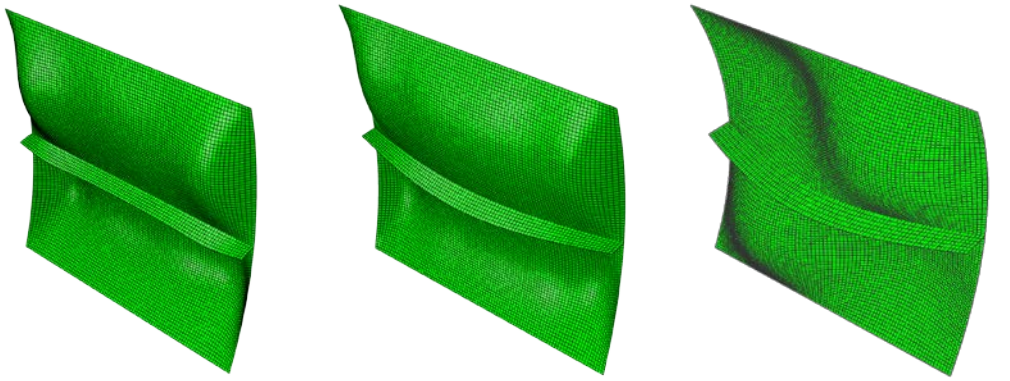

Eigenmode imperfection Modelled imperfection (SS) Modelled imperfection (MPSW)

a)

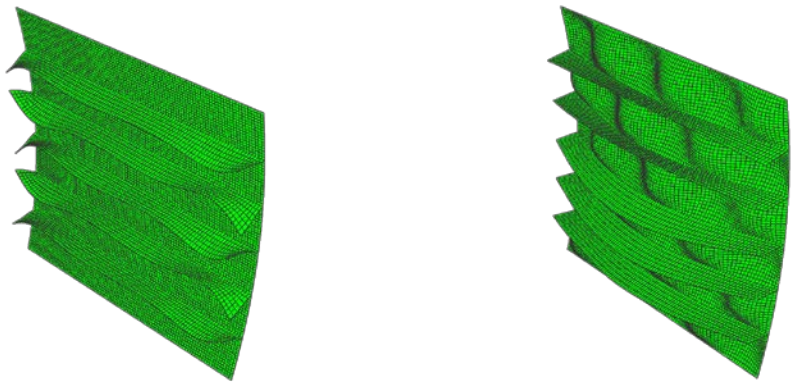

Eigenmode imperfection Modelled imperfection (MPSW)

b)

Figure 5.11: Comparison of the modelled imperfection (SS and MPSW) with the respective eigenmode: *a)* Z=100, n_s=1, α=1.0 and BCC and *b)* Z=50, n_s=5, α=1.0 and BCC (unscaled)

is given to the latter in the posterior parametric study.

In order to exemplify what has been said, in Figure 5.11 several stiffened panels are modelled with different imperfection patterns: *a)* Z=100 with n_s=1 and *b)* Z=50 with n_s=5, both cases for α=1.0 and BCC. It is possible to verify that both the imperfection from the eigenmode (EM) and the imperfection with a local pattern given by the sum of sines (SS) are very similar in case *a)*. However, it should be noted that the eigenmode does not contain the global imperfection, contrarily to the SS imperfection, reason why the deformation of the stiffeners are slightly different. On the other hand, the multi perfect semi-wave (MPSW) imperfection differs considerably from the previous cases on the local imperfections. Additionally, in case *b)* it is visible that the EM is unable to provide a reasonable deformation pattern for the panel because deformations are practically existent only in the stiffeners. Contrarily, the local MPSW imperfection together with the global and stiffener imperfections provides an efficient way to model realistic imperfections in stiffened panels.[6]

5.8 RESIDUAL STRESSES

Residual stresses are present in an unloaded element and they are due to manufacture and fabrication processes. In curved panels, residual stresses are mainly due to the roll bending process and welding.

The residual stresses due to the hot-rolling process are generally neglected in thin slender panels like the one in study. However, they become important for thick, low slenderness sections as shown by Alpsten [123] and Bjørhovde *et al.* [124]. In these studies, the minimum thickness considered is 12.7 mm but the corresponding width to thickness ratio (a/h) is only 12. The distribution of the residual stresses across the width of the studied plates was shown to be parabolic, with compression ($\sigma_{rs,c}$) at edges and tension ($\sigma_{rs,t}$) at the centre. The results of both studies are shown in Table 5.2 where it is possible to see a tendency of increasing magnitude of the residual stresses with the increasing of

[6] The figures are unscaled to facilitate the perception of the different components in the imperfection patterns.

Table 5.2: Effect of hot rolling process in the residual stresses of thick plates based on the studies by Alpsten [82] and Bjørhovde *et al.* [83]

	thickness, h [mm]	**width, a** [mm]	a/h	$\sigma_{rs,c}$ [MPa]	$\sigma_{rs,t}$ [MPa]	$\sigma_{rs,c}/f_y$ [%]	$\sigma_{rs,t}/f_y$ [%]
Alpsten [123]	12.7	152.4	12.0	-69.0	20.7	27.8	8.3
	25.4	508	20.0	-89.6	13.8	36.1	5.6
	50.8	304.8	6.0	-144.8	55.2	58.3	22.2
	88.9	609.6	6.9	-213.7	62.1	86.1	25.0
Bjørhovde *et al.* [124]	50.8	304.8	6.0	-110.3	58.6	44.4	23.6
	88.9	304.8	3.4	-110.3	69.0	44.4	27.8
	50.8	609.6	12.0	-131.0	55.2	52.8	22.2
	88.9	609.6	6.9	-158.6	86.2	63.9	34.7
	152.4	609.6	4.0	-196.5	93.1	79.2	37.5

the thickness of the plates.

The fabrication operation to apply curvature in panels (which are generally obtained from flat plates) through cold roll bending induce mainly circumferential residual stresses varying along the thickness which may be important only for panels mainly loaded in circumferential compression. The longitudinal component of the residual stresses has generally low values and in most cases it is not relevant [125][126].

The welding stresses result from the heat generated that affects the properties of the metal, which lead to differential thermal strains when the material cools. The tensile stresses are due to the thermal contraction of the heated metal close to welds. Taking into account the restraint against free thermal contraction, compression zones are also generated away from the weld. These compression residual stresses are responsible for decreasing the strength of a compressed element because the yielding process is modified.

In welded sections, only longitudinal stresses (parallel to the seam) are of practical relevance, because in the transversal direction residual stresses due to welding have low values and may be neglected [127][128]. Although the panels are usually welded along the edges in both directions, the most relevant situation is the one leading to the residual

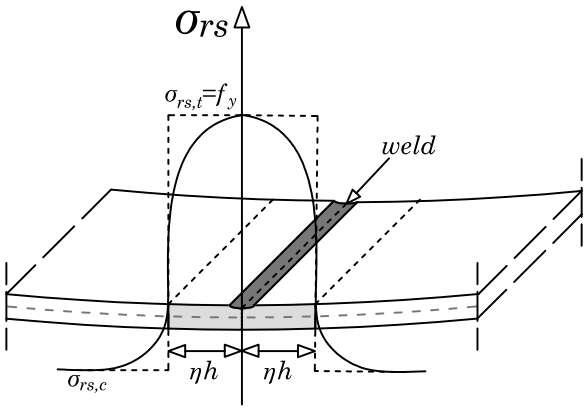

Figure 5.12: Real residual stresses distribution and simplified model

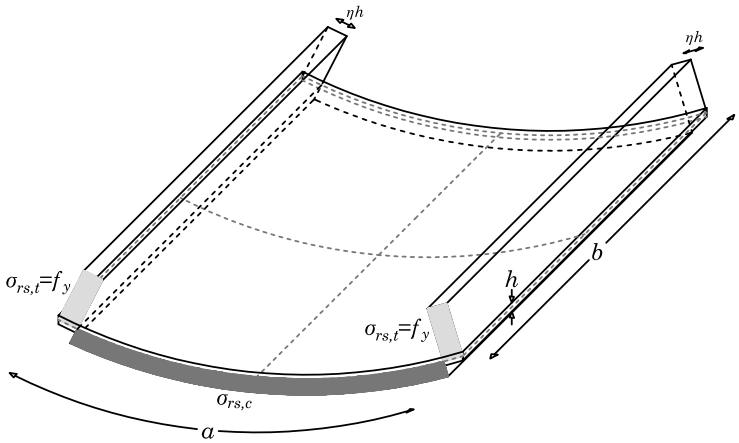

Figure 5.13: Residual stresses configuration for unstiffened curved panels

stresses in the load direction. Taking into account that only uniaxial compression is studied in detail, only the weld on the relevant direction are considered.

The real resulting residual stresses depend considerably on the welding process and input parameters used (*e.g.* heat, size of weld, etc.). For design purposes, the real stress distribution is usually represented by a simpler model with a parallel strip close to the weld with width ηh on each side for the tensile residual stresses with a constant value and in the zone away a constant value for the compression residual stresses, as schematically represented in Figure 5.12. The maximum value of the tensile residual stresses is conservatively considered to be the yield stress of the metal and by equilibrium the value of the residual stresses in the compression zone are determined as shown in Figure 5.13.

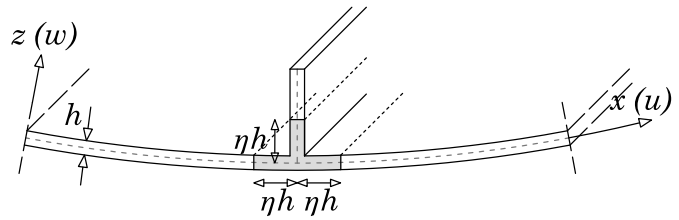

Figure 5.14: Residual stresses configuration for welding of stiffeners

From what has been said, the residual stresses configuration for unstiffened panels may be assumed as presented in Figure 5.13. These residual stresses are parallel to the welds, meaning that the longitudinal welds are the most unfavourable taking into account the considered direction for compression.

In a similar way, when stiffeners are present welds induce tensile residual stresses in parallel strips as represented in Figure 5.14, and compression residual stresses are determined by equilibrium.

According to the bibliography, *e.g.* Faulkner [129], Dubas and Gehri [130] and Ravn-Jensen and Tvergaard [131], depending of the welding process, the value of η, for the strip width of the tensile residual stresses, varies generally between 2 and 6.

Braun [132] performed a thorough study on the stability of steel plates under combined loading. The author considered a rectangular distribution for residual stresses with η=2.25 for the tension stress value equal to f_y.

For the case of stiffened plates, Chen and Guedes Soares [133] calibrated η in function of the yield stress and geometry of the stiffeners and plate using numerical and experimental results.

Consequently, whenever relevant residual stresses are considered in this work a value η=2.25 is assumed.

5.9 FE MODEL VALIDATION

The Finite Element models were validated for LBAs and GMNIAs (with Riks implementation).

Regarding the validation of the LBAs, the results from Martins [15] for unstiffened

Table 5.3: Validation of the numerical model for LBAs for unstiffened panels with Martins [15] in terms of the elastic buckling coefficient, k_σ (α=1.0, a=1.0 m, h=0.01 m)

	Z=0			Z=50			Z=100		
	Martins [15]	**Own FEA**	**Diff. [%]**	**Martins [15]**	**Own FEA**	**Diff. [%]**	**Martins [15]**	**Own FEA**	**Diff. [%]**
BUU	4.0	4.0	0.0%	16.3	16.32	0.1%	33.1	33.24	0.4%
BCU	4.0	4.0	0.0%	17.8	17.78	-0.1%	34.5	34.56	0.2%
BCC	4.0	4.0	0.0%	18.5	18.53	0.2%	35.1	35.12	0.1%

panels are used. The panels have aspect ratio α=1.0 with a width a=1.0 m. The thickness is considered with h=0.01 m and curvatures, Z, with 0, 50 and 100. The load is considered as pure compression. The comparison of the results are presented in Table 5.3, in terms of the elastic buckling coefficient, k_σ.

In the case of stiffened panels, the elastic critical stresses, σ_{cr}, obtained numerically were compared with the results obtained by EBPlate software [134] for flat plates (Z=0) with a=b=2.5 m, h=0.015 m and stiffeners with h_s=0.015 m and d_s=0.15 m. Boundary conditions BCU were considered. In Table 5.4 the results are presented for up to 3 stiffeners. The maximum difference is -4.19%.

The validation of the GMNIAs are done with the results of Martins [15] for unstiffened and Tran [14] for stiffened panels. The same conditions of these numerical models were replicated (geometry, imperfections, material, boundary conditions, etc.). Distinct

Table 5.4: Validation of the numerical model for LBAs for stiffened plates with EBPlate [134] in terms of the elastic critical stresses, σ_{cr} (Z=0, α=1.0, a=2.5 m, h=0.015 m, h_s=0.015 m and d_s=0.15 m, BCU)

	Own FEA [MPa]	**EBPlate [134] [MPa]**	**Diff. [%]**
n_s=0	27.33	27.33	-0.01
n_s=1	112.31	113.64	-1.17
n_s=2	256.78	264.83	-3.04
n_s=3	412.83	430.88	-4.19

Table 5.5: Validation of the numerical model for GMNIA with unstiffened curved panels from Martins [15] in terms of the reduction factor, χ

	Z=0 a=0.462 m b=0.462 m			Z=50 a=0.368 m b=0.921 m			Z=100 a=0.356 m b=1.270 m		
	Martins [15]	**Own FEA**	**Diff. [%]**	**Martins [15]**	**Own FEA**	**Diff. [%]**	**Martins [15]**	**Own FEA**	**Diff. [%]**
BUU	0.738	0.747	1.2%	0.412	0.423	2.7%	0.370	0.385	4.1%
BCU	0.752	0.759	0.9%	0.576	0.591	2.6%	0.512	0.539	5.3%
BCC	0.782	0.787	0.6%	0.580	0.590	1.7%	0.518	0.538	3.9%

boundary conditions were considered in both works: both considered simply supported conditions but the in-plane restrictions along the edges are different.

Imperfections in Martins [15] were given by the first eigenmode with an amplitude of min (a/200; b/200). The compression load is uniform across the width of the plate. The panels have thickness h=0.01 m and curvatures Z= 0, 50 and 100. The width, a, and the length, b, were calculated for a corresponding slenderness, λ, equal to 1.0. The results are compared in terms of the reduction factor, χ, for the ultimate strength in Table 5.5. A maximum difference of 5.3 % is obtained.

In Tran [14], the first global mode from eigenmodes was selected with an amplitude of min (a/400;b/400). The direction of the imperfection chosen in the centrifugal direction (compression induced on the stiffeners). The author considered stiffened panels composed by 8 flat stiffeners with h_s=0.016 m and d_s=0.15 m. The panels have h=0.012

Table 5.6: Validation of the numerical model with stiffened curved panels from Tran [14] in terms of the reduction factor, χ (BCU)

	Z=0			Z=192		
	Tran [14]	**Own FEA**	**Diff. [%]**	**Tran [14]**	**Own FEA**	**Diff. [%]**
α=0.5	16.9	17.81	5%	21.9	20.64	-6%
α=1.0	8.2	7.80	-5%	18.0	17.68	-2%
α=1.5	7.7	7.23	-6%	15.2	15.21	0%

m, a=b=4.8 m and α=0.5, 1.0 and 1.5. Two levels of curvatures were considered, Z=0 and Z=192. From Table 5.6 it is possible to verify that the maximum difference is -6%.

Taking into account the low values of the maximum differences verified for all cases, it is possible to consider the present numerical models validated.

5.10 SUMMARY

This chapter addressed the numerical modelling of the curved panels.

The types of analyses were briefly described and the way they were employed was explained. The assumed options regarding the boundary and loading conditions, the material properties and the type of element and mesh were described.

The modelling of the imperfections and the reason why they were modelled in a thorough manner (contrarily to the default approach of using the eigenmodes) were given. According to the bibliography, it was possible to conclude that the residual stresses due to the hot-rolling process may be neglected for these thin panels. Consequently, only the influence of weld induced residual stresses will be assessed in the next Chapter.

The numerical models were validated allowing its use in the following sections.

6 Characterization of the behaviour and ultimate load of unstiffened and stiffened curved panels under compression and out-of-plane loading

6.1 Introduction

In this chapter, the behaviour of both unstiffened and stiffened curved steel panels under uniaxial compression and out-of-plane pressure is assessed. This assessment is carried out using the Finite Element Method (FEM), through the ABAQUS software as described

in the previous chapter. The objective is to characterize the "real" behaviour of these panels accounting for a variety of imperfections and plasticity of the material, in the most realistic way possible. Consequently, an extensive parametric variation is carried out for all possible parameters, namely curvature, aspect ratio, boundary conditions, and geometry and arrangement of stiffeners, in the case of stiffened panels. The important effect of imperfections is studied in a very complete way.

The results are assessed in terms of the critical behaviour, nonlinear behaviour, through the equilibrium paths and in terms of the ultimate load. With this, it is expected to take useful conclusions in terms of the relevant parameters (curvatures, aspect ratios, level of imperfections, etc.) and understand the way they affect the behaviour of the curved panels.

Firstly, in section 6.2, a brief study on the impact of the geometric parameters on the critical behaviour of the unstiffened and stiffened curved panels is presented. In section 6.3 a preliminary study for the definition of the limits and parameters required to be incorporated in the parametric study is carried out using an elastic material. Next, in section 6.4, the effect of the nonlinearity of the material is introduced and assessed in comparison with an elastic material. The way this affects the equilibrium paths in comparison with the ones using an elastic material is analysed. The effect of residual stresses is addressed in the succeeding section. Its impact on the ultimate load is verified and the need for its use in the numerical analyses is discussed. In sections 6.6 and 6.7, the results of the parametric variation for the unstiffened and stiffened panels, respectively, are discussed in terms of the large deflection behaviour and ultimate load under uniaxial compression. Similar analyses are then performed for the unstiffened and stiffened panels under out-of-plane pressure in sections 6.8 and 6.9, respectively.

The results of the numerical analyses performed in this chapter will be useful in Chapter 7, where the semi-analytical formulation is applied and validated.

6.2 Critical behaviour of unstiffened and stiffened curved panels under uniaxial compression

6.2.1 Introduction

The objective of this section is to present some basic results on the critical behaviour of curved panels which are considered essential for the understanding of some concepts presented in the following sections. As previously referred, the main focus of the thesis is not on the critical behaviour of the curved panels. Consequently, the critical behaviour of curved panels is only briefly described in next paragraphs. The elastic buckling coefficient for unstiffened curved panels was studied in detail by Martins *et al.* [53] [54]. However, unlike these studies, besides unstiffened panels, stiffened curved panels are also addressed here.

The results presented in this section are obtained by FE analyses; however, for validation purposes of the critical load, some comparisons with the semi-analytical model will be presented posteriorly in Chapter 7.

6.2.2 Elastic buckling coefficient

The critical stress, σ_{cr}, of a curved panel may be characterized, similarly to flat plates, by:

$$\sigma_{cr} = k_{\sigma} \frac{\pi^2 E}{12\left(1-\upsilon^2\right)}\left(\frac{h}{a}\right)^2 \tag{6.1}$$

where k_{σ} is the elastic buckling coefficient, which for curved panels accounts with the curvature. The remaining variables were previously defined.

In Figure 6.1 the buckling coefficients, k_{σ}, are plotted for different curvatures and aspect ratios for boundary conditions *a)* BUU, *b)* BCU and *c)* BCC. Curvatures from Z=0 to Z=50 with steps Z=1 and aspect ratios from α=0.2 to α=5.0 with steps α=0.1 are presented. Consequently, a total of 7497 LBAs were performed for the construction of the graphs.

This range of parameters allows to cover most cases of unstiffened curved panels (even as a local panel between stiffeners) with practical significance.

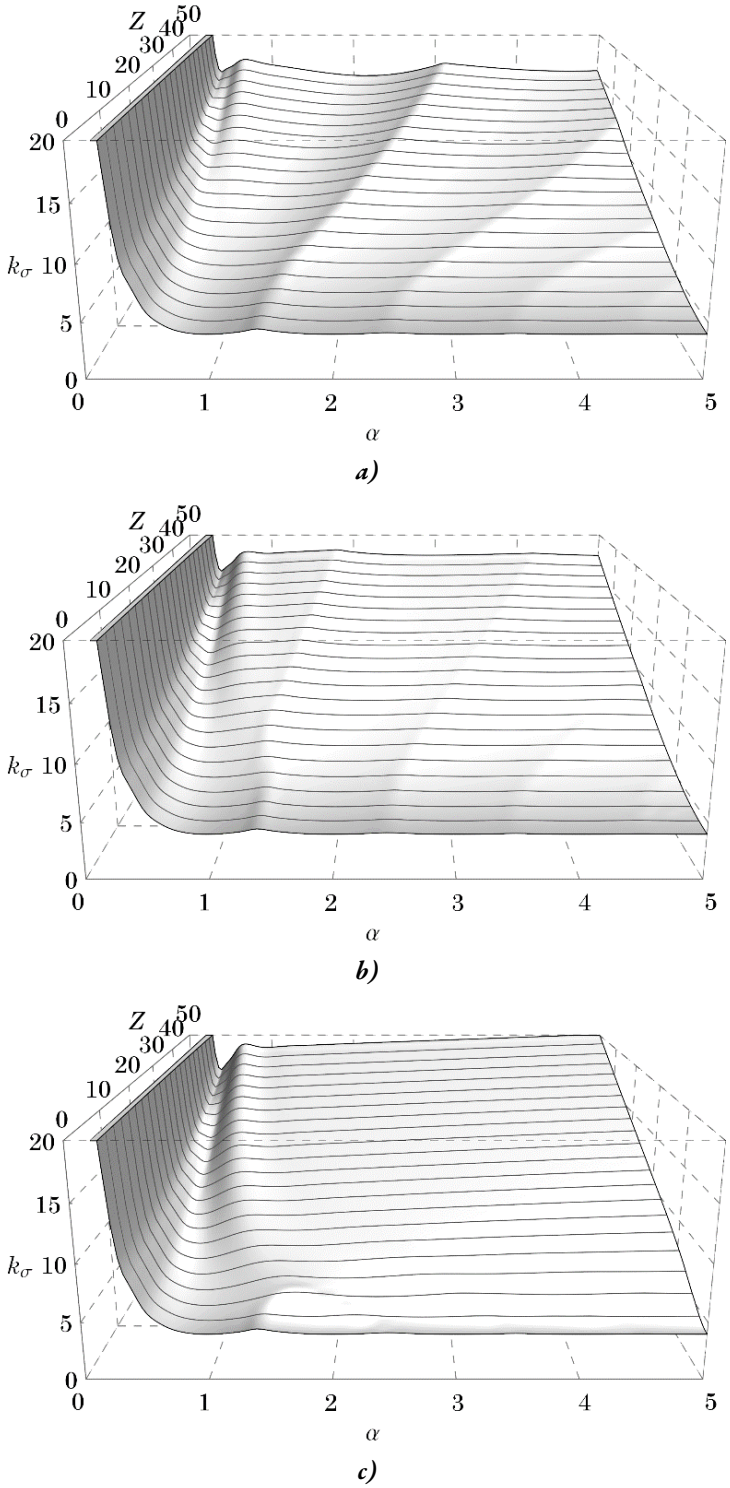

Figure 6.1: Plotting of the buckling coefficients, k_σ, for different aspect ratios and curvatures for boundary conditions *a)* BUU, *b)* BCU and *c)* BCC

The curvature is found to change dramatically the critical behaviour of the panels. It is possible to verify that for flat plates (Z=0) the buckling coefficients, k_σ, are not affected by the boundary conditions. The same is not true for curved panels. When Z>0, the surface given by the values of k_σ is relatively distinct for each type of boundary condition. However, the same tendency is verified, in general: *i)* low aspect ratios (α lower than ≈ 0.5) lead to considerably high values of k_σ, which increase very fast as α approaches 0; *ii)* as the aspect ratio increases, the buckling coefficient tends to stabilize, however local minimums are found along α. This effect vanishes the more restrained the boundary conditions are; *iii)* k_σ increases as the curvature increases with an approximately constant rate. This rate is larger the more restrained are the boundary conditions; and *iv)* k_σ increases as more in-plane restraints are considered for the boundary conditions, *i.e.* in a general way, one can say $k_{\sigma,BUU}<k_{\sigma,BCU}<k_{\sigma,BCC}$.

6.2.3 Effect of the boundary conditions

The influence of the three boundary conditions defined in section 3.4 are now assessed in terms of the elastic buckling coefficients and eigenmodes. In Figure 6.2, the first eigenmodes for unstiffened panels with curvatures Z=0 to Z=100 and aspect ratio α=1.0 for boundary conditions BUU, BCU and BCC (for the rectangular coordinate system) are presented. It is possible to verify that the curvature changes very considerably the first eigenmodes. While for flat and very low curvatures the pattern is well adjusted with a global semi-wave in each direction, for higher curvatures the complexity of the pattern increases significantly. The type of boundary condition changes also the pattern of the eigenmodes. For low curvatures, the differences are small but for Z=30 and Z=50, for example, they are very noticeable.

Still in regard to the boundary conditions, in Table 6.2 the differences in considering the boundary conditions defined in a rectangular or a cylindrical coordinate system (CS) are presented. The values are shown in terms of the elastic buckling coefficient, k_σ, for both coordinate systems and all types of boundary conditions, considering unstiffened panels with α=1.0 (a=b=1.0 m), h=0.01 m and curvatures from Z=0 to Z=100. The difference depends on the central angles which are in function of Z, h and a ($\theta=Zh/a$). The values used for these variables are typical of real geometries and, consequently, the differences

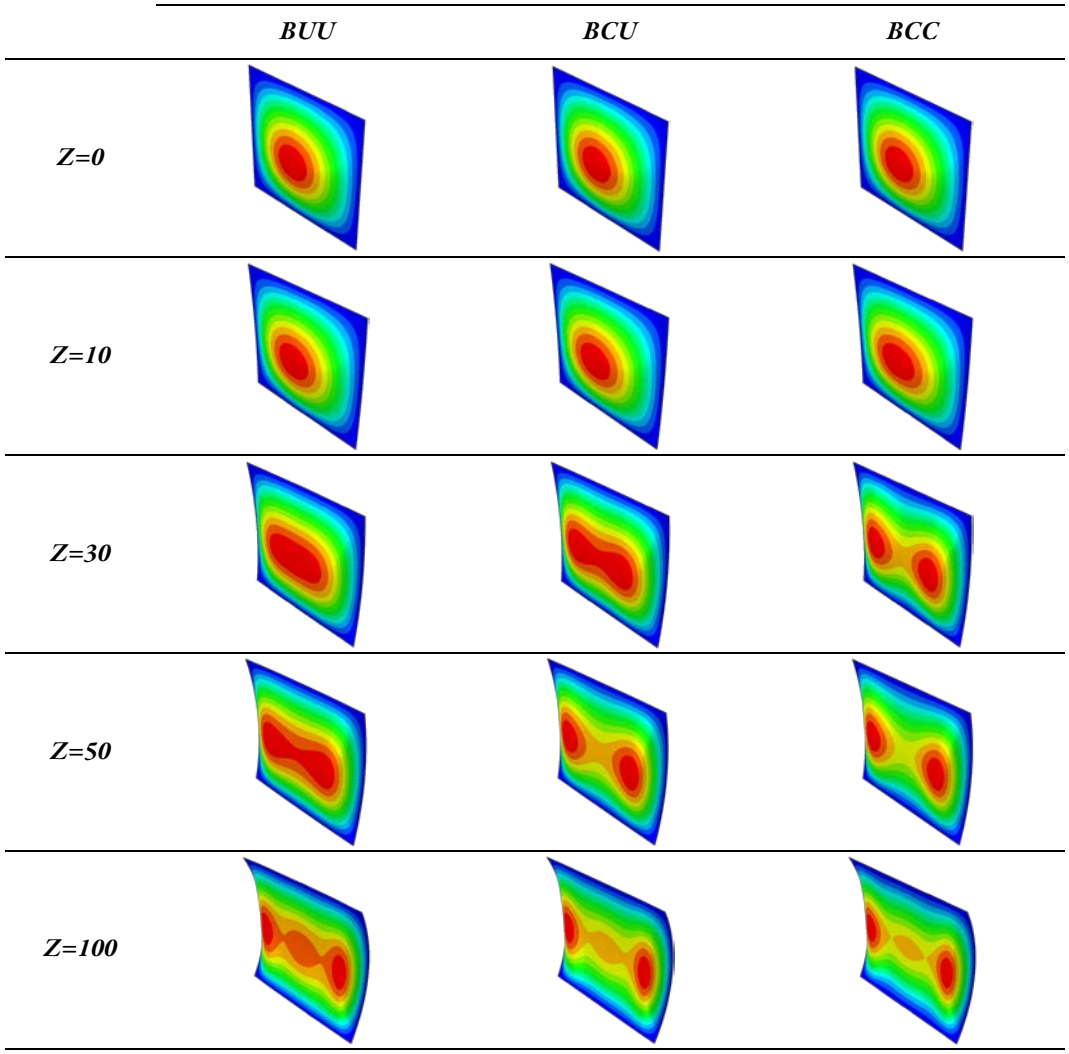

Figure 6.2: Effect of boundary conditions on the first eigenmode (α=1.0, n_s=0 and rectangular CS)

may be considered representative of real curved panels.

The cylindrical CS leads to slightly lower values of k_σ than the rectangular CS. As expected, the differences have the minimum value for Z=0 and the maximum for Z=100. It is verified that the maximum difference on the elastic buckling coefficient between both cylindrical and rectangular coordinate systems is -1.4%, -1.1% and -1.0% for BUU, BCU and BCC, respectively, for Z=100 (a large value of curvature) and a central angle θ=*1.0*. These values allow to conclude that the differences between both coordinate systems may be neglected for the critical load and consequently conclusions may be drawn

Table 6.2: Elastic buckling coefficients k_σ and differences for boundary conditions with rectangular and cylindrical coordinate systems (n_s=0, a=b=1.0 m, h=0.01 m)

		Z=0	Z=10	Z=20	Z=30	Z=40	Z=50	Z=60	Z=70	Z=80	Z=90	Z=100
		(θ=0)	(θ=0.1)	(θ=0.2)	(θ=0.3)	(θ=0.4)	(θ=0.5)	(θ=0.6)	(θ=0.7)	(θ=0.8)	(θ=0.9)	(θ=1.0)
BUU	$k_{\sigma,\,rect}$	4.00	4.79	6.95	9.87	13.02	16.29	19.64	23.03	26.42	29.80	33.18
	$k_{\sigma,\,cyl}$	4.00	4.79	6.92	9.81	12.92	16.14	19.44	22.76	26.09	29.40	32.71
	Diff [%]	0.0%	-0.1%	-0.4%	-0.6%	-0.8%	-0.9%	-1.0%	-1.1%	-1.2%	-1.3%	-1.4%
BCU	$k_{\sigma,\,rect}$	4.00	5.10	7.94	11.27	14.49	17.76	21.11	24.47	27.83	31.17	34.52
	$k_{\sigma,\,cyl}$	4.00	5.09	7.91	11.21	14.41	17.65	20.95	24.27	27.57	30.86	34.15
	Diff [%]	0.0%	-0.1%	-0.3%	-0.5%	-0.5%	-0.6%	-0.7%	-0.8%	-0.9%	-1.0%	-1.1%
BCC	$k_{\sigma,\,rect}$	4.00	5.70	9.21	12.28	15.31	18.52	21.83	25.15	28.46	31.76	35.08
	$k_{\sigma,\,cyl}$	4.00	5.70	9.19	12.24	15.24	18.42	21.69	24.96	28.22	31.47	34.72
	Diff [%]	0.0%	-0.1%	-0.2%	-0.3%	-0.4%	-0.6%	-0.7%	-0.8%	-0.9%	-0.9%	-1.0%

for the critical behaviour of curved panels without specifying the coordinate system considered.

The differences in k_σ due to the type of boundary conditions (BUU, BCU and BCC) are calculated in Table 6.1. Here, the differences are in some cases very important. The larger differences are verified between BUU and BCC and the maximum values occur for intermediate curvatures (Z=20). In this case, BCC shows a buckling coefficient 32.5% larger than the corresponding case for BUU. For flat plates (Z=0), the type of boundary conditions does not affect the value of k_σ (the differences are 0.0%) and for Z=100 the maximum difference is only 5.7%.

Table 6.1: Differences in the elastic buckling coefficient k_σ for boundary conditions BUU, BCU and BCC (n_s=0, a=b=1.0 m, h=0.01 m , rectangular CS)

	Z=0	Z=10	Z=20	Z=30	Z=40	Z=50	Z=60	Z=70	Z=80	Z=90	Z=100
BUU and BCU	0.0%	6.3%	14.1%	14.1%	11.2%	9.0%	7.5%	6.3%	5.3%	4.6%	4.0%
BUU and BCC	0.0%	19.0%	32.5%	24.4%	17.6%	13.7%	11.1%	9.2%	7.7%	6.6%	5.7%
BCU and BCC	0.0%	11.8%	15.8%	8.6%	5.2%	3.7%	2.7%	2.0%	1.4%	0.9%	0.6%

6.2.4 Effect of the aspect ratio

The effect of the aspect ratio both on the first eigenmodes and on the elastic critical buckling coefficient, k_σ, is very notorious. In Figure 6.3, the first eigenmodes for flat and curved panels are presented for different aspect ratios from short (α=0.5) to long panels (α=3.0). It is verified that for large aspect ratios, curved panels present more complex eigenmodes. For the flat case the complexity is the same only the number of perfect semi-waves increases. Consequently, if one wants to model this behaviour by semi-analytical models, the required number of degrees of freedom (see equation (4.85)), is much larger in curved panels than flat plates.

Regarding the influence of aspect ratio in k_σ, it is seen that, in general, short panels ($\alpha \leq 0.5$) show much higher values than a corresponding long panel. However, this tendency is not monotonic, because it has local minimum and maximum values, as previously shown in Figure 6.1. It is well known, that for flat plates the minimum value of k_σ is 4.0. For curved panels this value depends considerably on the curvature.

In Table 6.3 some values of k_σ are presented for panels with different curvatures and aspect ratios (BCC). It is possible to confirm with numerical values that the curvature

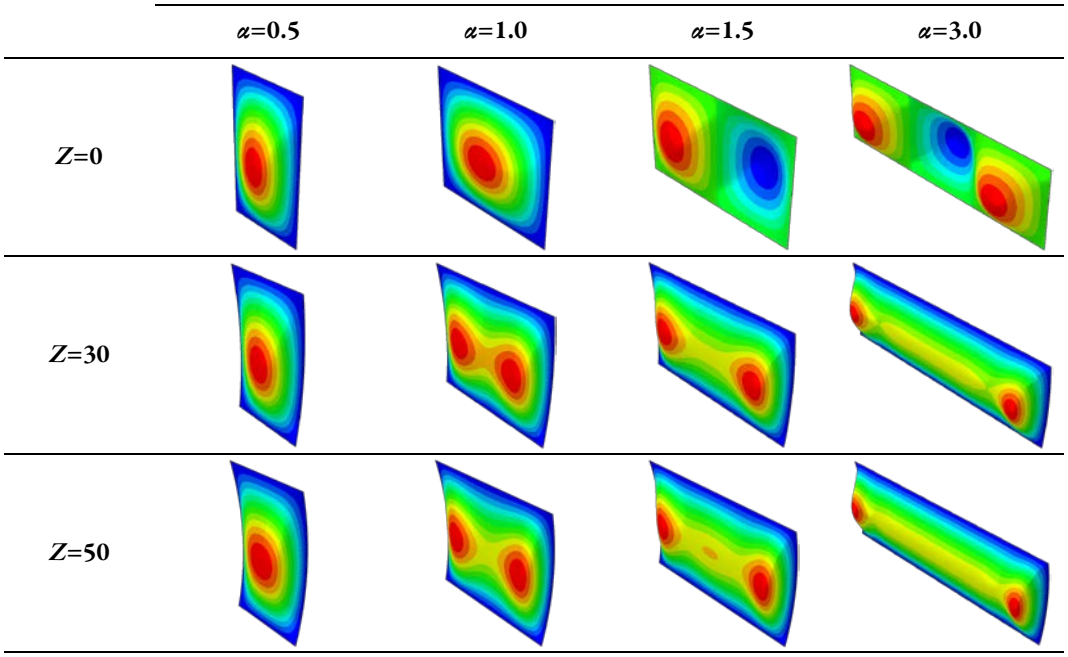

Figure 6.3: Effect of aspect ratio on first eigenmode (BCC, n_s=0 and rectangular CS)

Table 6.3: Elastic buckling coefficient k_σ for different aspect ratios (BCC, n_s=0, rectangular CS)

	α=0.3	α=0.5	α=1.0	α=1.5	α=3.0	α=5.0
Z=0	13.25	6.25	4.00	4.34	4.00	4.00
Z=10	13.43	6.74	5.70	6.64	7.13	7.67
Z=30	14.88	10.52	12.29	12.38	13.07	13.90
Z=50	17.74	17.27	18.53	18.79	19.36	20.09

shows a tendency to increase the values of k_σ for all the aspect ratios presented.

6.2.5 Effect of the curvature

The effect of curvature on the critical behaviour of curved panels has been presented together with the influence of the other variables. As it has been seen, the curvature changes drastically the critical load and the eigenmodes of the panels. Generally, the greater the curvature the greater is the critical load of the panels.

Until now only the first eigenmodes have been discussed; however, despite not showing a large practical interest, for comparison purposes the first 5 eigenmodes of a flat plate and a curved panel (Z=30) are compared in Figure 6.4. As it is seen the eigenmodes can be considerably changed with curvature.

	1st eigenmode	2nd eigenmode	3rd eigenmode	4th eigenmode	5th eigenmode
Z=0	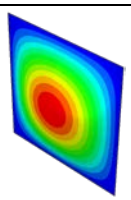	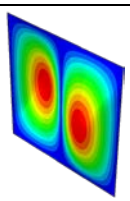	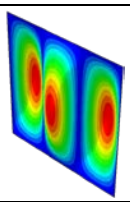	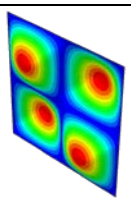	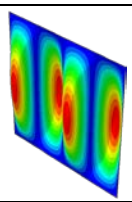
Z=30	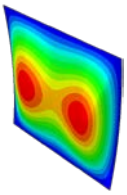	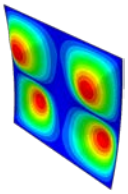	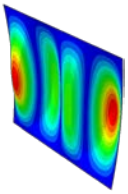	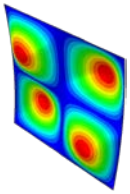	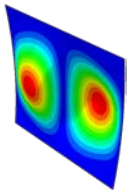

Figure 6.4: First 5 eigenmodes (BCC, α=1.0 and rectangular CS)

6.2.6 Effect of the stiffeners

The effect of the stiffeners is very important both in the values of k_σ and in the eigenmodes. Depending on the second moment of area of the stiffeners, the critical behaviour of these panels is completely changed. If the stiffeners have high second moment of area such that they constitute nodal lines, the panel buckles locally between stiffeners. On the other hand, if the stiffeners have a low second moment of area they will buckle together with the panel. This global buckling is easier to happen the greater the number of stiffeners because the panels approaches an orthotropic behaviour. This phenomenon is shown in Figure 6.5, where the first eigenmode is shown for 1 and 5

	n_s=0	n_s=1		n_s=5	
		low 2nd moment of area	high 2nd moment of area	Low 2nd moment of area	high 2nd moment of area
Z=0	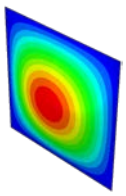	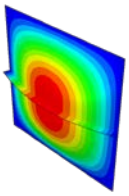	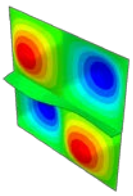	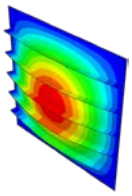	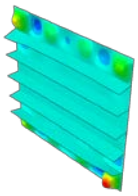
Z=30	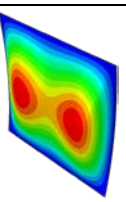	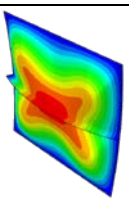	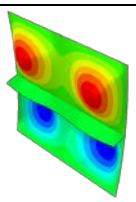	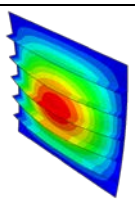	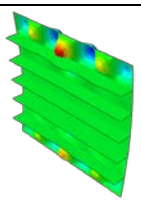

Figure 6.5: Effect of the number and 2nd moment of area of stiffeners on the first eigenmode (BCC, α=1, n_s=0, and rectangular CS)

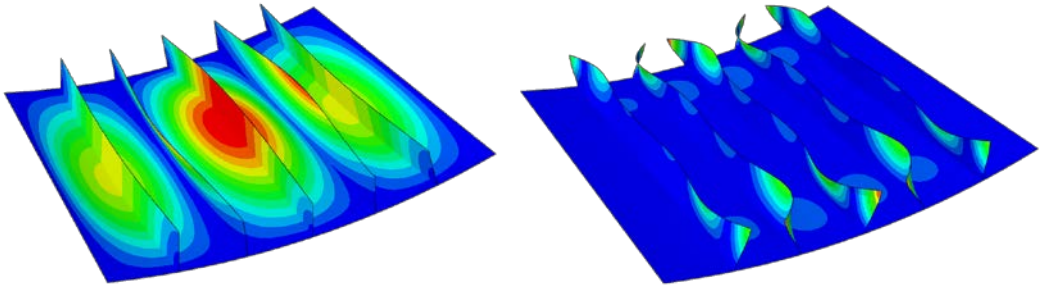

a) *b)*

Figure 6.6: Effect of the load applied *a)* only on the shell; and *b)* the shell and stiffeners. on the first eigenmode (BCC, α=1.0, Z=50 and n_s=5)

Table 6.4: Differences in the critical load, $P_{y,crit}$, and in the elastic buckling coefficient, k_σ when applying the load only on the shell or on the shell and stiffeners (a=b=1 m, h=0.01 m, h_s=0.01 m and d_s=0.1 m)

		Load on the shell		Load on the shell and stiffeners			
	Z	$P_{y,crit}$ [kN]	k_σ	$P_{y,crit}$ [kN]	k_σ	Diff. $P_{y,crit}$ [%]	Diff. k_σ [%]
n_s=1	0	3249	17.12	3438	16.47	-5.5%	3.9%
	30	4634	24.42	4913	23.53	-5.7%	3.8%
	50	5603	29.52	6020	28.83	-6.9%	2.4%
n_s=3	0	14355	75.63	15073	61.09	-4.8%	23.8%
	30	14683	77.36	15235	61.75	-3.6%	25.3%
	50	15300	80.61	15584	63.16	-1.8%	27.6%
n_s=5	0	27902	147.01	20597	72.34	35.5%	103.2%
	30	29429	155.05	20542	72.15	43.3%	114.9%
	50	28077	147.93	20512	72.05	36.9%	105.3%

stiffeners with low and high second moment of area and compared with the respective unstiffened panel. Flat and curved panels (Z=30) are used for comparison. The differences between the flat and curved panels are only in curvature, *i.e.* they have the same dimensions including the stiffeners. It is found that curvature can change significantly the buckling mode, especially for the case with less stiffeners.

Another import aspect is the way as the compression in-plane load is applied, if only on the panel or on the panel and stiffeners simultaneously. Table 6.4 presents the comparison of this aspect in terms of the critical load, $P_{y,crit}$, and in the elastic buckling coefficient, k_σ, for stiffened panels with 1, 3 and 5 stiffeners with a=b=1 m, h=0.01 m, h_s=0.01 m and d_s=0.1 m. Some conclusions may be drawn regarding this aspect. Firstly, when the load is applied also on the stiffeners the critical load is higher for 1 and 3 stiffeners, but not for 5 stiffeners, with significant differences. This is explained by the fact that in the first two cases the buckling occurs on the panel and stiffeners together while on the latter it occurs only on the stiffeners, see Figure 6.6. Despite being an

example, this case shows that the way the load is applied can change dramatically the critical behaviour of the panels. Secondly, due to the difference in the load application area in both cases, while for n_s=3, for example, while $P_{y,crit}$ is smaller when the load is applied only on the shell, k_σ is larger. For Z=50, the maximum difference in $P_{y,crit}$ is -1.8%, while in k_σ is 27.6%.

6.3 Preliminary analysis for the definition of the parametric study

6.3.1 Introduction

The objective of this section is to carry out a preliminary study for the definition of the limits and parameters to incorporate in the extensive parametric study that will be performed in next sections. This will be the first contact with the effect of the parameters on the large deflection of the panels and the aim is to understand the way they influence its behaviour in order to conclude about the need of their consideration. For this objective, unstiffened and stiffened under compression are considered. The parameters evaluated are the effect of the coordinate system, boundary conditions, aspect ratio, curvature and imperfections. The results are presented for some cases carefully chosen with the aim to be representative of the remaining cases. Only axial compression and an elastic material are considered in this phase.

6.3.2 Effect of coordinate system used for the boundary conditions

The influence of the coordinate system (CS) used to define the supports is assessed next in terms of the equilibrium paths. As previously discussed in section 3.4, the curvature of the panel changes the orientation of the supports. This influence was evaluated in section 6.2.3 for the critical loads and a negligible effect of the coordinate system was found. The objective is now to assess if the same is true for the post-critical behaviour of the panels.

From equation (3.34) and (3.38), it is possible to rewrite the central angle in function of the curvature, Z, and width to thickness ratio, a/h, as follows:

$$\theta = \frac{Z}{\left(\frac{a}{h}\right)} \tag{6.2}$$

In fact, the parameter θ is the main responsible for the differences in the results between both coordinate systems (see Figure 3.6).

In Figure 6.7 *a)*, *b)* and *c)*, the equilibrium paths of the panels with curvatures from Z=0 to Z=100 composed by an elastic material are plotted using the FEM for boundary conditions BUU, BCU and BCC, respectively, for rectangular and cylindrical coordinate systems.

The width, a, and thickness, h, of the panels presented in the charts are, respectively, 1.0 m and 0.01 m (*i.e.* a/h=100), which leads to the central angles presented in Table 6.5. The equilibrium paths are obtained considering an initial global imperfection $w_0=a/500$ (a perfect semi-wave in each direction) for aspect ratios, α=1.0. The equilibrium paths are plotted in function of the normalized out-of-plane displacement, δ, at the centre of the panel for the load normalized to the equivalent plastic load, χ, if a yield stress would be used f_y=355 MPa. It should be noted that no yield stress was used in the material law. This value is used only to normalize the load.

From the observation of the results it is possible to draw the following conclusions: *i)* the coordinate system does not change the behaviour of the panels, *i.e.* the equilibrium paths show exactly the same development; *ii)* the effect of the coordinate system is noticeable only on the final part of the curves. The curves obtained for the cylindrical CS are slightly below the ones for the rectangular CS. This effect is only noticeable with the increase in curvature. In fact, the differences for the flat plate (Z=0) are 0%, because both systems are equivalent. In Table 6.5 the maximum differences obtained between both coordinate systems are presented for all BCs. A very small difference is obtained for the worst case, 5.6%, for Z=100, which is already considered a very high value of curvatures. Besides that, the differences for all BCs are very similar. Taking into account that this maximum difference is obtained for a normalized load, $\chi\approx$2.0, one may conclude that in practice (where $\chi\leq$1.0, neglecting strain hardening) the differences may be neglected and the specification of the CS used to model the panels is unnecessary.

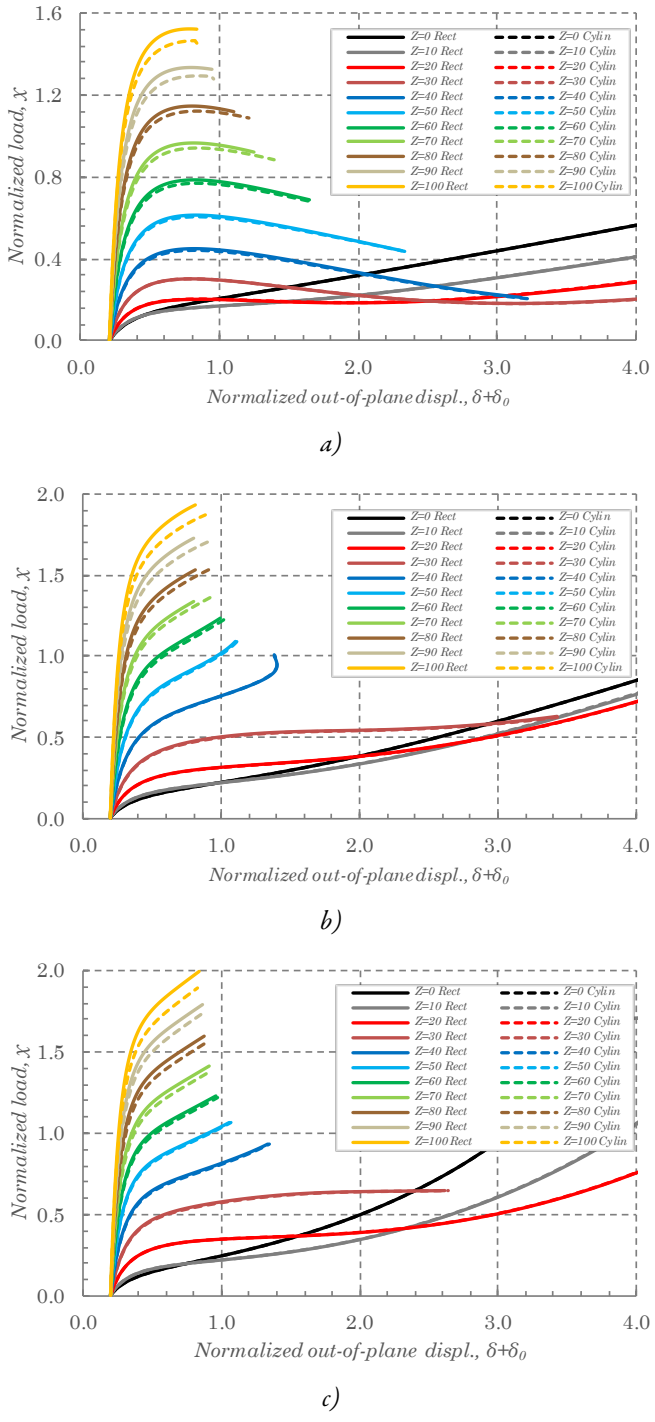

Figure 6.7: Comparison of equilibrium paths for boundary conditions *a)* BUU; *b)* BCU and *c)* BCC with rectangular and cylindrical coordinate systems (a=b=1.0 m, h=0.01 m and w_0=a/500)

Table 6.5: Maximum differences for the normalized load χ for boundary conditions BUU, BCU and BCC with rectangular and cylindrical coordinate systems

	Z=0	Z=10	Z=20	Z=30	Z=40	Z=50	Z=60	Z=70	Z=80	Z=90	Z=100
	(θ=0)	(θ=0.1)	(θ=0.2)	(θ=0.3)	(θ=0.4)	(θ=0.5)	(θ=0.6)	(θ=0.7)	(θ=0.8)	(θ=0.9)	(θ=1.0)
BUU	0.0%	0.1%	0.4%	0.6%	0.8%	1.1%	1.5%	1.9%	2.5%	3.2%	3.9%
BCU	0.0%	0.0%	0.1%	0.4%	0.4%	1.0%	1.2%	2.4%	3.6%	4.3%	5.4%
BCC	0.0%	0.0%	0.0%	0.6%	0.6%	0.9%	1.7%	2.8%	3.5%	4.5%	5.6%

In conclusion, despite not being exclusively dependent of the curvature, but instead of the central angle, the differences presented in Table 6.5, may be considered representative of most cases in practice: *i)* for isolated unstiffened panels, values of *a/h* less than 50 are not very common, even so, a value of θ=1.0 (for which the differences were assessed) implies at maximum a value of Z=50 (see equation (6.2)), which covers most situations in practice; *ii)* for stiffened panels, despite larger curvatures may be possible, larger *a/h* ratios (of the global panel) are equally usual. Assuming a reasonable limit value for *a/h* of 150, a value of θ=1.0 leads to Z=150 which allows to cover equally a large part of curved stiffened panel in real cases.

According to what has been discussed, unless otherwise stated a rectangular CS is used in the analyses along the thesis.

6.3.3 Effect of the boundary conditions

Comparing the equilibrium paths in Figure 6.7 it is possible to conclude that the larger differences are found between BUU and the remaining boundary conditions. In this particular example, the equilibrium paths of the curved panels for BUU, unlike BCU and BCC, are markedly unstable. On the other hand, the same panels show unstable equilibrium paths under BCU and BCC only if smaller imperfections were considered, as will be shown posteriorly in Figure 7.3.

This is justified by the fact that for BUU, due to the in-plane unrestrained edges the equilibrium paths present generally more unstable equilibrium paths, even in situations where larger imperfections are considered.

Other conclusion is that in some cases, like the one in of Figure 6.7, the equilibrium paths of a panel under BCU and BCC are very similar. Reason why in future, when the objective is to draw conclusions about a certain behaviour which is similar in both boundary conditions, the results will be presented in some cases only for one of these boundary conditions. However, this similarity is not verified in all cases. For example, in the same equilibrium paths, a considerable difference is shown for large deflections of the flat plate (Z=0).

The differences between the three boundary conditions are, generally, not negligible and, consequently, all of them would deserve to be studied independently. However, since the practical applicability of BUU is much lower than BCU and BCC, the main focus will be given on these latter ones. Even so, results for BUU will be given only for the sake of comparison whenever relevant.

6.3.4 Effect of the aspect ratio

In order to assess the influence of the aspect ratio, α, a refined variation of the parameter is required. For this, BCC is chosen. Values of 0.5, 0.75, 1.0, 1.25, 1.5, 2.0 and 3.0 are given to α, for curvatures, Z, 0, 10, 20 and 50. A global initial imperfection with a perfect semi-wave in each direction and an amplitude $w_0=a/500$ was considered. The width, a, and thickness, h, of the panels are considered, similarly to the ones in Figure 6.7, with 1.0 and 0.01 m, respectively.

The equilibrium paths for these cases are plotted in Figure 6.8 in function of the normalised out-of-plane displacements, $\delta+\delta_0$. These equilibrium paths are plotted for larger displacements than the ones in Figure 6.7. Analysing the results when larger displacements are considered, the out-of-plane displacement at the centre of the panel starts to follow the inverse direction, *i.e.* a dent starts to appear in the central zone of the panel. This phenomenon is usually accompanied by a decrease in the load and, generally, by the development of even larger displacements in the initial direction in other points of the panel. For even larger displacements, in some cases (see Z=0), the system regains stiffness and the load starts to rise again. This phenomenon is clarified in Figure 6.9, where the equilibrium path in which this phenomenon is more visible (Z=0) is plotted. The curve with α=1.0 is selected. The deformation shapes are presented for several points

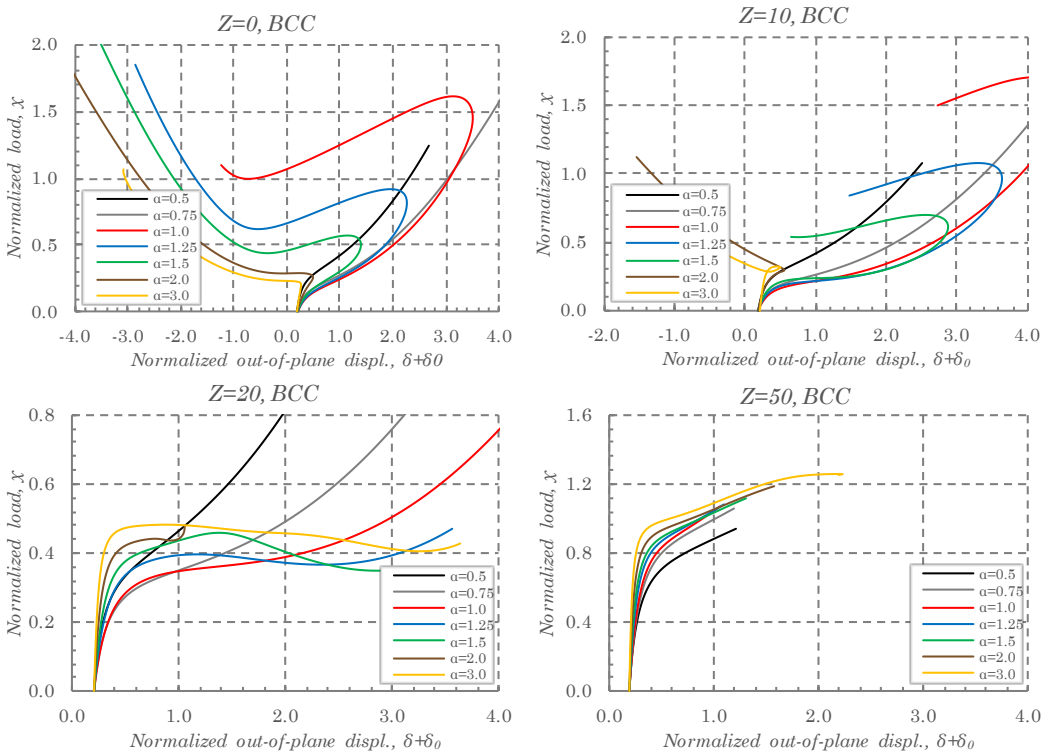

Figure 6.8: Comparison of equilibrium paths in function of the out-of-plane displacement for different aspect ratios (BCC and $w_0=a/500$)

along the curve: point A - χ=0.5; point B - χ=1.0; point C – maximum local for χ; and point D - minimum local for χ. It is visible that the deformation shape passes progressively from 1 semi-wave to 3 semi-waves in the longitudinal direction.

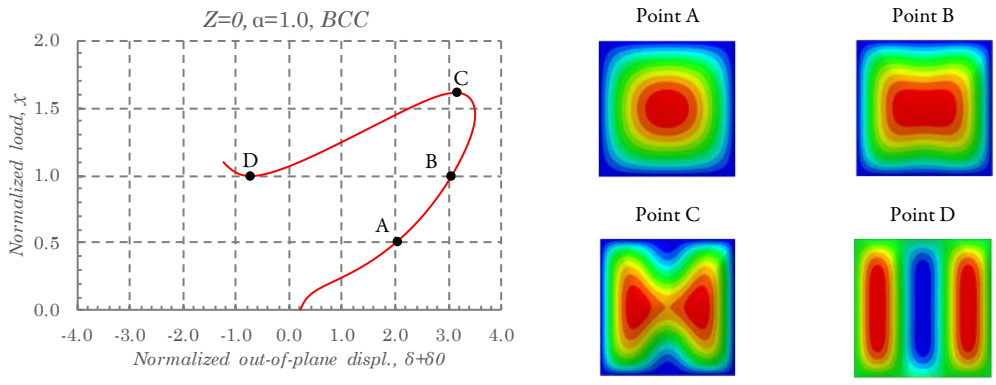

Figure 6.9: Equilibrium path and deformation shapes of a panel with Z=0, α=1.0 (BCC and $w_0=a/500$)

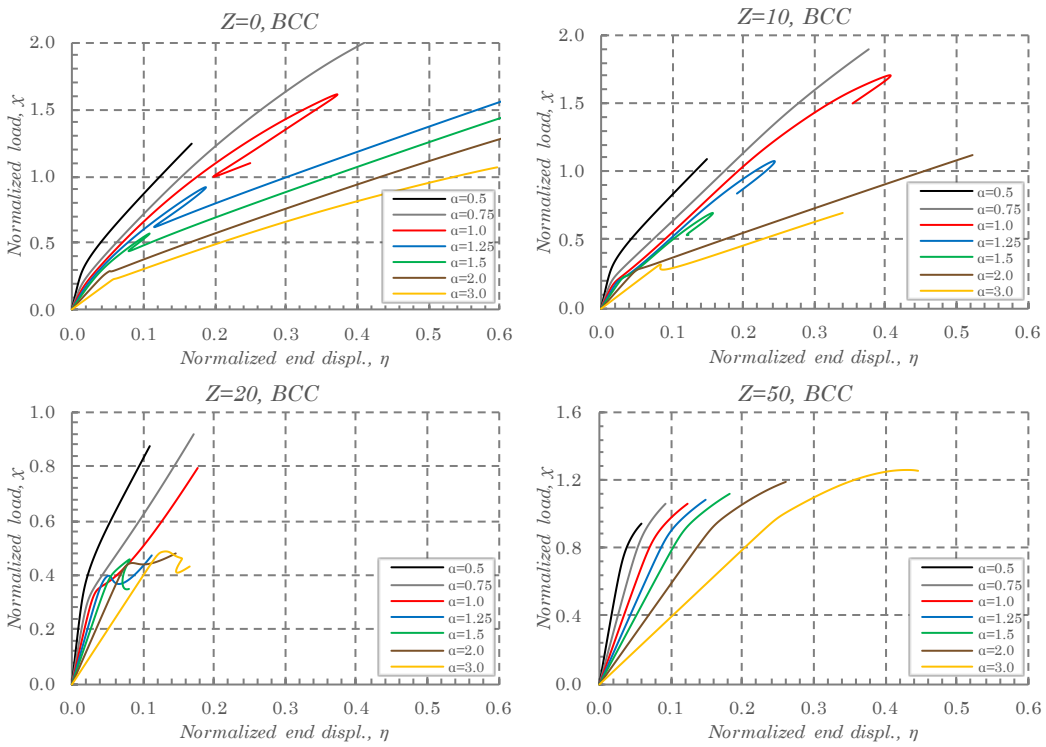

Figure 6.10: Comparison of equilibrium paths in function of the in-plane displacement for different aspect ratios (BCC and $w_0=a/500$)

However, this phenomenon happens more rarely in practice because when the plasticity of the material is considered (unlike this case), as will be seen in section 6.4, the effect of plasticity occurs first and the ultimate load is reached before, in a large percentage of the cases.

This phenomenon is more common in panels with large aspect ratios if a global initial imperfection is considered. This is due to the fact the deformation tends to follow more "natural" deformation shapes. This effect will be further explained in section 6.3.8, where the different types of initial imperfections are addressed.

In general, as the curvature increases, this phenomenon disappears progressively. The curvatures of Z=20 and Z=50 do not show this behaviour for the plotted displacement.

The same results are now plotted in terms of the end displacement normalised to thickness, η, in Figure 6.10. It is possible to verify that the stiffness of the panels decreases as the aspect ratio increases. Besides that, the complexity of the equilibrium paths

decreases as the curvature increases.

6.3.5 Effect of curvature

A preliminary discussion on the effect of the curvature may be done based on the results of Figure 6.7, Figure 6.8 and Figure 6.10. It is possible to verify that the curvature tends to increase the stiffness of the panels, in the initial part of the equilibrium paths. However, this is not verified for larger displacements of panels with lower curvatures. In fact, for $Z \leq 30$, many panels with larger curvatures show larger displacements for the same load level. This is clearly seen, comparing the panels with curvature $Z=0$ and $Z=10$ for BCC, where for $\chi=0.5$ the curved panel shows a displacement about 32% larger than the flat panel.

In Figure 6.11 the normalized loads are plotted for two levels of displacements, $\delta+\delta_{011}=0.5$ and $\delta+\delta_{011}=2.0$ for different curvatures. It is possible to verify that for the first case, there is a monotonic increase of the normalized load with the curvature and this increase is approximately linear from $Z=20$ up to $Z=100$. On the other hand, for $\delta+\delta_{011}=2.0$, there is a drop of the normalized load for $Z=10$ and $Z=20$ in comparison with the flat plate. Only for $Z=30$ the normalized load exceeds the one of $Z=0$.

Although with less practical meaning, for BUU this decrease for larger displacements is verified after a maximum load (with an elastic material) has been reached. In this case,

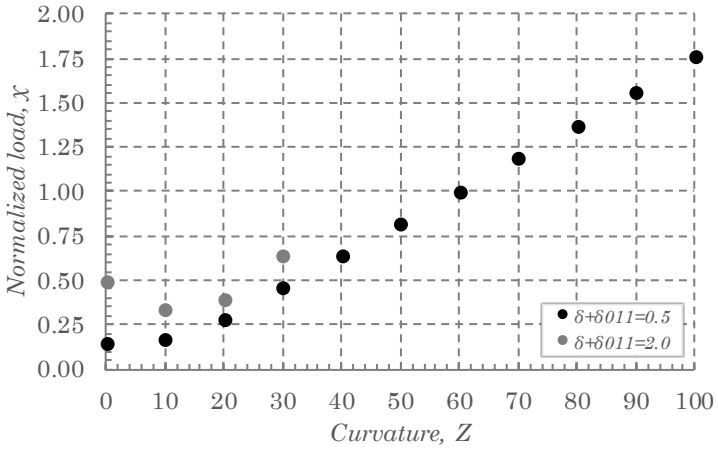

Figure 6.11: Normalized load in function of the curvature for displacements $\delta+\delta_{011}=0.5$ and 2.0

the panels show a negative stiffness crossing the curves of lower curvatures (see Figure 6.7*a)*).

This brief analysis allowed to conclude in a simplified way that the effect of the curvature is very important because it influences significantly the equilibrium paths of the panels. Additionally, this influence is not always very obvious which obliges to study in depth this parameter.

6.3.6 Effect of stiffeners

The effect of stiffeners was already discussed in section 6.2.6 in terms of the critical behaviour. In the same way, besides the number of stiffeners which is a parameter of utmost importance, it is expected that the ratio width to thickness of the local panels between stiffeners (see Figure 3.5), a_s/h, and the height to thickness ratio of the stiffeners, d_s/h_s, influence significantly the post-critical behaviour of stiffened curved panels. The objective is now to define the range of variation for these ratios based on a basic variation of these parameters together with reasonable values of practical interest.

The effect of the local slenderness of the subpanels is assessed in Figure 6.12. In these cases, limit values of 25 and 75 are chosen for the ratio a_s/h. A curved panel with Z=50 is chosen for comparison with the corresponding flat case; in all situations an aspect ratio α=1.0 is assumed. The results are plotted for 1 and 3 stiffeners with d_s/h_s=7.5 and a thickness of 0.01 m is fixed both for the panels (h) and stiffeners (h_s). A global

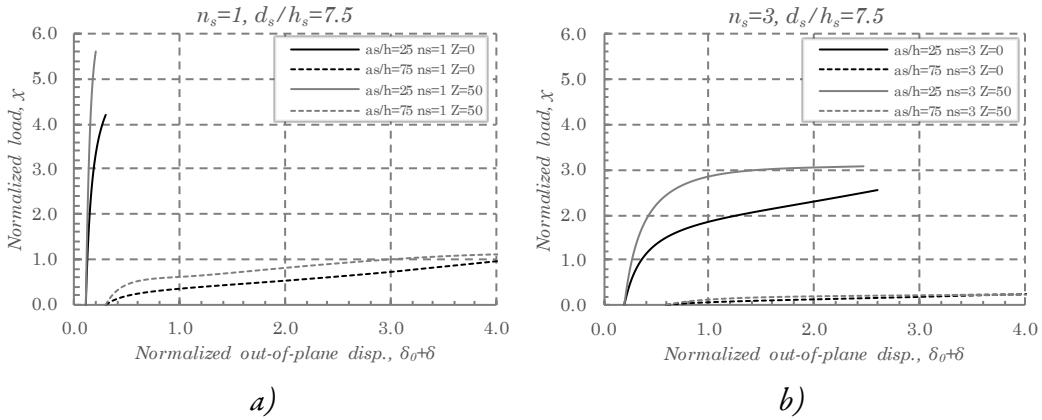

a) *b)*

Figure 6.12: Effect of the ratio a_s/h of the subpanels for stiffened panels with a) 1 and b) 3 stiffeners (BCC, h=h_s=0.01 m, α=1.0, w_0=min(a;b)/500)

imperfection with a single semi-wave in each direction with an amplitude w_0=min(a;b)/500 is assumed. This parameter is shown to influence quite significantly the equilibrium paths. A ratio 3 times larger changes completely the stiffness of the panels, thus providing reasonable limits for the assessment of the behaviour of the stiffened panels. As shown, the curvature of the panel can increase significantly the load for the same displacement.

In Figure 6.13 the equilibrium paths are compared for two values of d_s/h_s, 7.5 and 10.0 for 1, 3 and 7 stiffeners and a_s/h ratios of 25 and 75, as identified in the figure. A curvature of Z=50 is assumed for the curved panel and compared with the respective flat plate (Z=0). It is verified that an increase of 2.38 in the second moment of area of the stiffeners changes besides the equilibrium paths, the mode of deformation of the panels. This is exemplified for the case with n_s=1. For the flat plate, while for the stiffeners with lower second moment of area, a deformation shape close to a global mode occurs, for the stiffeners with higher second moment of area local deformation of the subpanel is

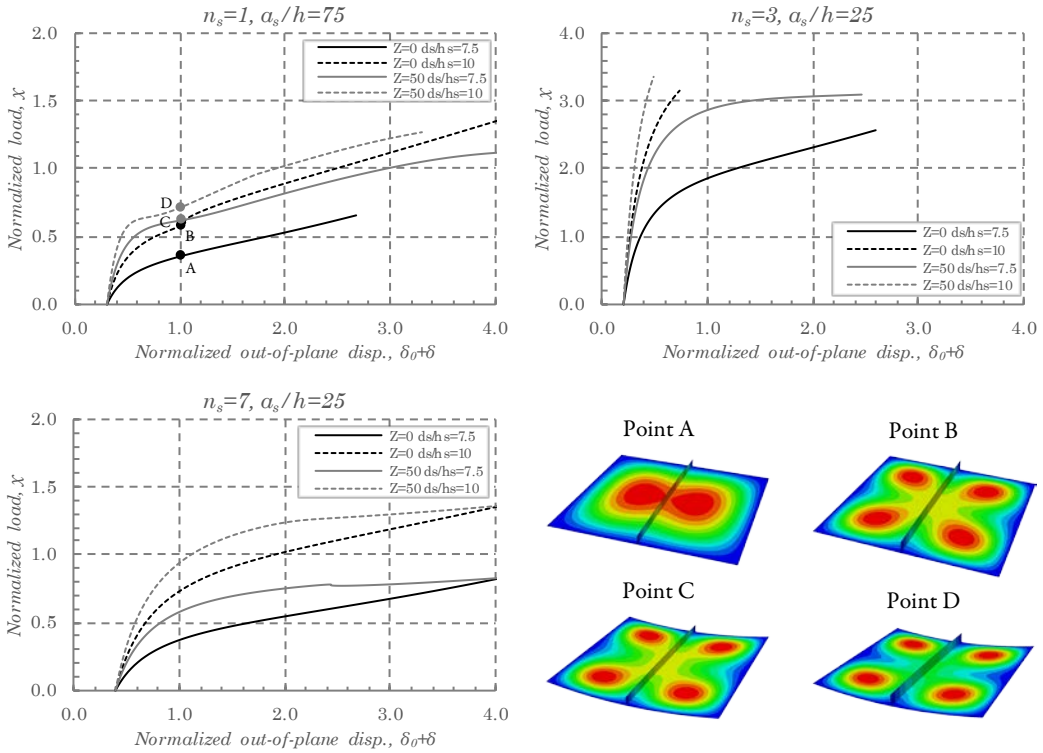

Figure 6.13: Effect of d_s/h_s ratio on the equilibrium paths and deformation shapes for different number of stiffeners and a_s/h ratios

verified, and the stiffeners induce a nodal line on the panel, *i.e.* there is a tendency to decrease the out-of-plane displacement along the stiffener. This is especially true for Z=0. With curvature this difference is not so obvious (see Point A and B for Z=0 and Point C and D for Z=50).

For any number of stiffeners, the effect of the d_s/h_s ratio is very notorious. In fact, this ratio, along with a_s/h, is responsible for the differentiation of global and local buckling in stiffened panels.

Given the significant difference verified in the elastic behaviour, both a_s/h and d_s/h_s deserve an in-depth study in the posterior sections. In comparison with the traditional flat stiffened plates, the effect of curvature is verified to play also an important role on this subject which must be clarified.

6.3.7 Effect of the load applied on the stiffeners

The differences obtained with the application of the in-plane compression load only on the panel and on the panels and also on stiffeners (as exemplified in Figure 5.2.) was found to be significant and consequently some comments should be given. This subject was already addressed for the critical behaviour in section 6.2.6.

The panels are loaded in compression by a stress corresponding to the yield stress, considered f_y=355 Mpa. However, as previously referred, two situations may be distinguished depending where this load is applied: *i)* only on the panel; and *ii)* on the panel and on the stiffeners (see Figure 5.2). Consequently, the applied force, F_{apl}, is given by the multiplication of f_y by the area of application. In Table 6.6, the critical load, F_{cr}, and the F_{cr}/F_{apl} ratio are presented for LBAs. Similarly, the ultimate load, F_{ult}, and the ratio F_{ult}/F_{apl} are presented. All cases are for panels with α=1.0 and BCU. The imperfections were considered as described in section 5.7, modelling the local imperfections with a sum of sines. It is shown that the values of the critical load are always higher when the load is applied also on the stiffeners with the exception of Z=0 and n_s=3. This is explained by the fact that in this case a global eigenmode occurs unlike to the cases with less stiffeners. On the other hand, the values of the ultimate load with the load applied also on the stiffeners lead, in all the studied cases, to higher values for the ultimate

Table 6.6: Comparison of the load applied on the panel with on the panel and stiffeners (α=1.0, d_s=0.15 m and h_s=0.015 m, Positive Imperfections with local SS, BCU)

		LBA						GMNIA					
		Panel		Panel+Stiffeners		Diff. F_{cr}/F_{apl} (%)	Diff. F_{cr} (%)	Panel		Panel+Stiffeners		Diff. F_{ult}/F_{apl} (%)	Diff. F_{ult} (%)
		F_{cr}/F_{apl}	F_{cr} [kN]	F_{cr}/F_{apl}	F_{cr} [kN]			F_{ult}/F_{apl}	F_{ult} [kN]	F_{ult}/F_{apl}	F_{ult} [kN]		
Z=0	n_s=1	0.323	4299.8	0.316	4464.4	-2.0%	3.8%	0.419	5572.7	0.465	6561.1	11.1%	17.7%
	n_s=2	0.758	10088.2	0.723	10784.7	-4.6%	6.9%	0.545	7252.1	0.629	9383.0	15.5%	29.4%
	n_s=3	1.399	18618.9	1.163[7]	18267.7	-16.9%	-1.9%	0.667	8873.7	0.770	12091.1	15.5%	36.3%
Z=50	n_s=1	0.487	6485.8	0.478	6739.4	-2.0%	3.9%	0.479	6381.7	0.486	6853.4	1.3%	7.4%
	n_s=2	0.854	11365.7	0.813	12120.2	-4.8%	6.6%	0.624	8309.8	0.632	9418.9	1.2%	13.3%
	n_s=3	1.458	19413.6	1.345	21126.7	-7.8%	8.8%	0.735	9783.5	0.776	12189.6	5.6%	24.6%
Z=100	n_s=1	0.819	10900.3	0.808	11404.6	-1.3%	4.6%	0.527	7020.5	0.533	7519.3	1.0%	7.1%
	n_s=2	1.115	14838.1	1.048	15621.2	-6.0%	5.3%	0.654	8704.7	0.647	9640.1	-1.1%	10.7%
	n_s=3	1.660	22094.8	1.505	23644.8	-9.3%	7.0%	0.798	10622.8	0.809	12703.4	1.3%	19.6%
Z=150	n_s=1	1.120	14908.7	1.114	15724.2	-0.5%	5.5%	0.575	7651.2	0.584	8241.7	1.6%	7.7%
	n_s=2	1.393	18540.3	1.319	19670.8	-5.3%	6.1%	0.714	9508.3	0.713	10637.9	-0.1%	11.9%
	n_s=3	1.929	25675.8	1.737	27278.2	-10.0%	6.2%	0.843	11217.6	0.844	13251.8	0.1%	18.1%

load. The effect is more noticeable as the number of stiffeners increases. The maximum observed difference in the ultimate load is 36.3% which shows that panels with the same geometry are able to withstand significant different loads depending on whether the load is applied only on the curved panel or also on the stiffeners.

This effect can be explained by the fact that when the load is applied only on the shell it is applied with an eccentricity (relatively to geometric centre) which has naturally an unfavourable effect. This means that considering the situation with the load applied also on the stiffeners may not be conservative for the cases when the load is not applied on the stiffeners. The case with the load applied also on the stiffeners corresponds to the majority of the cases in real situations, reason why unless otherwise stated this is the situation considered in further analyses of stiffened panels.

It should be noted that the differences between F_{ult} are generally higher than F_{ult}/F_{apl}. Even when in some cases the differences in the ratio are negative, the resulting F_{ult} is larger due to the larger cross-sectional area. The same is true for the critical loads.

[7] Corresponds to a global buckling mode, unlike to the cases with less stiffeners.

6.3.8 Effect of imperfections

The effect of imperfections is known to be of utmost importance in the study of shells. Hence, the objective is to assess the type of imperfections needed to be considered in the parametric study.

From what was discussed in section 5.7, in an unstiffened panel only global imperfections are required. The pattern given to this imperfection may be defined: *i)* automatically, from the eigenmodes of LBAs (the default approach in FEA); or *ii)* manually defining the coordinates for every point composing the deformed panel. The first approach has the advantage of being much easier to implement; however the second one provides more flexibility to choose imperfections as desired. In fact, from what was previously seen in section 6.2, some eigenmodes of curved panels present shapes which may be considered as poorly suited for an initial imperfection. Therefore, these imperfections will be compared with imperfections given by perfect semi-waves defined through the coordinates of the panel.

In Figure 6.14 the equilibrium paths of unstiffened panel with Z=0, Z=30 and Z=50 and α=1.0 are plotted for initial imperfections given by the first eigenmode (EM) and by a single semi-wave in each direction (a_{11}). Not less important, is the direction chosen for the imperfection. Additionally, both positive (P) and negative (N) directions are

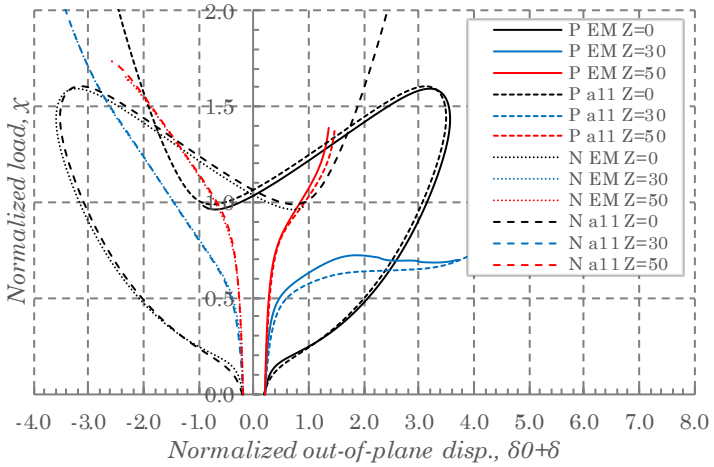

Figure 6.14: Comparison of the equilibrium paths for α=1.0 and different curvature using initial imperfections given by the first eigenmode (EM), single perfect semi-wave in each direction (a_{11}) with positive (P) and negative (N) directions (BCC)

considered for both cases. An amplitude w_0=min(a;b)/500 is assumed in all cases. It is concluded that: *i)* imperfection a_{11} can lead in some situations to equilibrium paths below (*i.e.* lower loads for the same displacement) the ones from EM (compare P a_{11} Z=30 with P EM Z=30 – for $\delta_0+\delta$=1.7, a difference of -14.2% is obtained); and *ii)* the consideration of the negative direction for imperfections changes completely the behaviour of the panels. While for the flat case, the equilibrium paths are completely symmetrical (as expected), in curved panels the development of the equilibrium paths is asymmetric.

In addition to the previous imperfections, an additional imperfection is necessary to be considered for the study of panels with large aspect ratios. This pattern of imperfection is given by multi perfect semi waves in the longitudinal direction.

In Figure 6.15, a flat and a curved panel (Z=30) with α=3.0 are compared in terms of their equilibrium paths for three different imperfections: *i)* first eigenmode (EM); *ii)* a single semi-wave in each direction (a_{11}); and *iii)* three semi-waves in the longitudinal direction and a single one in the transversal direction (a_{13}). Only the positive direction is considered for the imperfections and an amplitude for w_0=min(a;b)/200 is used in all cases. These initial imperfections are also presented in the same figure. It is shown that the initial pattern of imperfections affects significantly the response of the panels. As expected, for Z=0, the imperfections from EM and a_{13} are equivalent for the most part of the equilibrium path. However, while the imperfection EM, at $\delta_0+\delta$=-3.0, starts to develop the displacement in the opposite direction, the imperfection a_{13} continues the displacement in the initial negative direction[8]. This positive variation of the displacement (moving upwards) in EM is explained by a change in the deformation shape. While it had, in the initial phase, 3 longitudinal semi-waves, from that point, it passes, progressively, to show 5 (and eventually to present a positive deformation at the centre of the panel). However, the importance of this phenomenon is reduced in practice, because the yield of the material appears and the ultimate load is reached before. Furthermore, for the curved panel, imperfection a_{13} leads to a rather distinct equilibrium path from the one with EM. Especially relevant is the fact that in the first case the

[8] It should be noted that in these cases (and for Z=30 with a_{13}), positive imperfections lead to initial out-of-plane positions, at the centre of the panels, with negative values.

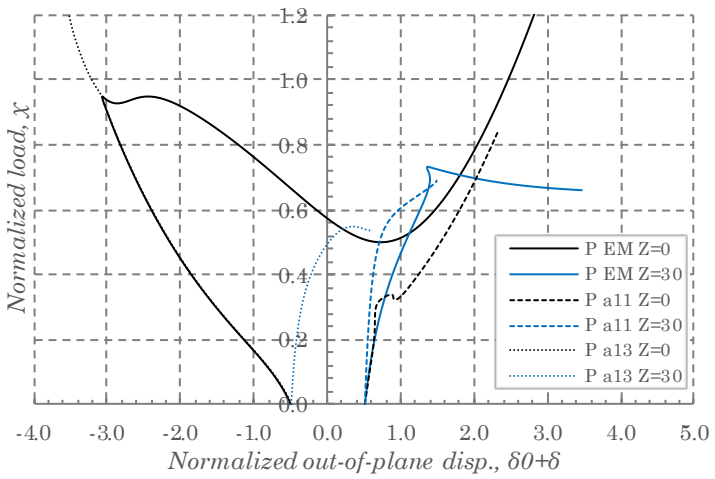

	EM	a_{11}	a_{13}
Z=0	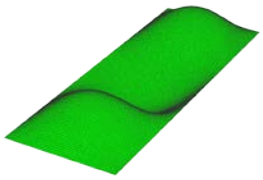	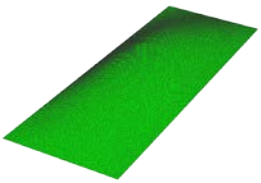	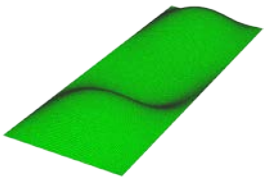
Z=30	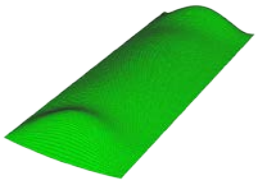	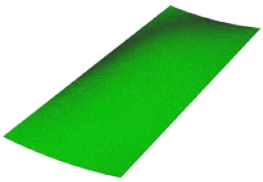	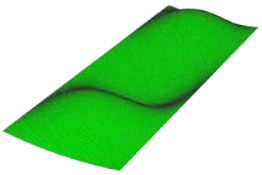

Figure 6.15: Comparison of the equilibrium paths and the respective imperfections for α=3.0 and curvatures Z=0 and Z=30 using initial imperfections given by the first eigenmode (EM), single semi-wave in each direction (a_{11}) and three semi-waves in longitudinal direction and a single one in transversal direction (a_{13}) (a=1.0 m, h=0.01 m, w_0=min(a;b)/200 and BCC)

equilibrium path has a maximum (χ=0.55), while for the second imperfection there is no maximum and the equilibrium path exceeds the that value. This allows to claim that imperfection a_{13} may lead to lower ultimate loads in curved panels, in comparison with the default approach of using EM as imperfections. This will be analysed in detail in section 6.6.

For stiffened panels, as discussed in section 5.7, for a thorough study of imperfections, two additional imperfections must be introduced: local imperfections between stiffeners and imperfections on the stiffeners. The only way to perform this in a systematic way is

using the second approach, defining the coordinates of the deformed panel.

In Figure 6.16*a)* the equilibrium paths of a stiffened panels (n_s=1 with a_s/h=75 and n_s=3 with a_s/h=25, both with d_s/h_s=10.0) are compared to study the effect of introducing imperfections on the subpanels and stiffeners. Thus, a global imperfection (ImpG) is compared with global, local and stiffeners imperfections (ImpGLS). The amplitudes are considered as in section 5.7 with 1/400*min(a;b) for global, 1/200*min(a_s;b) for local and 1/50 for the bow twist on stiffeners. It is possible to conclude that ImpGLS leads to equilibrium paths below the one with only a global imperfection. For the case with n_s=1, for $\delta_0+\delta$=0.6 using only the global imperfection leads to a value of χ 29% larger than considering also local and stiffeners imperfections. For the presented cases with n_s=3 the effect is the same, despite the differences not being so obvious.

In Figure 6.16*b)* the objective is to compare the effect of changing the direction of the imperfections. In this case, panels with n_s=5, a_s/h=25 and d_s/h_s=10.0 are considered. It is possible to verify that changing the direction of the initial imperfection leads to the developments of the out-of-plane displacements in the same direction, *i.e.* the displacements are amplified with the increase in load. Besides that, the equilibrium paths are not completely symmetric which implies that the behaviour is modified. Despite the differences in the elastic nonlinear behaviour are not very obvious for this particular case,

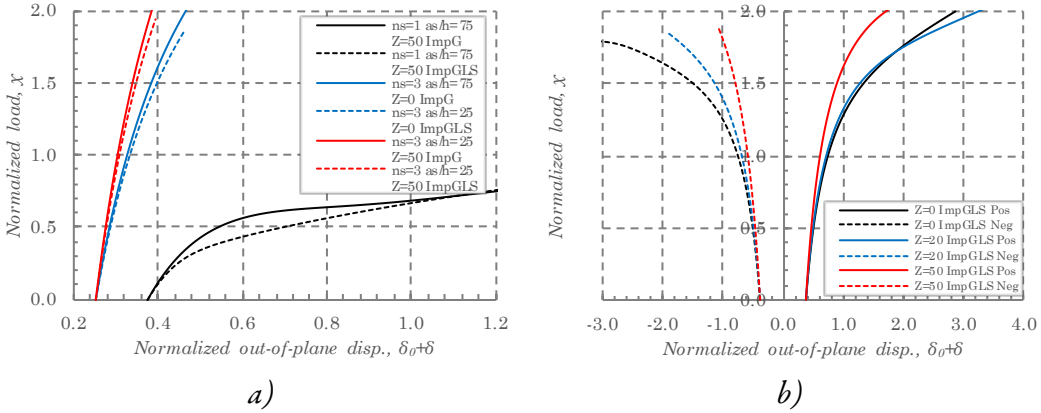

Figure 6.16: Effect of imperfections on stiffened panels: *a)* comparison of only global (ImpG) imperfections with global, local and stiffeners imperfections (ImpGLS); *b)* effect positive and negative directions for panel n_s=5, a_s/h=25, d_s/h_s=10.0 (α=1.0, h=h_s=0.01 m and BCC)

important differences are obtained for the ultimate load as will be discussed in section 6.6 (a reduction of about 24% is obtained in the ultimate load due to the consideration of negative direction for the imperfections).

In conclusion, it is not possible to choose *a priori* the most unfavourable imperfections, as neither of them can be *a priori* neglected. Hence, in the parametric study all of these imperfection will be considered.

6.4 Effect of the nonlinearity of the material

In Figure 6.17 and Figure 6.18 the equilibrium paths for unstiffened panels with BCU and BCC, respectively, are plotted considering an elastic and an elastic-plastic material (as described in section 5.5), allowing to assess the influence of the plasticity of the material on the behaviour of the panels.

The panels are considered with aspect ratios, α, from 0.5 up to 3.0 and curvatures, Z, from 0 up to 50. The width, a, and thickness, h, are 1.0 and 0.01 m, respectively. A global imperfection with a maximum amplitude $w_0=a/500$, with one semi-wave in each direction, a_{11}, is considered. As it is possible to see, the models with elastic-plastic material follow exactly the equilibrium paths of the corresponding elastic material up to certain point where the plasticity starts to occurs. In most cases, the effect of the plasticity takes place very "suddenly", *i.e.* the increase in displacement since the beginning of plasticity up to the point where the ultimate load is reached is usually small. This effect allows the use of strength criteria in semi-analytical models with satisfactory accuracy. Only in very rare cases, this displacement is large with a small increase in load, *e.g.* $\alpha=1.0$ and $Z=20$ for BCC (see Figure 6.18). In these cases, the strength criteria in the semi-analytical method should still be able to predict reasonably well the ultimate load although it may predict smaller corresponding displacements, because it naturally does not account for stress redistribution.

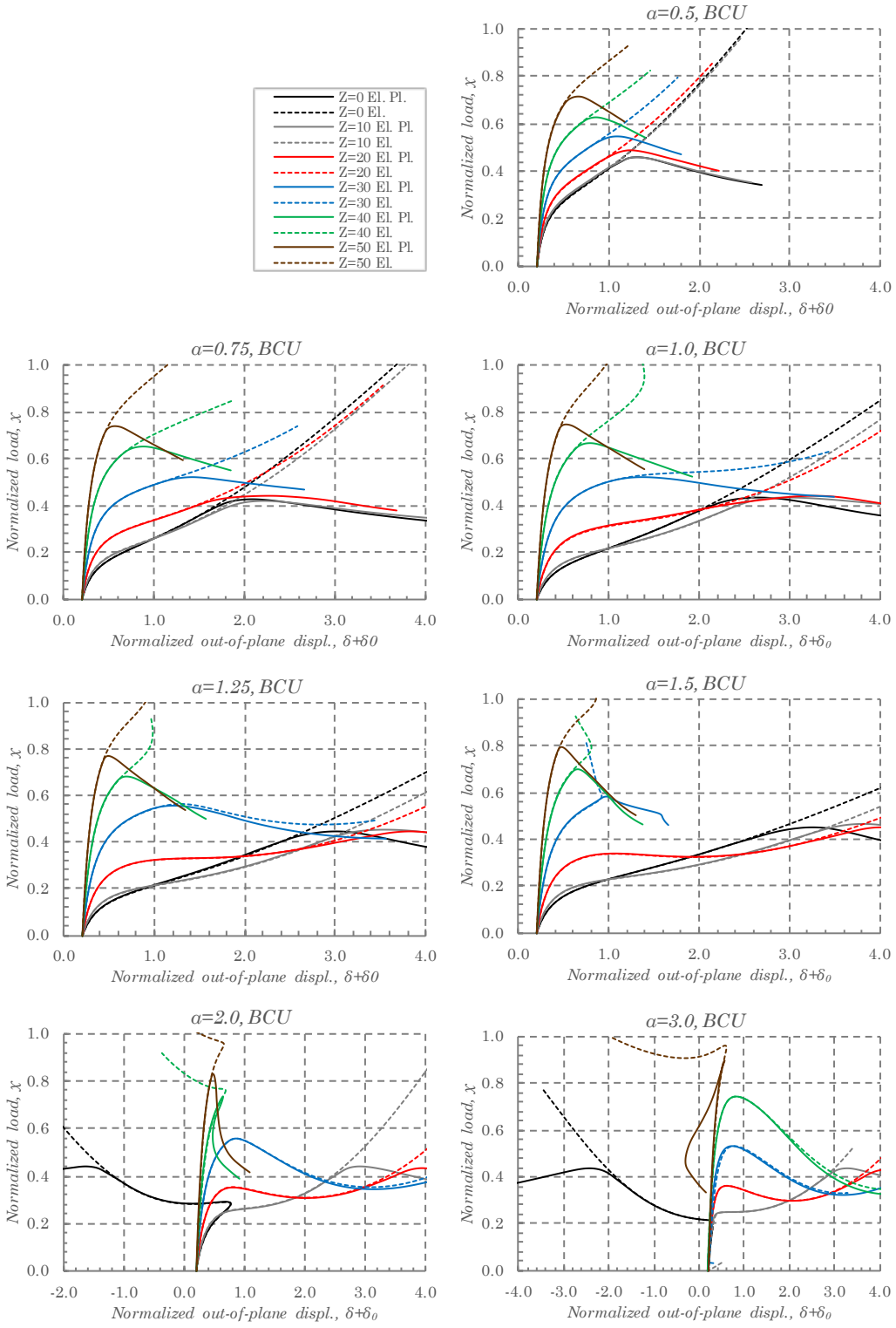

Figure 6.17: Effect of plasticity in the equilibrium paths for unstiffened panels with different curvatures and aspect ratios (global imperfection $w_0=a/500$ with a_{11} and BCU)

Moreover, it is possible to verify that the equilibrium paths for larger aspect ratios, mainly for BCC, become more unstable. In some cases, the direction of the displacement changes and the panel at that point (centre of the panel) deforms in the opposite direction. This is explained by the fact that an initial global imperfection with one semi-wave in each direction was considered and, as the deformation develops, a distinct deformation shape is followed. In fact, it is for the larger aspect ratios that the boundary conditions lead to larger differences in the equilibrium paths.

It is seen that the type of boundary condition may affect importantly the ultimate behaviour of the panels, *i.e.* while in many cases the ultimate load is controlled by elastic stability in BCU, in BCC they become controlled by plasticity. The cases of Z=30 with α=1.25 and Z=40 with α=1.25 are some examples.

6.5 EFFECT OF THE RESIDUAL STRESSES

The modelling of the residual stresses was already explained in section 5.8. Now, residual stresses are applied and its effect is compared with panels without them.

The influence on the equilibrium paths is assessed in Figure 6.19 *a)* and *b)* for unstiffened panels with different curvatures (Z=0, 30 and 50) with a=b=0.5 m and 1.0 m, respectively. The objective is to compare curved panels with different levels of slenderness, λ. Assuming a thickness h=0.01 m leads to panels with width to thickness ratios a/h=50 and 100, for a=b=0.5 m and 1.0 m, respectively. This range of curvatures and width to thickness ratios seeks to cover panels with practical application. An imperfection pattern from the first eigenmode is used for an amplitude w_0=a/500. The equilibrium paths are also plotted for the material without plasticity to comparison proposes. As expected, the cases with material plasticity follow exactly the same equilibrium paths up to plasticity begins to take place. In those points the ultimate load is generally reached for small increases in load. The introduction of the residual stresses leads to an earlier appearance of plasticity and slightly lower ultimate loads are obtained.

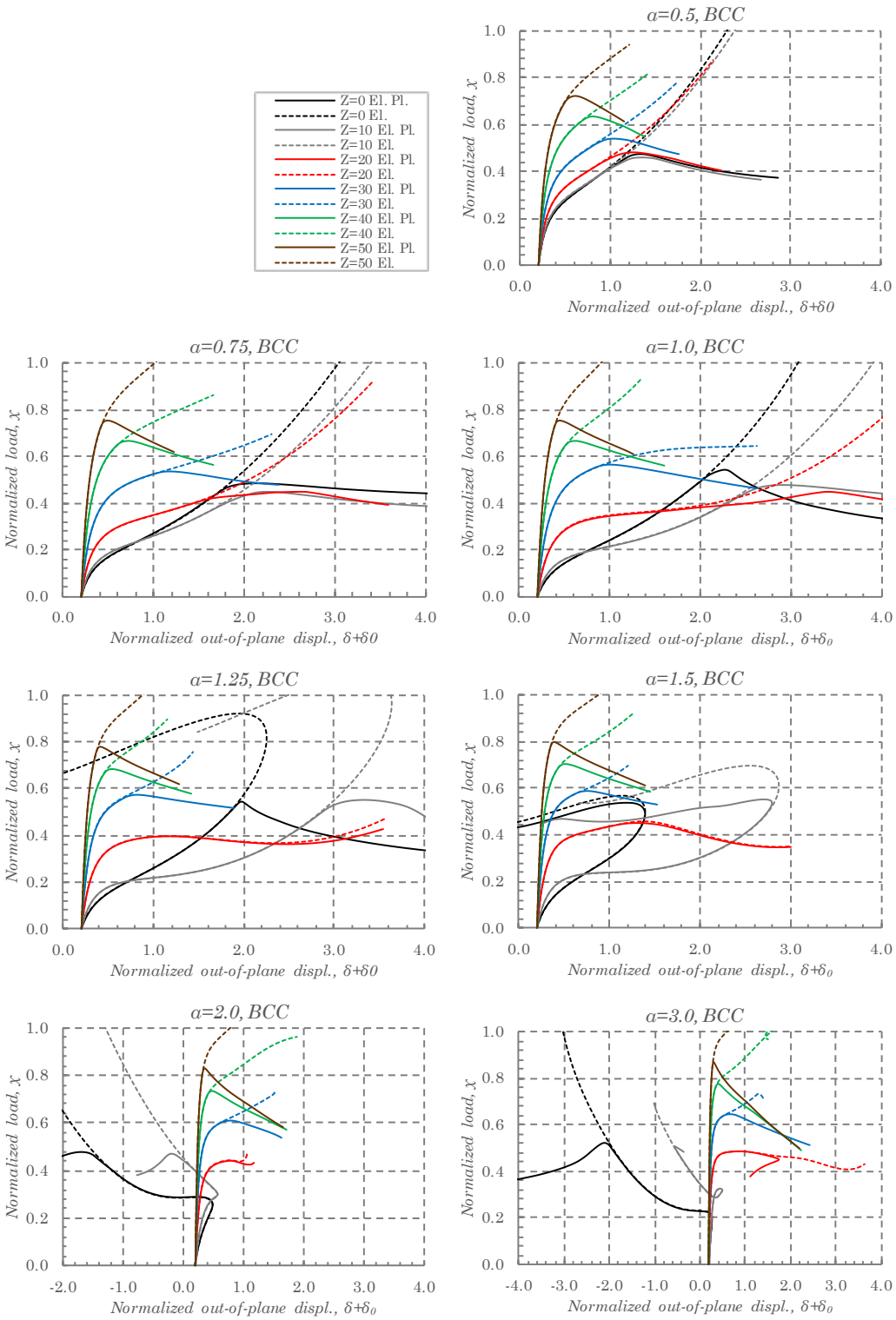

Figure 6.18: Effect of plasticity in the equilibrium paths for unstiffened panels with different curvatures and aspect ratios (global imperfection w_0=a/500 with a_{11} and BCC)

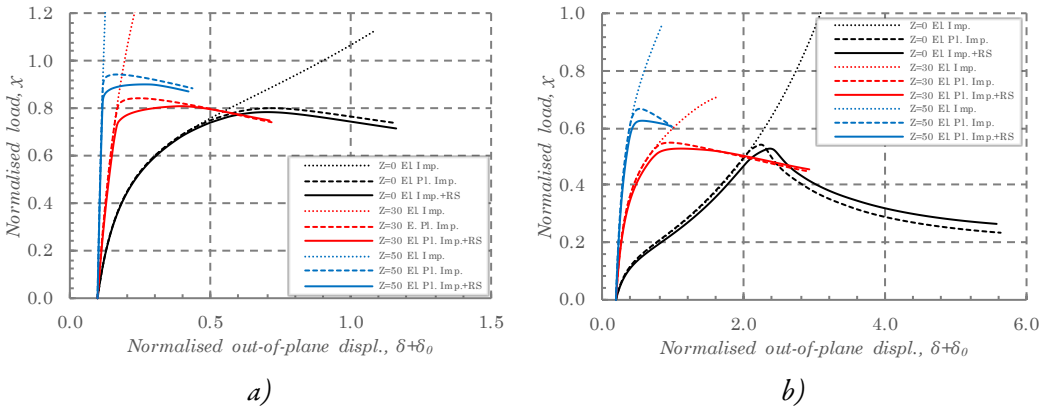

Figure 6.19: Effect of the residual stresses in the equilibrium paths for unstiffened panels with different curvatures: *a)* a=b=0.5 m and *b)* a=b=1.0 m (h=0.01 m, w_0=a/500 with imperfection pattern from 1st eigenmode and BCC)

The corresponding ultimate load is compared in Table 6.7 for the case with w_0=a/200 which may be used as an equivalent imperfection amplitude to obviate taking into account explicitly residual stresses. The maximum difference between the ultimate load obtained with and without residual stresses (with an amplitude w_0=a/500) is 6.2% for Z=50. For Z=30 the maximum difference is 5.0% for the panel a=b=0.5 m which has a low value of slenderness, λ=0.62. The values using an imperfection amplitude w_0=a/200 lead in all cases to lower values of ultimate load than using w_0=a/500 with residual stresses, with the exception for Z=0 and a=b=1.0 m. In this case, all values of ultimate load are very close. In fact, the reduction obtained using an imperfection 2.5 times larger, w_0=a/200, in comparison with w_0=a/500 is very small, χ=0.536 *vs* χ=0.540. For these values of slenderness, the panels show low sensitivity to imperfections. If residual stresses are incorporated χ=0.530. As expected for a panel with this high slenderness value, imperfections become less important.

In general, it is possible to conclude that for unstiffened panels the influence of residual stresses is not relevant, even for large values of curvatures and relatively small width to thickness ratios, and, consequently, the approach to use an equivalent imperfection to account for geometric imperfections and residual stresses in a simplified manner, is justifiable. The same conclusions have been obtained for flat plates by many authors, where the equivalent imperfections have been considered as sufficient [132].

Table 6.7: Effect of residual stresses on the ultimate load of unstiffened panels (imperfection pattern from the 1st eigenmode from LBAs and BCC)

	$a=b=0.5$ m					$a=b=1.0$ m				
Z	λ	χ_{imp} $a/200$	χ_{imp} $a/500$	χ_{imp} $a/500+RS$	Diff. [%]	λ	χ_{imp} $a/200$	χ_{imp} $a/500$	χ_{imp} $a/500+RS$	Diff. [%]
0	1.08	0.750	0.797	0.787	1.3%	2.16	0.536	0.540	0.530	1.7%
30	0.62	0.712	0.846	0.805	5.0%	1.23	0.497	0.549	0.530	3.7%
50	0.50	0.858	0.942	0.903	4.4%	1.00	0.575	0.665	0.626	6.2%

Consequently, residual stresses are only considered if their particular influence is to be assessed and otherwise stated they are not taken into account for unstiffened panels.

Residual stresses in stiffened panels assume, generally, greater importance than in unstiffened panels due to the larger quantity of welds (of the stiffeners) and because the width to thickness ratio of the subpanels, a_s/h, take usually smaller values. However: besides *i)* the modelling of residual stresses for such a large number of cases as carried out in next sections is more cumbersome in stiffened panels; *ii)* its benefit is not always justifiable because equivalent geometric imperfections are a reasonable and more practical alternative providing good predictions of the ultimate load. Reason why the default approach in flat stiffened panels has been usually to incorporate the effect of the residual stresses in the equivalent geometric imperfection.

6.6 LARGE DEFLECTION BEHAVIOUR AND ULTIMATE LOAD OF UNSTIFFENED CURVED PANELS UNDER UNIAXIAL COMPRESSION

6.6.1 Introduction

This section presents the parametric study carried out with FEM for the unstiffened curved panels under compression. The objective is twofold: *i)* to categorize the behaviour of unstiffened curved panels and conclude through an extensive number of results about the influence of geometric parameters, boundary conditions and imperfections; and *ii)*

to serve as basis for the validation of the semi-analytical method developed in Chapter 4. The results will be analysed in terms of the large deflection behaviour and ultimate strength.

The variation in geometry is done through the variation of curvature, Z, the aspect ratio, α, and width to thickness ratio, a/h. The values of Z are varied from 0 to 50 with steps of 10. These curvatures allow to cover most cases of practical applicability both in isolated unstiffened panels and local panels in stiffened panels (between stiffeners). For example, for local unstiffened panels in bridges the average value for the maximum limit of curvature is Z=15 [135]. In a similar way, the aspect ratio is varied to take into account not only isolated unstiffened panels but also local panels composing stiffened panels. Consequently, not only short panels with a low value of α (not unusual in isolated panels) but also long panels with considerably large values of this parameter (typical of local panel between stiffeners) are considered. The variation of the aspect ratio is 0.5, 1.0, 1.5, 2.0, 3.0, 5.0 and 7.5. The width to thickness ratio, a/h, is also an important parameter since it is the main responsible for defining the slenderness of the panel. In this case, this ratio is varied from 50 to 150 with steps of 25, thus covering from relatively stocky to slender panels. When performing the parametric variation for the stiffened panels, in section 6.7, a lower value of 25 will be given to the local width to thickness ratio of the panel between stiffeners, a_s/h, value which may be found in local panels between stiffeners but rarely in isolated panels. The thickness of the panels, h, can be fixed since a/h is varied, *i.e.* the change in slenderness is done with the change in the width of the panel. Consequently, h is fixed in most cases with 0.01 m. However, in some additional cases, a value of h=0.016 m is used to spot possible differences arising from the use of thicker panels.

As previously seen in section 6.2, the effect of the in-plane restraint of boundary conditions may be in some cases be very important. Consequently, all the three boundary conditions BUU, BCU and BCC are considered in the parametric study. Their influence will be further analysed together with a wider range of parameters.

The effect of imperfections is not only important for the elastic behaviour of the panels (briefly discussed in section 6.3.8), but especially for the ultimate load. Consequently, the consideration of different patterns of imperfections are of utmost importance in the parametric study carried out. An in-depth imperfection sensitivity study is carried out for

the curved panels. As previously explained in section 5.7, imperfections were modelled in FE analyses calculating the coordinates of each point composing the deformed panel. This approach allows to choose the desired imperfection and obviates the limitation to use only patterns given by the eigenmodes, usually the default approach in FEM software.

Three main groups of imperfections were considered for the unstiffened panels. Besides *i)* the default approach in FEA, *i.e.* the use of the pattern of the eigenmodes (named "EM") from LBAs, two additional groups of imperfections were considered: *ii)* a single perfect semi-wave in each direction (named "SPSW"), which corresponds to the geometrically simpler imperfection and seeks to simulate a global imperfection; and *iii)* multi perfect semi-wave in longitudinal direction (direction of the load) and a single perfect semi-wave in transversal direction (named "MPSW"), which seeks to introduce a larger number of waves, especially important in panels with larger aspect ratios.

The reason to develop these imperfection shapes through the coordinates of each point composing the mesh of the panels is related to the fact that as the curvature increases the eigenmodes tend to present patterns similar to a "horse saddle" (see section 6.2) and they cease to be in many cases the most unfavourable pattern for imperfections. This is even more critical for stiffened panels, since, the eigenmodes of stiffened panels do not allow to separate global, local and stiffeners imperfections.

Equally important, although often neglected, is the direction given to the imperfection. Despite irrelevant in flat unstiffened plates, imperfections with centripetal and centrifugal directions lead to distinct results in curved panel both whether they are unstiffened or stiffened panels. Imperfections with centripetal direction are considered as being positive ("POS"), while the ones with centrifugal direction are considered as being negative ("NEG").

Two amplitudes are considered for the imperfections: $\min(a;b)/200$ and $\min(a;b)/500$. The first amplitude corresponds to the one defined for local flat plates according to EN 1993-1-5 [1]. The second presents a lower amplitude and it is introduced to define a lower limit within which most amplitude imperfections in practice may be situated.

In conclusion, each panel is analysed with 12 distinct imperfections.

An elasto-plastic material, as described in section 5.5, is used in all analyses. This material

Table 6.8: Parametric variation of unstiffened curved panels under compression (GMNIA)

Panel				BC	Imperfection	Material
Z	α	a/b	b [m]			
0	0.5	50	0.01	BUU	POS(SPSW:min(a;b)/200)	Elasto-Plastic (S355)
10	1.0	75	(0.016)	BCU	NEG(SPSW:min(a;b)/200)	
20	1.5	100		BCC	POS(MPSW:min(a;b)/200)	
30	2.0	125			NEG(MPSW:min(a;b)/200)	
40	3.0	150			POS(EM:min(a;b)/200)	
50	5.0				NEG(EM:min(a;b)/200)	
	7.5				POS(SPSW:min(a;b)/500)	
					NEG(SPSW:min(a;b)/500)	
					POS(MPSW:min(a;b)/500)	
					NEG(MPSW:min(a;b)/500)	
					POS(EM:min(a;b)/500)	
					NEG(EM:min(a;b)/500)	

seeks to simulate a S355 steel and may be considered representative of a typical mild steel used in construction.

The parametric variation just described is summarized in Table 6.8, totalizing 7560 GMNIAs (without the extra cases for h=0.016 m) and 630 LBAs (for the imperfections of eigenmodes) performed for the unstiffened curved panels.

Given the huge amount of data generated with this parametric variation, it is convenient to compile and group the results in order to show certain behaviours, trends and characteristics of the curved panels. With this, it is pretended to obviate repetition and a tedious presentation of results. Whenever relevant, the reader is referred to the annexes present at the end of the thesis. The ultimate loads for all the geometries, using the positive eigenmode imperfection and the worst imperfection, can be consulted in Annex C.

6.6.2 Effect of the thickness

As already said, some of the cases of the parametric study were also considered with a thickness of h=0.016 m to assess the differences in the results. In Figure 6.20, some of those cases are compared in terms of the equilibrium paths with the out-of-plane

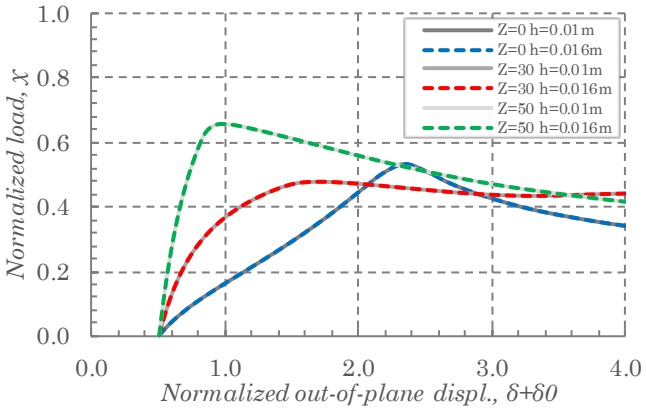

Figure 6.20: Effect of the thickness, h, in the equilibrium paths (positive SPSW imperfection, min(a;b)/200, α=1.0, BCC)

displacement at the centre of the panel normalized to the thickness, $\delta+\delta_{011}$. The same curvatures (Z=0, 30 and 50), width to thickness ratio (a/h=100), aspect ratio (α=1.0) and boundary conditions (BCC) are assumed for both thicknesses. It is possible to see that the (normalized) equilibrium paths for both thicknesses are precisely the same. This confirms the adequacy of the parameter of curvature, Z, to deal with curved panels. In fact, to assume the same a/h ratio means a proportional change in the dimensions and, consequently, in the imperfections, if they are defined as a function of a or b. If the panels are also defined with the same parameter of curvature, Z, it is possible to conclude, using equation (3.2), that the change in R should be proportional.

Consequently, in this section, only the results for h=0.01 m are presented, because once Z and a/h are fixed, they are representative of panels with different thicknesses.

6.6.3 Effect of the aspect ratio

The influence of the nonlinearity of the material was already discussed in section 6.4. Its effect was shown in terms of the equilibrium paths for curvatures from 0 to 50 and a wide range of aspect ratios in Figure 6.17 and Figure 6.18, respectively for BCU and BCC. It was found that the differences are greater for larger aspect ratios and lower curvatures. Not less important is the effect of the width to thickness ratio, a/h. The effect of this ratio is compared through the equilibrium paths in terms of the normalized (to thickness) in-

plane displacement, η, for a/h=50, 100 and 150, as a function of the curvature and aspect ratio in Figure 6.21*a)* and *b)*, respectively. In Figure 6.21*a)* an aspect ratio α=1.0 is assumed and curvatures of Z=0, 20 and 50 are used. In Figure 6.21*b)* a curvature of Z=20 is assumed and aspect ratios α=0.5, 2.0 and 5.0 are considered. It is shown that the increase in a/h has a very important effect decreasing the stiffness and the ultimate load. Although it seems at first sight that an increase in the curvature leads to an increase in the ultimate load, this is not true for all cases. As will be discussed later, cases with intermediate curvatures may show local minimums for the ultimate load. On the other hand, an increase in the aspect ratio leads generally to a decrease in the stiffness of the panels.

The effect of the aspect ratio on the ultimate load is much less obvious. This conclusion is sustained by Figure 6.22 which presents the ultimate load for more cases of a/h, Z and α, as described. It is possible to verify that while for BCU a change in the aspect ratio leads to much more scattered values of ultimate load for Z=50 than for Z=0, this is not verified in the same way for BCC. Additionally, for Z=0 while α=0.5 leads generally to the highest values of ultimate load for BCU, the same aspect ratio leads at most cases to the lowest value of the ultimate load for BCC. For Z=50, while the lowest ultimate load for BCU is generally obtained for α=7.5, for BCC it is obtained, for most cases of a/h ratio, for an intermediate aspect ratio α=3.0.

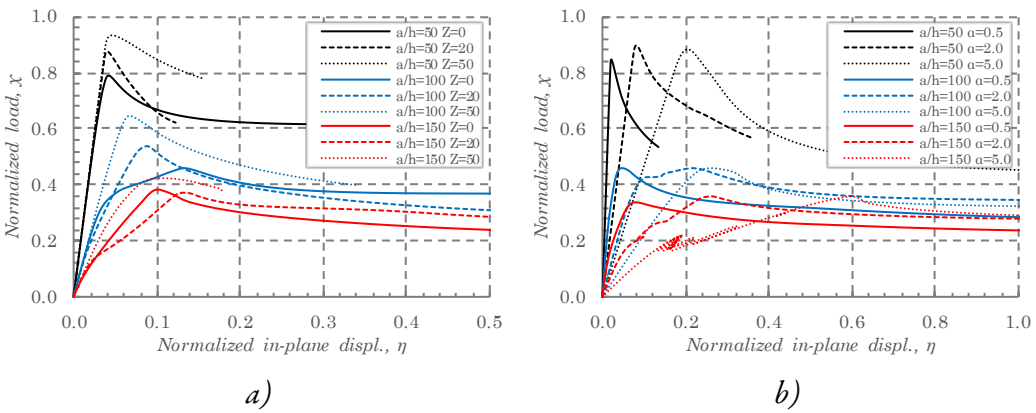

Figure 6.21: Effect of the ratio a/h in the equilibrium paths with *a)* the curvature (for α=1.0) and *b)* the aspect ratio (for Z=20) (positive imperfection from EM, min(a;b)/200, BCC)

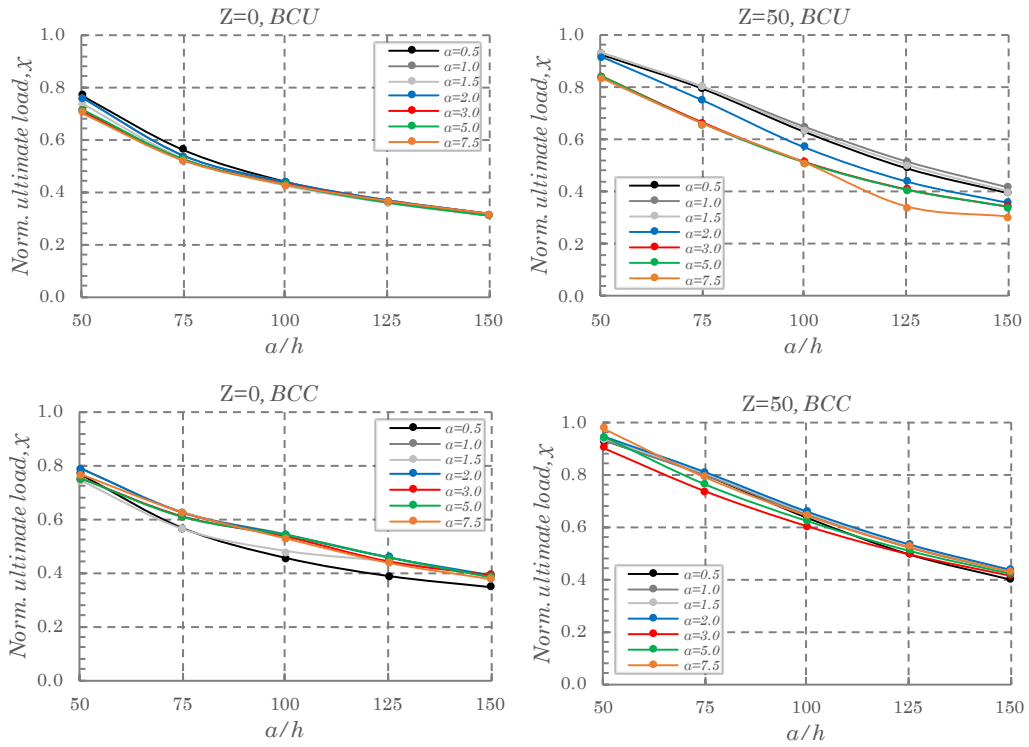

Figure 6.22: Normalized loads as a function of *a/h* for different aspect ratios (Z=0 and 50 and BCU and BCC, positive imperfection from EM; min(*a*;*b*)/200)

Taking into account that the results in Figure 6.22 may be considered representative of the generality of the curved panels, it can be concluded that the effect of the aspect ratio on the ultimate load is very dependent of the boundary conditions, curvature and *a/h* ratio, showing the complex relation between the aspect ratio and the ultimate load.

6.6.4 Effect of the boundary conditions

The effect of the type of boundary conditions on the ultimate load of the curved panels is assessed in Figure 6.23 for α=1.0, for all values of *a/h* and several values of curvature, as described. As the curvature increases the ultimate loads of BCU and BCC become closer and the differences for BUU become larger. However, for larger aspect ratios (α=5.0 in Figure 6.24) this trend is not verified because: *i)* the differences between BCU and BCC remain considerable even for larger curvatures because the in-plane restraint along the longitudinal edges becomes more important; and *ii)* the differences for BUU are not so obvious; they depend more on the *a/h* ratio and inclusively for lower values of *a/h* the

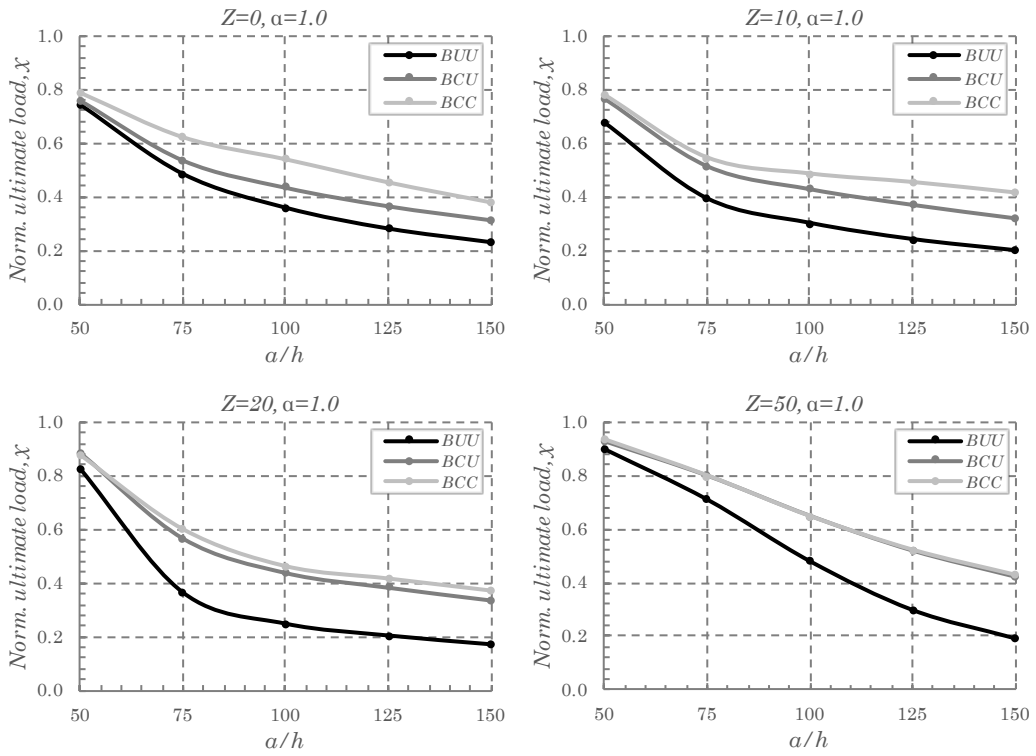

Figure 6.23: Normalized ultimate loads as a function of *a/h* for different boundary conditions (*α*=1.0, positive imperfection from EM; min(*a*;*b*)/200)

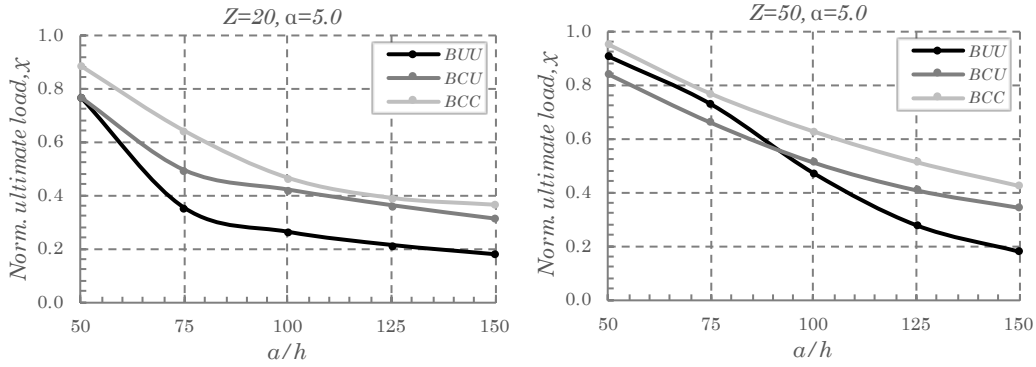

Figure 6.24: Normalized ultimate loads as a function of *a/h* for different boundary conditions (*α*=5.0, positive imperfection from EM; min(*a*;*b*)/200)

ultimate load of BUU can even exceed the one from BCU (for Z=50)

This is explained by the considerably distinct initial imperfection of the first eigenmode. While for BUU the eigenmode has two longitudinal semi-waves, BCU has three longitudinal semi-waves with very pronounced deformation closed to end edges which is

verified to be more detrimental for the ultimate load.

6.6.5 Effect of the width to thickness ratio, *a/h*

The effect of the width to thickness ratio, *a/h*, on the ultimate load may be assessed through Figure 6.22 to Figure 6.24. The increase of this ratio increases the slenderness of the panel and, consequently, it leads necessarily to a decrease on the ultimate load. Panels with higher slenderness are more prone to instabilities. In fact, from the results the reduction on the ultimate load may be rather abrupt depending of the boundary conditions, aspect ratio and curvature. As an example, the panel Z=20, α=1.0 and BUU shows a reduction of 56% if *a/h* passes from 50 to 75. When plotted as a function of the *a/h* ratio, the normalized ultimate loads show clear decreasing trends.

6.6.6 Effect of the imperfection pattern

An example of the effect of the imperfection pattern on the equilibrium path of a curved panel (Z=30, α=1.5, *a/h*=100 and BUU) is shown in Figure 6.25. It is verified that both the response and the ultimate load are completely changed with the initial imperfection pattern. It is possible to conclude that: *i)* the default approach in FEA of using the first Eigenmode (EM) from LBAs may not be the most unfavourable in terms of the ultimate load; *ii)* in this case, the most unfavourable pattern is the one with Multi Perfect Semi-

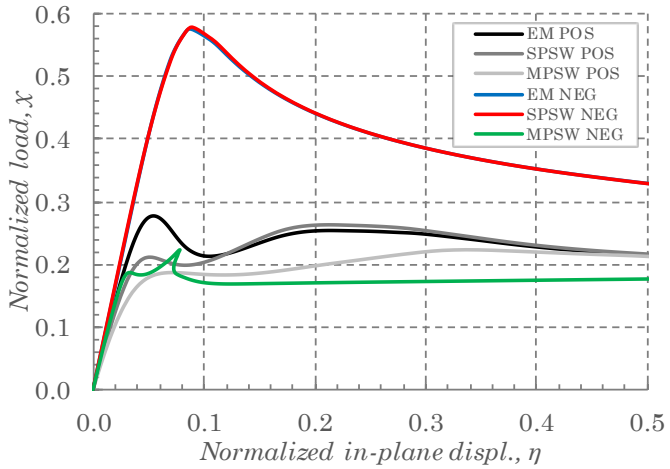

Figure 6.25: Effect of the different imperfection patterns (amplitude min(*a*;*b*)/200) in the equilibrium paths of a curved panel with Z=30, α=1.5, *a/h*=100 and BUU

Waves (MPSW) with negative (N) direction; *iii)* in curved panels, a Single Perfect Semi-Wave (SPSW) may lead to lower ultimate load than the first EM; *iv)* in this case the EM and the SPSW both with negative directions lead to very similar equilibrium paths; and *v)* in this case it is seen that the negative direction for the imperfections lead, depending of the pattern, to the lowest and the highest values for the ultimate load.

These results show how sensible to initial imperfections is the behaviour of curved panels.

The effect of the initial imperfection patterns in the equilibrium paths is shown in Figure 6.26: *a)* for different curvatures (α=1.0, a/h=50 and BCC) and Figure 6.26; *b)* for different aspect ratios (Z=40, a/h=150 and BCU). In the first case, imperfections given by the eigenmodes are compared with imperfection given by a single perfect semi-wave. It is shown that the second imperfection may lead to important reduction on the ultimate load in comparison with the EM, which proves that the default approach of considering only imperfections given by eigenmodes is not on the safe side. The same conclusion is taken from Figure 6.26 *b)* which shows equilibrium paths for several aspect ratios using imperfections from eigenmodes and multi perfect semi-waves. In this case, not only the ultimate load is greatly affected but also the nonlinear behaviour of the panels. As the aspect ratio increases the tendency to the development of snap-through phenomena increases. However, this phenomenon is inexistent with EM imperfections.

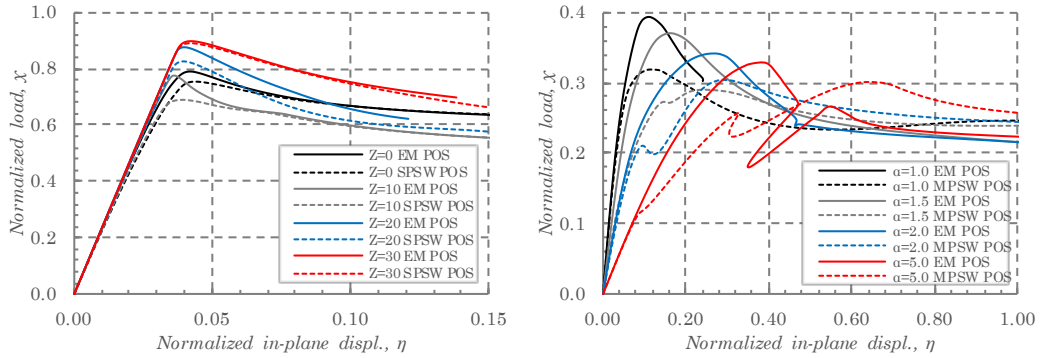

a) *b)*

Figure 6.26: Effect of the different imperfection patterns (amplitude min(a;b)/200) in the equilibrium paths *a)* for different curvatures (α=1.0, a/h=50 and BCC) and *b)* for different aspect ratios (Z=40, a/h=150 and BCU)

Overestimation of the ultimate load of the panels is verified with EM imperfection for all the aspect ratios. For α=1.0, if one uses the EM imperfection the strength of the panel is overestimated by 23.5% in comparison with other perfectly reasonable imperfection pattern[9].

In Figure 6.27 the percentage of the imperfection patterns leading to the lowest ultimate load is analysed as a function of the aspect ratio. The results are separated for flat and curved panels (Z=10 to Z=50), because, as previously explained, the direction of the imperfection in unstiffened flat plates is irrelevant, consequently only positive directions are considered. For flat plates, it is seen that for the lowest aspect ratio (α=0.5) the EM imperfection is the most unfavourable in 100% of the cases. For α=1.0, SPSW is the most unfavourable imperfection in 100% of the cases for BUU and BCU and 80% for BCC. As the aspect ratio increases the MPSW assume great importance. In BCU this imperfection leads in most cases to the lowest ultimate load. For BUU the importance is divided with EM and PMSW. Contrarily, for BCC, SPSW is important even for the larger aspect ratios. Regarding the panels with Z=10 to Z=50, it is verified that: *i)* EM is the most unfavourable imperfection for the lower aspect ratio (α=0.5) in all BC and in many situations for BCC; and *ii)* the negative imperfection SPSW is the most unfavourable only for very few cases. Beyond this, a large variability is verified regarding the most unfavourable pattern, being difficult to anticipate *a priori* the most adverse imperfection for a certain case. This means that the prediction of the ultimate load of curved panels must be done using all the imperfections patterns and the minimum ultimate load must be selected among all the cases.

In Figure 6.28 the percentage of the imperfection patterns leading to the lowest ultimate loads are grouped and compared for different a/h ratios. Once again, it is verified that the most unfavourable imperfection depends significantly of the case, despite the changing of the a/h ratio does not contribute so much for the changing in the worst pattern as the aspect ratio. Even so, there are cases where the changing the a/h ratio changes the pattern leading to the minimum ultimate load. For example, for Z=0 with BCC, while for a/h=50 in 57% of the cases the worst pattern is the MPSW, for a/h=150 the same pattern

[9] For α=1.0 the MPSW coincides with the SPSW imperfection because equation (5.13) gives n=1.

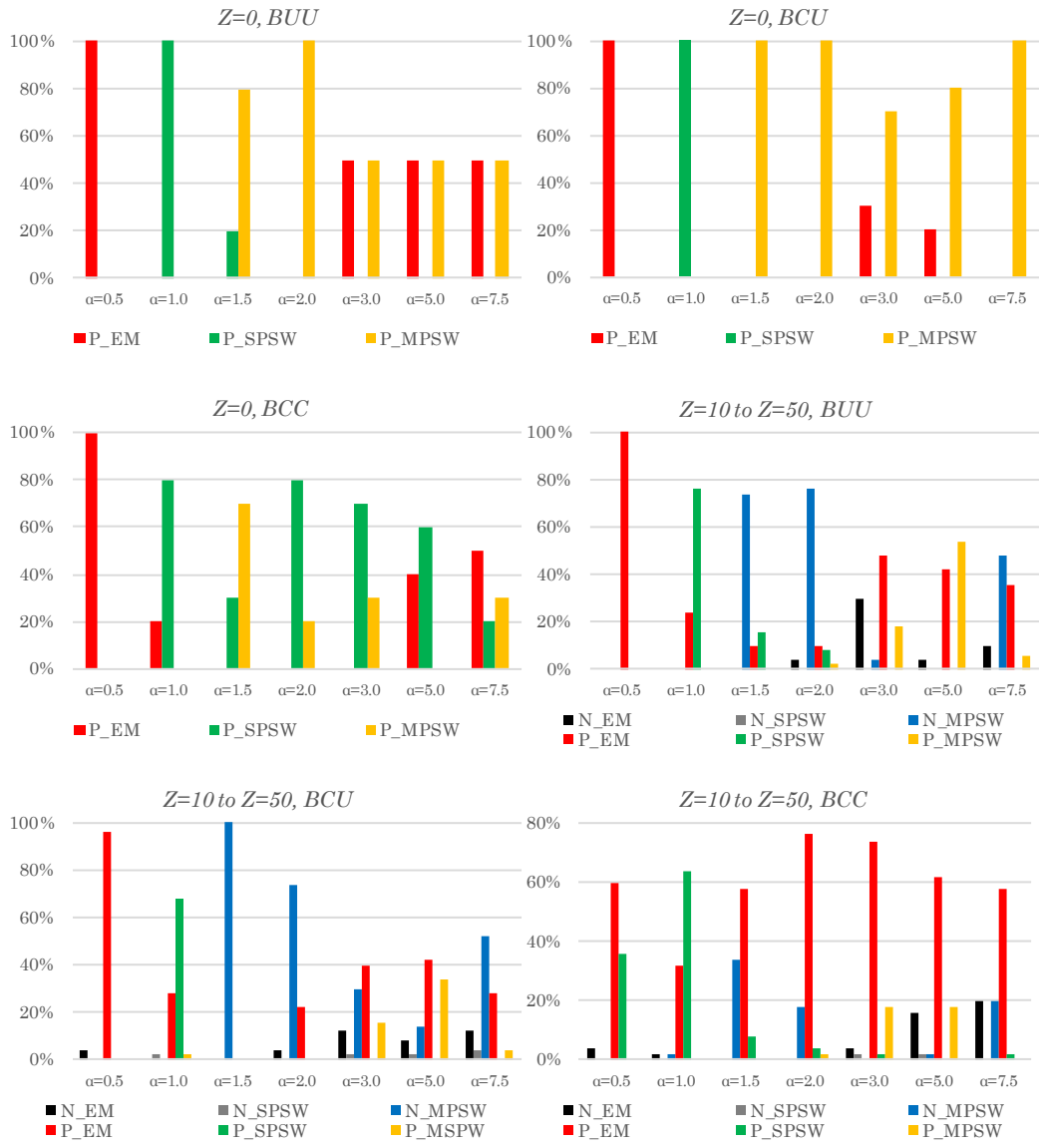

Figure 6.27: Percentage of the imperfection patterns leading to the lowest ultimate load as a function of the aspect ratio for Z=0 to Z=10 to Z=50 (for all cases with amplitudes min(a;b)/200 and min(a;b)/500)

is the worst only in 7% of the cases. For the panels with Z=10 to Z=50 EM, (positive and negative) imperfections led to the minimum ultimate load in only 51% of the cases. Negative imperfections led to the lowest values for the ultimate load in 33% of the cases.

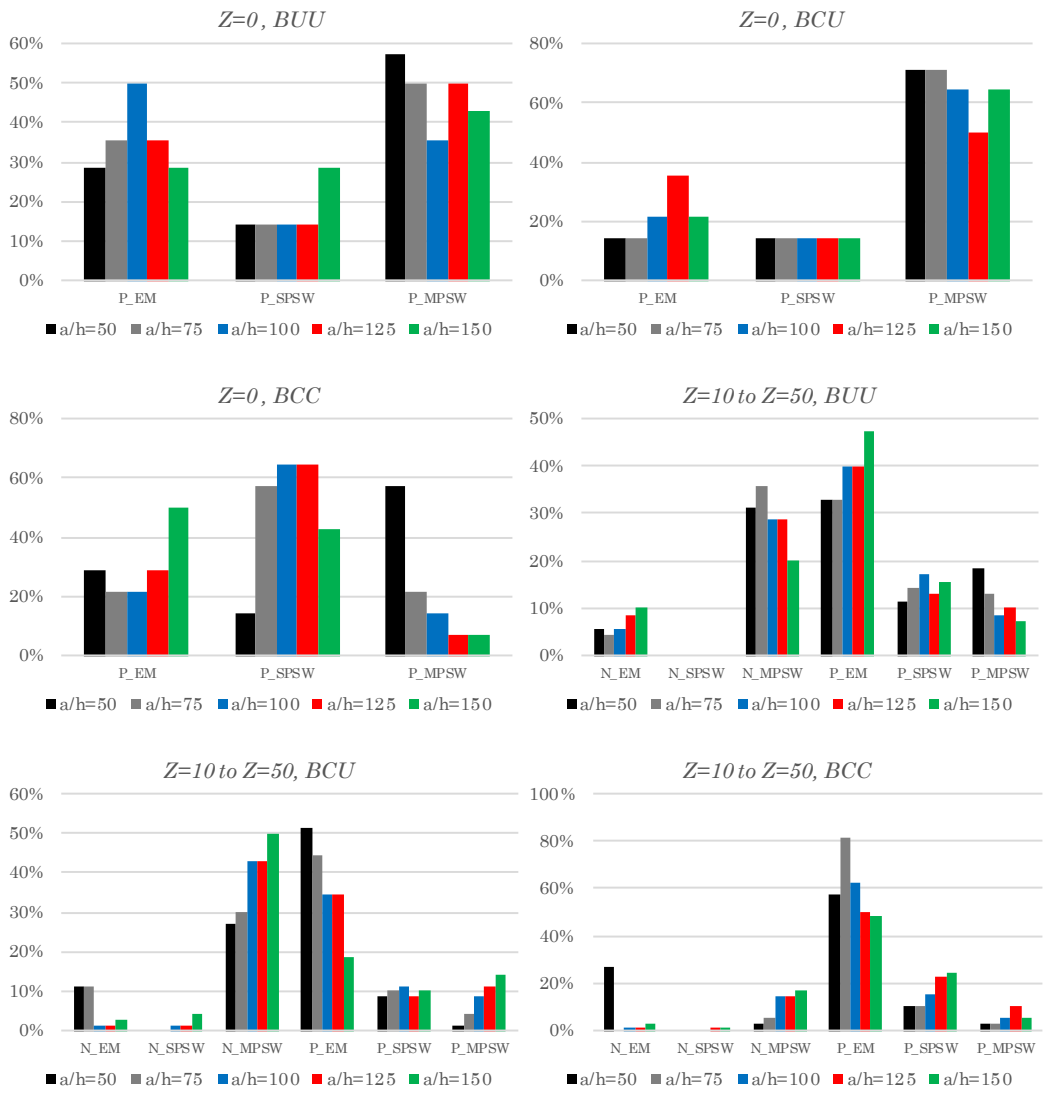

Figure 6.28: Percentage of the imperfection patterns leading to the lowest ultimate load as a function of a/h for Z=0 to Z=10 to Z=50 (for all cases with amplitudes min(a;b)/200 and min(a;b)/500)

The chart shows clearly the most important imperfections. Positive EM and negative MPSW are the imperfections patterns with more importance and the negative SPSW is the one with less importance.

6.6.7 Effect of the curvature

Supported by some of the previous conclusions, it is now possible to assess more clearly

the effect of curvature. As previously referred, the effect of curvature on the ultimate load is not monotonic, *i.e.* it shows local minima for intermediate curvatures. In order to clarify this aspect, in Figure 6.29, the minimum ultimate loads (*i.e.* the lowest obtained from all imperfections) are plotted as a function of the curvature for several levels of *a/h*. The amplitude for imperfections has the value min(*a*;*b*)/200. In this particular case, α=1.0 is chosen and all the three types of boundary conditions are studied.

The results show the existence of very pronounced local minimums for the ultimate load when plotted in function of the curvature. These minima depend very significantly on the *a/h* ratio regarding its value and positions (along *Z*). Generally, as *a/h* increases, the minimum is reached for larger values of *Z*. Depending of the *a/h* ratio, the minimum is generally reached for curvatures up to *Z*=30 or 40 (depending of the boundary conditions). The decrease is generally higher for the lower *a/h* ratios. The boundary conditions play also an important role in this behaviour. BUU show very pronounced

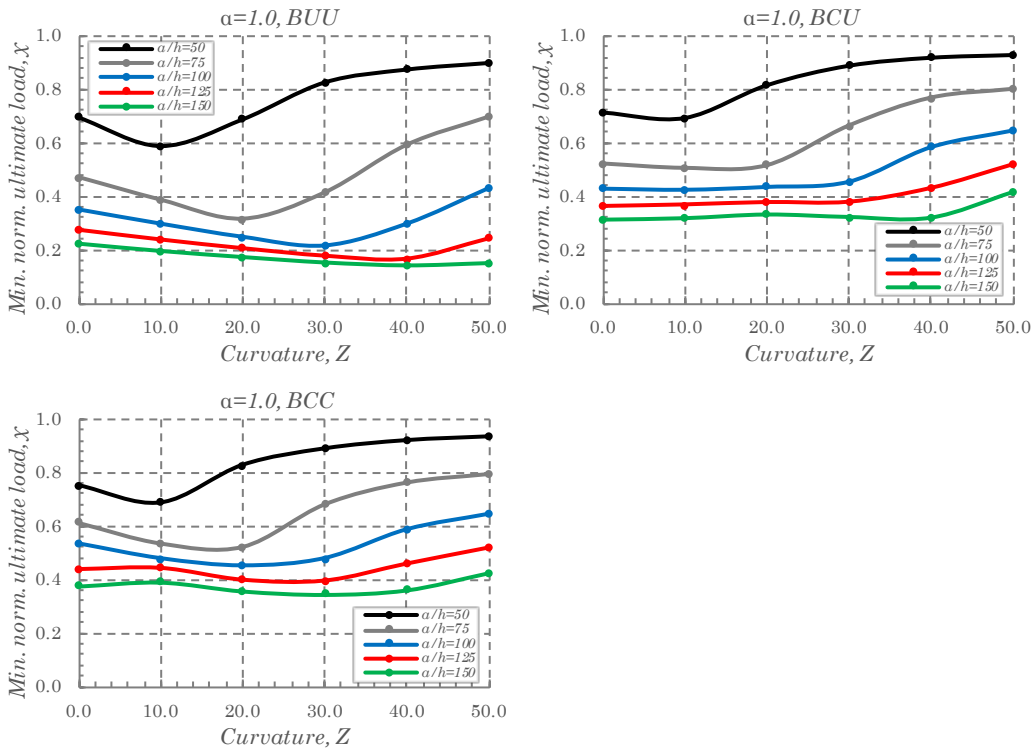

Figure 6.29: Minimum normalized loads as a function of curvature for different values of *a/h* (imperfection with amplitude min(*a*;*b*)/200)

decreases in χ while BCU show only slightly decreases. In this last case, χ shows almost constant values for the lower curvatures and then they start to increase from a certain curvature.

In this example, the reduction of the ultimate load comparatively to the flat plates (Z=0) reaches an extreme value of -41% for Z=40, a/b=125 and BUU. For BCU and BCC the maximum differences are -3% and -16%, respectively. For other aspect ratios, the differences relatively to Z=0 are not very different comparatively to the plotted case (α=1.0), see Annex C. The same is true for the amplitude min(a;b)/500, the maximum differences are similar[10].

6.6.8 Ultimate load of unstiffened curved panels

To analyse the results of the ultimate load it is convenient to define the normalized slenderness parameter, λ, which is defined as a function of the yield stress, f_y, and critical stress, σ_{cr}, as follows:

$$\lambda = \sqrt{\frac{f_y}{\sigma_{cr}}} \tag{6.3}$$

The critical stresses of the panel are calculated from the LBAs and a value of 355 MPa is considered for the yield stress. As an example, in Figure 6.30, the normalized slenderness of the unstiffened panels for α=0.5 and α=1.0 for BCC are compared. The numerical values of the normalized slenderness of the remaining unstiffened panels can be found in Annex B. From the observation of these results, it is possible to draw the following conclusions: *i)* the curvature decreases the normalized slenderness of the panels; *ii)* the width to thickness ratio, *a/b,* increases significantly the normalized slenderness; *iii)* the influence of *a/b* on the values of λ tends to decrease as the curvature increases; *iv)* the type of boundary conditions do not affect very significantly the results; however, the differences increase with the increase in curvature and *a/b* ratio; and *v)* lower aspect ratios tend to lead to lower values in λ for lower curvatures. This is not necessarily true for

[10] It should be noted that in the parametric study, steps of Z=10 were used for the curvature, which means that even larger differences may be obtained for the local minima of the ultimate loads of curved panels comparatively to the flat plates.

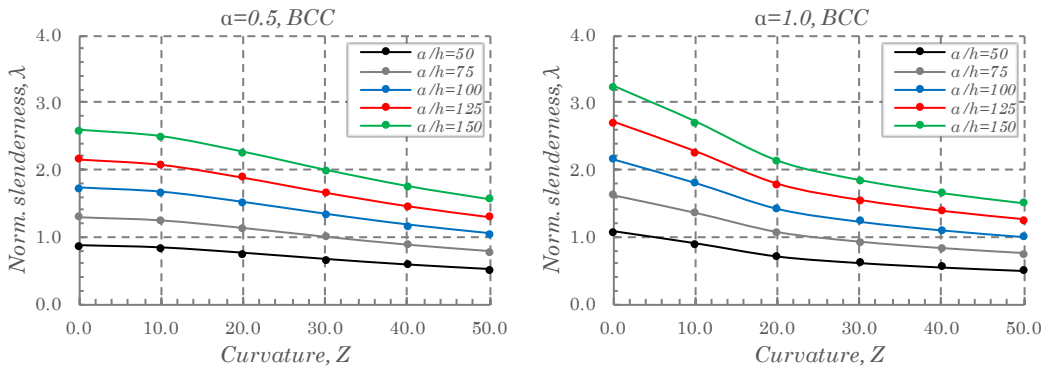

Figure 6.30: Normalized slenderness of panels for different curvatures, *Z*, and *a/h* ratios (*α*=0.5 and 1.0, BCC)

intermediate curvatures. Additionally, as the aspect ratio increases, the normalized slenderness tends to stabilize approximately to the same values, similarly to the buckling coefficient, k_σ (see section 6.2.2). In fact, λ may be written as a function of k_σ using equation (6.1) and (6.3).

Plotting the ultimate load as a function of the slenderness, the effect of the pattern of imperfection is easily seen. In Figure 6.31, the reduction factor, χ, is plotted as a function of the slenderness, λ, for the positive eigenmode imperfection and for the most unfavourable imperfection pattern, for different levels of curvature and α=1.5 and BUU.

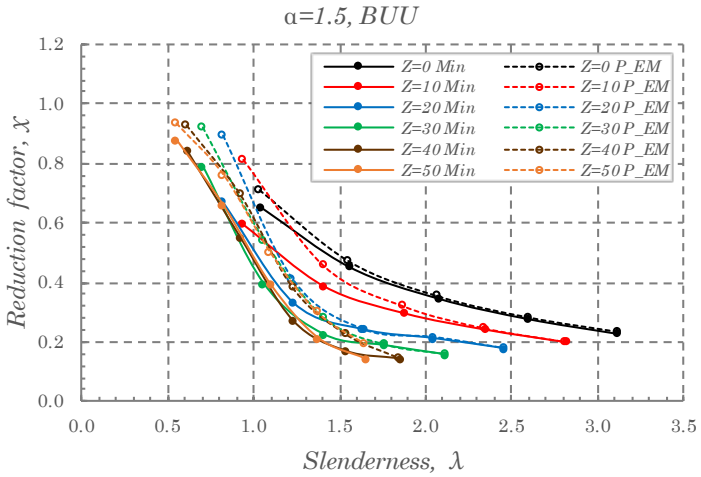

Figure 6.31: Reduction factor as a function of the slenderness for different values Z using positive EM imperfection and the most unfavourable imperfection (*α*=1.5, BUU and amplitude min(*a*;*b*)/200)

This case was chosen to show the important effect that the imperfection pattern may have in the reduction factor. The following conclusions may be drawn: *i)* the slenderness allows to define conveniently the reduction factor for the all the curvatures; *ii)* a clear effect of the curvature in seen; *iii)* the effect of the imperfection pattern on the reduction factor is very important. This effect is more visible for the intermediate slenderness, where the effect of imperfections is higher. The effect is reduced for high values of slenderness because the problem passes to be controlled by elastic instability and for small values of slenderness where the resistance is controlled by plasticity; *iv)* the decrease of χ is more evident as the curvature increases (the slope of the curves is greater).

In order to compare the effect of the aspect ratio and boundary conditions in the reduction curves, in Figure 6.32, they are plotted for α=0.5, α=1.0 and BUU, BCU and BCC. It is seen that the low value of α makes the reduction curves much less sensible to the curvature, with exception for BUU, where the effect of the curvature is still clearly seen. The differences between BCU and BCC are very small. On the other hand, increasing the aspect ratio for α=1.0 changes completely the curves. Here, the differences for different curvatures and boundary conditions are much larger. It is verified the existence of intermediate curvatures leading to reduction curves below the ones of larger curvatures, confirming what was previously said. This effect is amplified for the curves with the minimum values (see, for example, Z=20, α=1.0 and BCC).

As expected, the greater the amplitude of the imperfections, the lower is the ultimate load of a panel; however, it is possible to verify in Figure 6.33 that this effect is generally greater as the curvature increases. The reduction curves are plotted for two levels of amplitudes $\min(a;b)/200$ and $\min(a;b)/500$ for α=1.0 and all the boundary conditions. The effects of increasing the amplitudes are common to the three boundary conditions.

To assess the effect of the aspect ratio in the reduction curves, in Figure 6.34 flat and curved panels (Z=50) are compared for BCU and BCC in terms of the reduction curves. It is concluded that the effect of the aspect ratio is modified with the curvature, because while α=0.5 leads to the lowest values of χ for Z=0, it leads to the highest values is the curved panels in both boundary conditions. This effect is verified for both boundary conditions. On the other hand, for Z=50 the panels with larger values of α lead to the

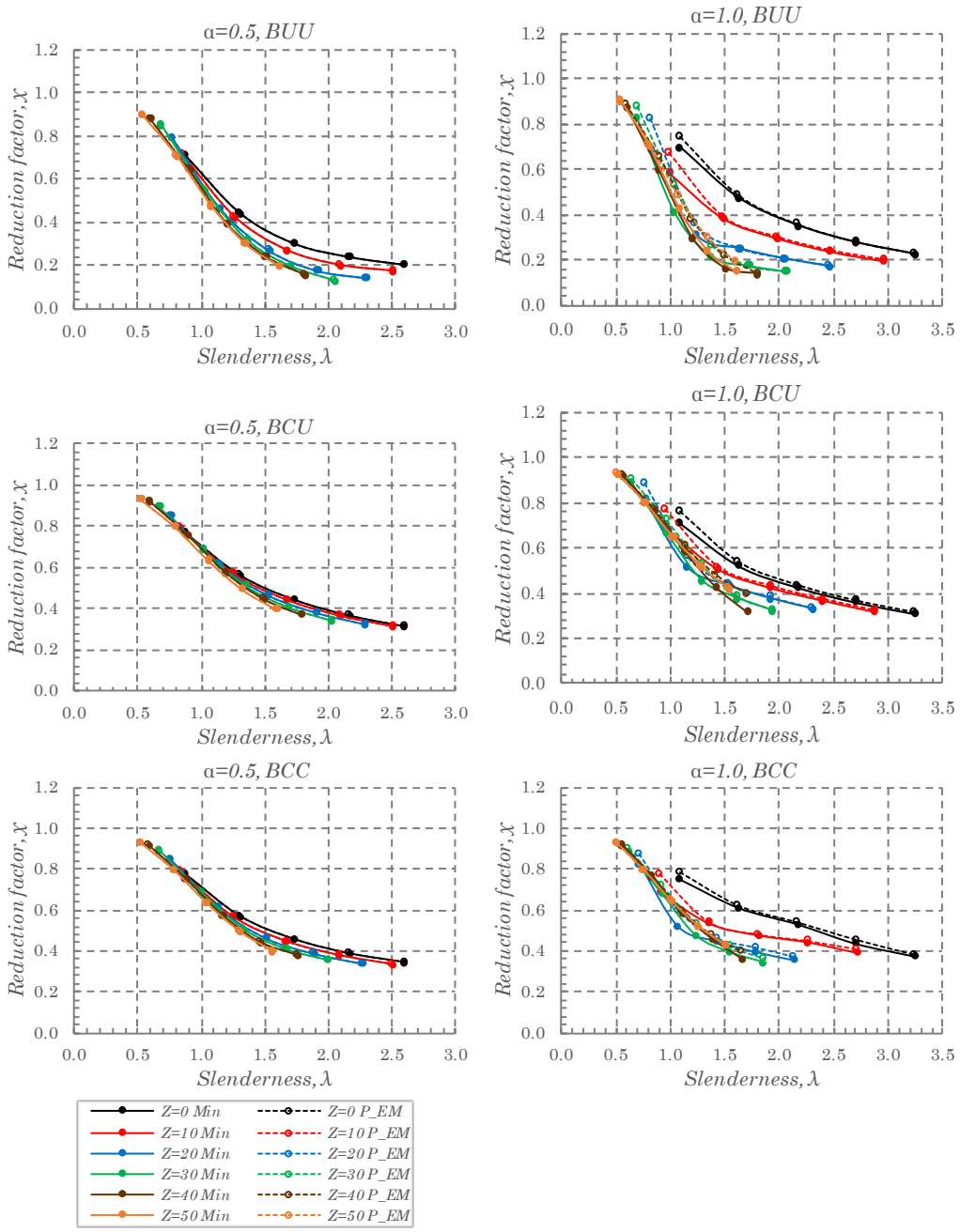

Figure 6.32: Reduction factor as a function of the slenderness for different values of Z using positive EM imperfection and the most unfavourable imperfection (α=0.5 and α=1.0, BUU, BCU and BCC and amplitude min(a;b)/200)

lowest values of χ for BCU and the intermediate values of α=3.0 leads generally to the lowest curve for BCC.

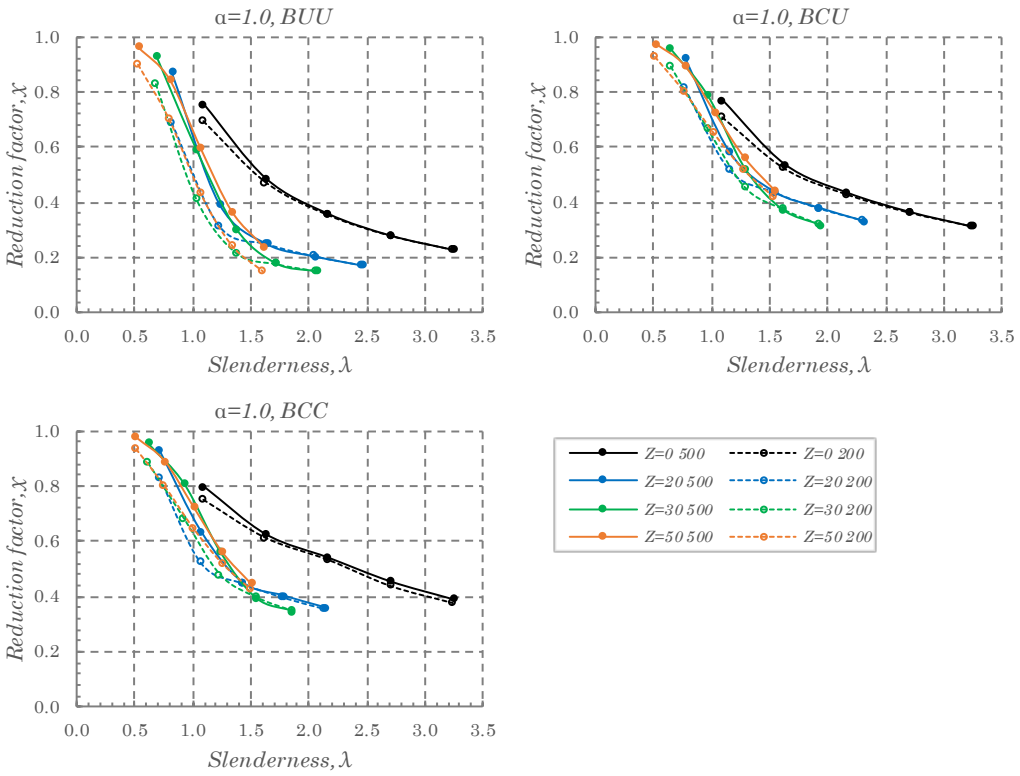

Figure 6.33: Effect of the amplitude of imperfection in the reduction factors (amplitude $\min(a;b)/200$ *vs* $\min(a;b)/500$)

The normalized ultimate loads for all the analyses carried out with amplitude for imperfections equal to $\min(a;b)/200$ and BCU are plotted in Figure 6.35. The imperfection patterns are distinguished. It is possible to verify a considerable variability of values of χ due to the several imperfection patterns. The minimum envelope changes considerably with the curvature.

6.7 LARGE DEFLECTION BEHAVIOUR AND ULTIMATE LOAD OF STIFFENED CURVED PANELS UNDER UNIAXIAL COMPRESSION

6.7.1 Introduction

This section is devoted to the study of the stiffened panels under uniaxial compression.

The curvatures, Z, are considered from 0 to 50 with steps of 10 and two additional cases

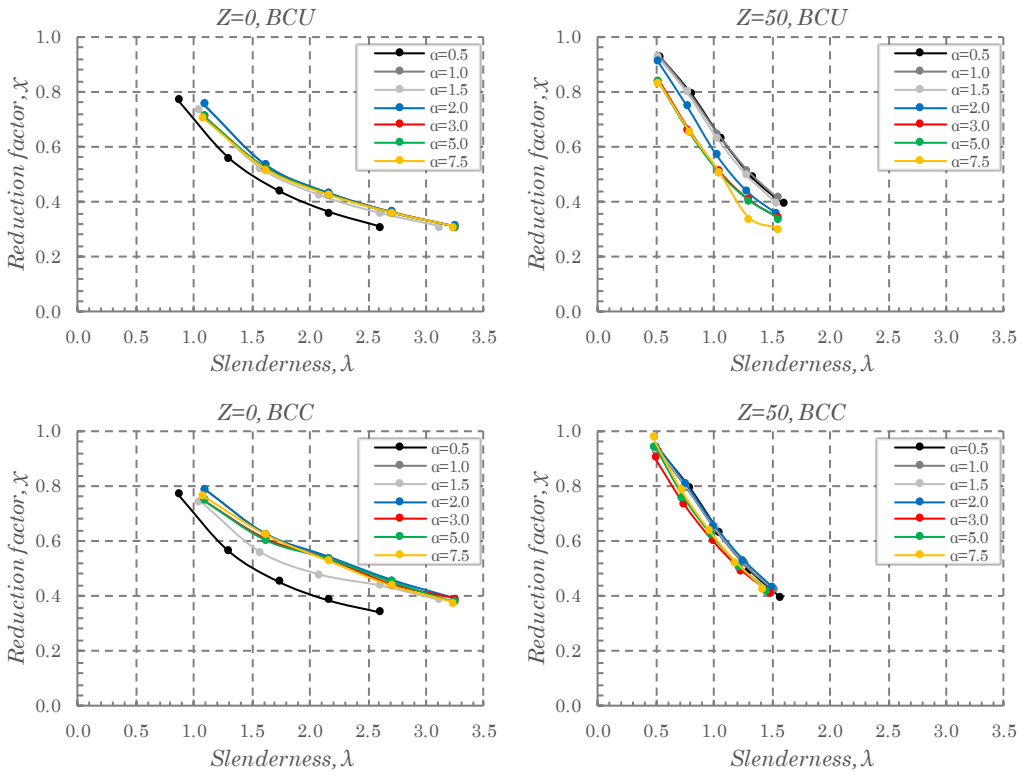

Figure 6.34: Effect of the aspect ratio in the reduction factors

with very large curvatures of 100 and 200 are considered for comparison. The aspect ratios, α, are varied from 0.5 to 1.5 with steps of 0.25. The thickness, h, is maintained constant with values of 0.01 m, however the local slenderness of the subpanels is varied with the width of the subpanels to thickness ratio, a_s/h, from 25 to 75 with steps of 25. In this way, the width of the panels changes correspondingly (from 0.5 to 6.0 m). This variation allows to assess the transition between local and global instability phenomena.

The stiffeners are considered flat with a constant thickness, h_s, of 0.01 m. The depth of the stiffeners are modelled with values of 0.075 m and 0.1 m. It should be noted that the depths of the stiffeners in the FEM, due to the utilization of shell elements, are modelled up to the middle surface of the panel and, consequently, they have to be explicitly modelled with the increase of half of the thickness, $h/2$. This means that, in comparison with the free dimension for the depth of the stiffeners, d_s, defined in Figure 3.5, $d_{s,FEM}=d_s+h/2$. However, for convenience in this Chapter 6, $d_{s,FEM}$ is named simply as d_s. (thus, d_s/h_s is defined in the same way, *i.e.* with values of 7.5 and 10.0). The proper

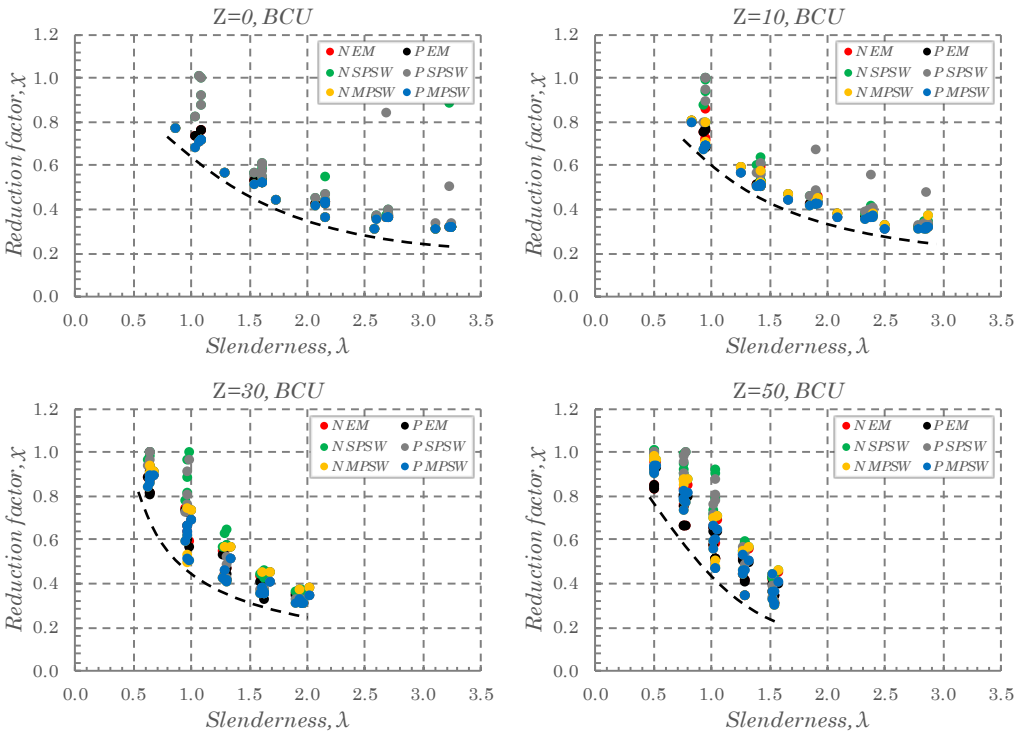

Figure 6.35: Normalized ultimate loads for all the imperfection patterns and aspect ratios (imperfection with amplitude min(a;b)/200 and BCU)

distinction between both depths will be done in the comparison with the results of the SAM, in Chapter 7. Consequently, for h=0.01 m, the free dimension of the stiffeners are respectively 0.07 m and 0.095 m, which have class 1 and 3, respectively, for a steel with f_y=355 MPa. The number of stiffeners, n_s, is considered as: 1, 2, 3, 5 and 7. In this way it is possible to analyse the change in behaviour that a low and a large number of stiffeners introduce to the panels.

The local curvature of the subpanels, Z_{loc}, defined by equation (5.8), varies between 0.16 (for Z=10 and n_s=7) and 50.0 (for Z=200 and n_s=1), values which were previously covered in the study of unstiffened panels, in section 6.6.

BUU are excluded from the analyses due to reduced practical applicability.

As previously discussed, the eigenmodes of stiffened panels do not allow to separate global, local and stiffeners imperfections, and consequently they are not a viable approach to model adequately imperfections in stiffened panels. Hence, the imperfections were separately considered for global, local and stiffeners through the definition of the

deformed coordinates. The global imperfection is modelled with a single perfect semi-wave (SPSW), and the local imperfection with multi perfect semi-waves (MPSW) depending of the local geometry of the subpanels, as described in section 5.7. The amplitudes for each component are considered as follows: min(a;b)/400 for the global imperfection, min(a;b)/200 for the local imperfection and h/50 for the rotation of the stiffeners. Additionally, positive and negative direction are considered for the imperfections.

The parametric variation for the stiffened panels is summarised in Table 6.9, corresponding to a total of 4800 GMNIAs.

The ultimate loads for the stiffened panels with d_s/h_s=10 can be consulted in Annex C.

Table 6.9: Parametric variation of stiffened curved panels under compression (GMNIA)

Panel				Stiffeners			BC	Imperfection	Material
Z_{Global}	α	a_s/h	h [m]	n_s	d_s/h_s	h_s [m]			
0	0.5	25	0.01	1	7.5	0.01	BCU	POS(SPSW:min(a;b)/400+	Elasto-Plastic
10	0.75	50		2	10.0		BCC	MPSW:min(a;b)/200+Stf:h/50)	(S355)
20	1.0	75		3				NEG(SPSW:min(a;b)/400+	
30	1.25			5				MPSW:min(a;b)/200+Stf:h/50)	
40	1.5			7					
50									
100									
200									

6.7.2 Effect of the width of the subpanel to thickness ratio

Figure 6.36 presents the normalized ultimate loads, χ, as a function of the curvature for different values of a_s/h and number of stiffeners for panels with α=1.0 and BCU. Imperfections were considered with positive and negative directions with amplitude min(a;b)/200. As expected larger values of the a_s/h ratio lead to lower values for the normalized loads because the panels are more prone to local instabilities. The increase in the number of stiffeners decreases also the values of χ because the dimensions of the panel increase correspondingly. Regarding the direction of imperfections, a great dependency on Z, n_s, and as/h is verified. However, it is possible to conclude that in general, negative

imperfections are the most conditioning for Z up to approximately 40 or 50, for a_s/h=50 and a_s/h=75, and, in general, for all curvatures for a_s/h=25. Some exceptions are found for n_s=1, where the negative direction is only the most unfavourable for Z=0 to 20. In some cases, the differences reach very significant values. For example, for n_s=7 with a_s/h=50 for Z=0 the negative direction leads to an ultimate load 48% lower than for the positive imperfection. In contrast, for Z=200, it is leads to the lowest ultimate load (25% lower than the negative direction).

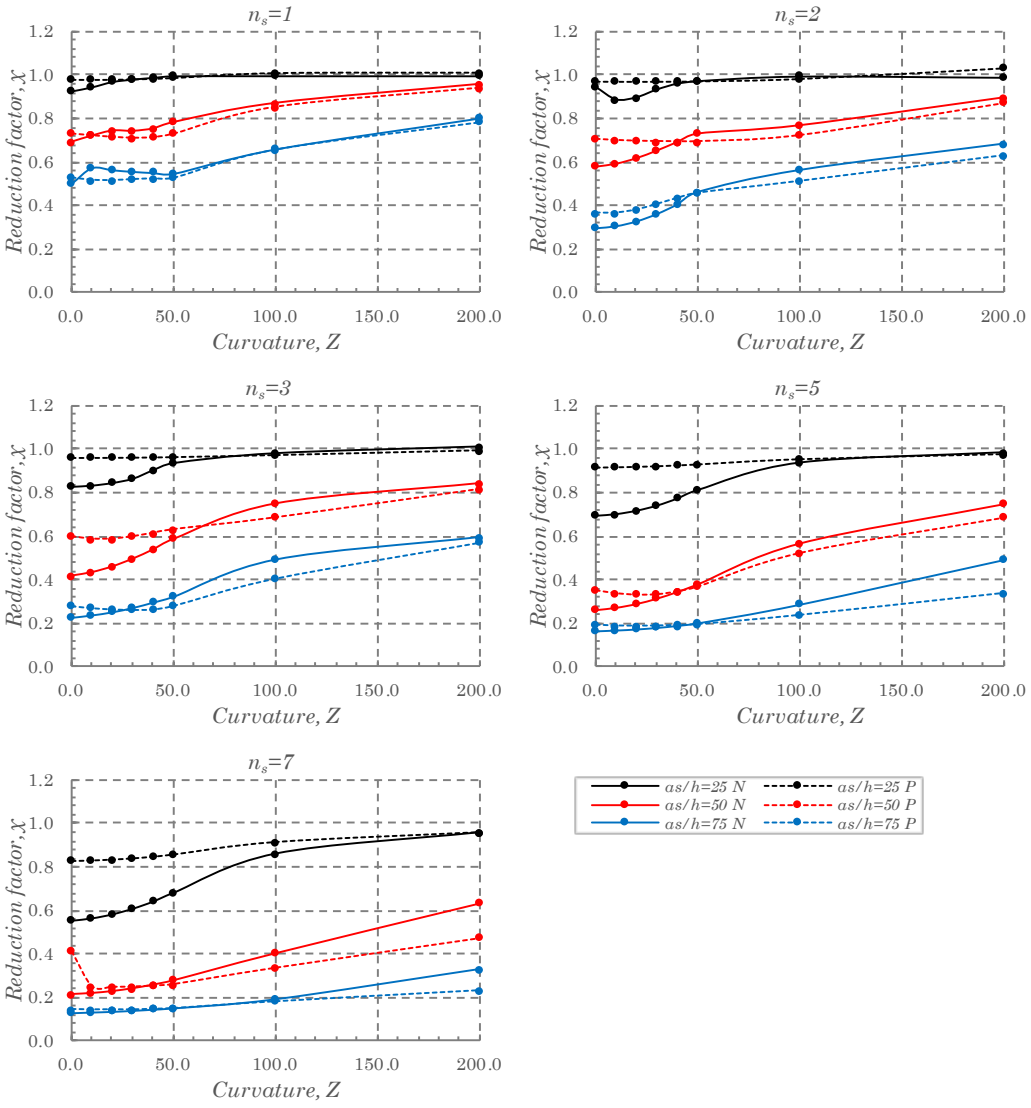

Figure 6.36: Reduction factor as a function of curvature for different values of a_s/h, number of stiffeners for positive and negative imperfections (α=1.0, d_s/h_s=10 and BCU)

6.7.3 Effect of the geometry of stiffeners

To assess the influence of the depth to thickness ratio, d_s/h_s, the reduction factors are plotted, in Figure 6.37, for values of 7.5 and 10.0, as a function of the curvature for different number of stiffeners and a_s/h ratios. Panels with α=1.0 with BCU and negative imperfection were considered. The increase in the ultimate load obtained by increasing the moment of inertia of the stiffeners depends on the curvature, a_s/h and the numbers of stiffeners. The benefit of increasing the moment of inertia of the stiffeners in panels with n_s≤3 is almost negligible for Z≥100 (exception for Z=100 and a_s/h=75).

As the a_s/h ratio increases, larger moments of inertia of stiffeners increase significantly the ultimate load for n_s=1. For a_s/h=75 the benefit is considerable for Z=0 (48.4%) and Z=10 (62.1%). However, for Z=30 it is only 2.7%, and for larger curvatures larger than that the gains are negligible. For n_s≥5 the benefit decreases for lower curvatures when a_s/h

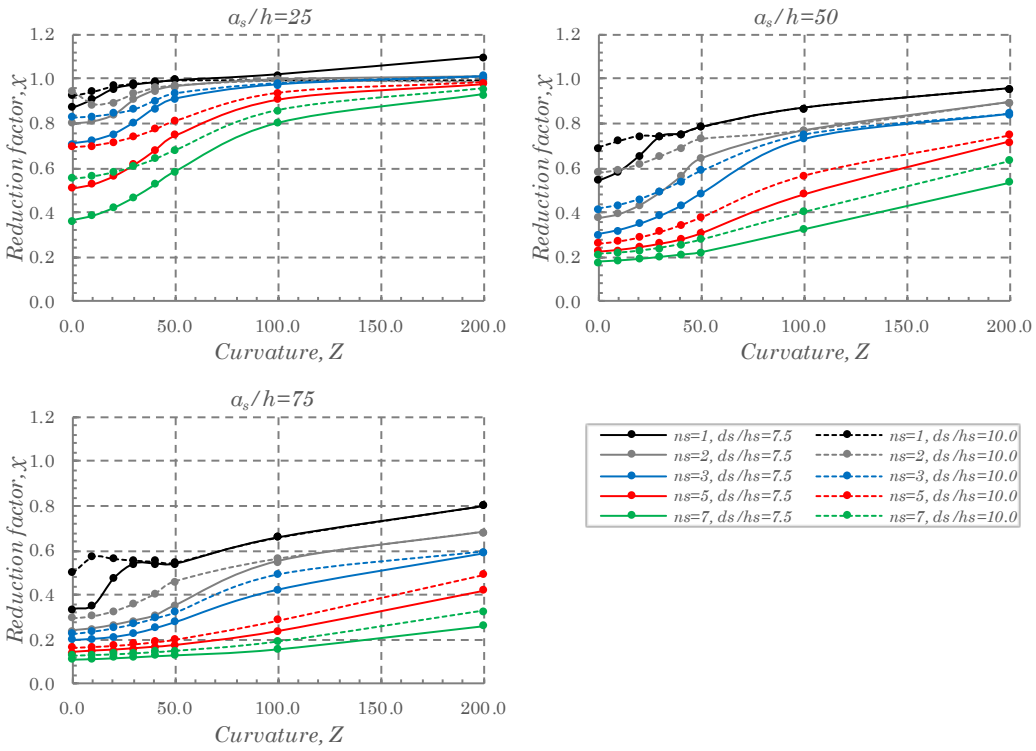

Figure 6.37: Reduction factor as a function of curvature for different number of stiffeners, d_s/h_s and of a_s/h ratios (α=1.0, negative imperfection and BCU)

increases. For example, while for n_s=7 and Z=0 the gain for a_s/h=25 is 51.8%, for a_s/h=75 it is only 15.6%.

6.7.4 Effect of the aspect ratio and boundary conditions

The Figure 6.38 analyses the effect of the aspect ratio and boundary conditions. For this, panels with a_s/h=50, d_s/h_s=10.0 and negative imperfections were used. In general, while Z=0 shows a decrease of the ultimate load with the increase in the aspect ratio, the panel

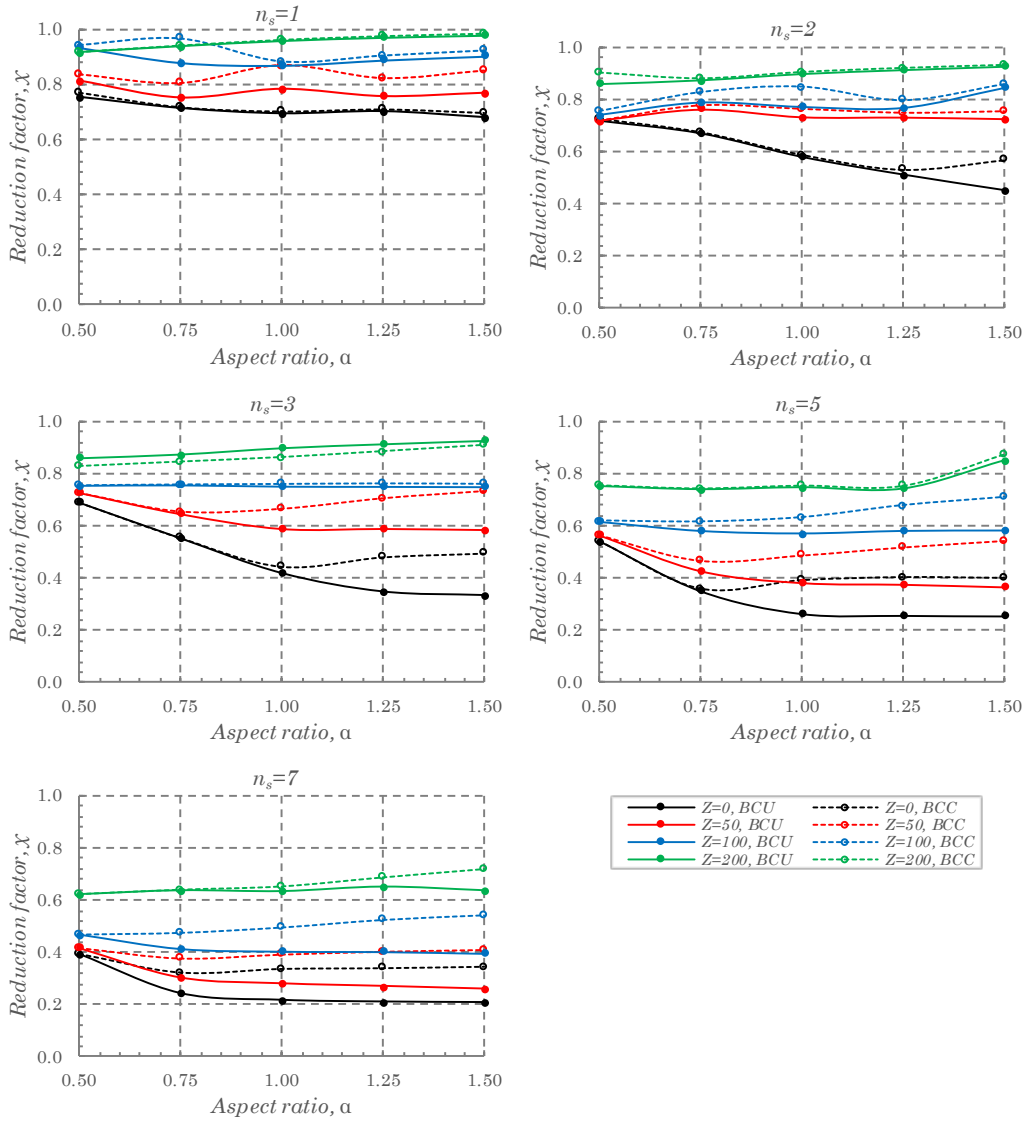

Figure 6.38: Reduction factor as a function of the aspect ratio for different curvatures, number of stiffeners and BCU and BCC (a_s/h=50, d_s/h_s=10.0 and negative imperfection)

with Z=200 is not very affected; in fact, a slight increase is verified.

For the larger number of stiffeners, as the aspect ratio increases, χ seems to tend for an approximately constant value within the plotted aspect ratios. The effect of boundary conditions follows the same tendency as previously identified for the unstiffened panels, *i.e.* the BCU leads in general to lower values of χ than BCC and this difference has tendency to increase as the aspect ratio also increases. While curved panels with BCU tend to stable values of χ, for BCC the aspect ratio seems to increase χ, leading to some cases to local minima.

The largest curvature (Z=200) is the least affected by the change in boundary conditions. As an example, with n_s=7, a_s/h=50, α=1.5 for Z=0 passing from BCU for BCC means an increase in the reduction factor of 67%, while for Z=200 it is only 13%.

6.7.5 Effect of the curvature

The effect of curvature has been assessed through the results presented from Figure 6.36 to Figure 6.38. Generally, the increase in Z increases the resistance of the panels. From observation of Figure 6.36, some exceptions are found, for example for n_s=2 with a_s/h=25. In this case, there is a reduction of χ for lower curvatures in comparison with Z=0, which is recovered with the increase in curvature (only for Z=40). The gain in χ with the curvature is larger for higher aspect ratios.

6.7.6 Imperfection sensitivity

The effect of the imperfection direction on the ultimate load in shown in Figure 6.39. It is possible to verify that in general as the curvature increases, the higher is the percentage of cases where the positive direction for the imperfection leads to the lowest ultimate load. These effect also depends on the number of stiffeners. For example, for Z=40, while for n_s=3 the lowest ultimate load is obtained with the negative direction in 55% of the cases, for n_s=1 the same happens only in 3% of the cases.

This can be confirmed in Table 6.10 where the percentages for all the analyses performed are presented only in function of the curvature. While for Z=0 the positive direction leads to the lowest ultimate load in only 7% of the cases, for Z=200 it happens for 80%.

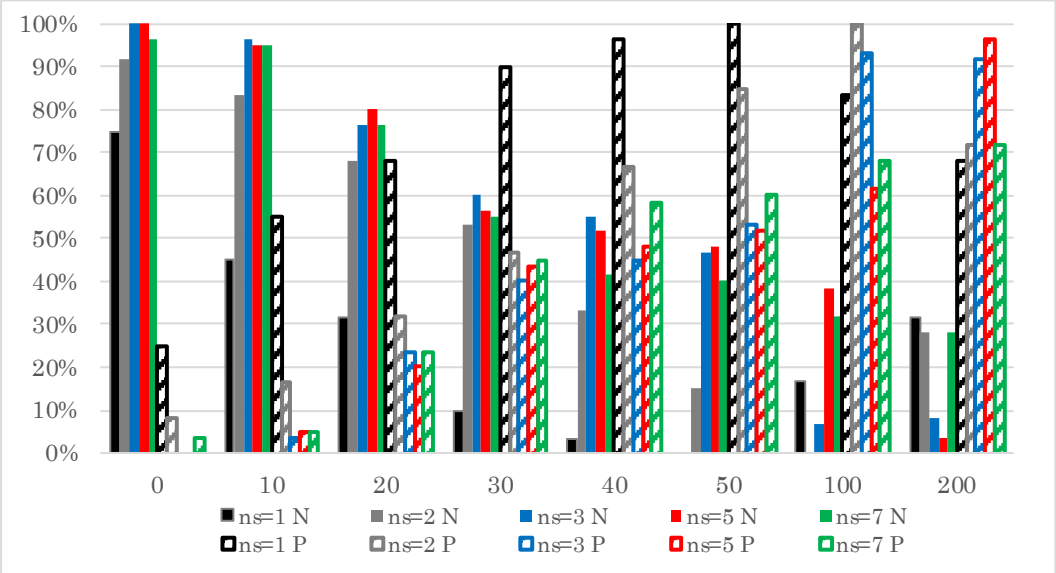

Figure 6.39: Percentage of the direction of imperfections leading to the minimum ultimate load as a function of the curvature for each number of stiffeners

Table 6.10: Percentage of the direction of imperfections leading to the lowest ultimate load

	Z=0	Z=10	Z=20	Z=30	Z=40	Z=50	Z=100	Z=200
POS	7%	17%	33%	53%	63%	70%	81%	80%
NEG	93%	83%	67%	47%	37%	30%	19%	20%

6.8 LARGE DEFLECTION BEHAVIOUR AND ULTIMATE LOAD OF UNSTIFFENED CURVED PANELS UNDER OUT-OF-PLANE PRESSURE

6.8.1 Introduction

In this section it is sought to study the behaviour of unstiffened curved panels under out-of-plane pressure. Interaction with in-plane compression is also assessed leading to some distinct load cases.

The geometric parameters are varied similarly to the previous case of in-plane

compression but now with a more reduced sample size (steps are increased). Taking into account that imperfections have less impact for out-of-plane pressure and its effect was already studied in detail in section 6.6, only the imperfection given by a single perfect semi-wave (SPSW) with positive direction and an amplitude of min(a;b)/200 is considered now. Depending on the order of application of the loads, two situations may be distinguished: *i)* initial in-plane compression (axial force - AxF) followed by out-of-plane pressure (P); and *ii)* initial out-of-plane pressure followed by axial compression. Furthermore, different levels of the initial preload are considered. For the initial in-plane compression, 0, 10 and 25% of the plastic load are considered, AxF0, AxF10 and AxF25, respectively. Depending on the direction for the out-of-plane pressure following this initial compression, positive and negative directions may be considered, +P and –P, respectively. For the initial out-of-plane pressure, 0 and 50 kPa are considered, P0 and P50, respectively. Additionally, the direction of the out-of-plane pressure. This parametric variation leads to 1512 different cases as summarized in Table 6.11.

Table 6.11: Parametric variation of unstiffened curved panels under out-of-plane pressure (GMNIA)

Panel				BC	Imperfection	Load case	Material
Z	α	a/b	b [m]				
0	0.5	50	0.01	BUU	POS(SPSW:min(a;b)/200)	AxF0+P	Elasto-Plastic (S355)
10	1.0	100		BCU		AxF10+P	
20	2.0	150		BCC		AxF25+P	
30	5.0					AxF0-P	
40						AxF25-P	
50						(P0+AxF)	
						P50+AxF	

6.8.2 Effect of the aspect ratio

The effect of the aspect ratio for panels loaded with positive (centripetal) out-of-plane pressure is shown in Figure 6.40. Aspect ratios are varied from 0.5 to 5.0 and curvatures from 0 to 50 as described. The panels are considered without initial axial preload (AxF=0%) and with a/b=100 for BCC. The aspect ratios are shown to change very considerably the stiffness of the panels. It is verified that the stiffness of the panels

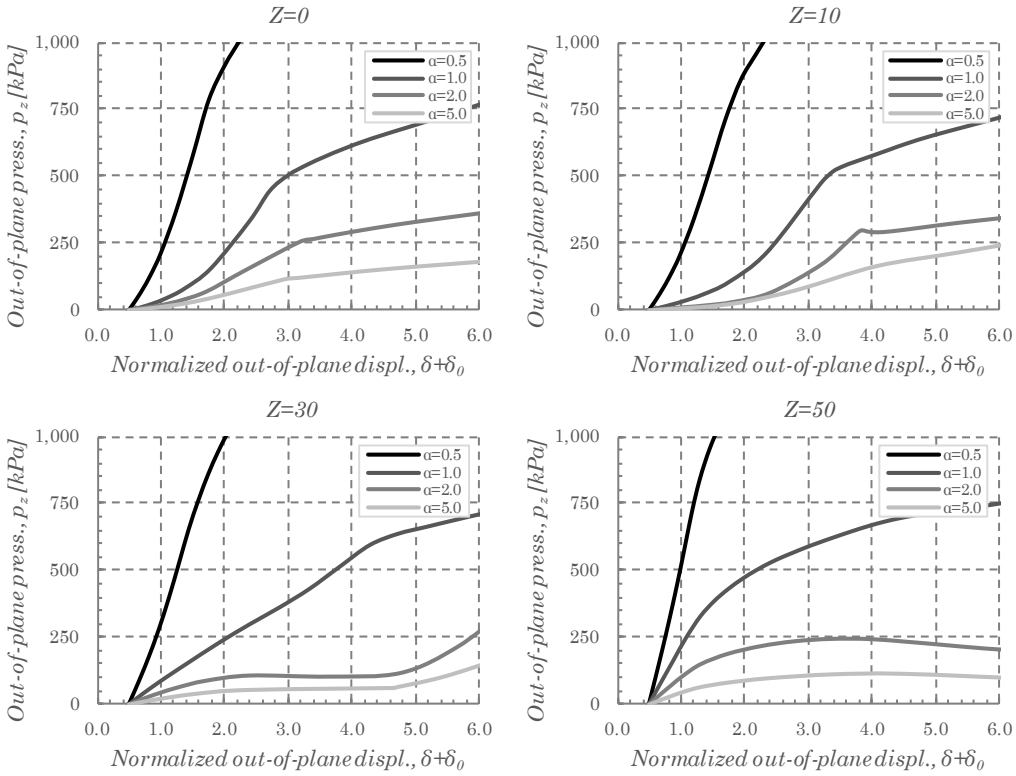

Figure 6.40: Effect of the aspect ratio for panels loaded with positive out-of-plane pressure for different levels of curvature (a/h=100, BCC, AxF=0)

decreases with the increase in the aspect ratio. This effect persists for the different curvatures despite larger curvatures increasing the initial stiffness of the panels. In fact, the equilibrium paths are greatly affected by the curvature.

A very markedly change in the slope of the curves is shown in the majority of the cases. This is due to the yielding which is propagated to the all section very quickly. In Z=50 this phenomenon is more gradual and the curves are smother.

It is verified that the equilibrium paths do not show maxima values, with the exception of two cases (Z=50 for α=2.0 and 5.0), even for very high values of out-of-plane displacements ($\delta+\delta_0$=6.0). Supported on the results obtained from the remaining analyses, this leads to the conclusion that, in general, under pure out-of-plane pressure, ultimate loads are not reached within practical displacements. Because fracture was not considered in the material law the displacements continue to develop up to unrealistic values. At some point fracture would be determinant. However, this question is of

reduced practical interest because that situation is not reached in practice. For these reasons the analyses of the ultimate load of the panels under out-of-plane pressure is more complex.

6.8.3 Effect of an initial in-plane compression

In Figure 6.41, the effect of the initial in-plane axial load (AxF=0% *vs* AxF=25%) is assessed. Thus, the panels are firstly compressed and then subject to a positive out-of-plane pressure. The results are compared for different levels of curvature and a/h ratios. All the panels are considered with α=1.0. The following conclusions may be drawn: *i)* larger a/h ratios decrease very significantly the loads developed for the same displacements; *ii)* the effect of the initial in-plane compression is very important. The in-plane compression changes completely the response of the panels. The initial in-plane compression induces instability phenomena that causes the appearance of ultimate loads,

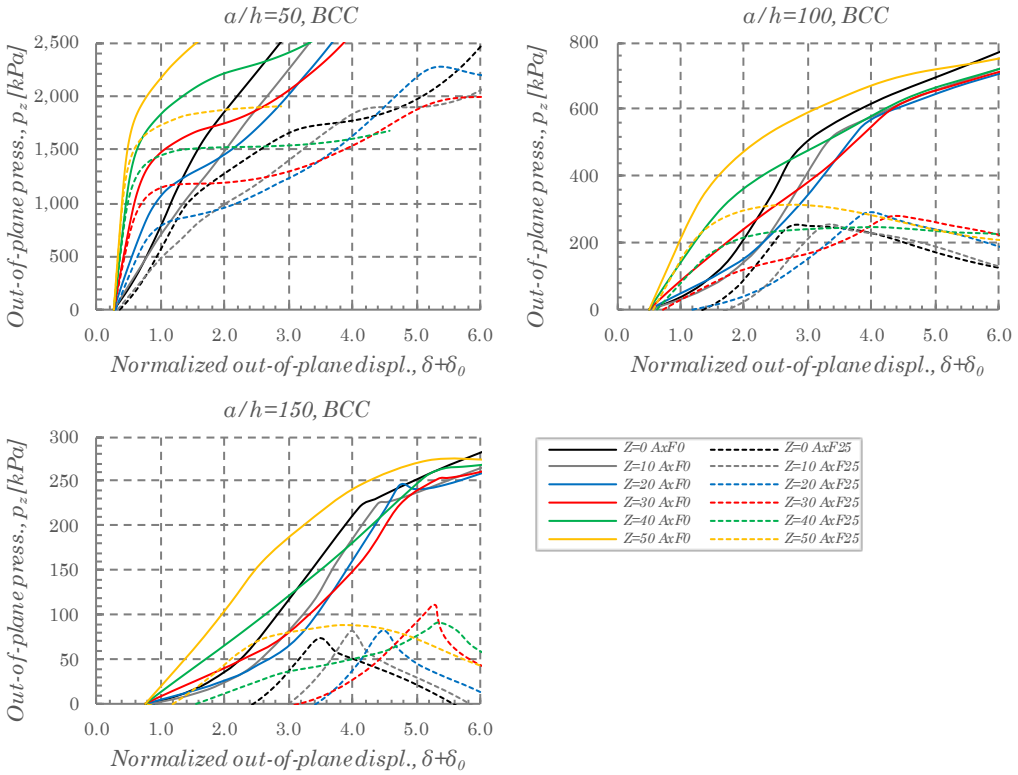

Figure 6.41: Effect of the initial in-plane axial load (AxF=0% *vs* AxF=25%) for panels loaded with positive out-of-plane pressure for different levels of curvature and a/h ratios (α=1.0)

contrarily to the panels without initial axial compression (AxF=0%). This effect is larger for larger values of a/h ratios. While a/h=50 does not practically deflect with the application of the initial in-plane compression, for a/h=150 a value of $\delta+\delta_0$=3.4 is developed for Z=20; *iii)* the curvature affects significantly the load-deflection behaviour, which is relatively complex because of the intersection of the curves. For example, Z=0 for low values of p_z develops considerably larger displacements that most of the curved panels. However, as the load increases it becomes stiffer (see, for example, the panel Z=40, within reasonable displacements ($\delta+\delta_0 \leq 3.0$)).

The values of ultimate loads of the cases represented in Figure 6.41 are shown in Table 6.12. The values for a/h=50 are not shown because they are not reached within the range of admissible displacements. Besides the usual reduction of the ultimate loads with the increase in a/h, it is observed that its evolution is not monotonic with curvature, showing the additional complexity of the interaction between in-plane and out-of-plane loading.

Figure 6.42 shows the equilibrium paths of panels with and without the pre-compression followed by negative (centrifugal) out-of-plane pressures. Once again, the panels without initial compression have always the values of p_z increasing with the displacements. Here, the effect of the curvature is more "predictable", *i.e.* the curvature increases the developed load for the same displacement approximately in a constant way along the all range of displacements and for all boundary conditions. In this case, the ultimate load obtained when the pre-compression exists is $p_{z,ulmBCC} > p_{z,ulmBCU} > p_{z,ulmBUU}$. This effect is shown in Table 6.13 where the values of the ultimate loads are compared.

The in-plane restraints along the edges become important when the behaviour is controlled by the membrane component. This effect would become more important if

Table 6.12: Ultimate load for the positive p_z in panels pre-compressed with AxF=25%, α=1.0 and BCC [kPa]

	Z=0	Z=10	Z=20	Z=30	Z=40	Z=50
a/h=50	-	-	-	-	-	-
a/h=100	251.2	255.3	291.0	277.9	246.1	312.9
a/h=150	74.4	80.6	83.2	111.8	90.8	88.5

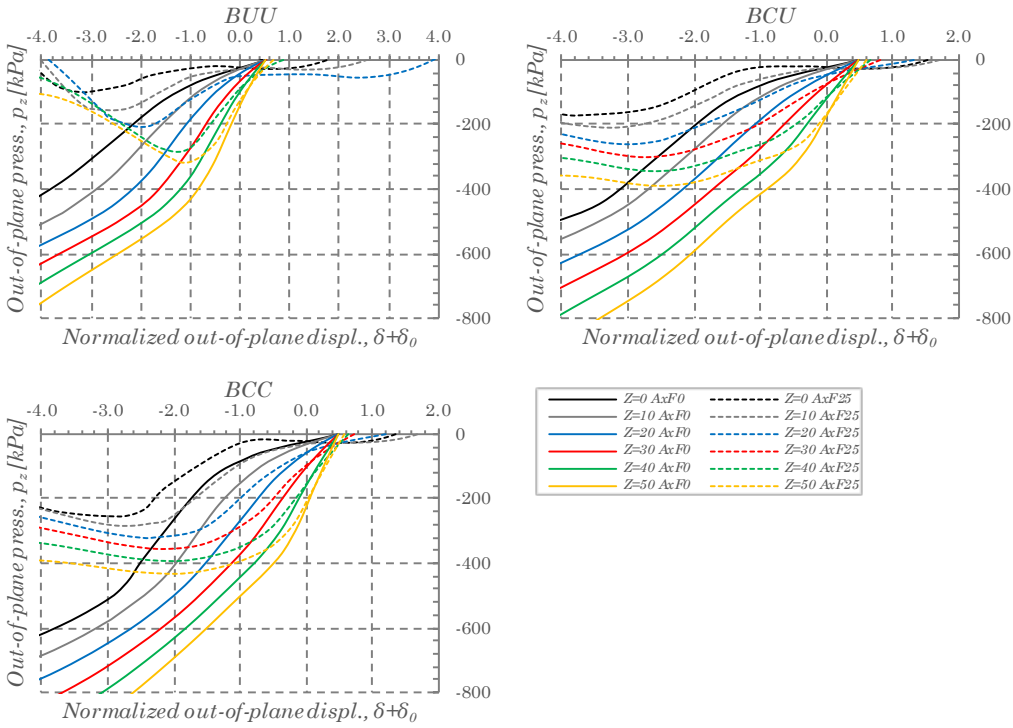

Figure 6.42: Effect of the initial in-plane axial load (AxF=0% *vs* AxF=25%) for panels loaded with negative out-of-plane pressure for different levels of curvature and different boundary conditions (a/h=100, α=1.0)

axial restraint existed along the edges, for example, in-plane fixed boundary conditions. In this case, because boundary conditions are simply supported the in-plane displacement are free, however there is a partial effect due to the relative displacement constraints assumed for the edges in BCU and BCC. This influence is noticeable in the results.

The differences on the displacements due to the initial compression are quite significant, especially between BUU and the remaining boundary conditions. In fact, it is verified

Table 6.13: Ultimate load for the negative p_z in panels pre-compressed with AxF=25%, α=1.0 and a/h=100 [kPa]

	Z=0	Z=10	Z=20	Z=30	Z=40	Z=50
BUU	-97.9	-153.1	-208.3	(AxF=21.6%)	-275.5	-317.4
BCU	-171.2	-210.2	-258.8	-301.0	-343.3	-387.4
BCC	-253.6	-282.7	-320.1	-355.0	-391.5	-431.7

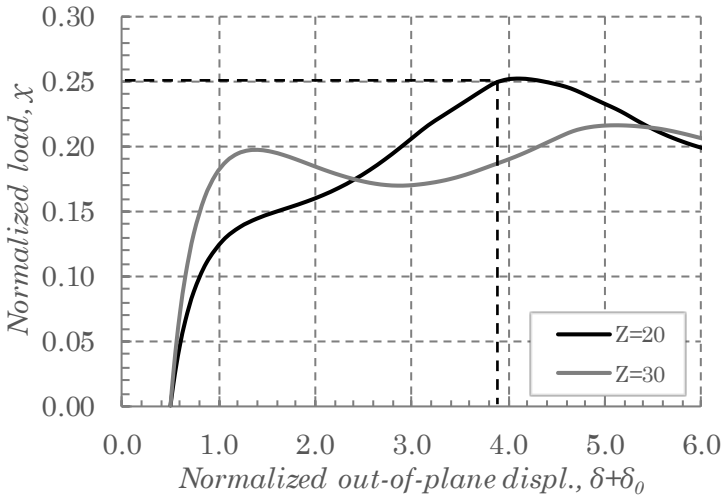

Figure 6.43: Comparison of the equilibrium paths for Z=20 and Z=30 under uniaxial compression for a/h=100, α=1.0 and BUU

that one panel (Z=30) in BUU is even unable to sustain the initial pre-compression. This is clarified in Figure 6.43 where the equilibrium path for Z=30 and Z=20 is plotted for pure compression. It is verified that the panel Z=30 is unable to reach 25% of the plastic load (21.6%), reason why the corresponding equilibrium path was not presented in Figure 6.42. On the hand, for exemplification, the panel Z=20 reaches the predefined in-plane load for $\delta+\delta_0$=3.9, which matches the initial displacement in Figure 6.42.

6.8.4 Initial out-of-plane pressure followed by in-plane compression

Figure 6.44 shows the load-deflection curves of in-plane compressed panels initially preloaded with a uniformly distributed out-of-plane pressure, p_z, of 50 kPa. The results are compared with the results without out-of-plane pressure from section 6.6. Different curvatures and aspect ratios are considered with BCC. It is verified that the behaviour is considerably distinct depending on the aspect ratio. The behaviour of the panels becomes much more unstable as the aspect ratio increases. This, in part, is explained by the initial imperfection pattern used. As previously discussed in section 6.6, this type of imperfection (SPSW) force this type of behaviour in panels with large aspect ratios. Nevertheless, the effect of the initial p_z is very noticeable and increases as the aspect ratio increases. In the initial state, the initial p_z can be seen as an amplification of the initial imperfection. For α=0.5 and 1.0, the behaviour follows approximately the same tendency

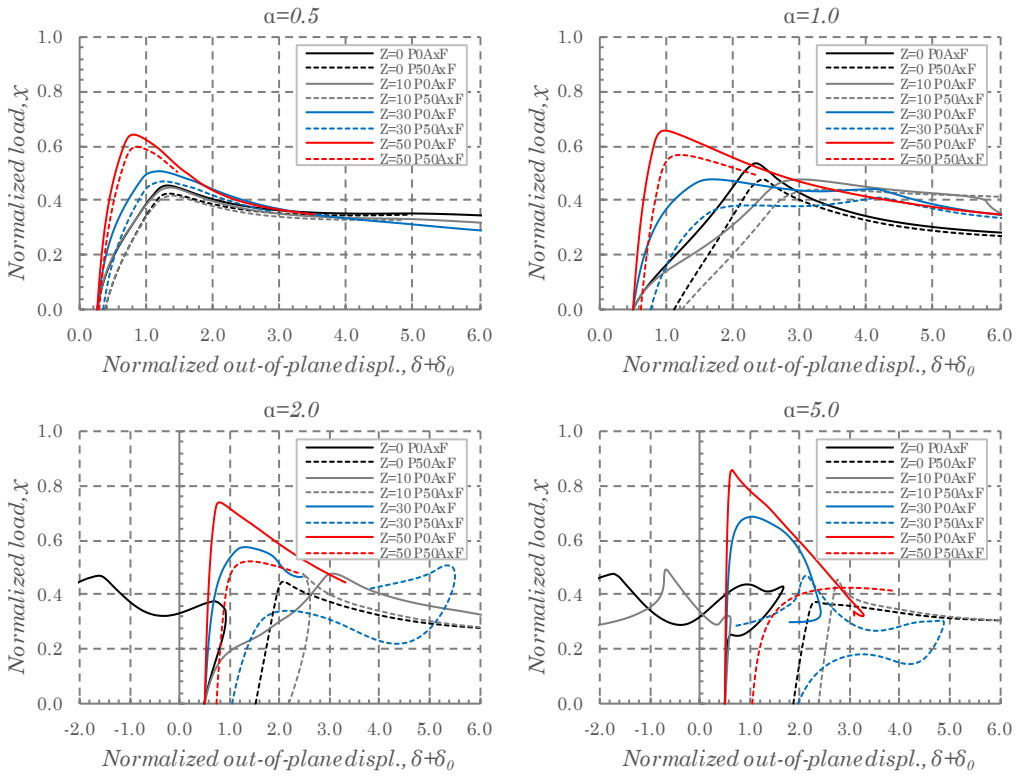

Figure 6.44: Effect of the initial out-of-plane pressure (p_z=0 kPa vs p_z=50 kPa) for panels loaded with in-plane compression for different levels of curvature and aspect ratios (a/h=100, α=1.0 and BCC)

reaching the ultimate load for lower values. In some cases, for the larger aspect ratios, the initial p_z has a stabilizing effect. For example, where the panels only loaded in compression changed the direction of deformation, they passed to deform only in one direction, *e.g.* Z=0 and α=2.0. However, in other cases for example Z=30 it is not sufficient to eliminate this effect.

The values of the ultimate load are compiled in Figure 6.45. The decrease in the ultimate load may be rather significant especially for the larger aspect ratios with large curvatures. The case with α=5.0 and Z=50 shows a reduction of 50.4%. For α=0.5 and α=1.0 the reduction is approximately constant along all the curvatures.

The ultimate loads for panels with a/h=100 subjected to an initial out-of-plane pressure of 50 kPa followed by in-plane compression can be consulted in Annex C.

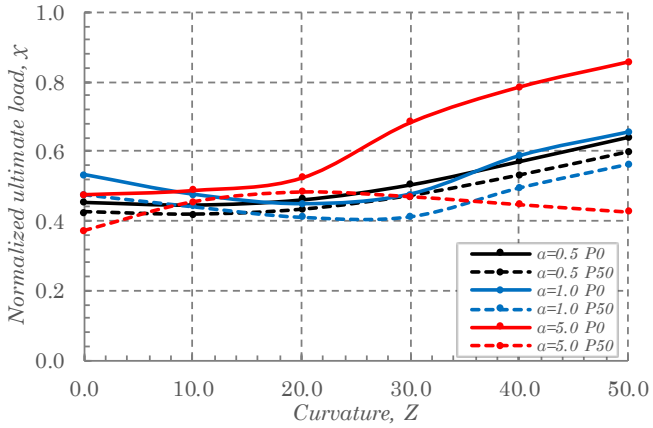

Figure 6.45: Effect of the initial out-of-plane pressure (p_z=0 kPa vs p_z=50 kPa) in the ultimate load for panels loaded with in-plane compression for different levels of curvature and aspect ratios (a/h=100, α=1.0 and BCC)

6.9 LARGE DEFLECTION BEHAVIOUR AND ULTIMATE LOAD OF STIFFENED CURVED PANELS UNDER OUT-OF-PLANE PRESSURE

6.9.1 Introduction

Similarly to the previous section, out-of-plane pressure is addressed but now for stiffened panels. The geometric variation is the same as in section 6.7, however with fewer intermediate cases to avoid unnecessary analyses. The effect of parameters like the aspect ratio, the curvature and boundary conditions is, in generic terms, similar to what has been said in previous sections. Consequently, less quantity of results will be presented to avoid repetition.

The objective is to characterize generically the behaviour of the stiffened panels under this new load situation and present its distinctive behaviour in comparison with the previous cases.

The load cases are similar to the ones defined in the previous section for the unstiffened panels. Table 6.14 summarizes the 2160 different situations considered.

Table 6.14: Parametric variation of stiffened curved panels under out-of-plane pressure (GMNIA)

Panel				Stiffeners			BC	Imperfection	Load case	Material
Z_{Global}	α	a_s/h	h [m]	n_s	d_s/h_s	h_s [m]				
0	0.5	25	0.01	1	7.5	0.01	BCC	POS(	AxF0+P	Elasto-Plastic
10	1.0	50		2	10.0			SPSW:min(a;b)/400	AxF25+P	(S355)
30	1.5			3				+MPSW:min(a;b)/200	AxF0-P	
50				5				+Stf:h/50)	AxF25-P	
100				7					(P0+AxF)	
200									P50+AxF	

6.9.2 Effect of the aspect ratio, a_s/h and d_s/h_s ratios

The effect of the width of the subpanel to thickness ratio, a_s/h, is shown in Figure 6.46 for different aspect ratios and curvatures for a panel with 3 stiffeners. As expected, the slenderness of the subpanels affects significantly the loads reached. For example for α=1.0 and Z=50, a panel with a_s/h=50 develops -89.9% smaller loads than with a_s/h=25 for δ=1.5 (discounting the effect of δ_0).

Smaller aspect ratios increase substantially the stiffness of the panels. For example, for a_s/h=25 and Z=50, the panel with α=1.5 develops a load 83.9% smaller than α=0.5 for $\delta+\delta_0$=2.0. For a_s/h=25 and α=1.0, a panel with Z=100 develops a load 157.3% larger than Z=0 for $\delta+\delta_0$=1.0.

Figure 6.47 shows the effect of increasing d_s/h_s=7.5 to d_s/h_s=10.0 (an increase of the moment of inertia of the stiffeners of 2.37 times) for different number of stiffeners and curvatures[11]. It is possible to conclude that the behaviour is not changed, only amplified with the increase in the d_s/h_s ratio. This increase is approximately constant along the displacement, however its effect tends to increase with the slenderness of the panels (a/h in this case proportional to the number of stiffeners) where the stiffeners are more important.

[11] The case with n_s=1 and Z=200 is not shown because this very high value of curvature for a_s/h=25 generates a panel with a small radius of curvature showing little practical applicability.

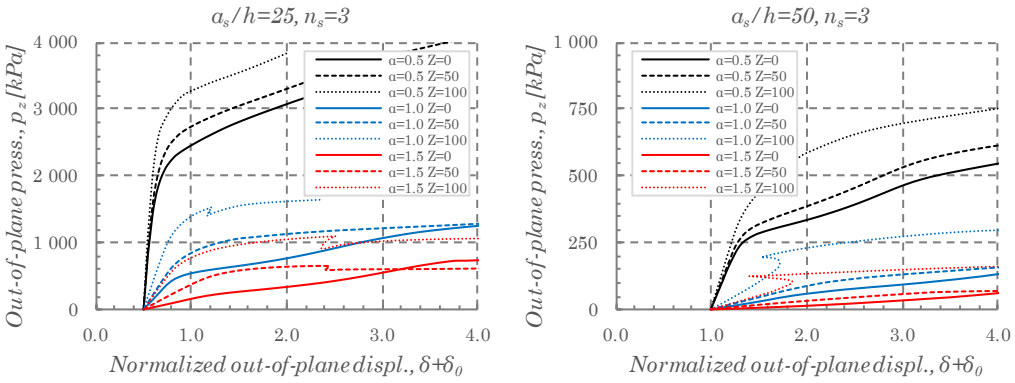

Figure 6.46: Effect of the aspect ratio and a_s/h ratio for panels loaded with positive out-of-plane pressure for different levels of curvature (BCC, AxF=0)

The reason for the peculiar equilibrium paths for the highest curvatures (Z=100 and Z=200) for a_s/h=50 in Figure 6.46 and n_s=7 in Figure 6.47 will be explained in the next section.

6.9.3 Effect of an initial in-plane compression

Figure 6.48 compares panels without initial in-plane compression with an initial in-plane compression equivalent to 25% of f_y (AxF25). Different number of stiffeners and curvatures are compared.

For curvatures up to 50, the initial in-plane compression increases the initial displacements and it lowers the equilibrium paths, *i.e.* the load reached for a same displacement is lower. The effect of the initial compression is found to be very important for Z=100 and Z=200, especially for larger a/h (proportional the number of stiffeners), where the behaviour is very unstable. The reason is that these panels are very unstable and prone to snap-through phenomena similarly to what has been shown in previous figures.

These snap-through phenomena occur in panels with very high curvatures Z>100 and large slenderness (increasing with n_s and a_s/h ratio). Panels with very high curvatures approach the classical case of snap-trough phenomena: an arch under pressure. They may also occur in a small number of stiffeners with large a_s/h ratios. In these cases, the stiffeners are stiff in comparison with the panel and local instabilities are susceptible to be developed. In these cases, the curvature may induce the development of larger

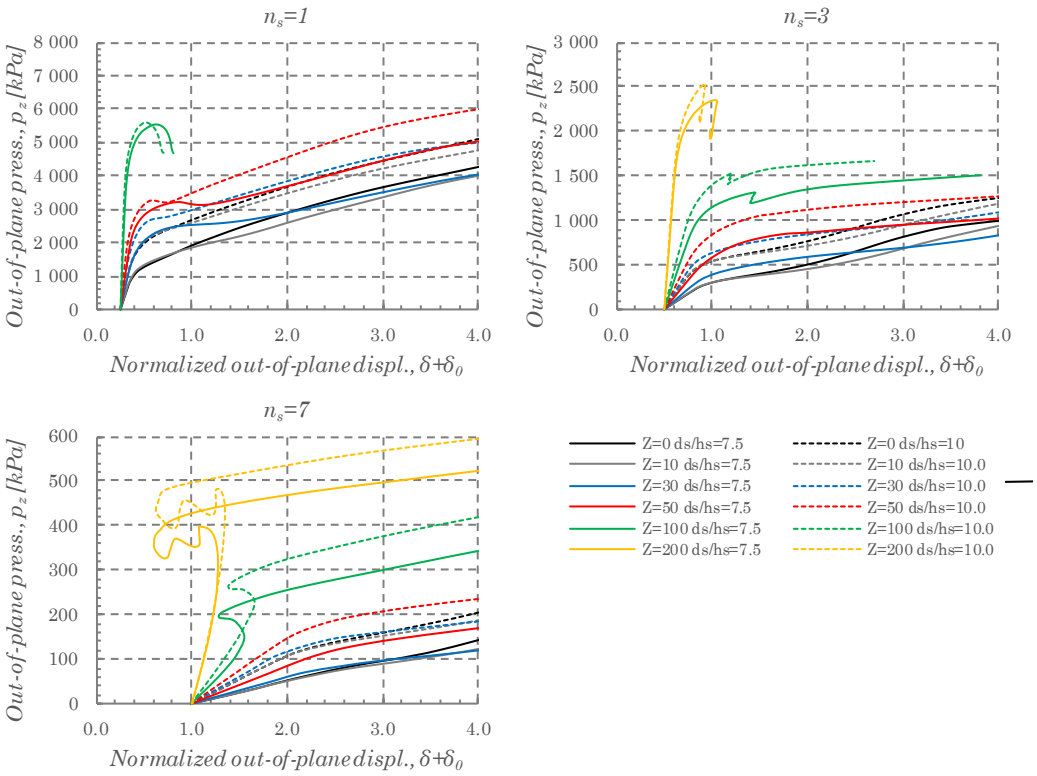

Figure 6.47: Effect of the d_s/h ratio for panels loaded with positive out-of-plane pressure for different levels of curvature (a_s/h=25, α=1.0, AxF=0 and BCC)

displacements in certain subpanels which due to the existence of stiffeners do not propagate to the adjacent subpanels. However, due to the compatibility of rotations, reverse displacements may be developed in the adjacent panels.

In order to exemplify this case, one of the most extreme cases found with this phenomenon is represented in Figure 6.49, corresponding to n_s=2, a_s/h=50, Z=100, α=1.0, AxF=0% and BCC. The equilibrium paths in function of the out-of-plane and in-plane displacement are plotted with several points marked in the equilibrium paths with the corresponding deformation shape. It is possible to confirm the development of larger displacements at the outer subpanels. This is due to the existence of stiffeners decreasing the displacements along them. By compatibility of rotations on the stiffeners, the displacements at the central panel is reduced (Point C). From that point, the system regains stiffness and the displacements increase again at the centre (Point D).

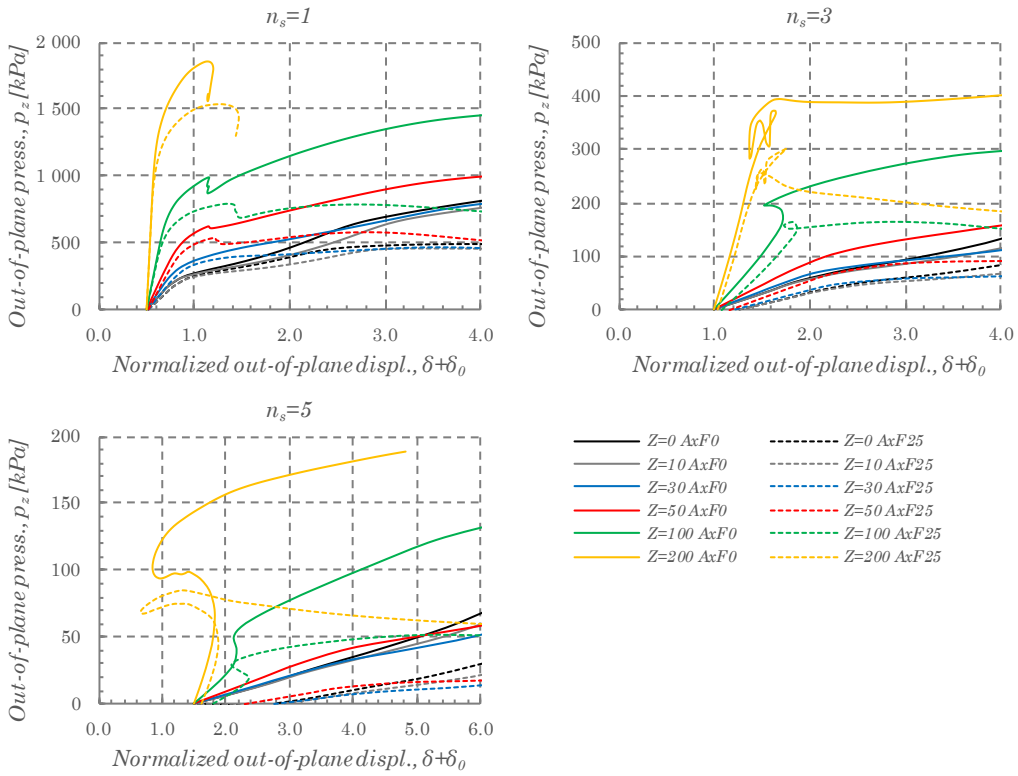

Figure 6.48: Effect of the initial in-plane axial load (AxF=0% *vs* AxF=25%) for panels loaded with positive out-of-plane pressure for different levels of curvature and number of stiffeners (a_s/h=50, α=1.0 and BCC)

Centrifugal (negative) pressures are applied in the panels of Figure 6.50. The effect of the initial in-plane compression is also evaluated. Similarly to what was concluded for the unstiffened panels, this centrifugal pressure induce more stable behaviours along the curvatures. Furthermore, as expected, snap-through phenomena are inexistent for this direction of the pressure.

The effect of the initial in-plane compression is approximately constant; however, a slight increase in the difference between AxF0 and AxF25 is verified for larger curvatures.

6.9.4 Initial out-of-plane pressure followed by in-plane compression

In this case, the out-of-plane pressure is first applied and then followed by in-plane compression. The equilibrium paths of the panels studied in section 6.7 (P0AxF) are compared with the ones with an initial pressure of 50 kPa. Two levels for the a_s/h ratio and n_s are considered as described in Figure 6.51.

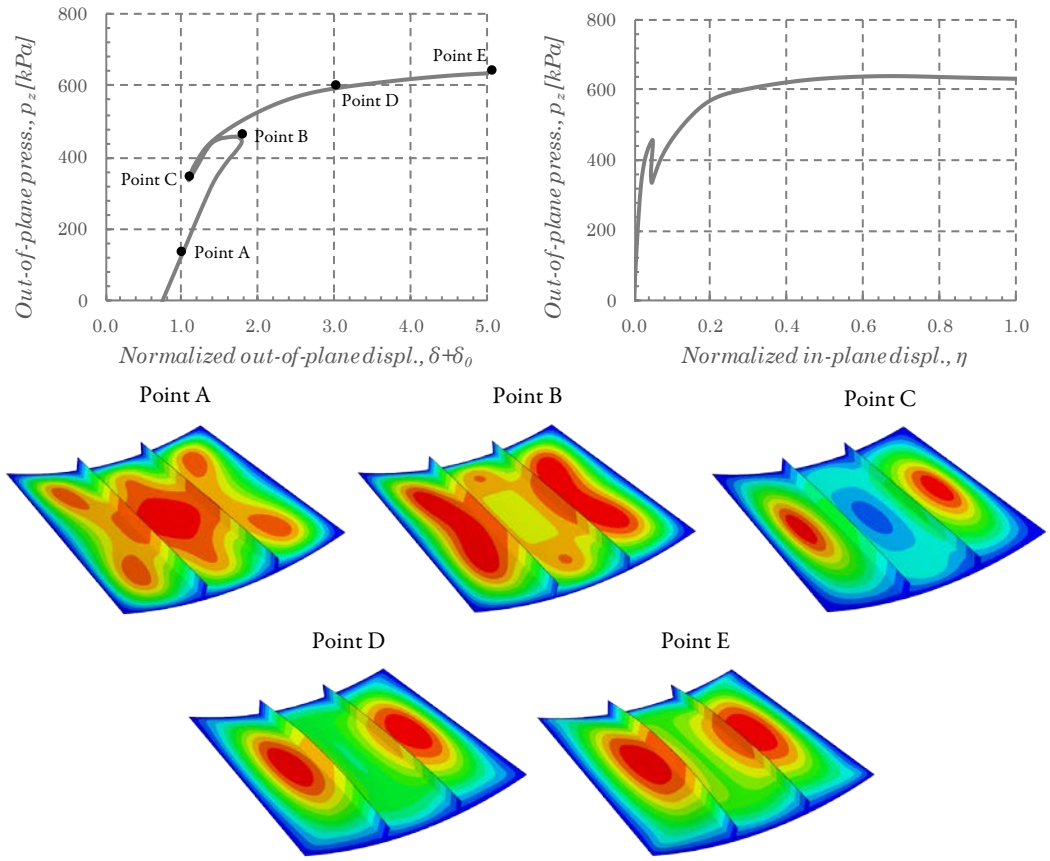

Figure 6.49: Evolution of the deformed shape for panels loaded with positive out-of-plane pressure for different levels of curvature and number of stiffeners (n_s=2, a_s/h=50, Z=100, α=1.0, AxF=0% and BCC)

The reduction of the ultimate loads is larger for smaller curvatures. For example, for a_s/h=50 and n_s=3 while the pressure leads to a reduction of 29.5% for Z=0, for Z=200 is only 7.7%.

The ultimate loads for panels with a_s/h=25 subjected to an initial out-of-plane pressure of 50 kPa followed by in-plane compression can be consulted in Annex C.

6.10 Summary

In this chapter, the behaviour of both unstiffened and stiffened panels was characterized for in-plane compression, out-of-plane pressure and interaction between both loads. The study was performed through FEA in the most realistic way possible for a wide range of

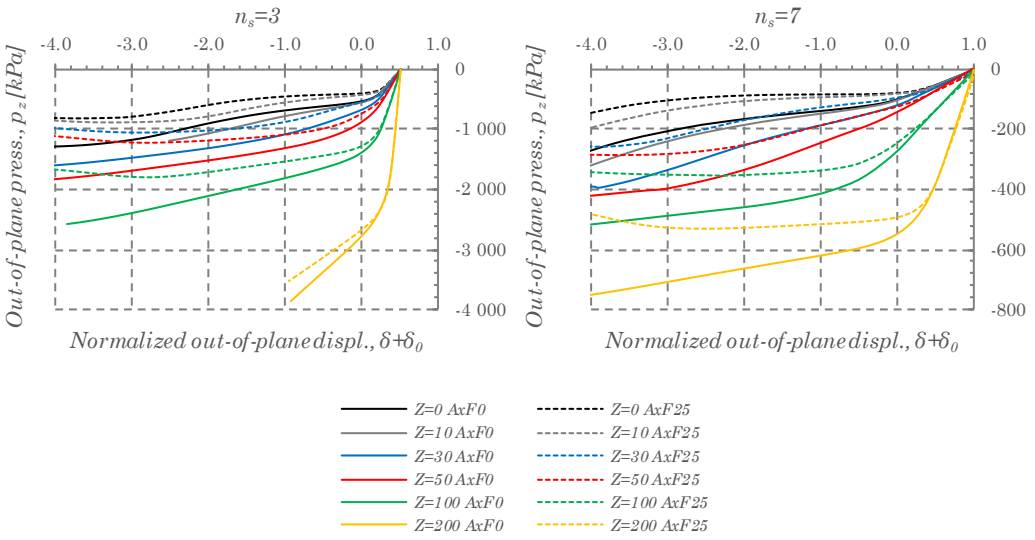

Figure 6.50: Effect of the initial in-plane axial load (AxF=0% *vs* AxF=25%) for panels loaded with negative out-of-plane pressure for different levels of curvature and number of stiffeners (a_s/h=25, α=1.0 and BCC)

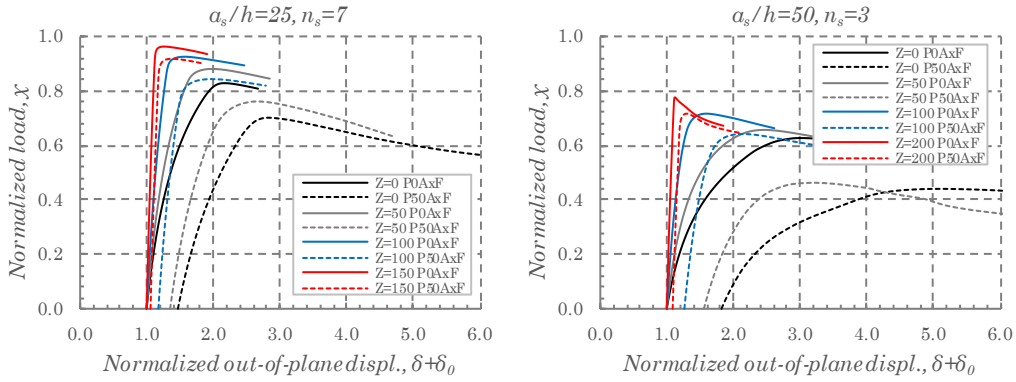

Figure 6.51: Effect of the initial out-of-plane pressure (p_z=0 kPa vs p_z=50 kPa) for stiffened panels loaded with in-plane compression for different levels of curvature: (α=1.0 and BCC)

situations (thousands of cases were analysed).

The chapter began with the analysis of the critical behaviour of the panels. This was found to be useful to explain certain behaviours in the following sections. The preliminary analysis on some of the parameters was found to be useful to analyse the importance to study certain parameters and to define the parametric study. The effect of the material nonlinearity was found to be very important on the large deflection behaviour of the panels. A brief study on the impact of residual stresses allowed to

conclude that the effect of residual stresses can be incorporated in a more convenient way by equivalent geometric imperfections.

The large deflection behaviour was then thoroughly analysed. The nonlinear behaviour and the ultimate load of unstiffened and stiffened curved panels subjected to in-plane compression was evaluated. A very detailed analysis of imperfection was carried out allowing to conclude about the utmost importance of the topic. For example, it was concluded that the consideration of initial imperfection patterns given by the eigenmodes from LBAs (usually assumed in many structural problems) may be non-conservative for curved panel. The global imperfection pattern, a_{11}, may lead, in some cases, to considerably lower values for χ.

The study was then extended to out-of-plane pressure and interaction with in-plane compression. In this case, taking into account that ultimate loads are not reached within displacements with practical significance more emphasis was given to the non-linear behaviour of the panels.

The analysed parameters were found to change dramatically the behaviour of the panels, which, in some cases, lead to unexpected results.

7 Validation of the Semi-Analytical Model for curved panels under in-plane compression and out-of-plane pressure

7.1 Introduction

In this chapter, the large displacement behaviour of unstiffened and stiffened curved panels are tackled with the Semi-Analytical Method (SAM) based on the formulation presented in Chapter 4. The results from the semi-analytical method are compared with the results of advanced finite element analyses. The objective is to validate the SAM for a wide range of situations both for unstiffened and stiffened panels under in-plane

compression and out-of-plane pressure. The results will be presented mainly in terms of the nonlinear equilibrium paths which were thoroughly analysed in Chapter 6.

Despite the critical behaviour not being the main subject of this thesis (as discussed in section 3.6, it is not able to characterize properly the behaviour of curved panels), the subject will be briefly addressed with the SAM for validation purposes in section 7.2. With regard to the post-buckling behaviour, the results are explored in greater detail and thoroughly compared with advanced non-linear FE analyses (as described in Chapter 5) in sections 7.3 and 7.4 for unstiffened and stiffened panels under in-plane compression, respectively. Out-of-plane pressure and its interaction with in-plane compression will be addressed in section 7.5.

As previously referred, an elastic material is considered in the analytical formulation and, consequently, the equilibrium paths in this chapter reflect that assumption. The effect of the plasticity of the material and the prediction of the ultimate load will be tackled in an approximate way through the utilization of a strength criterion in Chapter 8.

Linear elastic Bifurcation Analyses (LBAs) and Geometrically Nonlinear elastic Analyses with Imperfections included (GNIAs) were performed as described in detail in Chapter 5, for section 7.2 and sections 7.3 to 7.5, respectively. This means the use of a linear elastic material law with a modulus of elasticity, E, of 210 GPa and a Poisson's coefficient, ν, of 0.3 both in the SAM and FEM.

Residual stresses are possible to be incorporated in semi-analytical methods. Paik *et al.* [138] showed it for flat plates, for the case of weld induced residual stresses. This stress component is included in the stress function, F, simply as an initial stress field. However, as discussed in section 6.5, the explicit consideration of residual stresses is not crucial and, besides that, they may be conveniently accounted for through equivalent geometric imperfections, reason why they were not considered in the SAM.

Snap-through phenomena were found to be nonexistent in the analyses carried out. However, it should be noted that the semi-analytical formulation should be able to account for them properly, provided that an adequate method is chosen to solve the algebraic system of equations. The Newton-Raphson method in load-control fails to catch the equilibrium path when the tangent is zero, therefore requiring a displacement-control incrementation strategy or using an arc-length method.

In the SAM it is intended to use the minimum number of Degrees of Freedom (DOFs) possible to get a good approximation to the FEM results. This increases the efficiency of the method and, as it will be seen, in the case of a single DOF, closed-form expressions may be obtained, which is of enormous interest (subject to be studied in Chapter 8).

7.2 Critical behaviour of unstiffened curved panels under uniaxial compression

In order to assess the capability of the semi-analytical model to predict the critical behaviour, the elastic buckling coefficient of some unstiffened curved panels are compared with the numerical results.

The critical and the initial post-critical load-deflection curve of panels with Z=0, 10 and 20 are presented in Figure 7.1. These panels are considered free of imperfections, with boundary conditions BCC and an aspect ratio α=1.0. Taking into account what has been said, while the eigenmodes of panels with low curvatures are sufficiently well defined with few degrees of freedoms (DOFs), the eigenmodes of panels with larger curvatures require more degrees of freedom. For this particular case only 2 DOFs were used, b_{11} and b_{13}. Figure 7.1 corroborates what was schematically drawn previously in Figure 3.11. The

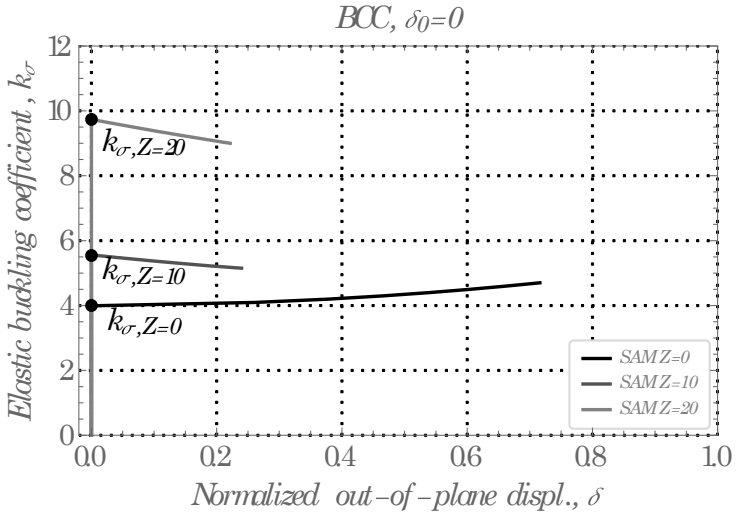

Figure 7.1: Critical and post-buckling behaviour in function of the out-of-plane displacement at the centre of the panels (BCC, n_s=0, and α=1.0)

equilibrium paths of a perfect plate (Z=0) and two perfect curved panels (Z=10 and Z=20) are obtained and compared directly by the SAM. The curves are plotted as a function of the normalized out-of-plane displacement at the centre of the panels, $\delta=w/h$. The differences in the behaviour are very clear. While the flat plate shows a stable post-critical equilibrium path, meaning that the load increases with the displacement, the curved panels show unstable equilibrium paths because the load decreases as the displacement increases. Additionally, the slope of the unstable equilibrium paths of curved panels increases as the curvature increases. Besides that, the graph shows that the curvature increases very significantly the elastic buckling coefficient, k_σ. For example, the panel with Z=20 has a value of k_σ 143% higher than the corresponding flat plate (k_σ=4.0).

In Table 7.1 the values of the elastic buckling coefficient, k_σ, obtained through SAM and FEM are presented and the differences between both methods are calculated. Corroborating what Martins *et al.* [54] concluded, for long panels ($\alpha\geq1$), it is very difficult to get satisfactory results for the critical stresses of panels with large curvatures when a small number of DOFs are employed. This is due to the fact that a large number of DOFs is required to approximate the correct eigenmodes (see section 6.2). The curvature increases very considerably the complexity of eigenmodes in comparison to flat panels. To evidence this, in Table 7.1, the elastic buckling coefficient, k_σ, is calculated only with 2 DOFs (b_{11} and b_{13}) and compared with the finite element analyses for aspect ratios α=0.5 and α=1.0, for various levels of curvatures. It is possible to conclude that the values of k_σ for α=0.5 obtained by the semi-analytical methods match perfectly the values

Table 7.1: Comparison of the elastic buckling coefficient k_σ calculated through SAM and FEM (BCC and n_s=0)

		Z=0	Z=10	Z=20	Z=30	Z=40	Z=50
α=0.5	**SAM**	6.24	6.68	8.15	10.47	13.56	17.29
	FEM	6.24	6.74	8.19	10.53	13.63	17.28
	Diff. [%]	0.0	-0.8	-0.4	-0.6	-0.5	0.1
α=1.0	**SAM**	4.00	5.55	9.73	14.51	-	-
	FEM	4.00	5.70	9.21	12.28	15.31	18.52
	Diff. [%]	0.0	-2.6	5.6	18.1	-	-

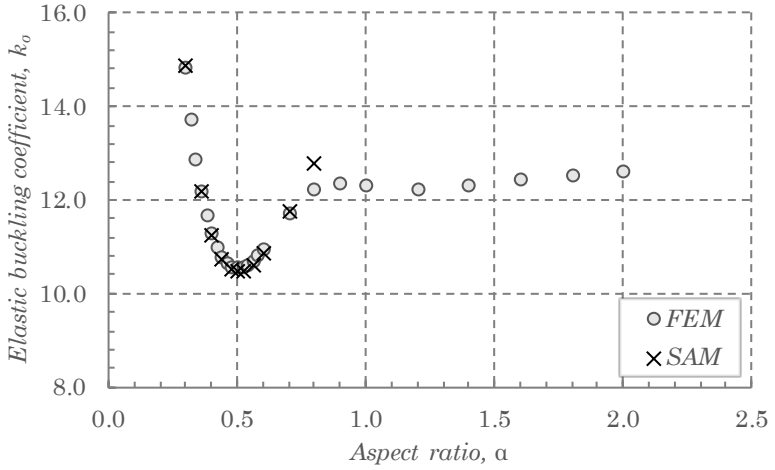

Figure 7.2: Elastic buckling coefficient k_σ calculated through SAM (b_{11} and b_{13}) and FEM (BCC, n_s=0, and Z=30)

obtained by FEM. For longer panels, the values match well only for curvature up to Z=20. This fact is explained with Figure 6.3, observing that only the eigenmodes of the shorter panels and the ones of the longer panels with Z=0 can be well approximated with very few DOFs. On the other hand, for long curved panels the complexity of the eigenmodes increases significantly and a larger number of DOFs are required.

A reasonable solution is to determine the minimum critical stresses for a given curvature which it is verified to occur for short aspect ratios ($\alpha \leq 1.0$) which can easily be estimated with only 1 or 2 DOF. For example, for a curvature Z=30 with 2 DOFs (b_{11} and b_{13}) the elastic buckling coefficient, k_σ, is perfectly matched up to aspect ratios α=0.7 which covers perfectly the minimum value of k_σ, as seen in Figure 7.2 where the SAM and FEM results are compared.

7.3 Large deflection behaviour of unstiffened curved panels under in-plane compression

7.3.1 Introduction

In this section, the elastic non-linear load-deflection behaviour of unstiffened curved panels under uniaxial in-plane compression is calculated through the semi-analytical

model and compared with the non-linear FEA. The main objective is to assess the validity of the semi-analytical method.

The panels are considered with initial imperfections which are considered the same in both approaches for the sake of comparison. The influence of imperfections was thoroughly assessed in Chapter 6 and it is not objective to introduce that variable again in the results of the SAM. Consequently, imperfections will be considered given, for convenience, simply by perfect semi-waves (the number depends of the aspect ratio).

The formulation with a MDOF solution is tested with square and long panels (α=3.0) for curvatures up to Z=50, for boundary conditions BCU and BCC and two levels of imperfections. The equilibrium paths are compared as a function of the in-plane and out-of-plane displacements.

7.3.2 Equilibrium paths and validation of the semi-analytical procedure

The number of semi-waves with more relevance for the aspect ratios studied is generally odd. Consequently, only symmetrical deflection modes with respect to both axes are relevant. Hence, only odd numbers are used for the number of semi-waves in the transversal and longitudinal directions, m and n, respectively in equation (4.85).

In a first phase, numerical calculations were performed for curvatures up to Z=50 and aspect ratios α=1.0 and 3.0. The width, a, and the thickness, h, is fixed to 1.0 and 0.01 m, respectively. Two imperfection amplitudes normalized to thickness, $\delta_0=w_0/h$, were used: δ_0=0.2 (equivalent to a/500) and δ_0=0.5 (equivalent to a/200). Depending on the aspect ratio, the number of perfect longitudinal semi-waves for the pattern of imperfections was chosen between 1 and 3.

It was found that only two degrees of freedom are enough for a reasonable characterization of the post-buckling behaviour of the panels in study, taking into account the range of curvatures with practical applicability. Therefore, for the MDOF solution, in panels with aspect ratios equal to 1.0 the DOFs were used with m=1 and n=1 and 3 (b_{11} and b_{13}); for aspect ratios equal to 3.0 the DOFs were used with m=1 and 3 and n=3 (b_{13} and b_{33}). On the other hand, it was found that a SDOF is not able to accurately reproduce the post-buckling behaviour of panels with large curvatures because

the need for a MDOF solution increases significantly as the curvature increases.

In order to facilitate the analysis of the results, a dimensionless load factor, $\overline{P_y}$, is defined as follows:

$$\overline{P_y} = p_y \frac{a^2}{E\,h^2} \tag{7.1}$$

To corroborate what has been said in the previous chapters, Figure 7.3 illustrates the response, obtained with the SAM, of a flat plate (Z=0) and a curved panel with low curvature (Z=10) without and with two levels of initial imperfections with one semi-wave in each direction (δ_{011}=0.01 and 0.2). The normalized load $\overline{P_y}$ is computed in function of the out-of-plane displacement normalized to the thickness, $\delta=w/h$, at the centre of the panel ($x=0$ and $y=0$, see Figure 3.4). The examination of the response of the perfect cases clearly shows a stable post-buckling behaviour for the flat plate while the curved panel exhibits an unstable post-buckling behaviour. For this case, this unstable response is only visible for small imperfections because of the subsequent re-stiffening of the curved panel. The unstable behaviour is significantly affected by curvature, boundary conditions and imperfections, as previously explained.

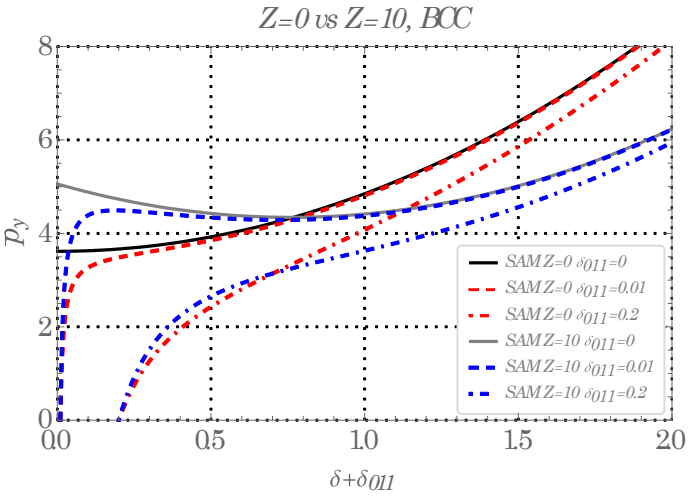

Figure 7.3: Equilibrium paths for the out-of-plane displacements at the centre of a flat plate (Z=0) and a low curvature panel (Z=10) without and with various levels of imperfections (BCC and α=1.0)

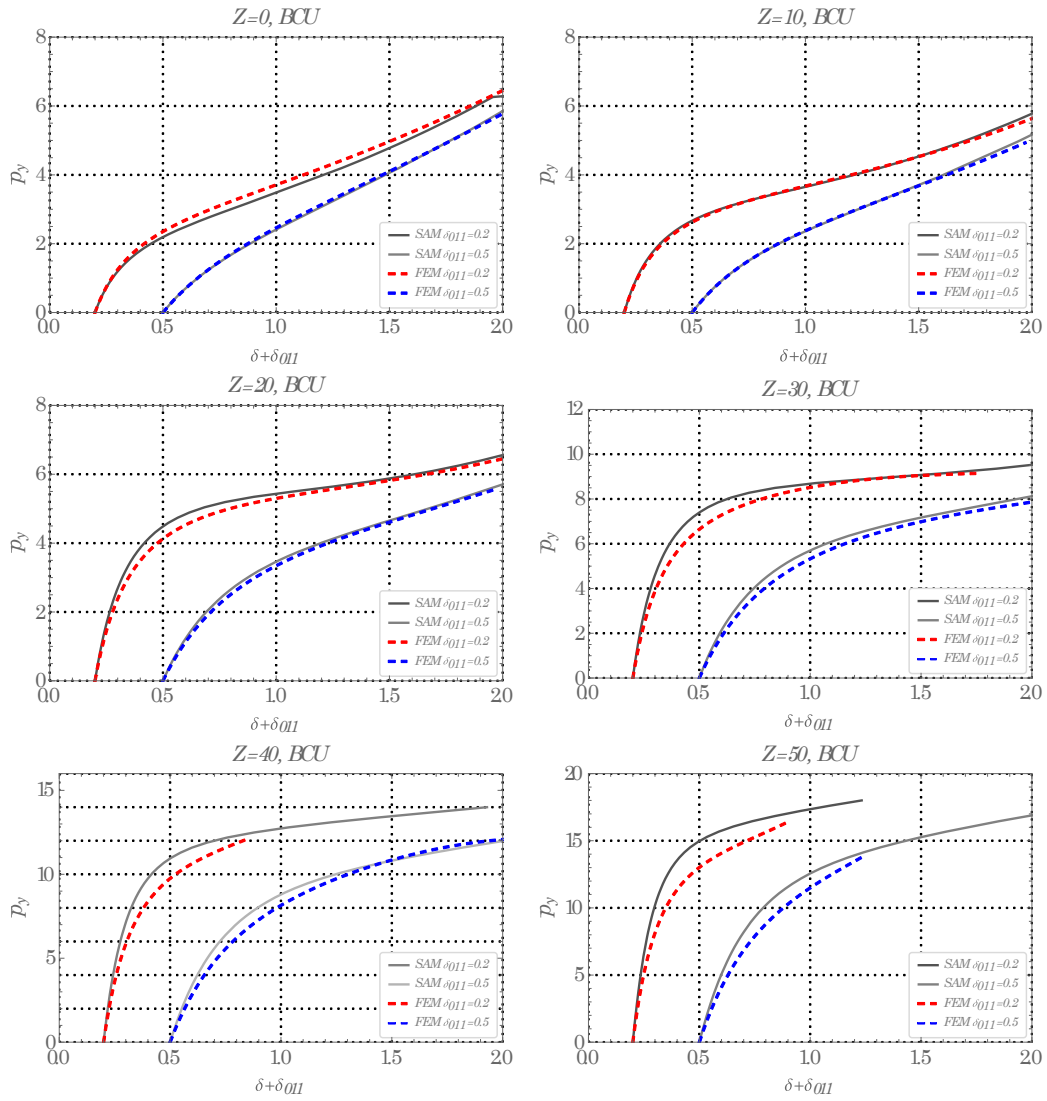

Figure 7.4: Equilibrium paths for the out-of-plane displacements at the centre of the panels (BCU and α=1.0)

The equilibrium paths obtained by the SAM are plotted up to: *i)* numerical divergence of the problem or *ii)* until a sufficient value for the load is reached.

The equilibrium paths of the panels previously described are computed in function of the out-of-plane displacement normalized to the thickness in Figure 7.4 and Figure 7.5 for α=1.0, respectively, for boundary conditions BCU and BCC. Comparison of the equilibrium paths obtained by the SAM and the FEM is done. A good agreement is verified for both boundary conditions as shown by the very good match for both

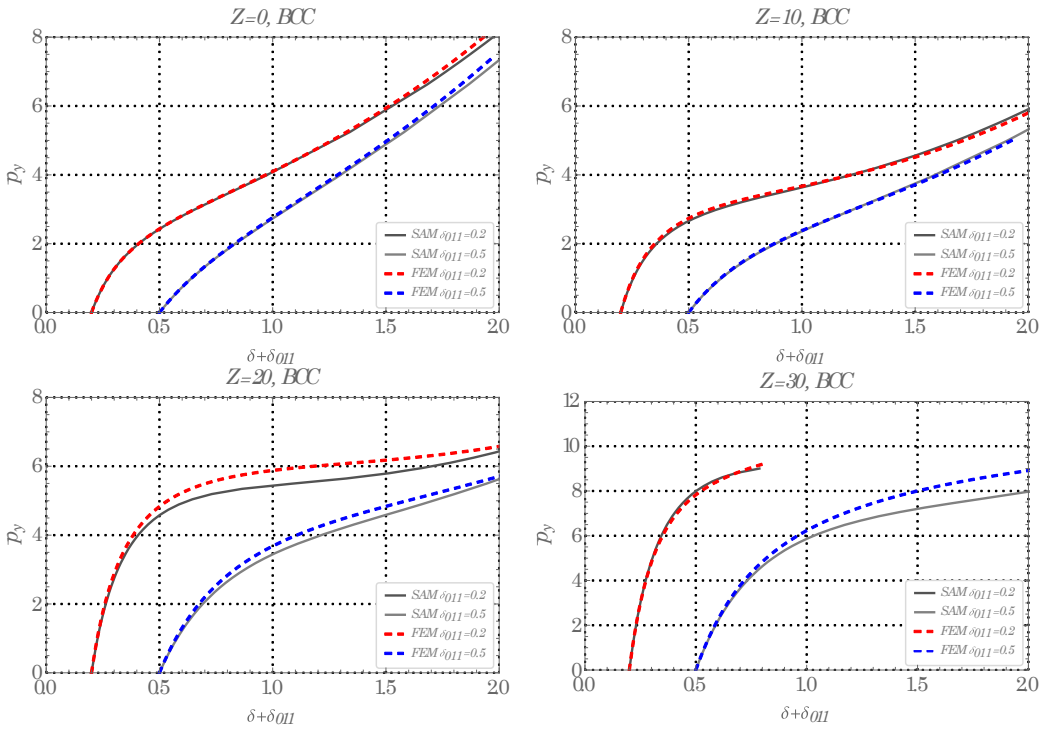

Figure 7.5: Equilibrium paths for the out-of-plane displacement at the centre of the panels (BCC and α=1.0)

imperfections, even using only 2 DOFs. However, as the curvature increases, the modal participation of higher modes is larger. Consequently, if larger curvatures were desired, more DOFs would be required. Despite the maximum error for boundary conditions BCU being still acceptable (≈15% for Z=50), it is possible to verify that the differences between the SAM and FEM results become larger from Z=40 onwards. For boundary conditions BCC it was found that the same 2 DOF lead to larger errors for Z=40 and Z=50 and the results are only shown for Z up to 30. Even so, it should be noted that a curvature Z=30 is enough to cover most of the unstiffened curved panels used in real bridges, for example, where the maximum values are approximately Z=15 [135].

The same load is also computed as a function of the in-plane displacement normalized to thickness, $\eta=v/h$, at the middle of the loaded edge ($x=0$ and $y=-b/2$, see Figure 3.4) in Figure 7.6 and Figure 7.7, for aspect ratios equal to 1.0, respectively for boundary conditions BCU and BCC. Again, a good agreement between the SAM and FEM results is verified. For boundary conditions BCU the equilibrium paths very well match for the

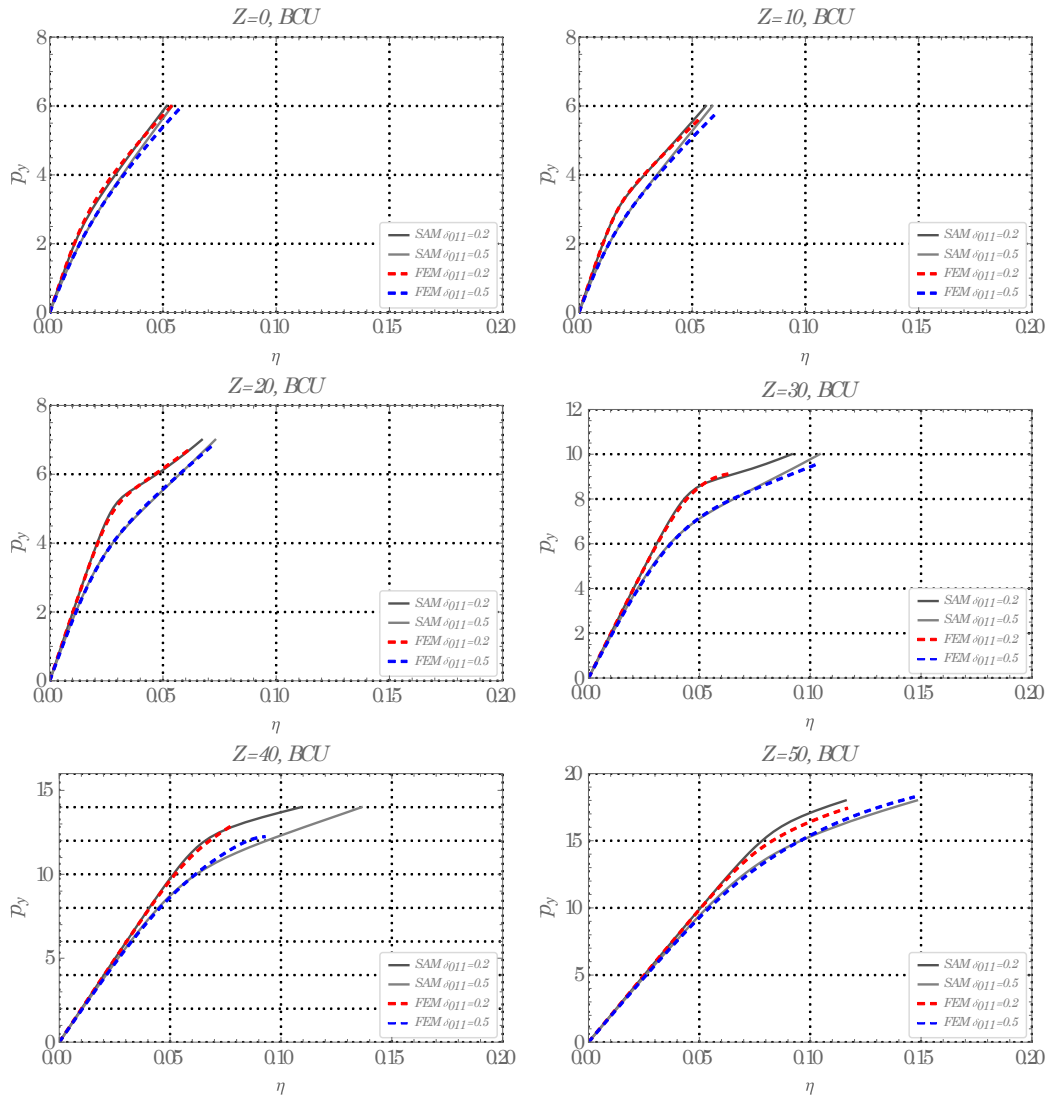

Figure 7.6: Equilibrium paths for the in-plane displacements at the middle of the loaded edges (BCU and α=1.0)

plotted range of in-plane displacements. For boundary conditions BCC, the initial stiffness is perfectly obtained, but some differences become visible for large values of η when the panels start losing stiffness. However, this only happens for very high load levels. In this case, even curvatures of Z=40 and Z=50 are reasonably assessed.

The validity of the semi-analytical model is also assessed for larger aspect ratios (α=3.0) in Figure 7.8 for out-of-plane displacements and BCU assuming an imperfection δ_{013}=0.2 and in Figure 7.9 for in-plane displacements and BCC for an imperfection δ_{013}=0.5. In

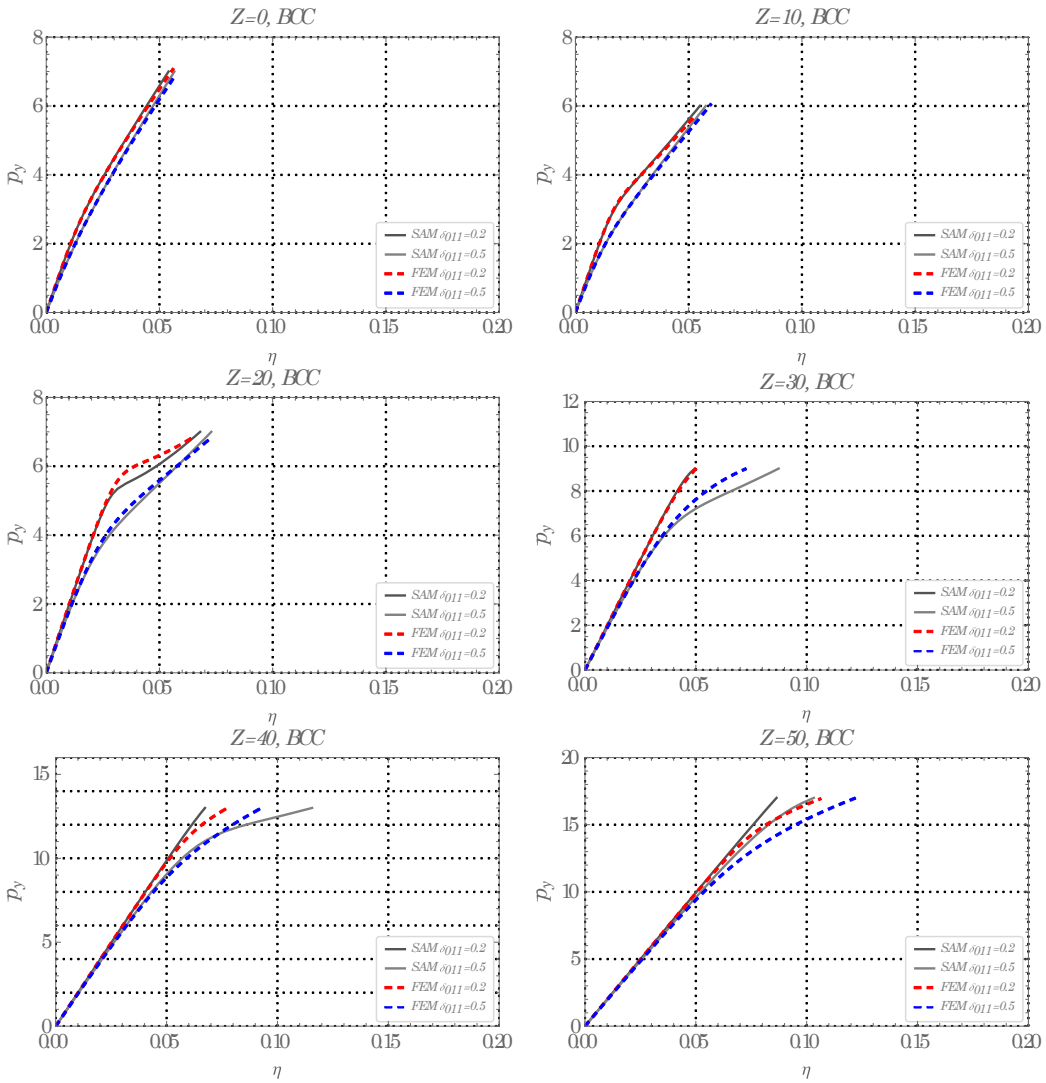

Figure 7.7: Equilibrium paths for the in-plane displacements at the middle of the loaded edges (BCC and α=1.0)

both cases, a good agreement is obtained. It is verified that the in-plane stiffness decreases as the aspect ratio increases. Comparing Figure 7.7 and Figure 7.9 it is possible to conclude that for a same load level, a panel with a larger aspect ratio develops larger in-plane displacements than one with a smaller aspect ratio.

It is clear that a good solution for generic aspect ratios and curvatures of the panels requires a sufficient number of DOFs. This will impact the efficiency of the SAM in terms of calculation times and convergence. Naturally, equally good solutions may be obtained using a small number of DOFs, provided that the most relevant modes are

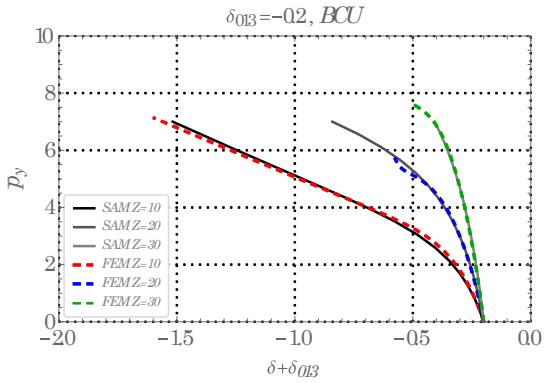

Figure 7.8: Equilibrium paths for the out-of-plane displacement at the centre of the panels (BCU and α=3.0)

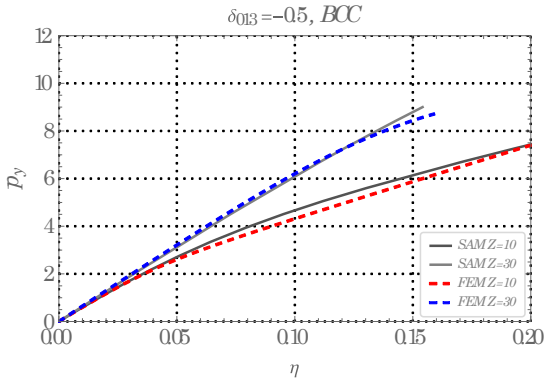

Figure 7.9: Equilibrium paths for the in-plane displacements at the middle of the loaded edge (BCC and α=3.0)

appropriately chosen. For longer panels, the pattern of displacements (w) and initial imperfections (w_0) of the semi-analytical model needs to match the real behaviour, obtained from the FEM analyses. Hence, for a panel with an aspect ratio α=3.0 and an imperfection a_{13}, the deformation shape has 3 longitudinal semi-waves which is mainly represented by the mode b_{13}. This is shown in Figure 7.10 where the deformation shapes are represented with the vertical displacements in z obtained from the FE analyses for panels with boundary conditions BCU, Z=10 and α=1.0 and α=3.0 in *a)* and *b)*, respectively, for a load level $\overline{P_y} = 4$. Figure 7.11 shows the corresponding out-of-plane displacements (w) obtained with the semi-analytical model.

From the previous results it is possible to corroborate what was concluded in Chapter 6 about the curvature. In general, for most cases, greater curvatures lead to the development

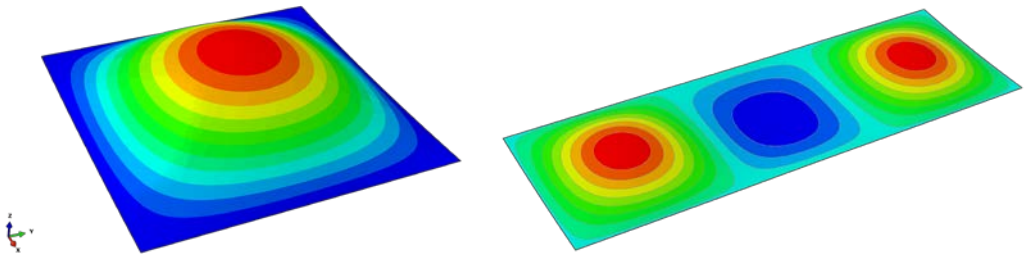

a) *b)*

Figure 7.10: Vertical displacements in z from the FEM for *a)* α=1.0 and *b)* α=3.0 with BCU, Z=10 and P_y^-=4.0

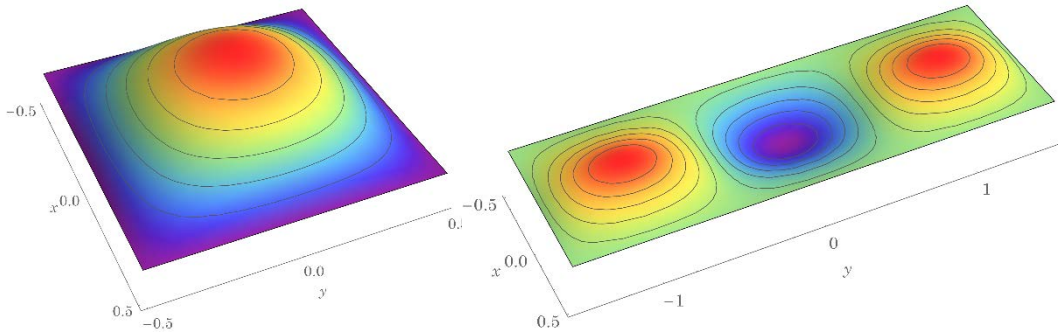

a) *b)*

Figure 7.11: Out-of-plane displacements (w) from the SAM for *a)* α=1.0 and *b)* α=3.0 with BCU, Z=10 and P_y^-=4.0

of higher loads for the same displacement. However, this is not always the case for low curvatures. For example, for boundary conditions BCC, the flat panel leads to higher loads for the same out-of-plane displacement when compared to the corresponding curved panel with Z=10 (see Figure 7.5).

The effect of the restraint of the longitudinal edges to remain straight was thoroughly analysed in Chapter 6 with the FEM. The same general effect was now obtained with the SAM. It is concluded that the in-plane restraint has a variable effect on the post-buckling behaviour of curved panels. As expected, the most restrained boundary conditions BCC lead generally to higher forces for the same displacement in the equivalent panel with boundary conditions BCU. However, these differences are not so notorious, especially for in-plane displacements of panels with aspect ratios equal to 1.0. The differences between boundary conditions are generally larger for larger aspect ratios. Anyway, the SAM was shown to be able to catch these effects quite well.

Finally, as previously concluded, it was found that imperfections play a fundamental role on the behaviour of curved panels under compression because they can decrease significantly the development of force in the elements. In all cases the SAM predicted very well the effect of the imperfections.

7.4 Large deflection behaviour of stiffened curved panels under in-plane compression

7.4.1 Introduction

In this section the validity of the orthotropic formulation developed in section 4.3 is assessed for stiffened curved panels under in-plane compression. This approach is applied to stiffened panels: *i)* composed by stiffeners not too strong so they do not constitute nodal lines; or *ii)* by a large number of stiffeners where the stiffeners buckle together with the panel (overall buckling occurs). To assess the applicability of this approximation, different configurations of stiffeners (in number and geometry) are considered. The number of stiffeners is varied between 3 to 7 stiffeners. To better assess this, in this section, the width of the panels are maintained fixed increasing the number of stiffeners. Later, in Chapter 8, when validating the proposed closed-form expressions for the equilibrium paths of stiffened curved panels, different geometric configurations (aspect ratio, width, thicknesses of the stiffeners, etc.) will also be assessed.

Despite a MDOF being required in some cases, a SDOF solution is sufficient for most of the analysed cases, where curvatures up to Z=50 and boundary conditions BCC are considered.

Contrarily to Chapter 6, very high values of curvature (Z=100 and 200) are not considered in the SAM for two reasons: *i)* a large number of DOFs are required, which decreases the efficiency of the method; and *ii)* the applicability of panels with so large curvatures is more reduced, not deserving so much attention.

7.4.2 Equilibrium paths and validation of the semi-analytical procedure

In a first phase, numerical calculations were performed for curvatures from Z=0 (flat

panels for comparison purposes) up to Z=50 and aspect ratios $\alpha=b/a$=1.0 and 3.0. Values of 1.0 m and 0.01 m were assumed for the width (a) and thickness (h), respectively. In order to obtain numerical values, three types of stiffeners were considered. Flat stiffeners with three different geometries were considered. Stiffener types A, B and C were assumed to have thicknesses (h_s) of 0.01 m in all cases and depths (d_s) of 0.045, 0.07 and 0.095 m, respectively[12]. In order to assess the validity of the orthotropic model, the number of stiffeners (n_s) are considered to be 3, 5 and 7. These stiffeners configurations induce behaviours of overall collapse mode as assumed for the orthotropic model. Moreover, this variation allows to assess the validity of the orthotropic model for a different number of stiffeners and, additionally, it allows to assess the influence of the slenderness of the stiffeners on the results, although class 4 stiffeners were not considered.

In real cases, these panels are not free from initial imperfections and residual stresses (due to welding). Due to the extreme complexity to account for the real initial scenario, the usual procedure is to assume an equivalent imperfection accounting for all the referred effects and, consequently, a value of an equivalent initial geometric imperfection should be given to a_{mn}. Two reasonable imperfection amplitudes normalized to thickness ($\delta_0=w_0/h$) were used: δ_0=0.2 (equivalent to a/500) and δ_0=0.5 (equivalent to a/200). The pattern for the initial imperfections was assumed to be given in all cases by a global mode (a_{11}: 1 perfect semi-wave in both directions).

It was found that a single degree of freedom (SDOF) is enough for a reasonable characterization of the post-buckling behaviour of the panels with an aspect ratio α=1.0. This is due to the fact that for this aspect ratio (and for the range of displacements considered) the first mode (b_{11}) is dominant and higher modes can be neglected. However, the same is not true for larger aspect ratios. In order to assess the validity of the semi-analytical model for larger aspect ratios, panels with aspect ratios α=3.0 are also assessed. Despite being a relatively large value for stiffened panels this aspect ratio, unlike

[12] It should be noted that the depths of the stiffeners in the SAM have discounted half of the thickness of the panel, h, in comparison with the values used in Chapter 6, although in practice they correspond to the same stiffener (*e.g.* for h=0.01 m, $d_{s,FEM}$=0.10 m → $d_{s,SAM}$=0.095 m). This is because in the FEM due to the utilization of shell elements the height of the stiffeners has to be explicitly modelled with the increase by h/2. On the other hand, in the SAM d_s is the real free dimension, as described in Figure 3.5. In fact, $d_{s,FEM}=d_s+h/2$, however for convenience in Chapter 6 $d_{s,FEM}$ was named simply as d_s.

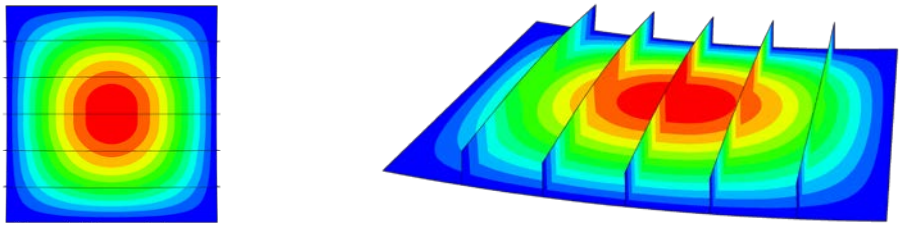

a) *b)*

Figure 7.12: Out-of-plane deformation for a panel with Z=20, α=1.0 and 5 stiffeners of type B for χ=2.0, *a)* top view and *b)* perspective view

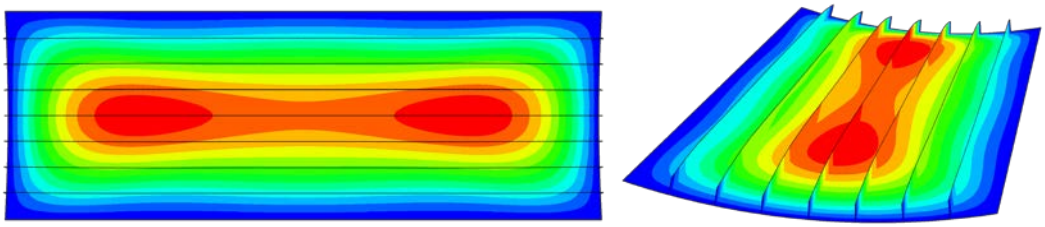

a) *b)*

Figure 7.13: Out-of-plane deformation for a panel with Z=50, α=3.0 and 7 stiffeners of type A for χ=2.0, *a)* top view and *b)* perspective view

panels with α=1.0, allows to catch the interaction between different modes and, consequently, more than one DOF is required. Comparing Figure 7.12 and Figure 7.13, where the out-of-plane deformation of panels with α=1.0 and α=3.0 are represented, respectively, one can conclude that while a unique DOF is sufficient for the first case (1 longitudinal semi-wave, b_{11}), at least 2 DOFs for the second case are needed (1 longitudinal semi-wave, b_{11}, and 3 longitudinal semi-waves, b_{13}). Therefore, for the analyses with α=3.0, a multiple degree of freedom displacement field (with 2 DOF) was used.

As previously explained, the depths of the different types of stiffeners previously defined are now increased by half of the thickness of the panel (for equivalence with the shell elements in the FEM) leading to 0.05, 0.075 and 0.10 m for stiffeners A, B and C, respectively.

In order to facilitate the analysis of the results, a normalized load factor χ is defined using the plastic load (corresponding to the total cross section of the stiffened panels) using a

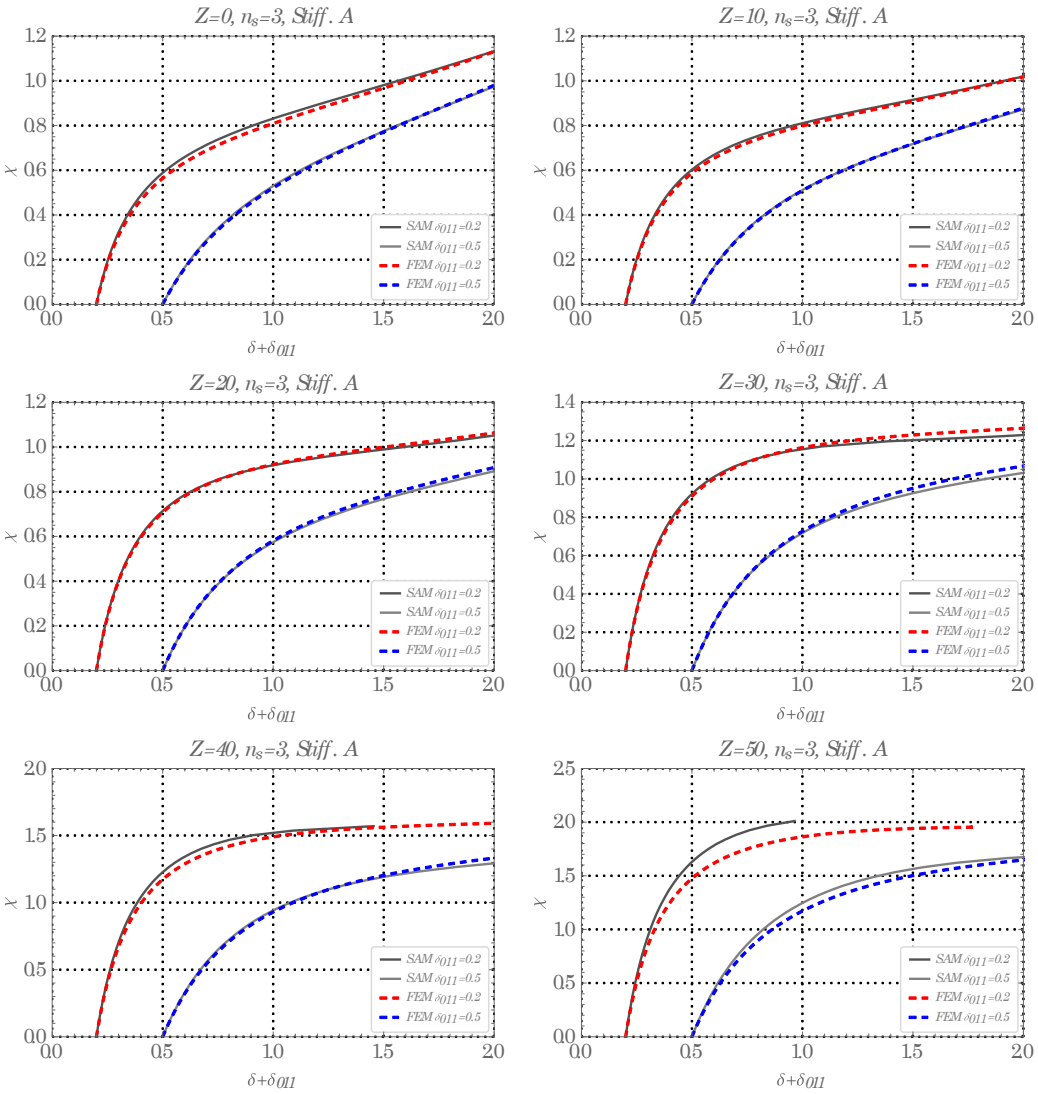

Figure 7.14: Equilibrium paths in function of the out-of-plane displacement at the centre of the panel for panels with α=1.0 and 3 stiffeners of type A

steel with a yield strength f_y=355 MPa. It should be noted that this yield strength is used only to normalize the value of the load because the material is in all cases considered elastic. Hence, the load factor is χ=1.0 when the stiffened cross-section is fully yielded. The load factor χ is calculated for the semi-analytical model as:

$$\chi = \frac{p_y (a\,h)}{f_y (a\,h + n_s\,h_s\,d_s)} \tag{7.2}$$

The load factor χ from the semi-analytical method is computed in function of the out-of-

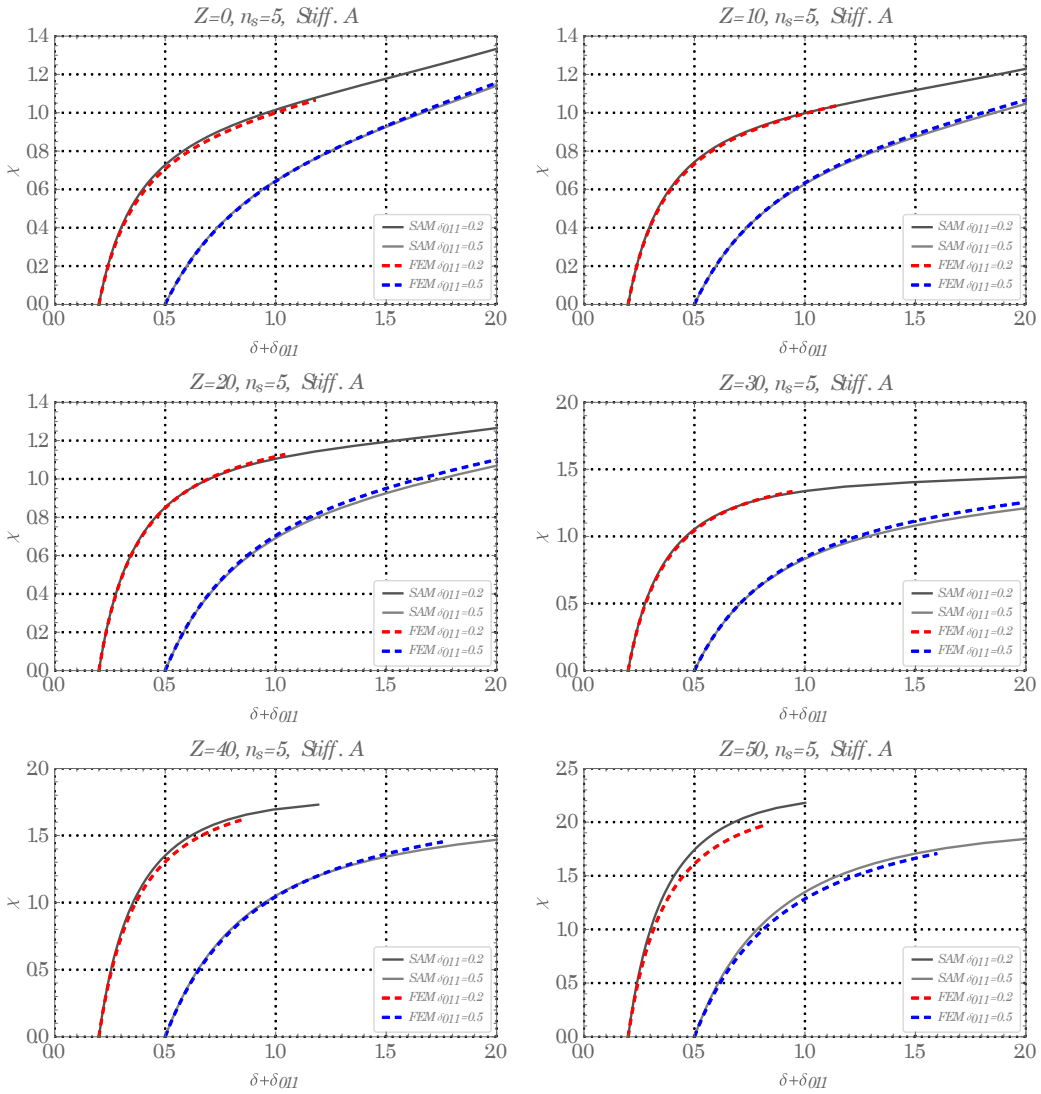

Figure 7.15: Equilibrium paths in function of the out-of-plane displacement at the centre of the panel for panels with α=1.0 and 5 stiffeners of type A

plane displacement normalized to the thickness $\delta=w/h$ at the centre of the panel ($x=0$ and $y=0$) and compared with the FEM results in the next graphs: Figure 7.14 to Figure 7.16 for stiffeners of type A and Figure 7.17 to Figure 7.19 for stiffeners of type B for panels with 3, 5 and 7 stiffeners and aspect ratio α=1.0. The comparison for stiffeners of type C are presented in Annex D for brevity reasons. The curves of the SAM are plotted at least up to χ=1.0. In some cases, larger values of χ are plotted to clarify the nonlinear behaviour of the panels.

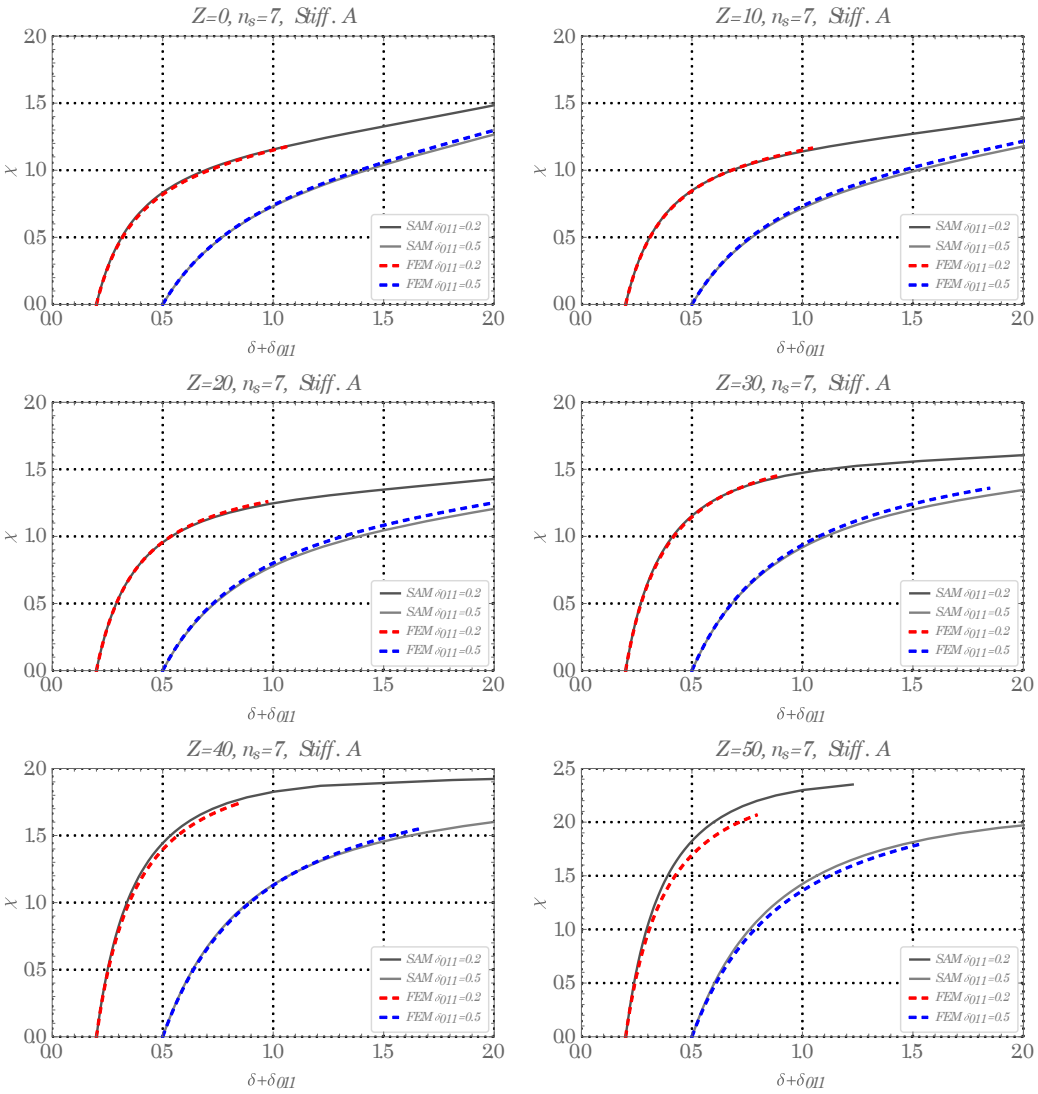

Figure 7.16: Equilibrium paths in function of the out-of-plane displacement at the centre of the panel for panels with α=1.0 and 7 stiffeners of type A

From these results it is possible to verify that in general a good agreement is obtained. As expected, the results are better the greater the number and the lower the slenderness of the stiffeners. The greater the number of stiffeners, the more the stiffened panels approach the orthotropic model. On the other hand, the greater the slenderness of the stiffeners the greater is the possibility of the stiffeners showing instability phenomena.

With n_s=3 the results are in good agreement only for stiffeners of type A and are acceptable for stiffeners of type B. However, it is important to mention that even for the

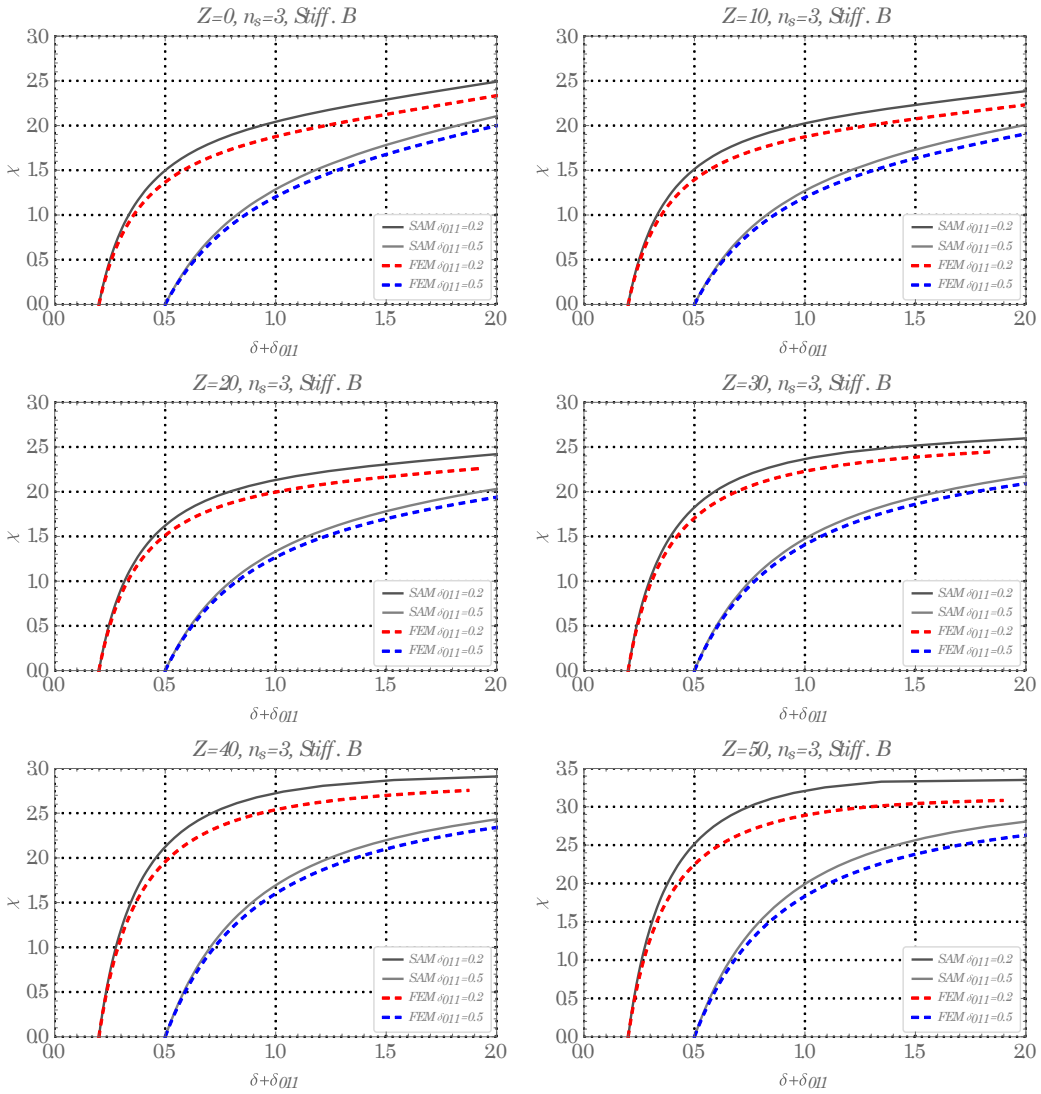

Figure 7.17: Equilibrium paths in function of the out-of-plane displacement at the centre of the panel for panels with α=1.0 and 3 stiffeners of type B

stiffeners with the highest slenderness, the differences only become relevant for values of the normalized load, χ higher than 1. For values of χ of practical interest ($\leq$1), the curves given by the SAM are in good agreement with the ones given by the FE analyses.

For n_s=5 and n_s=7 the results of the semi-analytical model are in excellent agreement with the FEM analyses, for all types of stiffeners and even for larger curvatures.

In general, the panels with the larger initial imperfection amplitude (δ_{011}=0.5) show a slightly better agreement than for the lower imperfection amplitude (δ_{011}=0.2).

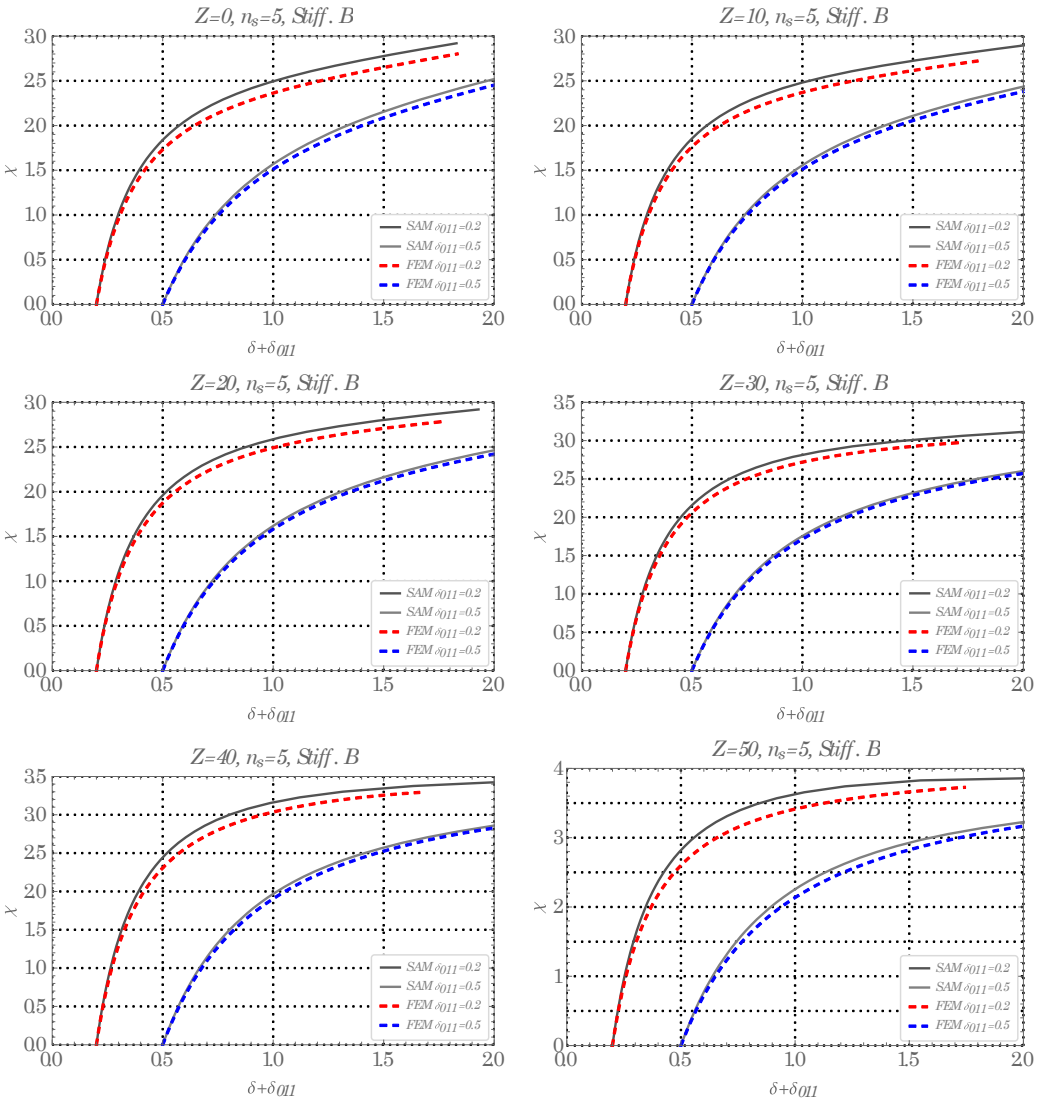

Figure 7.18: Equilibrium paths in function of the out-of-plane displacement at the centre of the panel for panels with α=1.0 and 5 stiffeners of type B

The level of normalized load achieved in the panels, for the range of displacements considered, varies from about 1 for slightly stiffened panels and low curvatures to about 7 times the plastic load for heavy stiffened panels and high curvatures. Hence, the elastic post-buckling solutions are able to reach and exceed all load levels of practical interest.

In Table 7.2 the results of the numerical models and the semi-analytical model are compared in terms of χ. The closest point to χ=1.0 is chosen and the displacement in this point is used to calculate χ in the semi-analytical model using only a SDOF. In this way,

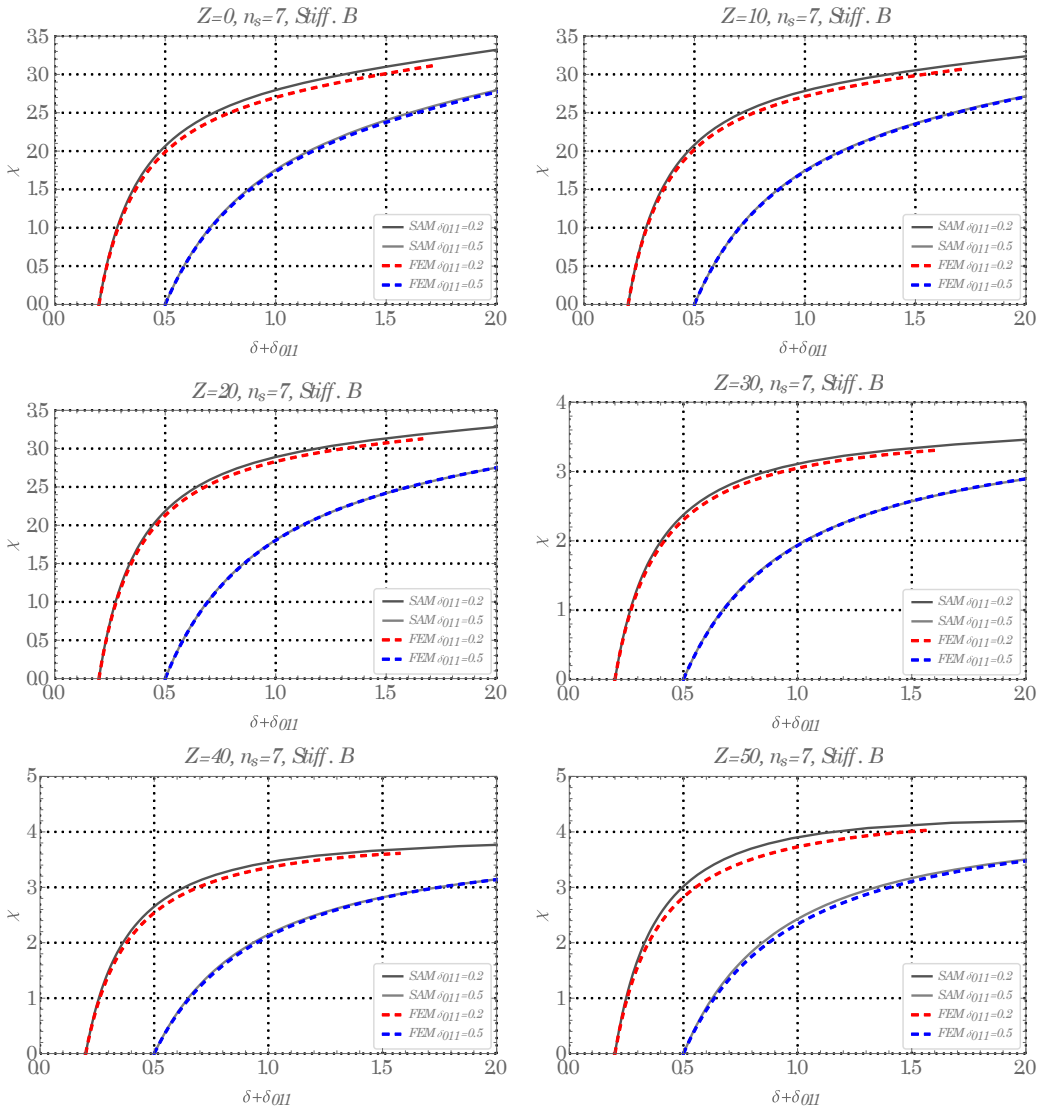

Figure 7.19: Equilibrium paths in function of the out-of-plane displacement at the centre of the panel for panels with α=1.0 and 7 stiffeners of type B

the maxima possible errors are given for those panels (only values of $\chi \leq 1.0$ have practical significance). The results are given for imperfections δ_{011}=0.5.

As expected, the larger the number of stiffeners the smaller is the difference between the FEM and the SAM. This corroborates the approximation to the orthotropic model. On the other hand, the larger is the slenderness of the stiffeners, the larger are the eccentricities and the possibility of instability phenomena. In these results this becomes visible for the stiffeners with the larger slenderness (stiffeners of type C) and the smallest

Table 7.2: Comparison of χ at the closest point in the numerical models leading to χ=1.0 for δ_{011}=0.5 (SDOF)

		Stiff. A				Stiff. B				Stiff. C			
		FEM		SAM		FEM		SAM		FEM		SAM	
	Z	χ	$\delta_{tot,FEM}$	$\chi_{(\delta_{tot,FEM})}$	diff. [%]	χ	$\delta_{tot,FEM}$	$\chi_{(\delta_{tot,FEM})}$	diff. [%]	χ	$\delta_{tot,FEM}$	$\chi_{(\delta_{tot,FEM})}$	diff. [%]
n_s=3	0	0.997	2.042	0.992	-0.6%	0.988	0.854	1.058	7.1%	0.951	0.633	1.071	12.5%
	10	1.005	2.398	0.996	-0.9%	1.009	0.867	1.072	6.3%	1.016	0.644	1.140	12.3%
	20	1.002	2.408	0.987	-1.6%	1.006	0.828	1.059	5.3%	1.025	0.639	1.144	11.5%
	30	0.999	1.677	0.969	-3.0%	0.989	0.768	1.040	5.2%	0.986	0.623	1.100	11.5%
	40	1.005	1.097	1.014	0.9%	1.006	0.724	1.068	6.2%	1.005	0.614	1.121	11.6%
	50	0.999	0.863	1.068	6.9%	1.015	0.686	1.109	9.2%	1.023	0.605	1.156	13.0%
n_s=5	0	1.001	1.648	0.993	-0.8%	1.020	0.760	1.062	4.1%	1.018	0.610	1.093	7.3%
	10	1.001	1.807	0.983	-1.7%	1.019	0.757	1.052	3.2%	1.020	0.610	1.095	7.4%
	20	1.001	1.652	0.974	-2.7%	1.000	0.732	1.028	2.9%	1.026	0.607	1.098	7.0%
	30	0.998	1.233	0.976	-2.3%	0.990	0.702	1.021	3.1%	0.973	0.595	1.043	7.2%
	40	0.997	0.955	1.006	0.9%	0.981	0.672	1.025	4.5%	0.983	0.590	1.065	8.3%
	50	1.003	0.813	1.081	7.8%	1.019	0.654	1.087	6.7%	0.994	0.584	1.090	9.6%
n_s=7	0	1.001	1.393	0.985	-1.6%	0.990	0.704	1.007	1.7%	0.981	0.591	1.021	4.1%
	10	0.998	1.451	0.971	-2.8%	0.991	0.702	1.000	0.9%	0.982	0.590	1.013	3.2%
	20	0.998	1.310	0.965	-3.3%	1.006	0.694	1.013	0.7%	0.986	0.588	1.017	3.2%
	30	1.001	1.075	0.979	-2.2%	0.984	0.671	0.999	1.6%	0.992	0.585	1.030	3.8%
	40	0.996	0.892	1.006	1.0%	1.013	0.657	1.043	2.9%	1.000	0.581	1.049	4.8%
	50	1.001	0.785	1.057	5.6%	0.990	0.634	1.048	5.9%	1.009	0.577	1.080	7.1%

number of stiffeners n_s=3 the average difference is 12.1%. On the other hand, for stiffeners of type A and n_s=7 the average difference is 2.8%. The semi-analytical model is thus able to deal accurately with a reduced number of stiffeners provided that they do not induce local effects, *i.e.* an overall buckling collapse mode occurs.

In Figure 7.20 the equilibrium paths for the out-of-plane displacement of the panels with α=3.0 are represented for low and high curvatures for different types of stiffeners (A and B). For all cases, a global pattern for initial imperfections with an amplitude of δ_{011}=0.5 was used and a solution with 2 DOFs was required. In all cases the semi-analytical model shows a good agreement with the FEM analyses. The curvature Z=10 is compared with Z=0 to show that for a same load level, the panel with Z=10 develops considerable larger

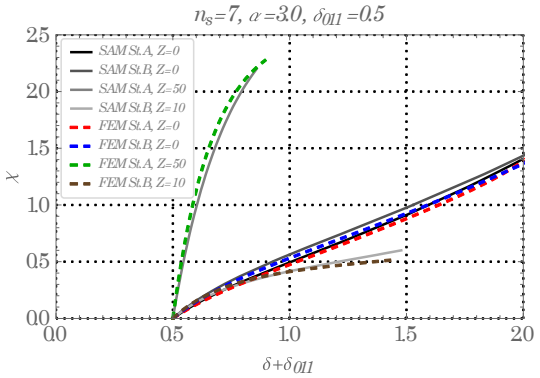

Figure 7.20: Equilibrium paths in function of the out-of-plane displacement at the centre of the panel for panels with α=3.0 and 7 stiffeners of type A and B for imperfections δ_{011}=0.5

out-of-plane displacements than the corresponding flat panel. This effect is even more visible for α=3.0 than for α=1.0. As for α=1.0, this may be explained by the fact that a low curvature may work like an imperfection and, consequently, it may lead to the development of larger deformations. In these cases, the gains with the introduction of curvature are not evident in comparison with the flat case. This aspect had already been identified previously.

Based on the presented results the semi-analytical method was proven to be able to deal with considerable high values of curvature (Z up to 50) and different aspect ratios of stiffened panels, provided that the deformation modes are properly chosen and the stiffened panels approach an orthotropic behaviour.

7.5 Large deflection behaviour of unstiffened and stiffened curved panels under combined uniaxial compression and out-of-plane pressure

7.5.1 Introduction

The main objective of this section is to show that the proposed methodology works well in a different number of situations under combined compression and out-of-plane loading. For all cases: *i)* the boundary conditions are considered simply supported with all edges forced to remain straight, BCC; *ii)* the aspect ratio is considered as $\alpha=b/a$=1.0

(different aspect ratios will be considered for validation of the closed-form expressions in Chapter 8)*; iii)* the imperfection amplitude was normalized to thickness ($\delta_0=w_0/h$) with a value of δ_0=0.2 or δ_0=-0.2 for centripetal and centrifugal out-of-plane pressure, respectively, and assumed with a pattern given by a single semi-wave in both directions (δ_{011}) which corresponds to a global imperfection mode.

Two distinct load cases were considered: *i)* the panels are considered first pre-loaded with one of three levels of in-plane compression and then subjected to increasing out-of-plane pressure (p_z); *ii)* the panels are considered first pre-loaded with one of three levels of out-of-plane pressure and then loaded with increasing in-plane compression (p_y). The equilibrium paths for both situations are compared by the semi-analytical method (SAM) and the Finite Element Method (FEM), as described in the previous sections.

Taking into account the sequence of the loads acting on the panels, two consecutive steps were defined for the FEM analyses. A first general static step was used for the first load (either the in-plane or out-of-plane loading), and a subsequent second step with an arc-length method of type Riks (see details in Chapter 5).

7.5.2 Equilibrium paths and validation of the semi-analytical procedure

7.5.2.1 Introduction

Taking into account what was previously said, the study incorporates unstiffened and stiffened panels, mainly for different curvatures and load cases. For the stiffened panels, a number of 7 stiffeners was assumed, which have a thickness (h_s) of 0.01 m and a depth (d_s) of 0.045 m (*i.e.* 0.05 m in FEA for the equivalence with the shell elements - increased by half the thickness of the panel). Values of 1.0 m and 0.01 m were assumed for the width (a) and thickness (h), respectively. The numerical calculations were performed, depending of the cases, for curvatures from Z=0 (flat panels) up to Z=50.

For comparative purposes, a normalized load factor χ is defined using the plastic load (corresponding to the total cross section of the stiffened panels) using a steel with a yield strength f_y=355 MPa. The load factor χ is calculated for the semi-analytical model as previously defined by equation (7.2).

The results are presented with the equilibrium paths in terms of the normalized out-of-plane deformation $\delta+\delta_{011}$ at the centre of the panels.

7.5.2.2 In-plane compression followed by out-of-plane pressure

In this situation, the panels are considered first pre-loaded with three levels of compression for a load factor χ=0% (case without compression), 10% or 25% and subsequently subjected to an increasing out-of-plane pressure (p_z).

It was attempted to use the minimum number of Degrees of Freedom (DOF) that are able to provide a sufficiently good response. Depending on the analyses, the deformation shapes can be more complex and a larger number of DOF is required. For example, in Figure 7.21 and Figure 7.22, the deformation shapes are compared for an unstiffened and a stiffened panel with the same curvature, respectively. Taking into account the considerably different patterns of deformation, the participation of the degrees of

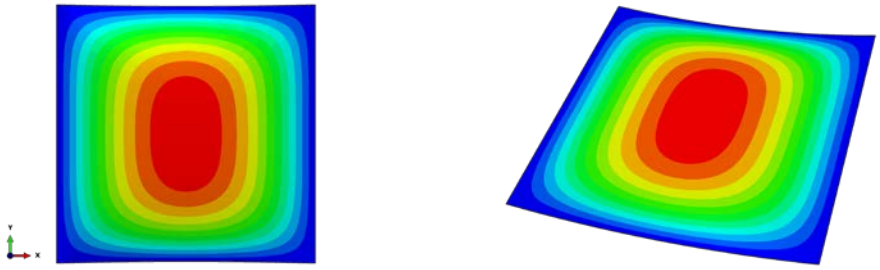

a) *b)*

Figure 7.21: Deformation for an unstiffened panel with Z=30 and α=1.0 (first loaded with χ=0% and then loaded up to p_z=50 kPa), *a)* top view and *b)* perspective view

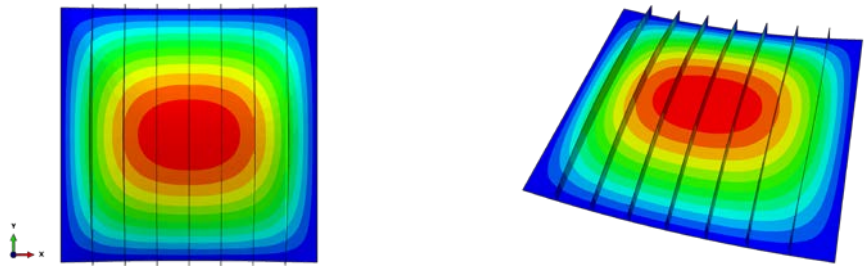

a) *b)*

Figure 7.22: Deformation for a stiffened panel with 7 stiffeners, Z=30 and α=1.0 (first loaded with χ=0% and then loaded up to p_z=50 kPa), *a)* top view and *b)* perspective view

freedom is expected to be different. While for the unstiffened panel the second most important contribution (after the global mode b_{11}) is mode b_{13}, for the stiffened panel the second most important contribution is mode b_{31}. It should be noted that in general with the increase of the curvature the complexity of the deformation shape also increases and more DOF are generally necessary.

The equilibrium paths for the unstiffened panels are plotted in Figure 7.23 with 2 DOF (b_{11} and b_{13}). It is verified that as the curvature increases the need for more degrees of freedom is higher. However, for the lower curvatures (up to Z=20) 2 DOFs are sufficient for a good characterization of the nonlinear behaviour. In this case the effect of the initial in-plane compression is very notorious because the panels are not very stiff. Besides that, it is interesting to compare the panels Z=0 and Z=10 with Z=20 and Z=30. A considerable effect of the curvature is visible in the development of the curves and also comparing, for example, the value of the out-of-plane displacement for p_z=0. Despite this very intricate behaviour, the semi-analytical formulation is able to predict it perfectly well.

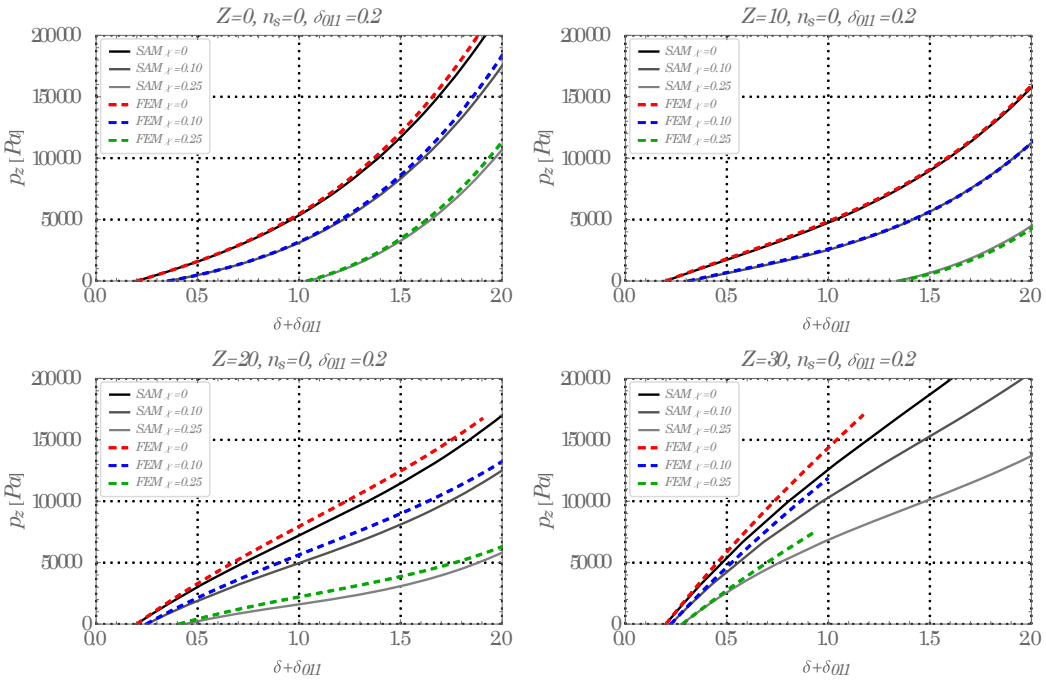

Figure 7.23: Equilibrium paths for unstiffened panels with α=1.0 for load case with initial in-plane compression and increasing out-of-plane pressure (2 DOFs: b_{11} and b_{13})

To evidence the need for a multi degree-of-freedom (MDOF) solution and to assess the influence of the number of DOFs, the equilibrium paths for the same unstiffened panels from Figure 7.23 for the load case without in-plane pre-compression (χ=0) are presented in Figure 7.24 for 1 DOF (b_{11}) and 4 DOFs (b_{11}, b_{13}, b_{31} and b_{33}). For reference purposes of the load level installed in the panels, the point where the first yield occurs (assuming f_y=355 MPa) is plotted. As expected, the deviation from the FEM results is much smaller for the solution with 4 DOFs in comparison with 1 DOF and 2 DOF (shown in Figure 7.23) leading to the conclusion that the accuracy of the results increases as the number of DOFs increases. A perfect agreement is verified for curvatures up to Z=20. An error of 0, 2% and -3% is verified for Z=0, 10 and 20, respectively. For the largest curvature, Z=30, an error of ≈-8% is verified for 4 DOFs at the point corresponding to first yield, in contrast with ≈−16% and ≈−13% for 1 and 2 DOFs, respectively. For the case with Z=30, despite being perfectly acceptable for such a complex deformation shape, the difference indicates that for curvatures larger than Z=30 even more DOFs may be needed.

Another expected evidence is related with the lower value of p_z needed to reach the first yield in the panel, as the initial level of χ increases. It was found that the differences are considerable. For example, for Z=30, while for χ=0 the panel reaches the first yield only for p_z≈173 kPa, for χ=0.25 it occurs only for ≈87 kPa.

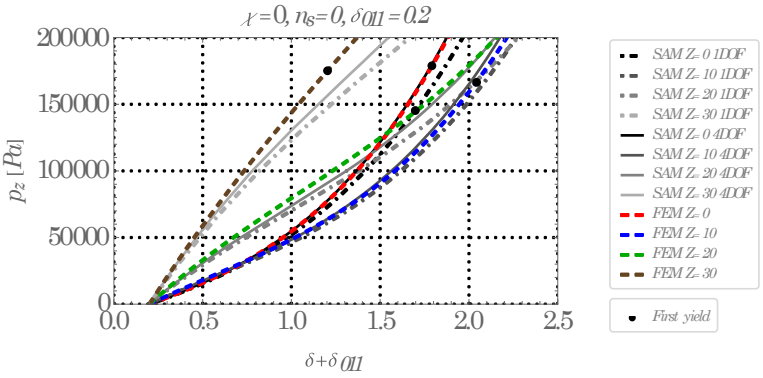

Figure 7.24: Equilibrium paths for unstiffened panels with α=1.0 for load case without initial in-plane compression (χ=0) and increasing out-of-plane pressure for 1 DOF (b_{11}) and 4 DOFs (b_{11}, b_{13}, b_{31} and b_{33}) and comparison with FEM

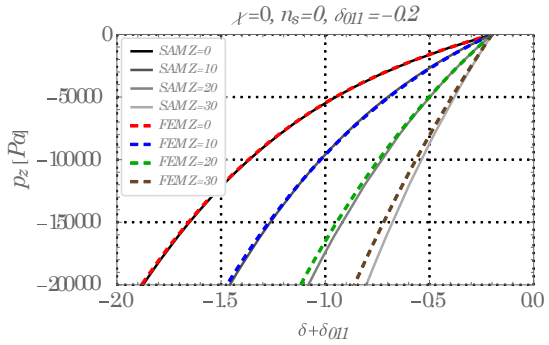

Figure 7.25: Equilibrium paths unstiffened panels with α=1.0 for load case without initial in-plane compression (χ=0) and increasing centrifugal out-of-plane pressure (4 DOF: b_{11}, b_{13}, b_{31} and b_{33})

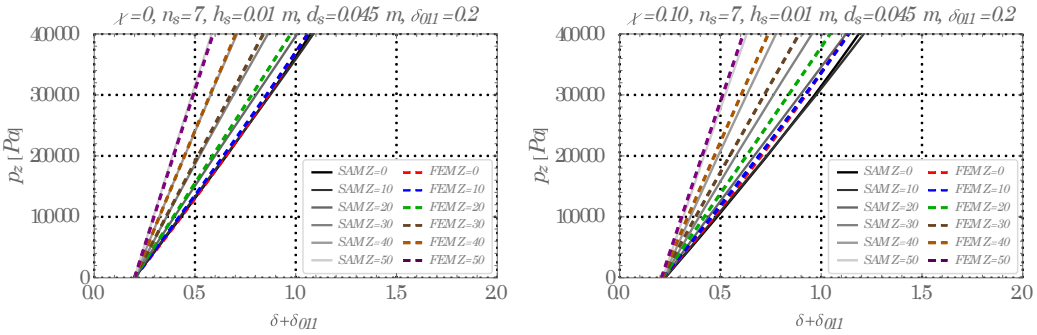

Figure 7.26: Equilibrium paths for stiffened panels with 7 stiffeners and α=1.0 for load case with initial in-plane compression and increasing out-of-plane pressure (4 DOF: b_{11}, b_{13}, b_{31}, b_{33})

The applicability of the semi-analytical formulation for centrifugal pressures is tested next for unstiffened panels. The panels are now considered with a symmetric imperfection δ_{011}=-0.2 (initial imperfection towards the pressure). The equilibrium paths of the unstiffened panels with in-plane compression χ=0 and increasing centrifugal out-of-plane pressure are plotted in Figure 7.25 with 4 DOF. It is possible to verify a very good adjustment between the semi-analytical formulation and the FEM analyses.

For the stiffened panels, a solution with 4 DOFs was required (b_{11}, b_{13}, b_{31} and b_{33}) even for smaller curvatures. The comparison of the equilibrium paths is presented in Figure 7.26, for χ=0 and χ=0.10. The agreement between the SAM and FEM is very good. As expected, in general, with the presence of pre-compression, a lower value for p_z is needed

to reach the first yield. Consequently, for lower curvatures the first yield is reached for relatively small values of p_z. For example, for the case of χ=0.10 for Z=0, the first yield (assuming f_y=355 MPa) occurs only for ≈187 kPa (where the agreement with FEM is very good) and consequently the relevance of very large pressures, presented in the chart for this case, is reduced because plasticity begins to be important. On the other hand, for the larger curvatures the pressures leading to the first yield are closer to the maximum value presented in the graph, where the agreement is verified to be also very good.

7.5.2.3 Out-of-plane pressure followed by in-plane compression

In this load case, the panels are considered first pre-loaded with one of three levels of an out-of-plane pressure p_z=0 (case without out-of-plane pressure), 10 or 50 kPa and subsequently loaded with increasing compression given in terms of the load factor χ. These are reasonable values for the initial out-of-plane pressure taking into account the initial effect on the studied panels.

Similarly, to what was said for the previous load case, the deformation of unstiffened and stiffened panels with the same curvature may also be considerably different. The comparison is done in Figure 7.27 and Figure 7.28, respectively, for the unstiffened and stiffened panel with Z=30. However, in this case, there is the particularity that the deformation shape for the stiffened panel is closer to the global mode b_{11}; hence, a single DOF is able to characterize well the nonlinear behaviour of the stiffened panels.

The equilibrium paths for the unstiffened panels first loaded with the out-of-plane pressure and then increasingly loaded with in-plane compression are presented in Figure

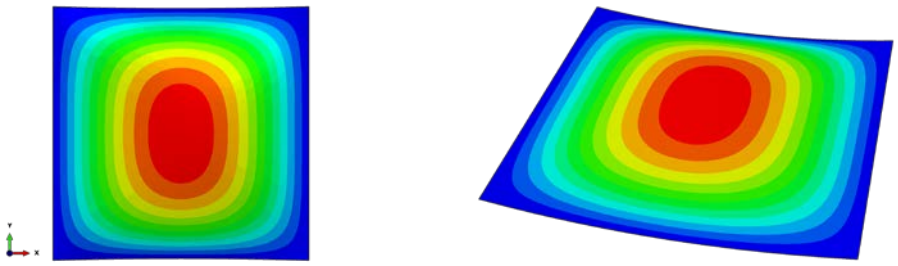

a) *b)*

Figure 7.27: Deformation for an unstiffened panel with Z=30 and α=1.0 (for p_z=50 kPa and χ=50%), *a)* top view and *b)* perspective view

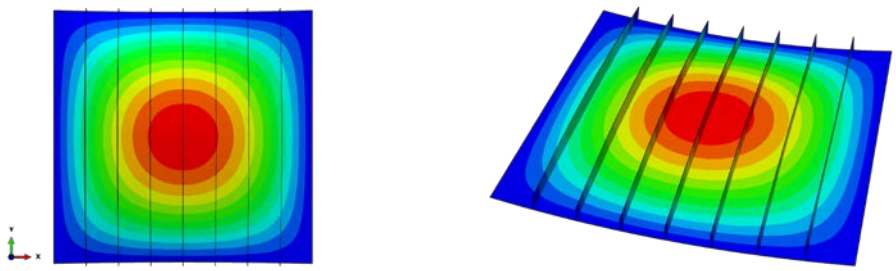

a) *b)*

Figure 7.28: Deformation for a panel with Z=30, α=1.0 and 7 stiffeners (first loaded with p_z=50 kPa and then loaded up to χ=100%), *a)* top view and *b)* perspective view

7.29. It is possible to verify that the 2 DOFs (b_{11} and b_{13}) for which the results were calculated are able to describe accurately the nonlinear for the presented curvatures but at the same time they let anticipate the need for more degrees of freedom if larger curvatures are desired, especially with higher levels of initial out-of-plane pressure.

The equilibrium paths for the stiffened panels are presented in Figure 7.30. As previously

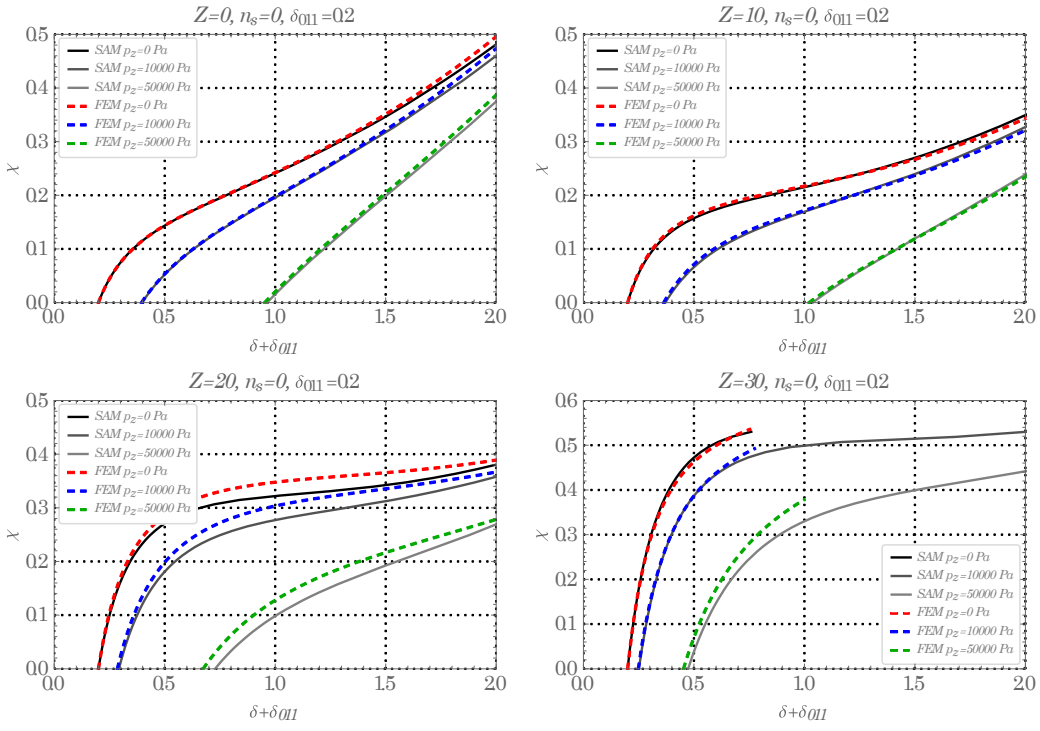

Figure 7.29: Equilibrium paths for unstiffened panels with α=1.0 for load case with initial out-of-plane pressure and increasing in-plane compression (2 DOF: b_{11} and b_{13})

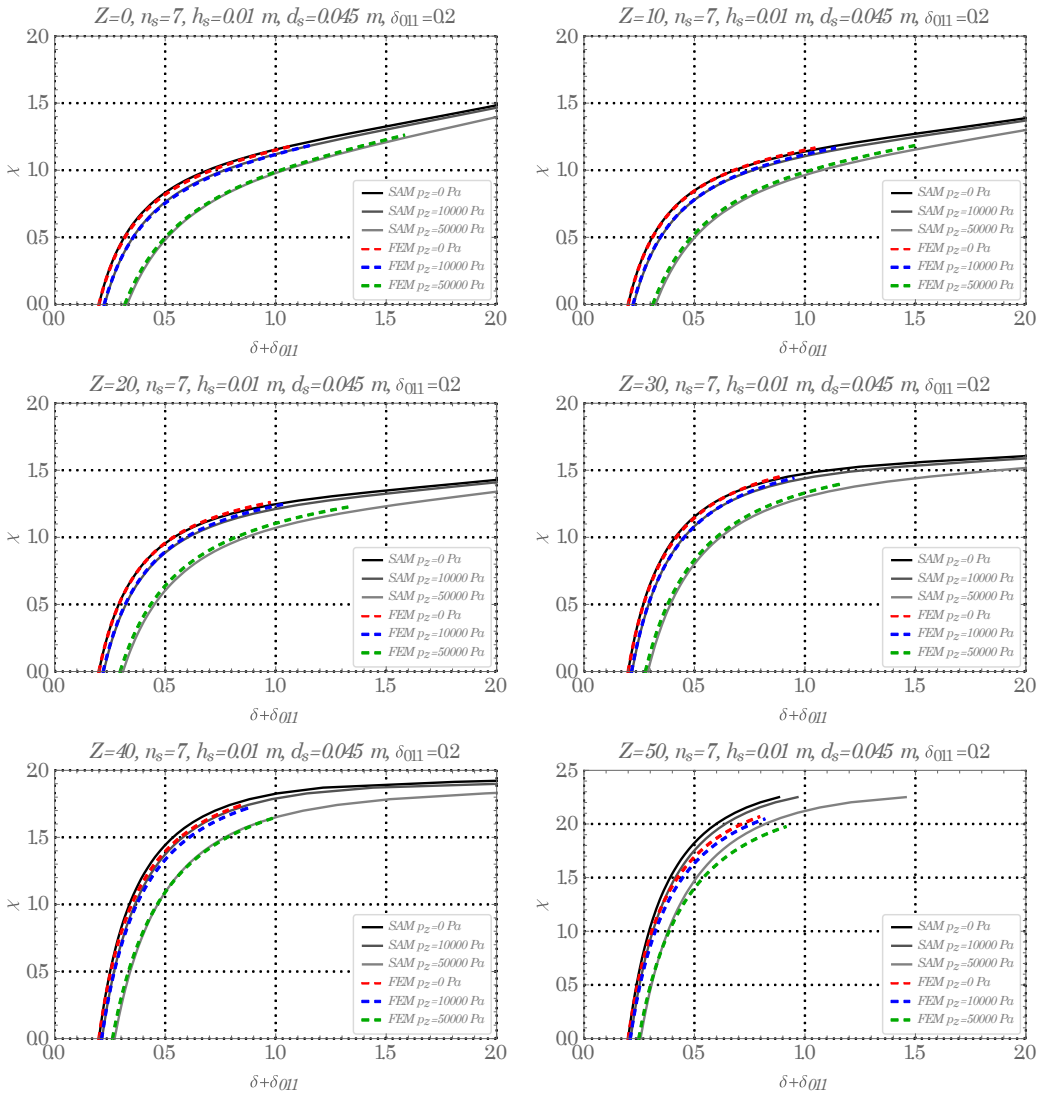

Figure 7.30: Equilibrium paths for stiffened panels with 7 stiffeners and α=1.0 for load case with initial out-of-plane pressure and increasing in-plane compression (1 DOF: b_{11})

explained, in this case only a single DOF (b_{11}) is sufficient to reproduce the behaviour of these panels with excellent accuracy for curvatures up to Z=50. It is observed that the situation with or without out-of-plane pressure is correctly characterized in the semi-analytical model.

In order to test the applicability of the semi-analytical formulation under centrifugal pressures, the equilibrium paths for the stiffened panels first loaded with p_z=-50 kPa and then loaded in compression are presented in Figure 7.31. As previously explained, the

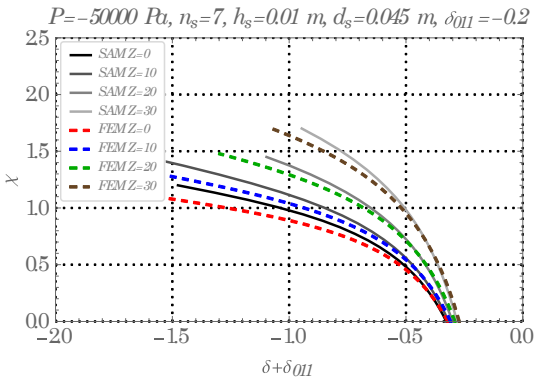

Figure 7.31: Equilibrium paths for stiffened panels with 7 stiffeners and α=1.0 for load case with initial out-of-plane pressure p_z=-50 kPa and increasing in-plane compression (1 DOF: b_{11})

initial imperfection δ_{011} was defined with the value -0.2. The same single DOF as in the previous graphs (b_{11}) was used. A single DOF is still able to provide a reasonable characterization of the nonlinear behaviour of these panels up to relevant values of χ. For reference purposes the first yield of Z=0 and Z=30 occurs for values of χ=0.38 and χ=0.58, respectively.

7.6 SUMMARY

A very good agreement between the semi-analytical method and FE analyses was obtained for the equilibrium paths in all the considered situations. It was found that, generally, as the curvature is increased, the modal participation of higher modes is larger and, consequently, the need for more DOFs is greater. Nonetheless, few DOFs are, generally, able to characterize accurately the behaviour of most unstiffened curved panels of practical interest. It is noted that for bridge applications, for example, the range of curvatures (Z) of unstiffened curved panels varies from 0 to 15 [135]. Hence, the semi-analytical method perfectly covers this range of curvatures.

In accordance with the conclusions drawn in Chapter 6, it was verified that even small curvatures change dramatically the behaviour of the panels and consequently the effect of the curvature needs to be deeply understood. The restraint of the longitudinal edges has an impact on the post-buckling behaviour of curved panels. Imperfections play a

fundamental role on the post-buckling behaviour of these elements once they can decrease significantly the load for a same displacement. In all cases, the SAM was perfectly able to deal with these situations.

8 Design oriented closed-form equations for the elastic large displacement behaviour and ultimate resistance of curved panels

8.1 Introduction

The semi-analytical method has just been validated, in the previous chapter, for the elastic large displacement behaviour. Closed-form expressions to predict this behaviour are proposed in this chapter (section 8.2). They are derived based on a SDOF solution and their validity is assessed for unstiffened and stiffened curved panels under in-plane and out-of-plane loading.

In chapter 6, the load-deflections curves of curved panels subjected to in-plane compression and out-of-plane loading were assessed, in detail, considering an elastic and a plastic material by FEM. The subject of section 8.3 is to assess the ultimate load of the unstiffened curved panels under in-plane compression by the semi-analytical method (SAM). The main outcome of this section is the derivation of closed-form expressions to predict the ultimate load of unstiffened curved panels (subsection 8.3.6). The accuracy of these expressions is shown to be very good.

Expressions of this type, have an obvious practical interest and, in the last section, they are applied to predict the large displacement behaviour and ultimate load of real curved panels.

8.2 Closed-form equations for the elastic large displacement behaviour of curved panels

8.2.1 Introduction

A MDOF solution hinders the obtainment of a usable simple expression for the equilibrium paths of the panels. Hence, a simple closed-form solutions was pursued by solving analytically the SAM with SDOF approximations. It was found that, although the SDOF solutions are not able to reproduce in absolute terms the exact (numerical) results of panels with large curvatures, they approximate well the elastic non-linear large-displacement behaviour of a large part of the panels with practical applicability.

The main advantage of using a SDOF is that it allows to obtain an exact explicit expression for the load (p_y or p_z) as a function of the normalized displacement (δ_{11}). However, the resulting closed form expression, obtained using the software Mathematica [116], is too long for practical interest. Consequently, in order to obtain a usable expression that may be easily implemented in a spreadsheet, some higher order terms were neglected. These terms were carefully selected and, consequently, the resulting expression may be used without any correction because the differences between the simplified and the original expression are negligible.

In the next subsections, closed-form expressions are derived for the curved panels. They are first derived for the isotropic curved panels under in-plane compression, in subsection

8.2.2. The validity of the expressions is assessed for several values of curvature, aspect ratio and width to thickness ratio. From the simplification of the most general expressions, simple expressions for flat plates are derived confirming established theoretical results. In subsection 8.2.3, similar expressions are derived for the orthotropic curved panels under in-plane compression. Finally, in subsection 8.2.4, the most general closed-form expressions are given for the orthotropic curved panels under combined in-plane compression and out-of-plane pressure. Different expressions are given depending of the explicit load (for p_z or p_y).

8.2.2 Unstiffened curved panels under in-plane compression

The closed-form expression presented in equation (8.1) is applicable to isotropic curved panels accounting for all the possible parameters, including the aspect ratio, α. Imperfections are explicitly incorporated with the imperfection pattern a_{11}, being included through the normalized imperfection δ_{011}. Boundary conditions BCC were selected. This expression can be easily calculated in a spreadsheet and it gives accurate values for all cases where a global SDOF is appropriate to simulate the behaviour of the panels.

$$p_y = -\frac{4\alpha}{\pi^2\left(\delta_{011}+\delta_{11}\right)}\left[\delta_{11}\left(\delta_{011}{}^2 C_1 + C_2 + C_3\right) + \delta_{11}{}^2\left(\frac{3}{2}\delta_{011}C_1 + C_4\right) + \frac{1}{2}\delta_{11}{}^3 C_1\right] \tag{8.1}$$

with the following constants:

$$\begin{aligned}
C_1 &= -\frac{Eh^2\pi^4\left(1+\alpha^4\right)}{32a^2\alpha^3}\\
C_2 &= \frac{Eh^2\left(c_1{}^6\pi^4 + 12Z^2\alpha^4\left(-1+\upsilon\right)\left(1+\upsilon\right)\left(-1-\alpha^2\upsilon+\alpha^4\left(1+4\upsilon\right)\right)\right)}{48a^2c1^4\alpha^3\left(-1+\upsilon^2\right)}\\
C_3 &= -\frac{1}{8a^2c_1{}^5\pi}Eh^2Z^2\alpha^2\,\mathrm{csch}\left[\frac{\pi\alpha}{2}\right]^2 \\
&\quad \left(\pi\left(\alpha+\alpha^3\right)\left(2\alpha^2\left(c_1-\upsilon\right)-\upsilon\right)+\pi\left(\alpha+\alpha^3\right)\left(2+\upsilon+2\alpha^2\left(1+\upsilon\right)\right)\right.\\
&\quad \left.\cosh\left[\pi\alpha\right]+2\left(-3+\alpha^6+\alpha^4\left(-1+4\upsilon\right)-\alpha^2\left(5+4\upsilon\right)\right)\sinh\left[\pi\alpha\right]\right)\\
C_4 &= \frac{1}{128a^2c_1{}^2c_2{}^2}Eh^2Z\alpha
\end{aligned} \tag{8.2}$$

$$\left(4\left(256+\alpha^2\left(256\left(2+\alpha^2\right)-64c_1{}^2\upsilon+3c_2{}^2\pi\left(2+\alpha^2+\upsilon\right)\right)\right)+3c_2{}^2\pi\alpha^3\right.$$
$$\left.\left(-2\left(5+3\upsilon+\alpha^2\left(3+\upsilon\right)\right)+\pi\left(\alpha+\alpha^3\right)\left(1+\upsilon\right)\coth\left[\frac{\pi\alpha}{2}\right]\right)\operatorname{csch}\left[\frac{\pi\alpha}{2}\right]\right)$$

$$c_1=1+\alpha^2$$

$$c_2=4+\alpha^2$$

A useful simplification is for the case α=1.0 which is given by equation (8.3).

$$p_y=-\frac{4}{\pi^2\left(\delta_{011}+\delta_{11}\right)}\left[\delta_{11}\left(\delta_{011}{}^2C_1+C_2+C_3\right)+\delta_{11}{}^2\left(\frac{3}{2}\delta_{011}C_1+C_4\right)+\frac{1}{2}\delta_{11}{}^3C_1\right] \tag{8.3}$$

with

$$C_1=-\frac{Eh^2\pi^4}{16a^2}$$

$$C_2=\frac{Eh^2\left(16\pi^4+9Z^2\upsilon\left(-1+\upsilon^2\right)\right)}{192a^2\left(-1+\upsilon^2\right)}$$

$$C_3=\frac{Eh^2Z^2\operatorname{csch}\left[\frac{\pi}{2}\right]^2\left(-\pi\left(4-3\upsilon+\left(4+3\upsilon\right)\cosh\left[\pi\right]\right)+8\sinh\left[\pi\right]\right)}{128a^2\pi} \tag{8.4}$$

$$C_4=\frac{Eh^2Z}{6400a^2}\left(-512\left(-4+\upsilon\right)+75\pi\left(6+2\upsilon+\right.\right.$$
$$\left.\left.\left(-4\left(2+\upsilon\right)+\pi\left(1+\upsilon\right)\coth\left[\frac{\pi}{2}\right]\right)\operatorname{csch}\left[\frac{\pi}{2}\right]\right)\right)$$

For comparison purposes, the previous expression for p_y is now even more simplified for the more traditional case of flat plates (Z=0). As shown in equation (8.5), for this case, the expression simplifies significantly.

$$p_y=-\frac{4}{\pi^2\left(\delta_{011}+\delta_{11}\right)}\left[\delta_{11}\left(-\delta_{011}{}^2\frac{Eh^2\pi^4}{16a^2}+\frac{Eh^2\pi^4}{12a^2\left(-1+\upsilon^2\right)}\right)+\right.$$
$$\left.-\delta_{11}{}^2\delta_{011}\frac{3Eh^2\pi^4}{32a^2}-\delta_{11}{}^3\frac{Eh^2\pi^4}{32a^2}\right] \tag{8.5}$$

The plotting of this expression is shown in Figure 8.1 for the perfect (δ_{011}=0) and an imperfect plate with δ_{011}=0.2 along with numerical results for the three boundary conditions. It is seen that the curve from the expression matches very well the numerical

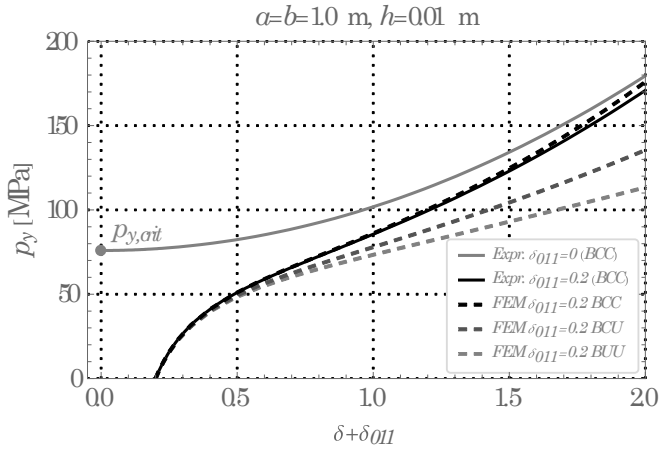

Figure 8.1: Comparison of the equilibrium paths of a flat plate obtained by equation (8.5) and FEM for the three boundary conditions

curve for BCC, for which it was developed. In fact, the differences between boundary conditions are, for this case, significant. The perfect equilibrium path is shown to assess the importance of imperfections. It is also pertinent to assess the critical stress of the panel which is easily obtained using δ_{11}=0 (and δ_{011}=0) in equation (8.5). Doing this, equation (8.6) is obtained for the critical stresses of flat plates, which is the same as equation (6.1) using k_σ=4.0. For the panel with a=1.0 m and h=0.01, a value of $p_{y,crit}$=75.92 MPa is obtained, matching perfectly the value obtained by FEM for the same conditions.

$$p_{y,crit} = \frac{\pi^2 E}{3\left(1-\upsilon^2\right)}\left(\frac{h}{a}\right)^2 \tag{8.6}$$

Back to the behaviour of the curved panels, the validity of equation (8.1) is assessed for several aspect ratios and a/h ratios. A flat plate and a curved panel with Z=20 are used for comparison. It is seen that for the flat plate aspect ratios α=1.5 are well adjusted for a considerable part of the displacements. For the curved panel aspect ratios up to α=1.25 are yet reasonably predicted while for α=1.5 the SDOF approximation is scarce and the agreement becomes worst. This effect tends to increase as the a/h ratio increases, because more complex deformation shapes occur. To corroborate this, in Figure 8.3 the equilibrium paths are compared for or α=0.5 and a/h=50 for a wide range of curvatures. It is shown that equation (8.1) is able to predict perfectly well a very large value of curvature, Z=75. This proves that the formulation is able to account for high values of

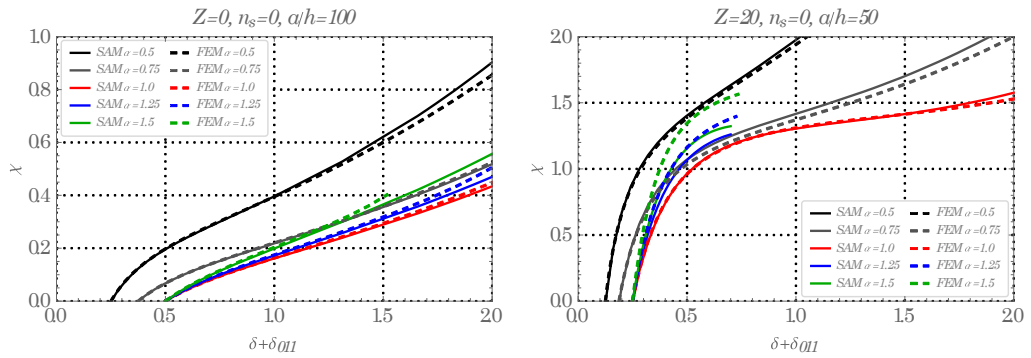

Figure 8.2: Comparison of the equilibrium paths of a flat and a curved panel obtained by equation (8.1) and FEM for different aspect ratios and *a/h* ratios (BCC)

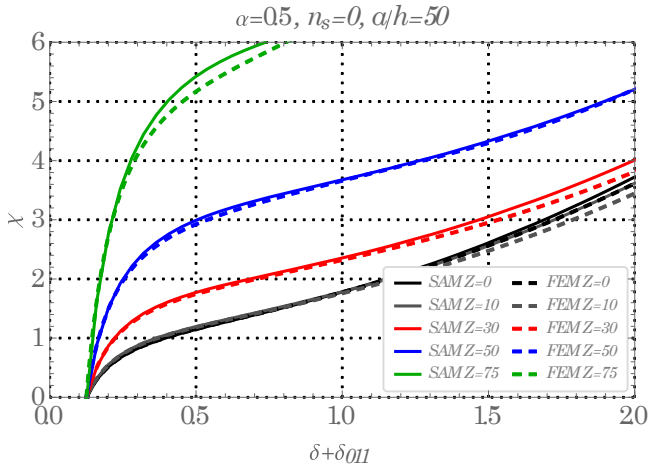

Figure 8.3: Comparison of the equilibrium paths for *α*=0.5 and *a/h=50* obtained by equation (8.1) and FEM for several curvatures (BCC)

curvature provided that the displacement function approximates properly the real deformation shapes of the panels.

A last series of results for a/h=100 obtained by equation (8.1) is compared in Figure 8.4 for various aspect ratios and curvatures. Two amplitudes for the imperfections are used, corresponding to w_0=min(a,b)/500 and w_0=min(a,b)/200. A good general agreement between the SDOF solution and FEM analyses is obtained. Naturally, it is visible that for large displacements, if larger curvatures and aspect ratios are considered, a MDOF solution may be required.

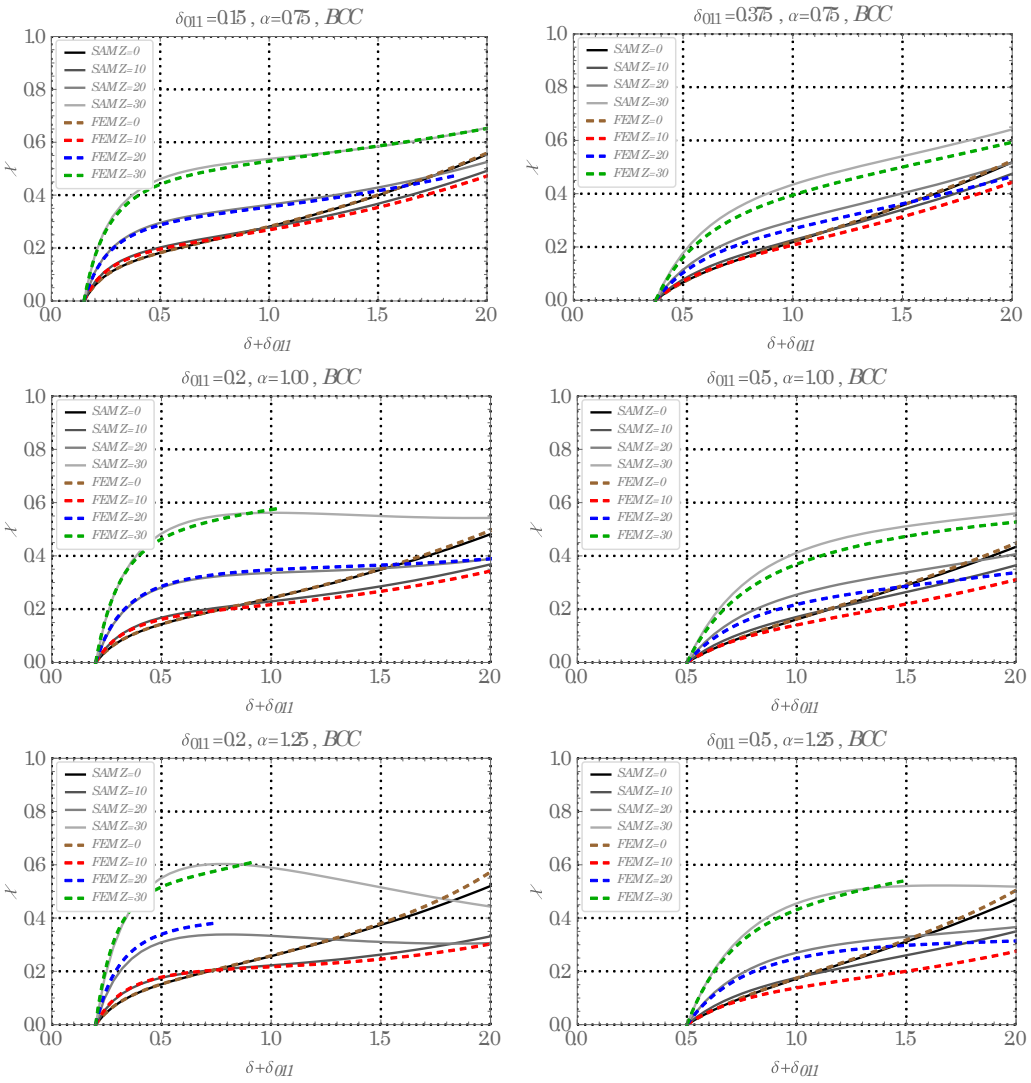

Figure 8.4: Comparison of the equilibrium paths for a/h=100 obtained by equation (8.1) and FEM for several curvatures, aspect ratios and amplitudes for imperfections (BCC)

The procedure adopted for the derivation of the closed-form expressions is general and it can be used to derive similar closed-form solutions for other ranges of application, provided that the SDOF is appropriately chosen. Naturally, for a longer panel (*e.g.* α=3.0 with a_{13}), the selected mode should match the controlling deformation mode (b_{13} in this particular case).

8.2.3 Stiffened curved panels under in-plane compression

As previously discussed, a SDOF model is sufficient to provide an accurate representation

of the post buckling behaviour of stiffened panels approaching and overall deformation mode. The panels are considered with a global imperfection pattern a_{11} (included through the normalized imperfection δ_{011}) and boundary conditions BCC.

Applying a similar procedure, the load-deflection of orthotropic curved panels (for any aspect ratio, α) is given by the same equation as previously defined for the isotropic panels:

$$p_y = -\frac{4\alpha}{\pi^2\left(\delta_{011}+\delta_{11}\right)}\left[\delta_{11}\left(\delta_{011}{}^2 C_1 + C_2 + C_3\right) + \delta_{11}{}^2\left(\frac{3}{2}\delta_{011}C_1 + C_4\right) + \frac{1}{2}\delta_{11}{}^3 C_1\right] \tag{8.7}$$

but now the constants are as follows:

$$\begin{aligned}
C_1 &= -\frac{h^2\pi^4\left(E_y + E_x\alpha^4\right)}{32a^2\alpha^3}\\
C_2 &= -\frac{\pi^4\left(D_y + 2\left(2D_S + D_{xy}\right)\alpha^2 + D_x\alpha^4\right)}{4a^2h\alpha^3} + \\
&\quad \frac{E_xE_yG_{xy}h^2Z^2\alpha}{8a^2}\left(-\frac{1}{E_1} + \frac{-5E_xG_{xy}\alpha^4 + E_y\left(-1+4\alpha^2\right)\left(G_{xy}+E_x\alpha^2\right)}{E_1{}^2}\right)\\
C_3 &= -\frac{1}{384a^2c_1E_1{}^2\pi}E_xE_yG_{xy}h^2Z^2\alpha^2\,\mathrm{csch}\left[\frac{\pi\alpha}{2}\right]^4\Bigg(-2c_1\pi\alpha\\
&\quad \left(-E_yG_{xy}\left(-3\left(17+5\upsilon_x\right)+\alpha^2\left(-3\left(6+\alpha^2\right)+3\left(8+\alpha^2\right)\upsilon_x+2c_1{}^2\pi^2\left(1+\upsilon_x\right)\right)\right)+\right.\\
&\quad E_x\left(E_y\left(-33+2\left(3+\pi^2\right)\alpha^2+\left(3+4\pi^2\right)\alpha^4+2\pi^2\alpha^6\right)-\right.\\
&\quad \left.\left.G_{xy}\left(-3-33\upsilon_y+\alpha^2\left(2c_1{}^2\pi^2\left(1+\upsilon_y\right)+3\left(6+\alpha^2\left(-5+\upsilon_y\right)+8\upsilon_y\right)\right)\right)\right)\right)-\\
&\quad 2c_1\pi\alpha\left(-E_yG_{xy}\left(39+9\upsilon_x+\alpha^2\left(-3\left(6+\alpha^2\right)\left(-1+\upsilon_x\right)+c_1{}^2\pi^2\left(1+\upsilon_x\right)\right)\right)+\right.\\
&\quad E_x\left(E_y\left(33+\alpha^2\left(6+c_1{}^2\pi^2-3\alpha^2\right)\right)-G_{xy}\left(3+33\upsilon_y+\right.\right.\\
&\quad \left.\left.\left.\alpha^2\left(c_1{}^2\pi^2\left(1+\upsilon_y\right)-3\left(2+\alpha^2\left(-5+\upsilon_y\right)+6\upsilon_y\right)\right)\right)\right)\right)\cosh\left[\pi\alpha\right]-\\
&\quad 12\pi\left(\alpha+\alpha^3\right)\left(-2E_y\left(G_{xy}+E_x\alpha^2\right)+E_yG_{xy}\left(-1+\alpha^2\right)\upsilon_x+E_xG_{xy}\alpha^2\left(2+\upsilon_y\right)\right)\\
&\quad \cosh\left[2\pi\alpha\right]-6\left(E_yG_{xy}\left(-5\left(7+\upsilon_x\right)+\right.\right.\\
&\quad \left.\left.\alpha^2\left(35+29\upsilon_x+2c_1{}^2\pi^2\left(3+\alpha^2+2\upsilon_x\right)+\alpha^2\left(7+\alpha^2+\upsilon_x-\alpha^2\upsilon_x\right)\right)\right)+\right.\\
&\quad \left.E_x\left(E_y\left(5+\alpha^2\left(-45-4c_1{}^2\pi^2+15\alpha^2+\alpha^4\right)\right)+G_{xy}\left(1-5\upsilon_y+\alpha^2\left(15-\right.\right.\right.
\end{aligned} \tag{8.8}$$

$$2c_1^2\pi^2\left(-1+\alpha^2-2\upsilon_y\right)+29\upsilon_y+\alpha^2\left(-45-\alpha^2\left(-5+\upsilon_y\right)+\upsilon_y\right)\Big)\Big)\Big)$$

$$\sinh[\pi\alpha]+3\Big(E_yG_{xy}\left(-\alpha^6\left(-1+\upsilon_x\right)-5\left(7+\upsilon_x\right)+\alpha^4\left(7+\upsilon_x\right)+\right.$$

$$\left.\alpha^2\left(35+29\upsilon_x\right)\right)+E_x\Big(E_y\left(5-45\alpha^2+15\alpha^4+\alpha^6\right)+G_{xy}$$

$$\left(1-5\upsilon_y+\alpha^2\left(15+29\upsilon_y+\alpha^2\left(-45-\alpha^2\left(-5+\upsilon_y\right)+\upsilon_y\right)\right)\right)\Big)\sinh[2\pi\alpha]\Big)$$

$$C_4=\frac{1}{128a^2E_1}E_xh^2Z\alpha\Bigg($$

$$\frac{1}{c_2^2}4\Big(E_y\left(256c_1^2G_{xy}+3c_2^2E_x\pi\alpha^2-2G_{xy}\left(16c_1^2+3c_2^2\pi\right)\alpha^2\upsilon_x\right)+E_xG_{xy}\alpha^2$$

$$\left(-32c_1^2\upsilon_y+3c_2^2\pi\left(\alpha^2+\upsilon_y\right)\right)\Big)+3G_{xy}\pi\alpha\Bigg(4\left(-1+\alpha^2\right)\left(E_y\upsilon_x-E_x\upsilon_y\right)\coth\left[\frac{\pi\alpha}{2}\right]+$$

$$\alpha^2\Bigg(-2E_y\left(5+3\alpha^2\right)-2E_x\left(3+\alpha^2\right)\upsilon_y+\pi\left(\alpha+\alpha^3\right)\left(E_y+E_x\upsilon_y\right)\coth\left[\frac{\pi\alpha}{2}\right]\Bigg)$$

$$\operatorname{csch}\left[\frac{\pi\alpha}{2}\right]+2c_1\pi\alpha\left(E_y\upsilon_x-E_x\upsilon_y\right)\operatorname{csch}\left[\frac{\pi\alpha}{2}\right]^2\Bigg)\Bigg)$$

$$E_1=E_xG_{xy}\alpha^4+E_y\left(G_{xy}+E_x\alpha^2-2G_{xy}\alpha^2\upsilon_x\right)$$

$$c_1=\left(1+\alpha^2\right)$$

$$c_2=\left(4+\alpha^2\right)$$

All the orthotropic properties are calculated as defined in section 4.3.

Simplifying the expression for α=1.0, equation (8.9) is obtained.

$$p_y=-\frac{4}{\pi^2\left(\delta_{011}+\delta_{11}\right)}\left[\delta_{11}\left(\delta_{011}{}^2C_1+C_2+C_3\right)+\delta_{11}{}^2\left(\frac{3}{2}\delta_{011}C_1+C_4\right)+\frac{1}{2}\delta_{11}{}^3C_1\right] \tag{8.9}$$

with

$$C_1=-\frac{\left(E_x+E_y\right)h^2\pi^4}{32a^2}$$

$$C_2=\frac{1}{4a^2h}\left(-\left(4D_S+D_x+2D_{xy}+D_y\right)\pi^4-\frac{2E_x{}^2E_y{}^2G_{xy}h^3Z^2}{E_1{}^2}\right) \tag{8.10}$$

$$C_3=\frac{E_xE_yG_{xy}h^2Z^2}{96a^2E_1{}^2\pi}\operatorname{csch}\left[\frac{\pi}{2}\right]^4\Bigg(E_yG_{xy}\left(-2\pi^3\left(1+\upsilon_x\right)\left(2+\cosh[\pi]\right)+\right.$$

$$12\pi\left(-8+\left(-1+\upsilon_x\right)\cosh\left[\pi\right]\right)\sinh\left[\frac{\pi}{2}\right]^2+12\pi^2\left(2+\upsilon_x\right)\sinh\left[\pi\right]-$$
$$6\left(1+3\upsilon_x\right)\left(-1+\cosh\left[\pi\right]\right)\sinh\left[\pi\right]\Big)+E_x\left(2G_{xy}\left(-\pi^3\left(1+\upsilon_y\right)\left(2+\cosh\left[\pi\right]\right)+\right.\right.$$
$$6\pi\left(4+\left(-1+\upsilon_y\right)\cosh\left[\pi\right]\right)\sinh\left[\frac{\pi}{2}\right]^2+6\pi^2\upsilon_y\sinh\left[\pi\right]-$$
$$9\left(-1+\upsilon_y\right)\left(-1+\cosh\left[\pi\right]\right)\sinh\left[\pi\right]\Big)+E_y\left(\pi\left(3\left(5-6\cosh\left[\pi\right]+\cosh\left[2\pi\right]\right)+\right.\right.$$
$$\left.\left.\left.\left.2\pi\left(\pi\left(2+\cosh\left[\pi\right]\right)-6\sinh\left[\pi\right]\right)\right)+9\left(-2\sinh\left[\pi\right]+\sinh\left[2\pi\right]\right)\right)\right)$$

$$C_4=\frac{E_x h^2 Z}{1600a^2E_1}\left(2\left(E_y\left(75E_x\pi-2G_{xy}\left(-512+64\upsilon_x+75\pi\upsilon_x\right)\right)+E_xG_{xy}\left(-128\upsilon_y+\right.\right.\right.$$
$$\left.\left.\left.75\pi\left(1+\upsilon_y\right)\right)\right)+75G_{xy}\pi\left(-8E_y-4E_x\upsilon_y+\pi\left(E_y+E_x\upsilon_y\right)\coth\left[\frac{\pi}{2}\right]\right)\operatorname{csch}\left[\frac{\pi}{2}\right]+$$
$$\left.150G_{xy}\pi^2\left(E_y\upsilon_x-E_x\upsilon_y\right)\operatorname{csch}\left[\frac{\pi}{2}\right]^2\right)$$

$$E_1=E_x\left(E_y+G_{xy}\right)+E_yG_{xy}\left(1-2\upsilon_x\right)$$

Neglecting the stiffeners, the equations for isotropic panels (n_s=0) presented in the previous subsection are obtained.

For validation purposes, the equilibrium paths of some randomly-selected panels with α=1.0 are calculated by expression (8.9) and compared with those obtained by FEM analyses in Figure 8.5. The geometry of some panels used in Chapter 6 are used for comparison and new values for the geometric variables are also introduced, as the thickness of the stiffeners, as described in the figure. To assess the validity of the orthotropic expressions for unstiffened panels (with the corresponding simplifications) the results for unstiffened panels are also assessed.

In Figure 8.6, the equilibrium paths of a curved stiffened panel with several aspect ratios are plotted with equation (8.7) and compared with the FEM.

As shown, the agreement of the previous expressions with the FEM results is, in all cases, very good, even for values of χ larger than 1.0, showing the wide applicability of the expressions for distinct situations.

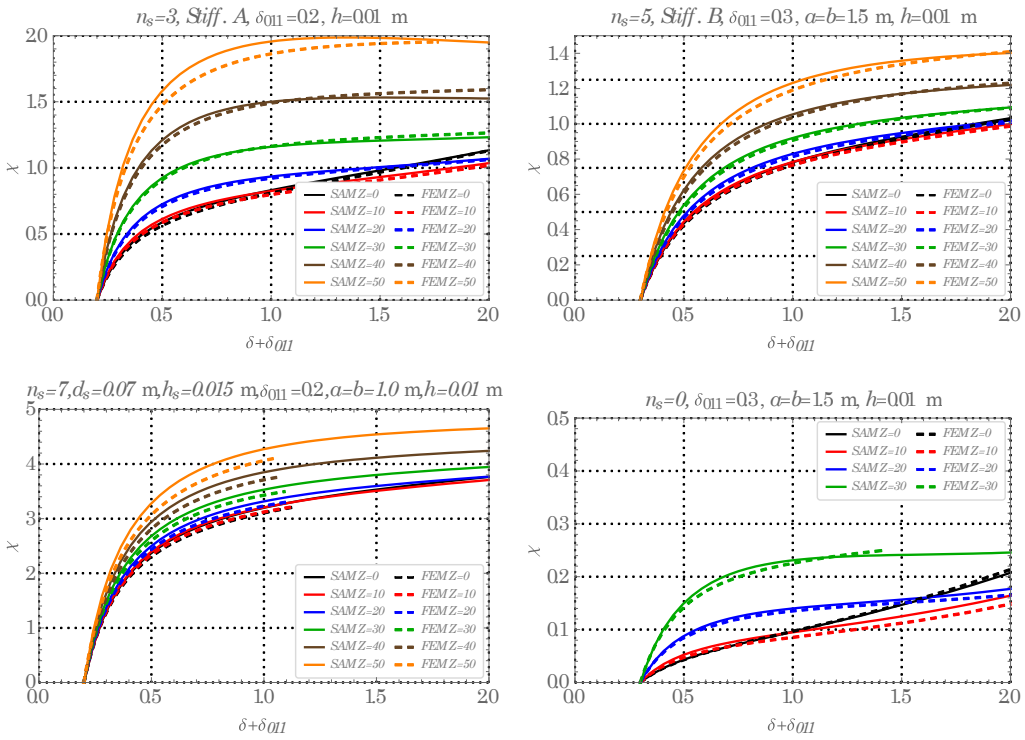

Figure 8.5: Comparison of the equilibrium paths for α=1.0 obtained by equation (8.9) and FEM for several geometric configurations (BCC)

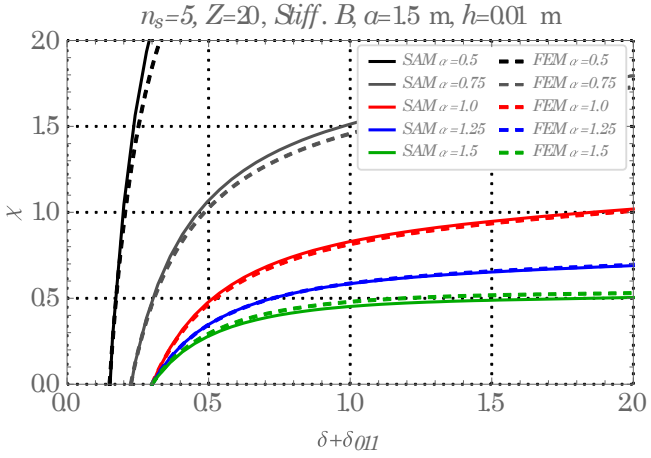

Figure 8.6: Comparison of the equilibrium paths for several aspect ratios obtained by equation (8.7) and FEM (w_0=min(a;b)/500, BCC)

8.2.4 Unstiffened and stiffened curved panels under combined in-plane compression and out-of-plane pressure

The expressions provided in subsections 8.2.2 and 8.2.3 for isotropic and orthotropic panels, respectively, are now extended to account for out-of-plane pressure, p_z. This extension is done through the introduction in the same expressions of only one additional term $C_0 p_z$, as shown in equation (8.11). This expression is directly applicable to the load case with initial out-of-plane pressure followed by in-plane compression.

$$p_y = -\frac{4\alpha}{\pi^2\left(\delta_{011}+\delta_{11}\right)}\left[C_0 p_z + \delta_{11}\left({\delta_{011}}^2 C_1 + C_2 + C_3\right) + {\delta_{11}}^2\left(\frac{3}{2}\delta_{011}C_1 + C_4\right) + \frac{1}{2}{\delta_{11}}^3 C_1\right] \tag{8.11}$$

where

$$C_0 = \frac{4a^2\alpha}{h^2\pi^2} \tag{8.12}$$

and the remaining constants are given in subsection 8.2.2 or 8.2.3 for isotropic or orthotropic panels, respectively.

Solving equation (8.11) for the out-of-plane pressure, p_z, equation (8.13) corresponds to the load case with initial in-plane compression followed by out-of-plane pressure.

$$p_z = \frac{1}{C_0}\left[-\frac{\pi^2}{4\alpha}\left(\delta_{011}+\delta_{11}\right)p_y - \delta_{11}\left({\delta_{011}}^2 C_1 + C_2 + C_3\right) - {\delta_{11}}^2\left(\frac{3}{2}\delta_{011}C_1 + C_4\right) - \frac{1}{2}{\delta_{11}}^3 C_1\right] \tag{8.13}$$

It is emphasized that these expressions, in its most general form, equations (8.11) and (8.13), give accurate values for all cases where a global SDOF is appropriate to simulate the behaviour of the panels therefore covering both unstiffened and stiffened curved panels with any number and geometry of stiffeners for BCC boundary conditions.

The validation of the expressions (8.11) and (8.13) are shown in Figure 8.7 and Figure 8.8, respectively. In both cases unstiffened and stiffened panels with α=1.0 are considered. The validation for several aspect ratios is shown in Figure 8.9 for panels initially loaded with an out-of-plane pressure p_z=50 kPa followed by in-plane compression (compare

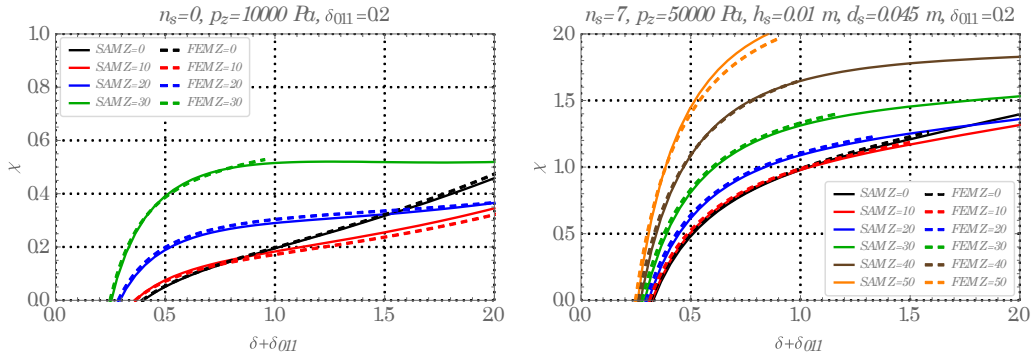

Figure 8.7: Comparison of the equilibrium paths for α=1.0 obtained by equation (8.11) and FEM for several geometric configurations of panels initially loaded with out-of-plane pressure followed by in-plane compression (a=1.0 m, BCC)

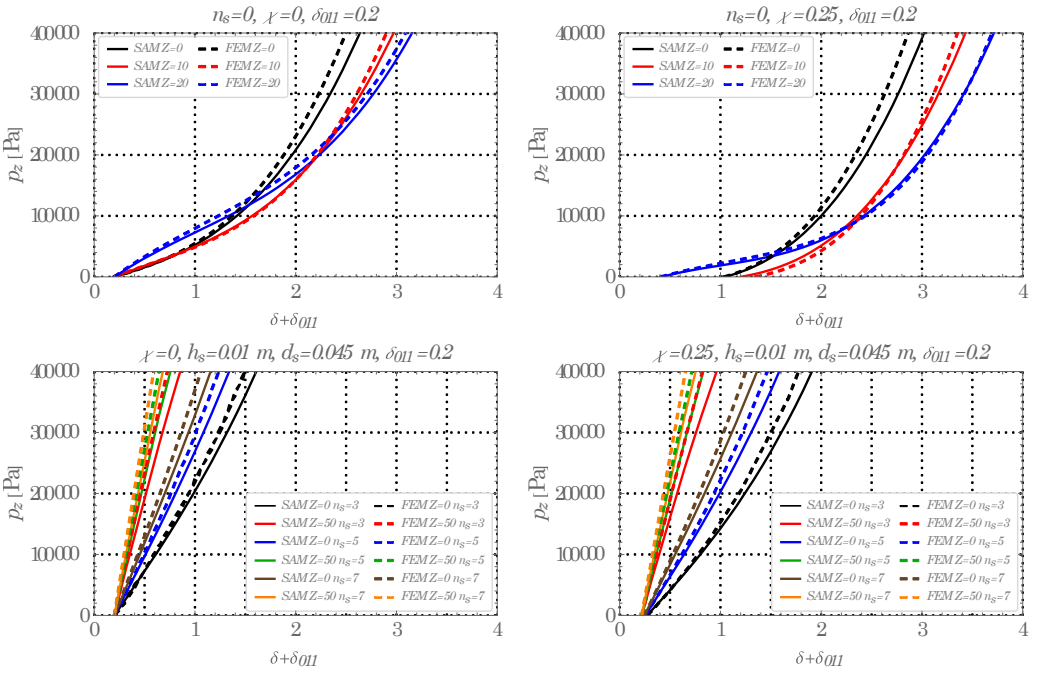

Figure 8.8: Comparison of the equilibrium paths for α=1.0 obtained by equation (8.13) and FEM for several geometric configurations of panels initially loaded with in-plane compression followed by out-of-plane pressure (a=1.0 m, BCC)

with Figure 8.6 for the same panels without initial out-of-plane pressure).

A very good agreements is obtained in all cases under complex loading conditions and geometric configurations, corroborating the excellent accuracy of the developed closed-form expressions in any situation.

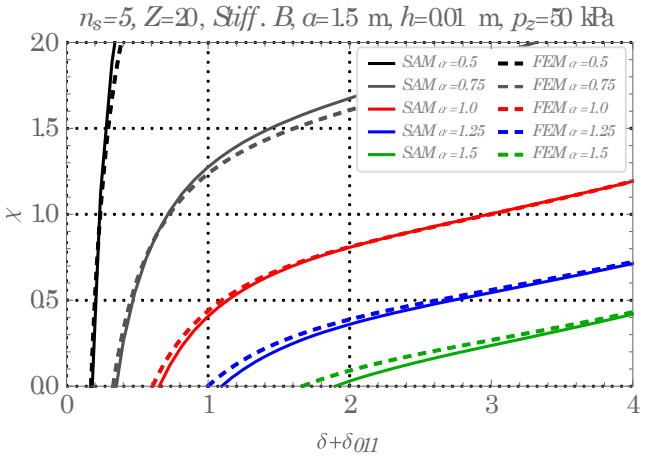

Figure 8.9: Comparison of the equilibrium paths for several aspect ratios obtained by equation (8.11) and FEM for panels initially loaded with out-of-plane pressure (p_z=50 kPa) followed by in-plane compression (w_0=min(a;b)/500, BCC)

8.3 ULTIMATE RESISTANCE OF UNSTIFFENED CURVED PANELS

8.3.1 Introduction

The plasticity of the material, in the FEM, is taken into account as described previously in section 5.5, considering an elastic-plastic material with strain hardening. However, accounting for this complex material in a semi-analytical model is difficult to implement and the efficiency of the procedure is greatly affected. Hence, the usual approach is to account for the plasticity in a simplified manner, using strength criteria. In subsection 8.3.2, a brief review of the utilization of strength criteria in the literature is presented. In subsection 8.3.3, the strength criterion adopted in the SAM is described and its assumptions are discussed. The first yield criterion applied to the von Mises' stresses using the membrane stresses is found to be a good compromise between accuracy and safety. Based on what was described in the previous chapters, subsection 8.3.4 discusses some fundamental concepts with particular importance for the study of the ultimate load by the semi-analytical model.

In subsection 8.3.5, the ultimate load of unstiffened curved panels under uniaxial compression is calculated by the SAM for a wide parametric variation of geometries considering different amplitudes and patterns of imperfections, boundary conditions and

even yield stresses. The influence of each of these parameters is calculated and validated with the results of the FEM. In order to assess the influence of the geometry on the resistance of the curved panels, the curvature parameter, Z, the aspect ratio, α, and the width over thickness, a/h, are varied with the objective to cover most cases of unstiffened curved panels with practical applicability.

8.3.2 Utilization of strength criteria in the literature

It was shown by Byklum [136] that it is possible to include a non-linear (elastic-plastic) material in semi-analytical methods for flat stiffened plates. However, this implies increasing considerably the complexity of the computational model; for example, analytical integration is lost, and besides that, the accuracy of the results decreases due to the incorporation of additional simplifications. Due to these disadvantages, the author opted to use a first yield criteria based on the von Mises stresses with an elastic material to predict the results of his analyses. Further work was done on the subject by Byklum and Amdahl [29] and Byklum *et al.* [137], which led to its implementation in the computer program PULS (DNV), preserving the same yield criteria for design purposes.

Paik *et al.* [138] and Paik and Lee [139] developed a semi-analytical method to predict the strength of flat plates. The authors also referred the difficulty to include explicitly material nonlinearity on the formulation. Therefore, they dealt numerically with the progress of the plasticity subdividing the plate in mesh regions. The von Mises yield criteria was then assessed for each region. If yield occurs the contribution of the yielded regions is removed from the stiffness matrix.

Brubak and Hellesland [140] applied the first yield criterion to the von Mises' membrane stresses at critical points along the edges of arbitrarily stiffened plates. The authors proved that this strength criterion is reasonable. However, it seems to indicate that for thick arbitrarily stiffened plates bending stresses may become important and membrane stresses may lead to non-conservative predictions for some cases. Later, Brubak and Hellesland [141] reinforced the same idea and used the bending stresses at three quarters of the plate thickness ($z=3h/8$) because the authors found that accounting for the bending stresses at the surface ($z=h/2$) may lead to too conservative results for those cases. Based on the findings of the last study, Ferreira and Virtuoso [30] used the strength

criterion at a quarter of the thickness ($z=h/4$) on the study of stiffened plates.

8.3.3 Strength criterion for the semi-analytical method

In the present study, the need to account for the contribution of the stresses along the thickness in the strength criterion was assessed. Using the membrane stresses instead of the stresses at the surface of the panel allows the development of some additional strength. The unstiffened panels studied are, generally, considered as thin and, consequently, this criterion was found to lead to satisfactory results. As it will be posteriorly identified, only for a very small part of the cases, this strength criterion predicted larger resistances than the finite element method. However, taking into account that this errors are small, in those cases, approximately less than 5%, it was not considered relevant to use a more conservative strength criteria, *i.e.* accounting for the contribution of the bending stresses along the thickness of the panels.

Hence, the von Mises' stresses, σ_{vM}, are calculated for the membrane stresses ($z=0$) by equation (8.14) and the strength criterion is considered to be reached when they equal the yield strength, f_y, at any point.

$$\sigma_{vM} = \sqrt{\sigma_x^{\,2} + \sigma_y^{\,2} - \sigma_x \sigma_y + 3\tau_{xy}^{\,2}} = f_y \tag{8.14}$$

Whenever relevant and unless otherwise stated, the yield strength is considered to be 355 MPa.

The location of the critical points has to be found for each case taking into account that its location is not fixed and it may change depending on geometrical parameters such as the curvature, Z. It was found that curvature changes completely the distribution of the von Mises stresses at first yield. To illustrate this, the distribution of the von Mises' stresses at the bottom extreme surface ($z=-h/2$) corresponding to the first yield are plotted in Figure 8.10 *a)* and *b),* for $Z=0$ and $Z=30$, respectively. While, for $Z=0$ the von Mises' stresses are larger along the longitudinal edges, for $Z=30$ the location of the larger stresses is along the transversal edges. Increasing the loading, yielding propagates to other points of the panel up to the ultimate load, as shown in Figure 8.11 *a)* and *b),* for $Z=0$ and $Z=30$, respectively. It is possible to see that the flat panel shows a larger area yielded in comparison with the curved panel, meaning in general that the increase in

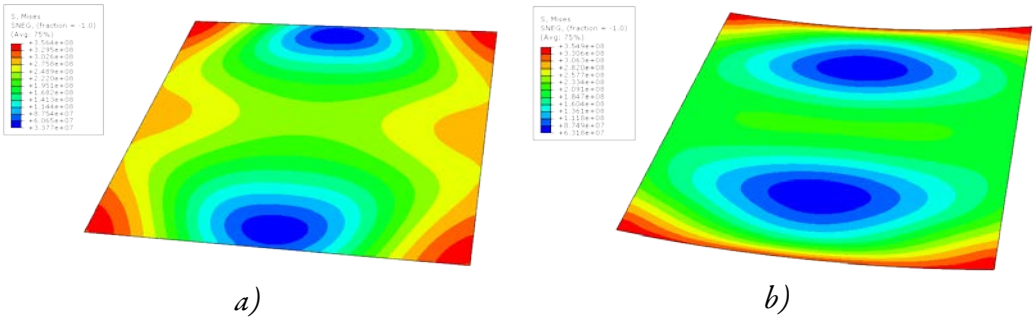

a) *b)*

Figure 8.10: Distribution of the von Mises' stresses at first yield for a panel with α=1.0 (a=b=1.0 m) and h=0.01 m (BCC) obtained by FEM for *a)* Z=0 and *b)* Z=30

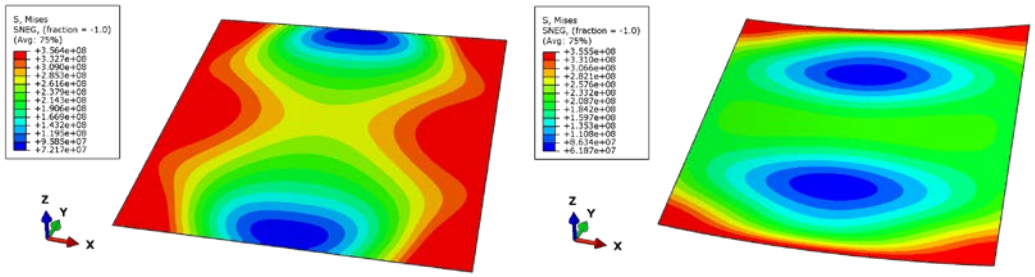

a) *b)*

Figure 8.11: Distribution of the von Mises' stresses at the ultimate load for a panel with α=1.0 (a=b=1.0 m) and h=0.01 m (BCC) obtained by FEM for *a)* Z=0 and *b)* Z=30

displacements between the first yield and the ultimate load is larger.

The location of the critical points obtained by the SAM, are analysed later; however, they were found to be in good agreement with those obtained by FEM.

8.3.4 Ultimate load of unstiffened curved panels under uniaxial compression

The effect of imperfections was already thoroughly discussed in Chapter 6; however, some concepts are discussed again with particular interest for application in the semi-analytical model. As previously shown, the initial imperfection pattern is able to influence significantly the development of the equilibrium paths.

In Figure 8.12, the equilibrium paths using three different imperfection patterns, a_{11}, a_{13} and 1st eigenmode from LBA, are plotted for unstiffened panels with α=3.0 and curvatures Z=0, Z=10 and Z=30 assuming the material with plasticity (contrarily to the figures of subsection 6.3.8, where an elastic material was used). The amplitudes of the

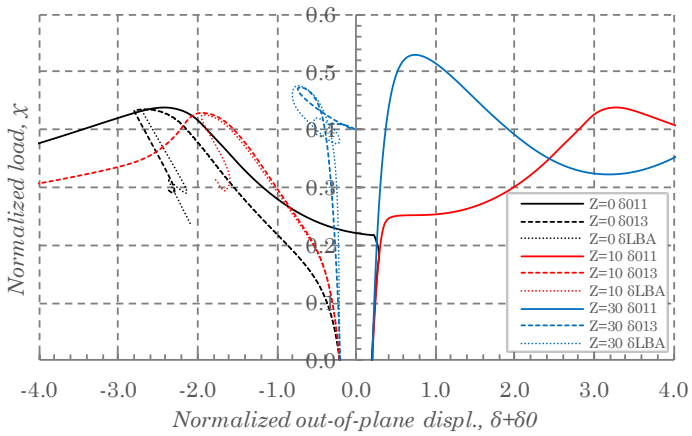

Figure 8.12: Effect of the initial imperfection for unstiffened panels with α=3.0 and imperfection patterns a_{11}, a_{13} and 1st eigenmode from LBA with amplitudes w_0=min(a;b)/500 (BCU)

imperfections are w_0=min(a;b)/500 and BCU are assumed. This aspect ratio is considered to assess the influence of taking into account a different number of semi-waves in the initial imperfection pattern and how they compare with the 1st eigenmode from LBA. It is seen that imperfection a_{11} leads to considerably distinct equilibrium paths in comparison with the remaining imperfection patterns, a_{13} and 1st eigenmode, which lead to very similar behaviours. When a_{11} is used, the displacement at the point at the centre of the panel may follow different directions comparatively to the remaining patterns and consequently different behaviours are obtained. In fact, only for the flat panel, Z=0, the displacement changes direction approaching the behaviour of the imperfection patterns a_{13} and 1st eigenmode.

In terms of the ultimate load, the results are very similar for all the three patterns, with the exception of Z=30, where a_{11} leads to a slightly larger value (χ=0.530) than a_{13} (χ=0.473) and 1st eigenmode (χ=0.476). In fact, the initial imperfection pattern can influence significantly the ultimate load value, even for panels with not so large aspect ratios. In order to exemplify this, in Figure 8.13 the reduction factors, χ, of unstiffened panels are compared using the initial imperfection pattern given by the first eigenmode obtained from linear buckling analyses (LBAs) and the global mode with one semi wave in each direction, a_{11}, for an aspect ratios α=1.0 and different curvatures. Values of w_0=min(a;b)/500 are considered for the amplitudes of imperfections and BCU are

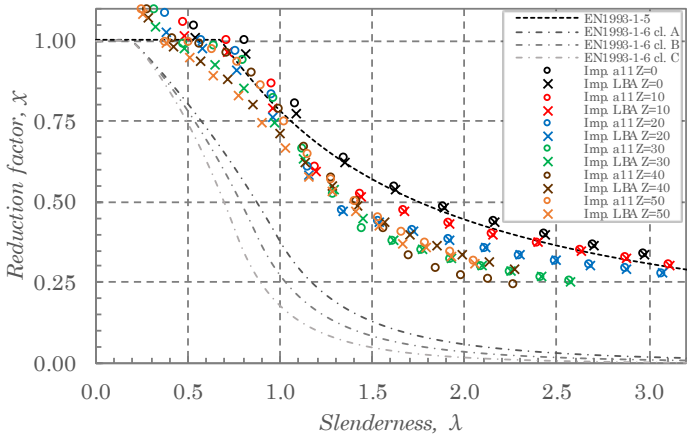

Figure 8.13: Effect of the initial imperfection pattern (eigenmode from LBA *vs* global mode a_{11}) on the reduction factor, χ, of unstiffened panels with amplitudes w_0=min(a;b)/500 (α=1.0 and BCU)

assumed. The ultimate load is plotted for tight intervals of the slenderness parameter, λ, as previously defined by equation (6.3). For comparison purposes, the reduction curves from EN1993-1-5 and EN1993-1-6, for flat plates and closed cylindrical shells, respectively, are plotted.

The following conclusions may be drawn: *i)* as expected, the curve from EN1993-1-5 is well adjusted to the results for flat panels (Z=0), since this curve is best obtained using a similar equivalent imperfection value (w_0=min(a/420; b/420), according to Zizza [142]); *ii)* the curves from EN1993-1-6 are too conservative for the curvatures considered, even considering the element with the best quality fabrication class (class A); and *iii)* the imperfection pattern corresponding to the first eigenmode of LBAs may not lead to the lowest value of χ for all curvatures. For larger slenderness, the global imperfection pattern, a_{11}, may lead to considerably lower values for χ.

The differences on the reduction factors obtained using both initial imperfection patterns are presented in Table 8.1, where a maximum difference of 25.7% is found for Z=40 and λ=1.85. As already concluded in Chapter 6, but now for lower increments in slenderness, this fact allows to claim that the consideration of initial imperfection patterns given by the eigenmodes from LBAs, which is usually assumed in many structural problems, may be non-conservative for curved panels and, consequently, the

Table 8.1: Difference of the initial imperfection pattern (eigenmode from LBA *vs* global mode a_{11}) on the reduction factor, χ, of unstiffened panels for Z=0 and Z=40 (α=1.0 and BCU)

	a=b [m]	0.25	0.375	0.5	0.625	0.75	0.875	1.0	1.125	1.25	1.375	1.5	1.625	1.75	1.875	2.0
Z=0	λ_{num}	0.54	0.81	1.08	1.35	1.62	1.89	2.16	2.43	2.70	2.97	3.24	3.51	3.78	4.05	4.32
	$\chi_{Imp\ LBA}$	1.009	0.959	0.771	0.623	0.539	0.480	0.436	0.398	0.366	0.339	0.314	0.293	0.273	0.257	0.242
	$\chi_{Imp\ a11}$	1.041	0.995	0.801	0.632	0.541	0.481	0.436	0.398	0.366	0.338	0.313	0.291	0.271	0.254	0.241
	Diff. [%]	-3.1%	-3.5%	-3.8%	-1.3%	-0.5%	-0.2%	0.0%	0.1%	0.2%	0.3%	0.3%	0.4%	0.7%	1.1%	0.6%
Z=40	λ_{num}	0.28	0.43	0.57	0.71	0.85	0.99	1.14	1.28	1.42	1.56	1.70	1.85	1.99	2.13	2.27
	$\chi_{Imp\ LBA}$	1.068	0.983	0.936	0.877	0.799	0.709	0.622	0.549	0.489	0.439	0.398	0.365	0.337	0.313	0.292
	$\chi_{Imp\ a11}$	1.091	1.004	0.988	0.960	0.898	0.786	0.665	0.572	0.500	0.413	0.331	0.290	0.271	0.255	0.242
	Diff. [%]	-2.2%	-2.1%	-5.2%	-8.6%	-11.0%	-9.8%	-6.5%	-4.1%	-2.3%	6.2%	20.4%	25.7%	24.5%	22.6%	20.7%

minimum value of χ using imperfection patterns from eigenmodes and perfect global modes should be considered.

Despite the implications of the imperfection pattern, for validation purposes of the SAM, the use of the perfect semi-waves with global imperfection mode, a_{11}, is assumed (the pattern a_{13} is also used in some cases for larger aspect ratios). The justifications for this assumption are: *i)* this initial imperfection mode is preferable because it is easily defined the same in the SAM (and in the FEM with the developed approach). In order to match exactly the eigenmode from LBAs for curved panels in the SAM, a large number of semi-waves in equation (4.86) would be required; *ii)* the analysis of the effect of imperfections was already carried out in Chapter 6 and it is not the objective of this chapter.

8.3.5 Validation of the SAM for the ultimate load

The semi-analytical formulation of Chapter 4 was formulated to account for multi degrees of freedom (MDOF) and, consequently, the number of DOFs incorporated in the model may be as large as desired. However, for computational efficiency reasons, it is desirable to keep the number of DOFs as low as possible. As previously discussed in Chapter 7, for the equilibrium paths, in cases with more complex geometries, a MDOF may be required to characterise the elastic behaviour of the panels with an acceptable error. The same is true for the ultimate load of the panels. As will be seen next, the

number of DOFs has in some cases a large influence on the calculated values of the ultimate load of curved panels. This influence is usually higher the greater the curvature of the panels. However, it is shown that only 1 or 2 DOFs, provided that they are properly chosen, are enough to characterise reasonably well the behaviour of most panels with practical relevance. Consequently, 1 or 2 DOFs show the best "cost-benefit" and are used to calculate the results in the following paragraphs.

Two distinct boundary conditions were formulated in Chapter 4 and assessed in Chapter 7 for the equilibrium paths. In next paragraphs, the ultimate load is also assessed for both boundary conditions and comparison between the results of the SAM and FEM are provided. However, when the objective is, for example, to show certain trends and behaviours, the results are provided for BCU or BCC indistinctly to avoid repetition, since, in general, the same conclusion may be drawn for the two boundary conditions.

The differences of using an elastic material to simulate the behaviour of the panels, in comparison with the non-linear material law used in the FEM, were discussed in section 6.4. The SAM is now applied to plot the equilibrium path and to predict the ultimate load of one of those panels (Z=10, α=1.0) with the equilibrium paths presented in Figure 6.18. In Figure 8.14, the load-deflection curve obtained with the SAM is compared with two curves obtained with the FEM, one considering the material as elastic and the other as elastic-plastic. The equilibrium path obtained with the SAM is represented up to the

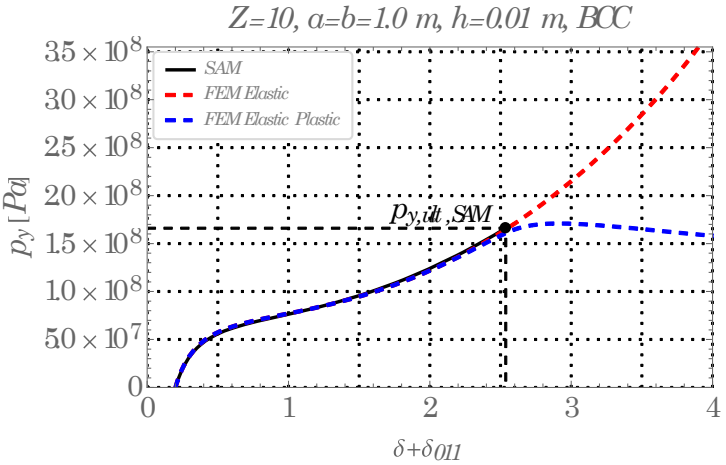

Figure 8.14: Comparison of the ultimate load by the SAM (2 DOF) and FEM (Z=10, a=b=1 m, h=0.01 m, imperfection w_0=min(a;b)/500 with a_{11} and BCC)

predicted ultimate load of the panel ($p_{y,ult,SAM}$), which is 166 MPa assuming that the strength criterion is reached when σ_{vM}=355 MPa. Up to this point, the curve follows exactly the two load-deflection curves of the FEM for the elastic and the elastic-plastic material. However, after the first yield, stress redistribution takes place and the curve deviates from the one with the elastic material, resulting in the maximum load point occurring for a slightly larger displacement, $\delta+\delta_{011}$=2.90 (against $\delta+\delta_{011}$=2.54 in the SAM) but for a very similar value of the maximum load, 171 MPa (which is, in fact, has much more practical relevance). This leads to reduction factors, $\chi=p_{y,ult}/f_y$, of 0.468 and 0.481, respectively for the SAM and FEM, which corresponds to an error in the SAM of -2.9%. However, it should be noted that these differences in the displacement are more prevailing in panels with lower curvatures. As seen in section 6.4, in the panels with larger curvatures, the point of the ultimate load occurs, in general, along the elastic equilibrium paths, *i.e.* the increase in displacement is lower.

If this procedure is followed for panels with different values of slenderness, λ, curves in terms of the reduction factor, χ, can be obtained as shown in Figure 8.15 and Figure 8.16, respectively for BCU and BCC. These curves are plotted for an aspect ratio α=1.0 and curvatures from Z=0 to Z=30, using only 2 DOFs. From the observation of these figures, it is possible to notice a good agreement between both approaches for the full range of slenderness. The maximum differences, despite perfectly acceptable, occur approximately for $0.5\leq\lambda\leq1.0$ when the ultimate load begins to be influenced not only by yielding of the material but by elastic-plastic interaction. For BCU, the curve from EN1993-1-5 is shown and the curves for larger curvatures (Z=30 and Z=40) are plotted for comparison. It is shown that the larger curvatures can be calculated with 2 DOF provided that the slenderness of the panels is not too high, because more complex deformation shapes occur and more DOFs are required.

The fact that the results from FEM may attain values of χ larger than 1.0 is explained by the consideration of hardening of the material and stresses larger than the yield stress may be developed, as previously explained. Naturally, this effect is not taken into account in the SAM.

An important aspect is the fact that the SAM provides safe values with exception of very

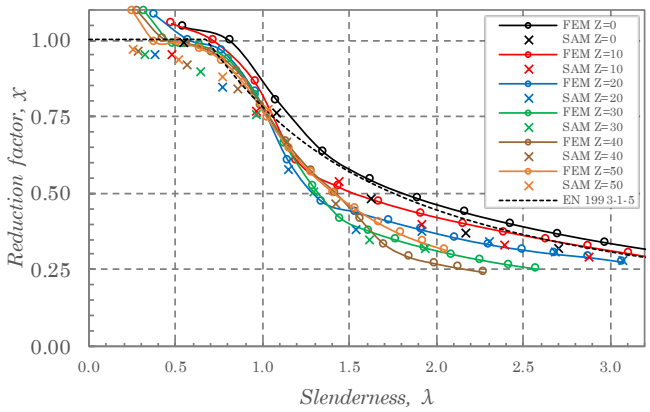

Figure 8.15: Comparison of the reduction curves obtained by the SAM (2 DOF) and FEM (α=1.0, global imperfection w_0=min(a;b)/500 with a_{11} and BCU)

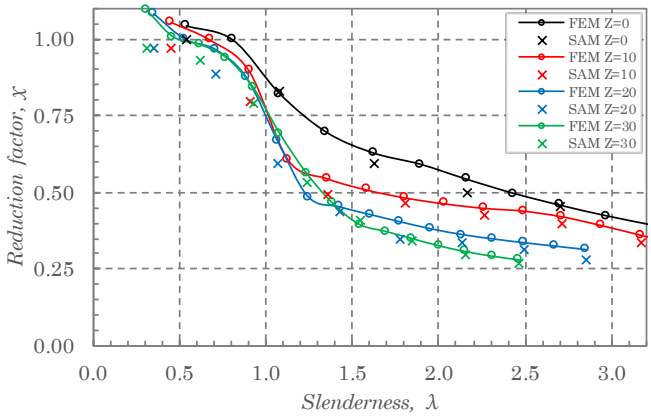

Figure 8.16: Comparison of the reduction curves obtained by the SAM (2 DOF) and FEM (α=1.0, global imperfection w_0=min(a;b)/500 with a_{11} and BCC)

few cases, however the maximum error on the unsafe side is only +3.6%. Taking this into account, it was not considered pertinent to use a more conservative strength criterion.

The same results are compared in scatterplots of Figure 8.17, for both boundary conditions, with the reduction factor, χ, obtained by the SAM and FEM. As verified, the values match reasonably well the line with slope 1.0. The statistical parameters, namely the coefficient of variation (CV), the correlation factor (Corr) and the mean absolute error (MAE), with respect to the values of the ultimate load calculated by the SAM and FEM are presented for each curvature in Table 8.2. All parameters corroborate the accuracy of the SAM. Not only the value of the correlation factor is very close to 1.0, but

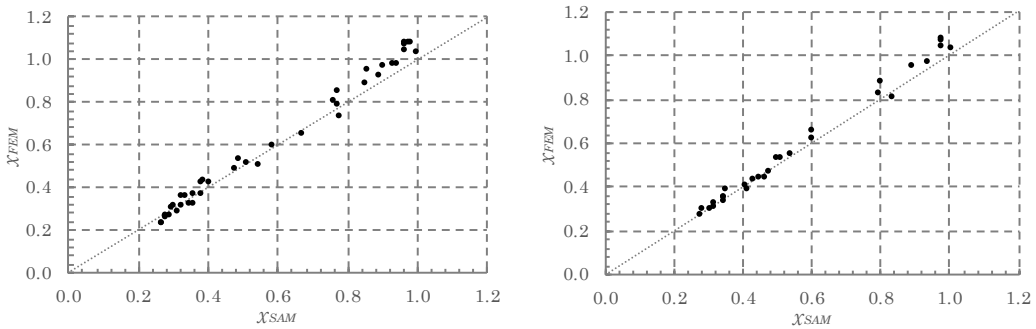

Figure 8.17: Comparison of the ultimate load by the SAM (2 DOF) and FEM for *a)* BCU and *b)* BCC (Z=10, a=b=1 m, h=0.01 m and global imperfection w_0=min(a:b/500) with a_{11})

also the mean absolute error shows a small negative error, as desired, with small dispersion.

It should be noted that, in some situations, the gains of introducing 2 DOFs in comparison with a SDOF are limited because: *i)* the deformation shapes are simple and a SDOF is enough; or *ii)* the deformation shapes are so complex that consistent improvements of the ultimate load would be only obtained with more DOFs; Nevertheless, the gains with the introduction of 2 DOFs are unquestionable, and they are justified in certain cases. In order to assess the influence of the number of DOFs in the prediction of the ultimate load, in Table 8.3 the comparison of the reduction factors, χ, obtained with 1 (b_{11}) and 2 (b_{11} and b_{13}) DOFs are presented for some random cases where the improvement are more noticeable. For comparison purposes the corresponding values of χ obtained by FEM are also presented. Three panels with Z=10, 20 and 30 with a/h=100, w_0=min($a;b$)/500 and BCC are considered. From the

Table 8.2: Statistical analysis of reduction factor, χ, of the error between the SAM and FEM

	BCU			BCC		
Z	CV	Corr	MAE	CV (%)	Corr	MAE (%)
0	7.8%	0.996	-3.3%	3.7%	0.988	-2.1%
10	7.1%	0.995	-3.4%	3.2%	0.998	-4.0%
20	7.2%	0.998	-3.9%	3.8%	0.998	-5.1%
30	4.5%	0.998	-5.4%	4.3%	0.998	-3.3%

Table 8.3: Comparison of the reduction factor, χ, obtained by the SAM with 1 DOF (b_{11}) and 2 DOFs (b_{11} and b_{13}) and FEM (a/h=100, a=1.0 m, w_0=min(a;b)/500 and BCC)

Z	α	χ_{FEM}	$\chi_{SAM,1DOF}$	$\chi_{SAM,2DOF}$	Diff. 1DOF vs FEM [%]	Diff. 2DOF vs FEM [%]
10	1.25	0.550	0.511	0.535	-7.13%	-2.69%
20	1.25	0.429	0.366	0.403	-14.70%	-6.13%
30	1.5	0.550	0.568	0.549	3.33%	-0.15%

observation of the results it is possible to verify that for these cases, the error decreases significantly when 2 DOFs are considered. While in some cases errors on the safe side are significantly reduced, in other cases small unsafe values replace safe values.

Additionally it was found that for flat plates the gains with the introduction of an additional DOF are, in general, more reduced, corroborating the idea that the need for more DOF is much larger in curved than flat panels.

In Table 8.4, the ultimate load obtained by the SAM, with DOFs b_{11} and b_{13}, and FEM are compared for different aspect ratios, α, and curvatures, Z. A global imperfection, a_{11}, is considered with and amplitude w_0=min(a;b)/500 for BCU. As previously discussed, the number of DOFs becomes important in the cases of large aspect ratios and curvatures. For these cases, 2 DOFs are insufficient to catch the very complex deformation shapes and more DOFs are required (for example, Z=30 and α=1.5). Even so, the results show

Table 8.4: Comparison of the ultimate load obtained by SAM (2 DOFs) and FEM for different aspect ratios and curvatures (a/h=100, a=1.0 m, w_0=min(a;b)/500 for BCU)

α	Z	λ	χ_{SAM}	χ_{FEM}	Error	Diff.	α	Z	λ	χ_{SAM}	χ_{FEM}	Error	Diff.
0.75	0	2.08	0.380	0.429	-11.4%	-0.049	1.25	0	2.11	0.400	0.443	-9.7%	-0.043
	10	1.90	0.431	0.423	1.8%	0.008		10	1.86	0.394	0.450	-12.3%	-0.056
	20	1.58	0.439	0.444	-1.0%	-0.004		20	1.51	0.392	0.446	-12.2%	-0.055
	30	1.31	0.470	0.523	-10.1%	-0.053		30	1.28	0.566	0.554	2.1%	0.012
1.0	0	2.16	0.372	0.436	-14.7%	-0.064	1.5	0	2.08	0.442	0.450	-1.8%	-0.008
	10	1.92	0.397	0.432	-8.0%	-0.034		10	1.86	0.414	0.464	-10.8%	-0.050
	20	1.54	0.380	0.439	-13.3%	-0.058		20	1.52	0.414	0.452	-8.5%	-0.038
	30	1.29	0.507	0.523	-3.0%	-0.016		30	1.27	-	0.580	-	-

that only 2 DOFs are able to provide good results for most curvatures of practical applicability, which for unstiffened panels in bridges, for example, is $Z \leq 15$ [135].

In order to show that a SDOF is able to estimate reasonably well the cases where the deformation shapes are well represented by the assumed mode, in Table 8.5, panels with α=1.0 and a/h=100 and 150 are compared with the FEM. Additionally, to assess also the validity for different yield stresses, a value of f_y=235 MPa is considered for the latter a/h ratio. A general good agreement is verified and on the other hand, the decrease on the reduction factor, χ, obtained increasing the value of the curvature, as identified in Chapter 6, is also perfectly caught with the SAM. In fact, it is verified that the value of χ may be considerably lower for the curved panels than for the corresponding flat plate (Z=0). The generally better agreement for lower yield stress, even for considerably slender panels, may be explained by the fact that the ultimate load is reached earlier leading to the development of smaller displacements where the agreement is generally better.

In order to validate the results of the SAM for the ultimate load, other amplitudes and patterns for imperfections should be assessed. In Table 8.6 the reduction factors, χ, are calculated for global imperfections a_{11}, but now considering amplitudes w_0=min(a;b)/200. Panels with aspect ratio α=1.0 and BCC are considered. Although, the differences for the FEM increase with the curvature, they are acceptable and on the safe side.

Table 8.5: Comparison of the ultimate load obtained by the SAM (SDOF) and FEM for different a/h ratios, curvatures and yield stresses (α=1.0, a=1.0 m, w_0=min(a;b)/500 for BCC)

	a/h=125 (f_y=355 MPa)				a/h=150 (f_y=235 MPa)			
Z	χ_{SAM}	χ_{FEM}	Error	Diff. [%]	χ_{SAM}	χ_{FEM}	Error	Diff. [%]
0	0.457	0.455	0.4%	0.2%	0.459	0.465	-1.3%	-0.6%
10	0.431	0.448	-3.7%	-1.6%	0.436	0.450	-3.1%	-1.4%
20	0.388	0.402	-3.4%	-1.4%	0.397	0.408	-2.5%	-1.0%
30	0.363	0.394	-8.0%	-3.1%	0.382	0.400	-4.4%	-1.8%

Table 8.6: Comparison of the ultimate load obtained by SAM (2 DOFs) and FEM for α=1.0 and different curvatures (a/h=100, a=1.0 m, w_0=min(a;b)/200 and BCC)

Z	λ	χ_{SAM}	χ_{FEM}	Error	Diff.
0	2.16	0.485	0.536	-9.7%	-0.052
10	1.81	0.454	0.477	-5.0%	-0.024
20	1.42	0.403	0.450	-10.5%	-0.047
30	1.23	0.400	0.478	-16.2%	-0.078

It is possible to deal with larger aspect ratios, obviating the use of a large number of DOFs, if the DOFs are properly chosen. However, as discussed in previous chapters, long panels with large curvatures show very intricate deformation shapes and a large number of DOFs are usually required. Therefore, if a small number of DOFs is used, one cannot expect the same level of accuracy, however, most curvatures of practical applicability (Z≤15, for bridges, for example) may be simulated reasonably well if the DOFs are chosen in accordance with the deformation shapes of the panels. For example, the deformation shape of panels with aspect ratio close to α=3.0 and an imperfection pattern a_{13}, may be reasonably approximated with only the DOFs b_{13} and b_{33}. In order to exemplify this, in Table 8.7 the ultimate load of panels with α=2.5 and 3.0 is calculated for panels with curvatures up to Z=15. In this case, initial imperfections are considered with 3

Table 8.7: Comparison of the ultimate load obtained by SAM (2 DOFs) and FEM for large aspect ratios (a/h=100, a=1.0 m, w_0=min(a;b)/500 with a_{13} and BCU)

α	Z	λ	χ_{SAM}	χ_{FEM}	Error	Diff.
2.5	**0**	2.13	0.355	0.429	-17.3%	-0.074
	5	2.05	0.349	0.426	-18.0%	-0.077
	10	1.89	0.363	0.424	-14.4%	-0.061
	15	1.71	0.397	0.425	-6.5%	-0.028
3.0	**0**	2.16	0.394	0.436	-9.5%	-0.030
	5	2.09	0.394	0.432	-8.7%	-0.023
	10	1.91	0.411	0.429	-4.1%	-0.018
	15	1.71	0.437	0.427	2.3%	0.010

longitudinal semi-waves, a_{13}, with amplitudes $w_0=a/500$ for BCU. In spite of the fact that the error is larger for aspect ratios $\alpha=2.5$ than for $\alpha=3.0$ the difference are on the safe side and, consequently, they are acceptable.

Another important aspect is related to the variation of χ with the aspect ratio. Despite not being so notorious as for the curvature, the variation of χ with the aspect ratio is not always monotonic, *i.e.* there are intermediate aspect ratios leading to lower values of χ as shown in Table 8.8. The results are calculated for a yield stress $f_y=235$ MPa and a different amplitude for the imperfection, $w_0=\min(a;b)/200$. The SAM is able to catch this behaviour as shown by the agreement with the results from the FEM. The error increases with the increase of the aspect ratio but maintained within acceptable limits.

Table 8.8: Comparison of the ultimate load obtained by SAM (2 DOFs) and FEM using a yield stress, $f_y=235$ MPa (imperfection $w_0=a/200$ with a_{11}, $Z=10$ for BCC)

α	λ	χ_{SAM}	χ_{FEM}	*Error*	*Diff.*
0.5	1.67	0.519	0.518	0.2%	0.1%
0.75	1.86	0.485	0.489	-0.9%	-0.4%
1.0	1.81	0.494	0.511	-3.5%	-1.8%
1.25	1.71	0.511	0.566	-9.8%	-5.5%

8.3.6 Simplified expressions for ultimate load based on the SAM

Expressions to predict the ultimate load of unstiffened curved panels, based on a SDOF solution, are proposed in this subsection. As it has been discussed along this chapter, increasing the number of DOFs increases the accuracy of the ultimate load predicted by the SAM, especially for larger curvatures and aspect ratios. However, as it was already shown in the previous subsection and it will be shown in more detail next, a SDOF is, nevertheless, able to provide good estimates of the resistance for a large part of the panels.

Solving the problem for isotropic panels according the Chapter 4, the distribution of the von Mises' stresses, σ_{vM}, in equation (8.14) is transformed in equation (8.15).

$$\sigma_{vM} = \sqrt{\left(-p_y + T_1\right)^2 - \frac{Eh}{8}\left(-p_y + T_1\right)T_2 + \left(\frac{Eh}{8}T_2\right)^2 + T_3} \tag{8.15}$$

with p_y given by equation (8.1) as a function of the out-of-plane displacement, δ_{11}, and T_1, T_2 and T_3 are function of x and y given, in their more general form, by:

$$\begin{aligned}
T_1 = {} & \frac{Eh^2}{8a^2}\left(\frac{1}{\alpha^2}\pi^2\delta_{11}\left(2\delta_{011}+\delta_{11}\right)\cos\left[\frac{2\pi x}{a}\right] - \frac{1}{c_1^{\,2}}8Z\alpha^2\delta_{11}\cos\left[\frac{\pi x}{a}\right]\cos\left[\frac{\pi y}{a\alpha}\right] + \right. \\
& \frac{1}{\alpha^2}32\pi\cos\left[\frac{2\pi y}{a\alpha}\right]\left(\pi\cosh\left[\frac{2\pi x}{a\alpha}\right]A + \left(a\alpha\cosh\left[\frac{4\pi x}{a\alpha}\right] + \right.\right. \\
& \left.\left. +2\pi x\sinh\left[\frac{4\pi x}{a\alpha}\right]\right)B\right) - 8\pi^2\cos\left[\frac{\pi x}{a}\right]\left(\cosh\left[\frac{\pi y}{a}\right]C + y\sinh\left[\frac{\pi y}{a}\right]D\right)\Bigg) \\
T_2 = {} & \frac{h}{a^2}\left(-\frac{1}{c_1^{\,2}}8Z\delta_{11}\cos\left[\frac{\pi x}{a}\right]\cos\left[\frac{\pi y}{a\alpha}\right] + \pi^2\delta_{11}\left(2\delta_{011}+\delta_{11}\right)\cos\left[\frac{2\pi y}{a\alpha}\right] - \right. \\
& \frac{1}{\alpha^2}32\pi^2\cos\left[\frac{2\pi y}{a\alpha}\right]\cosh\left[\frac{2\pi x}{a\alpha}\right]\left(A + x\sinh\left[\frac{2\pi x}{a\alpha}\right]B\right) + \\
& \left. 8\pi\cos\left[\frac{\pi x}{a}\right]\left(\pi y\sinh\left[\frac{\pi y}{a}\right]D + \cosh\left[\frac{\pi y}{a}\right]\left(\pi C + 2aD\right)\right)\right) \\
T_3 = {} & \frac{3E^2h^4}{a^4}\left(\frac{Z\alpha\delta_{11}}{c_1^{\,2}}\sin\left[\frac{\pi x}{a}\right]\sin\left[\frac{\pi y}{a\alpha}\right] - \frac{1}{\alpha^2}\left(\pi\sin\left[\frac{2\pi y}{a\alpha}\right]\left(4\pi\sinh\left[\frac{2\pi x}{a\alpha}\right]A + \right.\right.\right. \\
& \left.\left(4\pi x\cosh\left[\frac{4\pi x}{a\alpha}\right] + a\alpha\sinh\left[\frac{4\pi x}{a\alpha}\right]\right)B\right) + \\
& \left.\left.\left.\pi\alpha^2\sin\left[\frac{\pi x}{a}\right]\left(\pi y\cosh\left[\frac{\pi y}{a}\right]D + \sinh\left[\frac{\pi y}{a}\right]\left(\pi C + aD\right)\right)\right)\right)^2
\end{aligned} \tag{8.16}$$

where A, B, C and D are constants that depend on the geometric properties of the panels and the displacement δ_{11}, given by:

$$\begin{aligned}
A = {} & \frac{Z\alpha^2\delta_{11}\,\mathrm{csch}\left[\frac{\pi}{\alpha}\right]}{8c_1^{\,2}\pi^2\left(-1+\cosh\left[\pi\alpha\right]\right)\left(6\pi\cosh\left[\frac{2\pi}{\alpha}\right] + 5\alpha\sinh\left[\frac{2\pi}{\alpha}\right]\right)}\Bigg(\\
& 2\alpha\sinh\left[\frac{2\pi}{\alpha}\right]\left(\alpha\left(-2c_4 - c_1\pi\left(-1+4\upsilon\right)\right) + c_1\pi\alpha^3\left(1+\upsilon\right)\cosh\left[\frac{\pi\alpha}{2}\right] + \right. \\
& \left. 2c_4\alpha\cosh\left[\pi\alpha\right] - 2c_5\alpha^2\sinh\left[\frac{\pi\alpha}{2}\right] - c_3\left(-1+4\upsilon\right)\sinh\left[\pi\alpha\right]\right) +
\end{aligned} \tag{8.17}$$

$$4\pi\cosh\left[\frac{2\pi}{\alpha}\right]\left(-\alpha\left(2c_4+c_1\pi\left(1+4\upsilon\right)\right)+c_1\pi\alpha^3\left(1+\upsilon\right)\cosh\left[\frac{\pi\alpha}{2}\right]+\right.$$
$$\left.2c_4\alpha\cosh\left[\pi\alpha\right]-2c_5\alpha^2\sinh\left[\frac{\pi\alpha}{2}\right]-c_3\left(1+4\upsilon\right)\sinh\left[\pi\alpha\right]\right)\Big)$$

$$B=\frac{-Z\alpha^2\delta_{11}\,\mathrm{csch}\left[\frac{\pi\alpha}{2}\right]^2}{2ac_1{}^2\pi\left(6\pi\cosh\left[\frac{2\pi}{\alpha}\right]+5\alpha\sinh\left[\frac{2\pi}{\alpha}\right]\right)}\Big($$
$$-2\alpha\left(c_4+2c_1\pi\left(1+\upsilon\right)\right)+c_1\pi\alpha^3\left(1+\upsilon\right)\cosh\left[\frac{\pi\alpha}{2}\right]+$$
$$\left.2c_4\alpha\cosh\left[\pi\alpha\right]-2c_5\alpha^2\sinh\left[\frac{\pi\alpha}{2}\right]-4c_3\left(1+\upsilon\right)\sinh\left[\pi\alpha\right]\right)$$

$$C=-\frac{Z\alpha\delta_{11}}{4c_1{}^2\pi^2}\left(2c_3+\pi\alpha c_1\coth\left[\frac{\pi\alpha}{2}\right]\right)\mathrm{csch}\left[\frac{\pi\alpha}{2}\right]$$

$$D=\frac{Z\alpha\delta_{11}}{2ac_1\pi}\mathrm{csch}\left[\frac{\pi\alpha}{2}\right]$$

$$c_1=1+\alpha^2$$

$$c_3=-1+\alpha^2$$

$$c_4=2+\alpha^2+\upsilon$$

$$c_5=5+3\upsilon+\alpha^2\left(3+\upsilon\right)$$

These expressions are general and they are applicable to any curvature and aspect ratio.

The objective is then to determine p_y (*i.e.* the ultimate load) for which the following condition is verified.

$$\sigma_{vM} = f_y \tag{8.18}$$

For this, it is first required to determine the corresponding displacement δ_{11} at the ultimate load. With due substitutions, equation (8.15) could be solved for the displacement δ_{11}, where σ_{vM} equals the yield stress, f_y. However, given the fact that the solution for δ_{11} is quite cumbersome, due to the high order of δ_{11}, and, consequently, not convenient to present here, an alternative approach is preferable. Since the geometry, imperfection and material properties are defined, only two additional parameters are needed to be defined: *i)* the displacement δ_{11}; and *ii)* the location where the von Mises'

stresses first reach f_y.

In fact, the location of the critical points is changed with the curvature, as seen in Figure 8.10 and Figure 8.11. Fortunately, the location of the critical points occurs generally along the edges and it may be approximately predicted depending on the curvature, as follows: *i)* x=0.5a and y=0 for Z=0 to Z=10; *ii)* x=0.35a to 0.45a and y=0.5b for Z>0 to Z=30; and *iii)* x=0 and y=0.5b for Z=10 to Z=30. This means that few points have to be tested, leading to a straightforward process. It should be noted that, for example, for Z=0 the SDOF model leads to x=a/2 and y=0, although in many cases in FEM the first yield occurs in x=a/2 and y=b/2 as shown in Figure 8.10 for the von Mises stresses on the bottom surface. However, it is important to mention that f_y is almost reached simultaneous in both points, as it is possible to confirm in Figure 8.11, *i.e.* the propagation of the yield stress passes very quickly to x=a/2 and y=0, and consequently the differences are very small. To clarify the location of the critical points, some plots with the distribution of the von Mises stresses are present in Figure 8.18

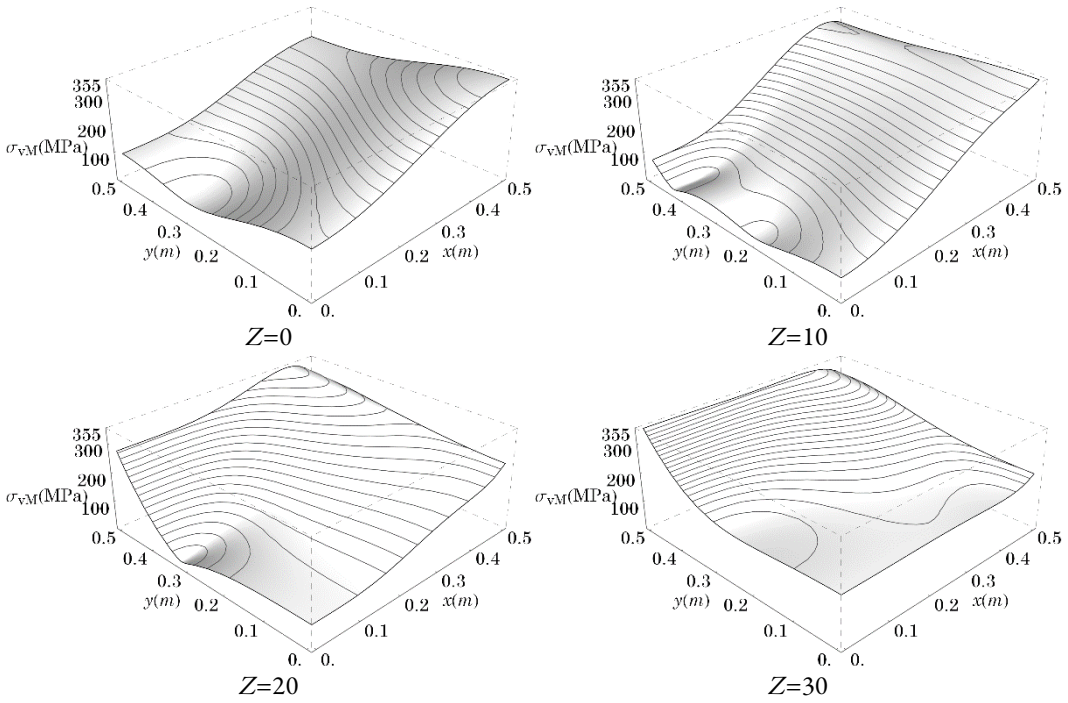

Figure 8.18: Comparison of the distribution of the von Mises' stresses for a panel with α=1.0 (a=b=1.0 m) and h=0.01 m (BCC) obtained by equation (8.15)

Once the location is determined, the next step is to increment δ_{11} until the condition (8.18) is verified, introducing this displacement in the load-deflection curves derived in Chapter 7, being equation (8.1) the most general, and to determine the corresponding load, *i.e.* the ultimate load.

A useful simplification of the problem is for aspect ratios α=1.0, leading to the following expression for T_1, T_2 and T_3.

$$
\begin{aligned}
T_1 = {} & \frac{Eh^2}{8a^2}\left(\pi^2\delta_{11}\left(2\delta_{011}+\delta_{11}\right)\cos\left[\frac{2\pi x}{a}\right]-2Z\delta_{11}\cos\left[\frac{\pi x}{a}\right]\cos\left[\frac{\pi y}{a}\right]+\right.\\
& 32\pi\cos\left[\frac{2\pi y}{a}\right]\left(\pi\cosh\left[\frac{2\pi x}{a}\right]A+\left(a\cosh\left[\frac{4\pi x}{a}\right]+\right.\right.\\
& \left.\left.+2\pi x\sinh\left[\frac{4\pi x}{a}\right]\right)B\right)-8\pi^2\cos\left[\frac{\pi x}{a}\right]\left(\cosh\left[\frac{\pi y}{a}\right]C+y\sinh\left[\frac{\pi y}{a}\right]D\right)\Bigg)\\
T_2 = {} & \frac{h}{a^2}\left(-2Z\delta_{11}\cos\left[\frac{\pi x}{a}\right]\cos\left[\frac{\pi y}{a}\right]+\pi^2\cos\left[\frac{2\pi y}{a}\right]\right.\\
& \left(\delta_{11}\left(2\delta_{011}+\delta_{11}\right)-32\cosh\left[\frac{2\pi x}{a}\right]A-16x\sinh\left[\frac{4\pi x}{a}\right]B\right)+\\
& \left.8\pi\cos\left[\frac{\pi x}{a}\right]\left(\pi y\sinh\left[\frac{\pi y}{a}\right]D+\cosh\left[\frac{\pi y}{a}\right]\left(\pi C+2aD\right)\right)\right)\\
T_3 = {} & \frac{3E^2h^4}{16a^4}\left(Z\delta_{11}\sin\left[\frac{\pi x}{a}\right]\sin\left[\frac{\pi y}{a}\right]-4\pi\sin\left[\frac{2\pi y}{a}\right]\left(4\pi\sinh\left[\frac{2\pi x}{a}\right]A+\right.\right.\\
& \left.\left(4\pi x\cosh\left[\frac{4\pi x}{a}\right]+a\sinh\left[\frac{4\pi x}{a}\right]\right)B\right)-\\
& \left.4\pi\sin\left[\frac{\pi x}{a}\right]\left(\pi y\cosh\left[\frac{\pi y}{a}\right]D+\sinh\left[\frac{\pi y}{a}\right]\left(\pi C+aD\right)\right)\right)^2
\end{aligned}
\tag{8.19}
$$

With the following constants:

$$
\begin{aligned}
A = {} & \frac{Z\delta_{11}\operatorname{csch}\left[\frac{\pi}{2}\right]^2\left(\pi\operatorname{csch}\left[\frac{\pi}{2}\right]+2\operatorname{sech}\left[\frac{\pi}{2}\right]\right)}{64\pi^2\left(\pi\cosh\left[\frac{\pi}{2}\right]+2\sinh\left[\frac{\pi}{2}\right]\right)\left(6\pi\cosh\left[2\pi\right]+5\sinh\left[2\pi\right]\right)}\Bigg(\\
& 4\pi^2\left(-1-4\upsilon+\left(1+\upsilon\right)\cosh\left[\frac{\pi}{2}\right]\right)\cosh\left[2\pi\right]+
\end{aligned}
\tag{8.20}
$$

$$8\left(\cosh\left[\frac{\pi}{2}\right]+\cosh\left[\frac{3\pi}{2}\right]\right)\sinh\left[\frac{\pi}{2}\right]^2\left(-2(2+\upsilon)+(3+\upsilon)\sinh\left[\frac{\pi}{2}\right]\right)+$$
$$\pi\left(2(3+\upsilon)\cosh[\pi]-4(3+\upsilon)\cosh[2\pi]+2(3+\upsilon)\cosh[3\pi]+\right.$$
$$\left.(17+9\upsilon)\sinh\left[\frac{3\pi}{2}\right]+2(1-4\upsilon)\sinh[2\pi]-(15+7\upsilon)\sinh\left[\frac{5\pi}{2}\right]\right)\Bigg)$$

$$B=\frac{Z\delta_{11}}{4a\pi\left(6\pi\cosh[2\pi]+5\sinh[2\pi]\right)}\Bigg(-2(3+\upsilon)-$$
$$\left(-4(2+\upsilon)+\pi(1+\upsilon)\coth\left[\frac{\pi}{2}\right]\right)\operatorname{csch}\left[\frac{\pi}{2}\right]+4\pi(1+\upsilon)\operatorname{csch}\left[\frac{\pi}{2}\right]^2\Bigg)$$

$$C=-\frac{Z\delta_{11}}{16\pi}\operatorname{csch}\left[\frac{\pi}{2}\right]^3\sinh[\pi]$$

$$D=\frac{Z\delta_{11}}{4a\pi}\operatorname{csch}\left[\frac{\pi}{2}\right]$$

For α=1.0, equation (8.3) is used for p_y.

For exemplification, the simplest possible case is obtained assuming Z=0. Taking into account that for Z=0, A=B=C=D=0, the following equations are obtained for the terms of equation (8.15).

$$T_1=\frac{Eh^2\pi^2\delta_{11}(2\delta_{011}+\delta_{11})}{8a^2}\cos\left[\frac{2\pi x}{a}\right]$$
$$T_2=\frac{h\pi^2\delta_{11}(2\delta_{011}+\delta_{11})}{a^2}\cos\left[\frac{2\pi y}{a}\right] \qquad (8.21)$$
$$T_3=0$$

Taking into account that the location of the point where the von Mises' stresses reach first the yield stress for Z=0 with a SDOF (x=a/2 and y=0), the expressions are further simplified, as follows:

$$T_1=-\frac{Eh^2\pi^2\delta_{11}(2\delta_{011}+\delta_{11})}{8a^2}$$
$$T_2=\frac{h\pi^2\delta_{11}(2\delta_{011}+\delta_{11})}{a^2} \qquad (8.22)$$
$$T_3=0$$

Substituting equation (8.5) for p_y and expression (8.22) in equation (8.15), the following expression is obtained for the von Mises' stress at the critical point.

$$\sigma_{vM} = \frac{Eh^2\pi^2\delta_{11}}{24a^2\left(\delta_{011}+\delta_{11}\right)\left(1-\upsilon^2\right)}\sqrt{\left(64+3\left(\delta_{011}+\delta_{11}\right)\left(2\delta_{011}+\delta_{11}\right)\right.} \Bigg/ \left(\left(-1+\upsilon^2\right)\left(-40+21\left(\delta_{011}+\delta_{11}\right)\left(2\delta_{011}+\delta_{11}\right)\left(-1+\upsilon^2\right)\right)\right) \tag{8.23}$$

To exemplify the procedure, the ultimate load of a flat plate with a=b=1.0 m, h=0.01 m and a global imperfection of w_0=min(a;b)/500 is calculated next.

Incrementing the value of δ_{11} until the von Mises' stress reaches the value of f_y, a value of 354.8 MPa is reached for a displacement δ_{11}=1.864. This process is exemplified in Table 8.9.

Table 8.9: Example of the calculation of the ultimate load by the proposed expressions for flat plates (calculation of the displacement at the ultimate load)

δ_{11}	1.5	1.8	1.85	1.86	1.864
σ_{vM} **[MPa]**	259.6	336.7	350.8	353.6	354.8

Inserting δ_{11}=1.864 in equation (8.5) a value of 177.9 MPa is obtained for the ultimate load, corresponding to a value of the normalized ultimate load χ=0.501. The value of χ calculated by the FEM is 0.541, meaning -7.4%, on the safe side.

Repeating the same procedure, changing the width of the panels, and consequently the width to thickness ratio, from a/h=50 to 150 for w_0=min(a;b)/500 and w_0=min(a;b)/200, Figure 8.19 is obtained. The results are in very good agreement with the FEM. However, it should be noted that the ultimate load predicted by the expression for a/h=50 (and w_0=min(a;b)/500) shows an error of 3.6% (χ_{SAM}=0.827 vs χ_{FEM}=0.798) on the unsafe side. This is a reasonable error taking into account the relatively low value of a/h. As previously, explained the von Mises' first yield criterion for the membrane stresses may lead to non-conservative predictions of the ultimate load for thick plates (in comparison with the width). In this cases, bending stresses start to be relevant and they should be accounted for in the strength criteria. The same phenomenon may be verified for small aspect ratios where the b/h ratio shows a low value. However, as a/h and b/h lesser than 50 were not considered and the error for the lowest ratios of the studied panels are small, it was not considered relevant to account for a more conservative strength

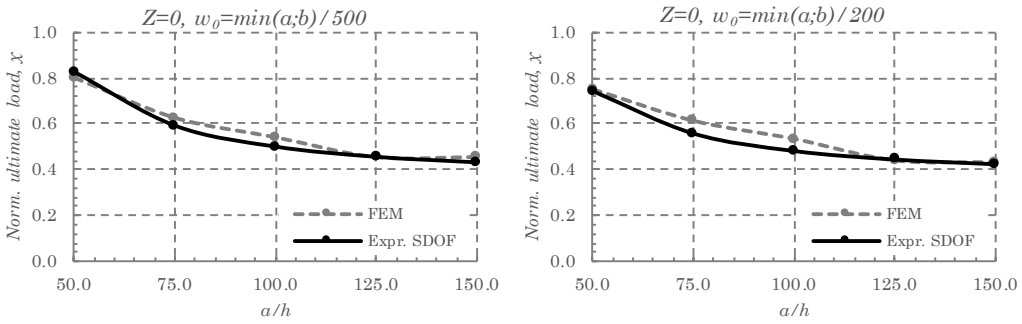

Figure 8.19: Comparison of the ultimate load calculated by equations (8.5) and (8.23) and FEM for flat plates as a function of the a/h ratio with imperfection *a)* w_0=min(a;b)/500 and *b)* w_0=min(a;b)/200 (α=1.0, h=0.01 m, BCC)

criterion.

Applying the procedure for the curved panels with α=1.0, through equations (8.3), (8.15) and (8.19), the normalized ultimate loads for Z=10 and Z=30 are plotted in Figure 8.20, as a function of the a/h ratio. For validation purposes, in Figure 8.21 similar results for Z=20 are obtained with a steel with f_y=235 MPa. The agreement between the analytical expressions and the FEM are generally very good. Only for Z=30 and a/h=75 the ultimate load predicted by the expression exceed in 5.5% (χ_{SAM}=0.854 vs χ_{FEM}=0.809) the value of the FEM. However, it should be noted that this curvature is considerably large taking into account that only 1 DOF is used (see Chapter 7). Additionally, the incorporation of bending stresses along the thickness in the strength criterion can be required for a conservative estimate.

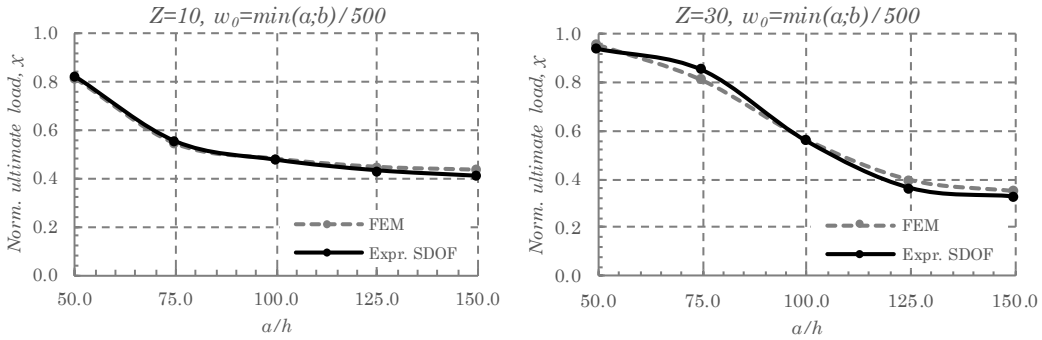

Figure 8.20: Comparison of the ultimate load calculated by equations (8.3) and (8.15)(8.19) and FEM for curved panels as a function of the a/h ratio (α=1.0, BCC)

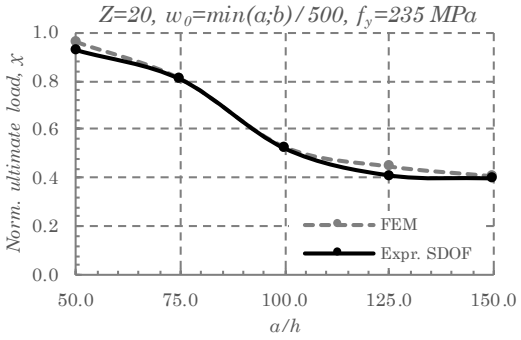

Figure 8.21: Comparison of the ultimate load calculated by equations (8.3) and (8.15) and FEM for curved panels as a function of the a/h ratio for f_y=235 MPa (α=1.0, BCC)

In order to validate the proposed expressions for what was previously discussed in Chapter 6 about the local minimums of χ when plotted as a function of the curvature, Figure 8.22 compares this effect with the FEM. The local minimum at Z=20 is caught and accurate safe values are provided for all curvatures (α=1.0, a/h=100).

The normalized ultimate loads of panels with different aspect ratios are plotted in Figure 8.23. A very good agreement is shown for aspect ratios between 0.75 and 1.25. The panel with α=0.5 shows an error of +6.8% which may be explained, once again, by the strength criterion considered. As previously explained, more conservative strength criteria should be applied to these cases. In fact, α=0.5 with a/h=100 seems to be more sensitive to this aspect than α=1.0 with a/h=50, despite both having b/h=50. For this reason, the

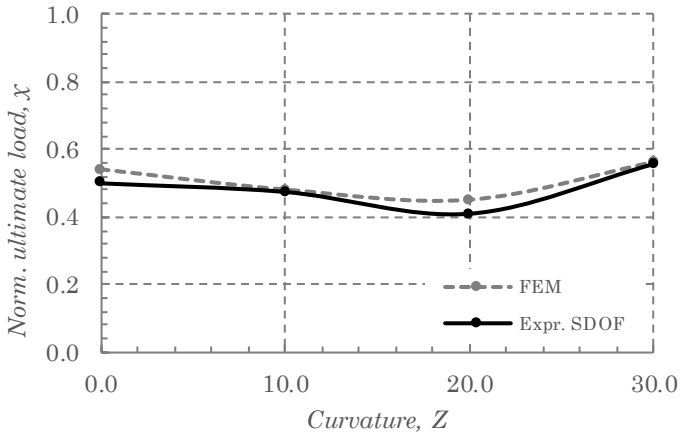

Figure 8.22: Comparison of the ultimate load calculated by equations (8.3) and (8.15) and FEM for several curvatures (w_0=min(a;b)/500, a=1.0 m, α=1.0, a/h=100, BCC)

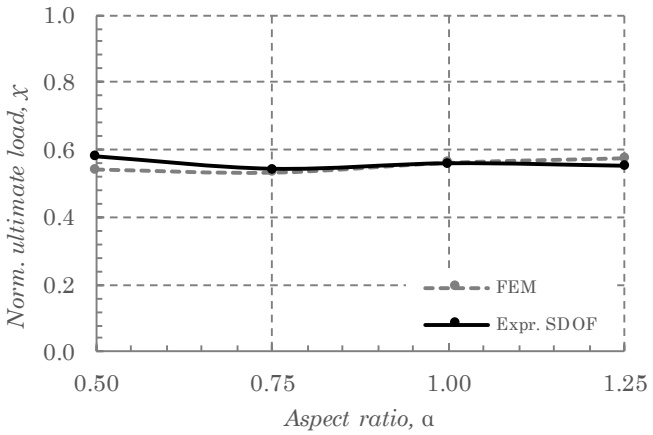

Figure 8.23: Comparison of the ultimate load calculated by equations (8.1) and (8.15) and FEM for a curved panel with Z=30 for several aspect ratios (w_0=min(a;b)/500, a=1.0 m, a/h=100, BCC)

calculation of panels with low aspect ratios (α<0.75) is not recommended. Additionally, aspect ratios α>1.25 do not should be used with the proposed expression due to the SDOF implications. For the remaining cases and according to the applicability assessed in Chapter 7, the proposed expressions showed, in the cases analysed, very good agreement with the nonlinear finite element analyses.

To corroborate this, Figure 8.24 presents all the results of χ calculated by the SAM in comparison with the FEM. The values fit well the line with slope 1.0 and are within the range of +10% and -10%. The good agreement is corroborated by the following statistical

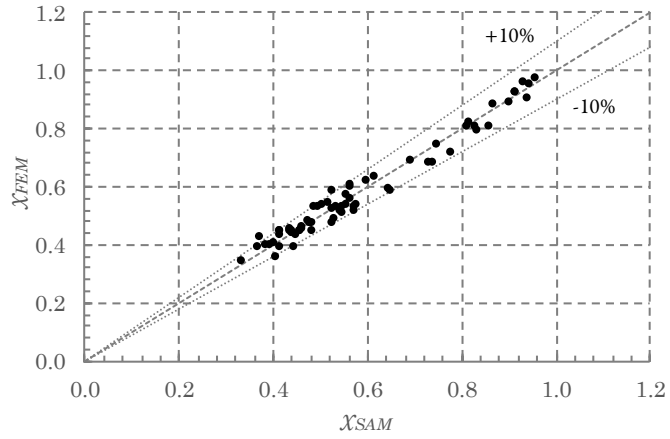

Figure 8.24: Comparison of the ultimate load calculated by the proposed expressions and FEM (BCC)

parameters: CV=5.8%, Corr=0.985 and MAE=-0.3%.

8.4 EXAMPLES OF APPLICATION

8.4.1 Introduction

In this section, the methodology proposed in the previous sections is used in two curved panels extracted from real cases. In the first example, the large deflection behaviour of a stiffened curved panel is studied and in the second example, the ultimate load of an unstiffened curved panel is predicted. The results of both examples are compared with FEM results showing good agreement.

8.4.2 Example 1: Large deflection behaviour of a stiffened curved panel

The objective of the first example is to apply the proposed expression to predict the large deflection behaviour of a stiffened curved panel under in-plane uniaxial compression.

The geometry of the panel is based on the information given in Tran *et al.* [84], Tran [14] and Reis *et al.* [135] for a stiffened panel from the Confluences bridge in Angers, France (see Figure 8.25). The information collected corresponds to a stiffened panel with a width, a, of 4.8 m, a radius, R, of 80 m, a thickness, h, of 16 mm, a length given by the distance between diaphragms, b, of 5.0 m and it is composed by 6 stiffeners, n_s, spaced by 0.8 m, a_s, in the central zone and 0.4 m and the extreme stiffeners are 0.4 m away from the boundaries, as identified in the figure. It is indicated that the stiffeners are flat, their geometry is omitted. Consequently, based on a survey done for similar cases, reasonable values of 0.18 m and 18 mm (*i.e.* d_s/h_s=10.0) were assumed, respectively, for the depth, d_s, and thickness of the stiffeners, h_s. As previously explained, to account in the numerical model for the overlap of the shell elements of the stiffeners and the panel, d_s is

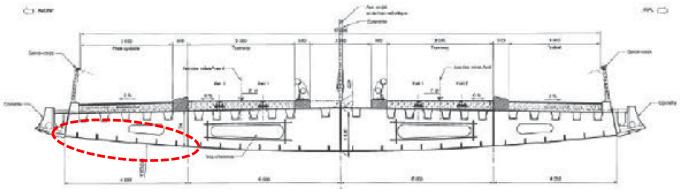

Figure 8.25: Cross-section of the Confluences bridge in Angers, France [14]

incremented in the FEM with half the thickness of the panel, $d_{s,FEM}$=0.188 m.

Taking into account the surrounding of the panel, BCC boundary conditions may be assumed.

The following geometric parameters are obtained for this panel:

$$Z = \frac{a^2}{Rh} = \frac{4.8^2}{80 \times 0.016} = 18.0 \tag{8.24}$$

$$\alpha = \frac{b}{a} = \frac{5}{4.8} = 1.041 \tag{8.25}$$

The spacing of the stiffeners for the panel of this example is different from the one used throughout the thesis. While previously the stiffeners were considered equally spaced by a distance $a_s=a/(n_s+1)$, the panel of this example is assumed with the spacing of the end panels half of the internal ones. This means a distance between stiffeners of $a_s=a/n_s$. Both cases are shown in Figure 8.26. This effect is non-negligible and, consequently, it should be taking into account in the study of the nonlinear behaviour of the panels.

To assess the accuracy of the expressions for this situation and to assess the differences between cases, both stiffener configurations are calculated next.

The first step is the calculation of the orthotropic properties of the panels as described in Chapter 4. Table 8.10 presents these values.

The next step is to introduce the geometric properties and the calculated orthotropic

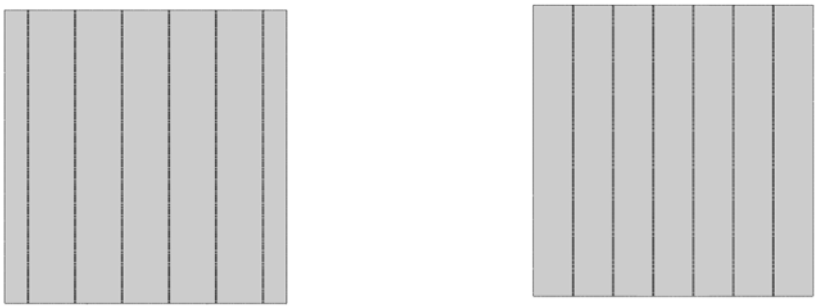

a) *b)*

Figure 8.26: Stiffener spacing configuration assumed for *a)* the panel of example 1 and *b)* throughout the thesis

Table 8.10: Calculation of the orthotropic properties for both stiffener spacing configurations

	$a_s=a/n_s$ =0.8 m	$a_s=a/(n_s+1)$ =0.685714 m		$a_s=a/n_s$ =0.8 m	$a_s=a/(n_s+1)$ =0.685714 m
z_0 [m]	0.0197955	0.0223426	G_{xy} [Pa]	8.87136×10^{10}	8.84808×10^{10}
I_s [m^4]	0.0000285637	0.0000272939	D_x [N·m]	80141.9	80346.5
v_x [-]	0.290273	0.293387	D_y [N·m]	9.05019×10^{6}	1.03192×10^{7}
E_x [Pa]	2.1×10^{11}	2.1×10^{11}	D_{xy} [N·m]	29151.5	29539.5
E_y [Pa]	2.63156×10^{11}	2.63156×10^{11}	D_{yx} [N·m]	2.62703×10^{6}	3.02752×10^{6}
v_y [-]	0.363748	0.367651	D_s [N·m]	30280.9	30201.4
v_{xy} [-]	0.324941	0.328427			

Table 8.11: Calculation of the constants C_1, C_2, C_3 and C_4

	C_1	C_2	C_3	C_4
$a_s=a/n_s$=0.8 m	-1.52995×10^{7}	-5.26631×10^{8}	-4.99045×10^{7}	2.09925×10^{7}
$a_s=a/(n_s+1)$=0.685714 m	-1.52995×10^{7}	-6.0105×10^{8}	-5.00496×10^{7}	2.09899×10^{7}

parameters in equations (8.8) to calculate the constants C_1, C_2, C_3 and C_4. The results for both cases are presented in Table 8.11.

Substituting these constants in equation (8.7), the expression for p_y appears as a function of the normalized imperfection, δ_{011}, and the normalized displacement, δ_{11}.

In this example, a global imperfection, a_{11}, with an amplitude $w_0=\min(a;b)/400$ is assumed, leading to the following normalized value of δ_{011}:

$$\delta_{011}=\frac{\min(a;b)/400}{h}=\frac{4.8/400}{0.016}=0.75 \tag{8.26}$$

Normalizing p_y through equation (7.2), assuming f_y=355 MPa, the equilibrium paths of both panels may be plotted as shown in Figure 8.27. It is possible to verify that the effect of the configuration of the stiffeners is noticeable. Additionally, the agreement between the proposed expression and the FEM is perfect, showing that it is able to deal accurately with stiffened panels of practical interest.

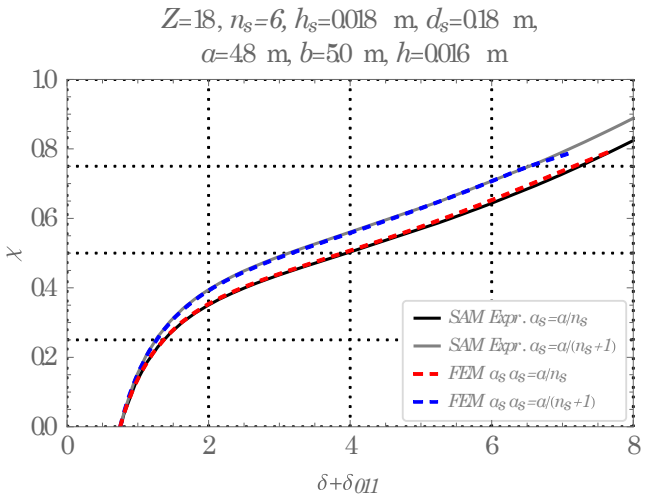

Figure 8.27: Comparison of the equilibrium paths for the stiffened panel of example 2 (w_0=min(a;b)/400)

8.4.3 Example 2: Ultimate load of an unstiffened curved panel

The second example aims to assess the ultimate load of a bilge panel under uniaxial compression of a container ship taken from Mohammed *et al.*[143] (see Figure 8.24). The selected panel is situated between two stiffeners considered, here, with a sufficiently high moment of inertia (370x13 bulb flats), so that the subpanel can be assumed as simply supported. Taking into account the location of the panel, BCC may be assumed. The selected subpanel has a thickness, h, of 21 mm, a width (between stiffeners), a, of 0.86 m and a radius of 4.9 m. The bulkheads are separated by 0.791 m, defining the length, b, of

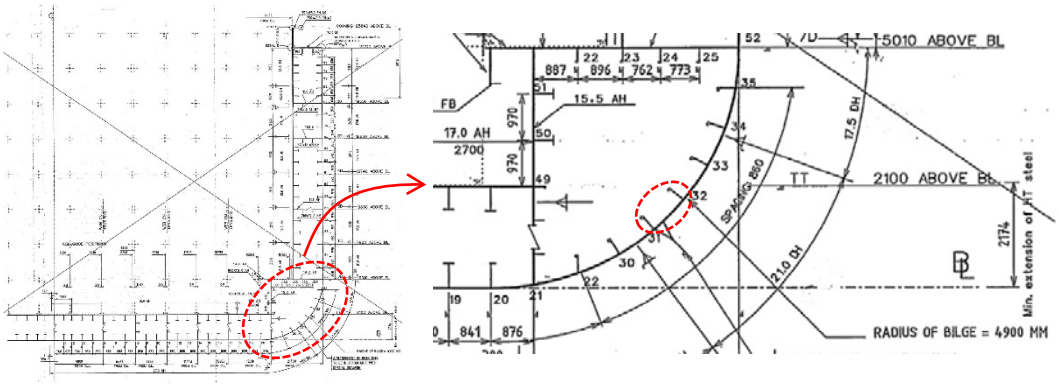

Figure 8.28: Midship section of a container ship and identification of the curved panel to study [143]

the panels. The panel is composed by a HT36 steel with a yield stress, f_y=355 MPa.

The following geometric parameters are obtained for this panel:

$$Z = \frac{a^2}{Rh} = \frac{0.86^2}{4.9 \times 0.021} = 7.188 \tag{8.27}$$

$$\alpha = \frac{b}{a} = \frac{0.791}{0.860} = 0.920 \tag{8.28}$$

A global imperfection, a_{11}, with an amplitude w_0=min(a;b)/500 is assumed, leading to a normalized value of δ_{011}:

$$\delta_{011} = \frac{\min(a;b)/500}{h} = \frac{0.791/500}{0.021} = 0.0753 \tag{8.29}$$

Substituting the geometric variables and the calculated parameters in equation (8.17), A, B, C and D are written in function of the normalized displacement δ_{11}. Introducing them in equations (8.16), T_1, T_2 and T_3 are written as a function of the x, y and δ_{11}. Substituting these expressions and equation (8.1) for p_y (also as a function of δ_{11}) in equation (8.15), the von Mises' stresses are written only in function of the coordinates (x and y) and the displacement δ_{11} which are the unknowns of the problem.

The point where the von Mises' stresses, σ_{vM}, reach first f_y should be determined. As previously explained, for this value of curvature, σ_{vM} is, generally, first reached for one of these two points: *i)* x=0.35a to 0.45a and y=0.5b*; and ii)* x=0.5a and y=0.

The first point may change along the transversal edge and the value of x, where the maximum stress occurs, should be determined. Assuming an initial value δ_{11}=0.1, x=0.35 m is determined as the one leading to the maximum value of σ_{vM}, as shown in Table 8.12.

Now, δ_{11} should be incremented until the von Mises' stress reaches the value of f_y. This process is shown in Table 8.13.

Table 8.12: Calculation of the x coordinate for δ_{11}=0.1 and y=b/2=0.3955 m

x [m]	0.32	0.33	0.34	0.35	0.36
σ_{vM} [MPa]	316.91	317.07	317.16	317.19	317.12

Table 8.13: Calculation of the displacement for $\sigma_{vM}=f_y$

δ_{11}	0.1	0.11	0.12	0.13
σ_{vM} [MPa]	317.19	330.88	343.34	354.75

A value of 354.75 MPa is reached for a displacement δ_{11}=0.13, which introduced in equation (8.1) leads to a value of p_y=329.21 MPa, corresponding to a value of χ=0.927.

The value of σ_{vM} should be now assessed for the second point, x=0.5a and y=0. For these coordinates, δ_{11}=0.13 leads to a value of σ_{vM}=325.80 MPa, meaning that this point is not the critical one.

The normalized ultimate load is obtained for the same panel by the FEM with the material properties previously described. A normalized ultimate load χ=0.923 is obtained for the panel, as shown in Figure 8.29. The error between both approaches is 0.4%.

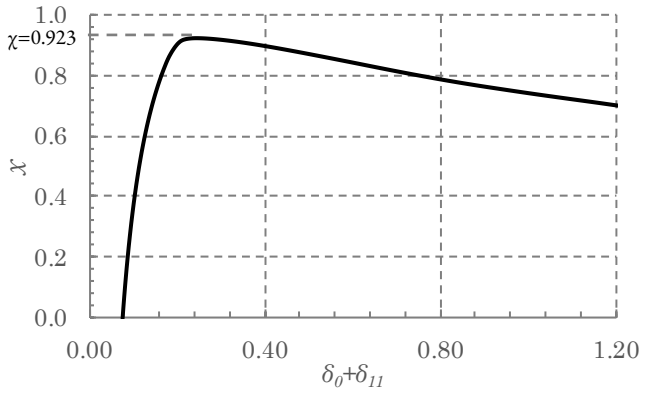

Figure 8.29: Equilibrium path and ultimate load of the unstiffened panel considered in the example 2

8.5 SUMMARY

Accurate closed-form analytical expressions for the post-buckling behaviour of curved unstiffened and stiffened curved panels based on a SDOF model were proposed. These expressions incorporate explicitly all the geometric parameters (including the aspect ratio) and are able to account for both in-plane and out-of-plane loading.

Despite being possible to include a non-linear material, as an elastic-plastic material, in the semi-analytical model, this is not a very practical strategy. The usual approach is to account for the plasticity in a simplified manner, using strength criteria. A first yield criterion was applied to the von Mises' stresses with the membrane stresses (z=0). Despite a more conservative criterion (*e.g.* accounting with the bending stresses along the thickness in the von Mises' stresses) would be desirable in some situations, it was not considered necessary to consider it, because for the studied panels the strength criterion using only the membrane stresses provided good results for most cases.

The effect of the curvature in the ultimate load was assessed in terms of the reduction buckling curves. Comparison with the provision of Eurocode 3 (EN1993-1-5 and EN1993-1-6) showed the total inadequacy of these standards to deal with curved panels. On the other hand, the predictions of the SAM matched with good accuracy the buckling curves for both BCU and BCC.

The validity of the SAM was then assessed for diverse situations of geometries and boundary conditions. A multi degree of freedom solution was employed whenever necessary. In this case, 2 DOFs were shown to increase the accuracy of the SAM especially for more complex deformation shapes for larger curvatures and aspect ratios. Nevertheless, a SDOF is able to deal reasonably well with a large part of the cases.

Finally, expressions to predict the ultimate load of unstiffened curved panels based on a SDOF were proposed and validated. They show good agreement with the FEM and they are able to account for the large part of the unstiffened curved panels used in practice.

9 Conclusions and outlook

9.1 Conclusions

The choice for the subject of this thesis was motivated by the recent growing interest in curved panels in several engineering fields and, at the same time, by the verified lack of robust provisions to deal with these structures. Consequently, it was proposed to address this topic through advanced numerical finite element analyses, but mainly, through semi-analytical methods. This decision was motivated by the fact that, although the FEM is able to deal accurately with the problem, it is time consuming and requires expertise, but mainly, it can only be used to derive design provisions necessarily involving empirical coefficients based on statistical assessment. On the other hand, analytical models allow to identify the key parameters that influence the behaviour of the panels and to develop expressions purely based on the physical background of the problem, which have a much greater interest.

In this sense, the derivation of a large deflection formulation for unstiffened and stiffened curved panels subjected to different loading conditions was derived. Special emphasis was

given to uniaxial compression which represent the key aspect in the stability of thin walled structures, but out-of-plane loading was also analysed.

The DMV theory based on the Donnell's theory and derived for shallow shells was shown to be the most adequate theory for application in the curved panels after a brief review was carried out comparing different shells theories available. The hypotheses on the basis of the theory and the consequences on the simplifications underlying the shallow shells assumptions were discussed. It was concluded that this theory combines simplicity and accuracy if certain limits are fulfilled (the present panels fall within this limits) and, consequently, it was chosen to formulate the problem.

The formulation was provided for isotropic and orthotropic panels with the number and geometry of stiffeners explicitly considered in the concave side of the curved panels for generic aspect ratios and curvatures. The formulation is able to account for generalized loading for two different simply supported boundary conditions depending of the in-plane restraint along the edges and it was derived for a multi degree of freedom solution solved with the Rayleigh-Ritz method.

Detailed finite element models able to describe accurately the behaviour of the panels were constructed. The modelling of the initial imperfections was considered in a relatively innovative way in comparison with the default approach used in most shell problems. This default approach, which consists in using the eigenmodes as initial imperfection, was found to overestimate, in some cases of unstiffened panels, the ultimate load in more than 25% the ultimate load in comparison with other perfectly admissible imperfections. This means that the consideration of initial imperfection patterns given by the eigenmodes from LBAs, which is usually assumed in many structural problems, may be non-conservative for curved panel. However, none of the considered imperfections may be considered always the most unfavourable one and, consequently, none of them can be *a priori* neglected. Additionally, to validate the SAM the same imperfection pattern must be used in the FEM and the followed approach is much more advantageous for this end. Other drawback of using the eigenmodes is that for stiffened panels they join the deformation of the panel and the stiffeners which makes impossible to define the correct amplitude to each type of imperfection separately. Consequently, the developed approach consisted in modelling the imperfections defining directly the

coordinates of the points composing the deformed panel. This alternative provides more flexibility to choose imperfections as desired. Despite neglected many times in the literature, the direction of imperfection is also an aspect of utmost importance, especially in stiffened panels. A negative imperfection (the one that induces compression on the stiffeners) is more detrimental than the positive one (which corresponds, generally, to the default direction of eigenmodes) in many cases. Although the importance of the negative direction decreases with the increase in curvature (for example, it leads to the lowest ultimate load in 93% and 20% of the cases, for Z=0 and 200, respectively) it is important and it cannot be neglected.

The behaviour of both unstiffened and stiffened panels was characterized for in-plane compression, out-of-plane pressure and interaction between both loading conditions through an extensive parametric variation with finite elements analyses. The results were discussed through the non-linear equilibrium paths and the ultimate loads.

The effect of the curvature on the equilibrium paths and ultimate load is very intricate. The existence of very pronounced local minimums for the ultimate load in function of the curvature was found. These effects depend very significantly of the width to thickness ratio, a/h, and the boundary conditions play also an important role in this behaviour. This effect is especially important for BUU. It was shown that a curved panel may have a decrease of more than 40% in the ultimate load when compared with the corresponding flat plate. This means that it may be quite unsafe to design a curved panel as if it was a flat plate. In contrast, this effect is much less severe for BCU. On the other hand, significant increases in resistance are obtained, in some cases, with the curvature. This shows that the design of curved panels has to be performed with a deep knowledge of this complex behaviour.

In spite of only simply supported boundary conditions were considered, the effect of the in-plane restraints along the edges is very evident. Large differences are found between BUU and the remaining boundary conditions both in the behaviour and in the ultimate load. BUU shows generally more unstable behaviours. Additionally, it is possible to say, as a rule of thumb, that the more in-plane restrained are the boundary conditions, the greater is the resistance.

Despite some conclusions are more or less generic and transversal to unstiffened and

stiffened panels, like the important effect of the curvature and aspect ratio, the additional contribution of stiffeners increases the number of parameters and, consequently, the complexity of the analysis because the dependency between variables increases. The local width to thickness ratio of the subpanels between stiffeners, a_s/h, and the ratio height to thickness of the stiffeners, d_s/h_s, play an important role in the response of the stiffened panels.

The study was then extended to out-of-plane pressure and interaction with in-plane compression. When only out-of-plane pressures are existent, ultimate loads are not usually reached within displacements with practical significance, and consequently more emphasis was given to the non-linear behaviour of the panels.

After being used to characterise thoroughly the behaviour of the unstiffened and stiffened panels, the finite element models were used to validate the semi-analytical model. This validation was first carried out in terms of the equilibrium paths and then in terms of the ultimate load.

It was found that, generally, as the curvature increases the modal participation of higher modes is larger. Nevertheless, few DOFs are, generally, sufficient to characterize accurately the behaviour of most curved panels of practical interest. Despite the complex behaviour identified for the panels, the SAM was able to account accurately with all the geometric parameters, boundary and loading conditions.

The orthotropic approach showed very good results in all cases where the assumed modes were able to describe the verified deformations, *i.e.* overall buckling of stiffened panels, which occurs for panels composed by stiffeners not too strong so they do not constitute nodal lines; or by a large number of stiffeners where the stiffeners buckle together with the panel.

Closed-form expressions were derived for the equilibrium paths of both unstiffened and stiffened curved panels. These expressions are able to provide very good accuracy covering a wide range of panels used in practice, and they are very useful once they incorporate explicitly all the considered parameters. Besides that, they are able to account for the interaction between in-plane and out-of-plane loading.

The ultimate load of unstiffened panels under compression was predicted using a first

yield criterion applied to the von Mises' stresses with the membrane components. This criterion was shown to provide good results for most cases under diverse situations of geometries and boundary conditions. The predictions of the SAM matched with good accuracy the buckling curves of curved panels for both BCU and BCC. The complex interaction of the several parameters in the ultimate load, identified firstly with the finite element analyses, was perfectly reproduced with the proposed formulation. Despite shown that a MDOF increases the accuracy of the SAM especially for more complex deformation shapes which occur for larger curvatures and aspect ratios, in most cases a SDOF is able to deal reasonably well with the large part of the cases. Based on this, expressions to predict the ultimate load of unstiffened curved panels based were proposed. They show good accuracy with only small differences in some cases in comparison with the FEM which may be explained by the lack of more degrees of freedom and by the strength criteria considered. However, only perfectly acceptable errors were shown for occasional cases, which are perfectly covered with the utilization of a small partial safety factor. Once these expressions are able to account for the large part of the panels used in practice they show a large practical interest.

9.2 OUTLOOK ON FURTHER WORK

Despite the fact that many of the issues raised at the outset of the research were successfully addressed, some others have arose as the work progressed and many more emerge from that would be the natural continuation of this work. Consequently, some recommendations for further work are identified next.

There is room to improve the efficiency of the resolution of the problem, for example in solving the system of equations when more degrees of freedom are considered. The formulation implemented with the software Mathematica can be further optimized to deal with a larger number DOFs more efficiently in terms of calculation times and convergence. Although there is no need for a very large number of DOFs for a reasonable characterization of most panels in practice, it was found that a larger number of DOFs would be desirable for some panels with larger curvatures and generic aspect ratios.

Snap-through phenomena were found to be rare in the analyses carried out with the semi-analytical method. However, as it was shown in the wide parametric study carried out

with FEM, some panels with large curvatures, aspect ratios and certain type of imperfections may be prone to snap-through phenomena. Although, the semi-analytical formulation is able to account for them properly, an arc-length method must be implement instead of the Newton-Raphson method.

The orthotropic approach was shown to be efficient to deal with stiffened panels approaching an overall buckling collapse. However, in some situations the panels are designed to local buckling occurs first. For these panels, which have generally slender subpanels, local deformations are generally more important than the global deformations. Consequently, for these panels, local modes of the subpanels should be assumed and the stiffeners should be considered as a separated member with assumed deformations (similarly to what is done for the panel). The process is identical to the one presented here with the additional energy components of the stiffeners and the conditions of continuity between the panel and stiffeners. In intermediate cases, interaction between local and global buckling may occurs and interaction between both approaches should be considered.

Some of the panels, namely the stockier ones, panels would benefit from using a more conservative strength criteria accounting with the bending stresses along the thickness, eliminating probably the use of a partial safety factor.

The prediction of the ultimate load of stiffened panels can also be addresses introducing strength criteria for stiffeners. The incorporation of residual stresses in the SAM can also be beneficial to tackle stiffened panels.

The present formulation was shown to have a large potential to extract expressions with a purely mechanical background. This kind of expressions has a huge practical interest. Although, several expressions were derived, much more can be obtained with the present formulation, as for example for other loading conditions (*e.g.* shear, biaxial compression, etc.) and for the remaining boundary conditions for which the formulation was already developed. Additionally, these expressions can be further simplified, in some cases, increasing the ease of its use for more design oriented formats.

9.3 SCIENTIFIC PRODUCTION

Journal papers

Manco, T., Rigueiro, C., Martins, J. P. and *Simões da Silva, L.:* Comparative assessment of the design of tubular elements according to offshore design standards and Eurocode 3. Steel Construction: Design and Research, Ernst & Sohn (a Wiley Company), Vol. 9, No. 4, 2016: 266–278.

Manco, T., Martins, J.P., Rigueiro, C. and *Simões da Silva, L.:* Semi-analytical model for the prediction of the post-buckling behaviour of unstiffened cylindrically curved steel panels under uniaxial compression. Marine Structures, Vol. 59; 2018: 387-400.

Manco, T., Martins, J.P., Rigueiro, C. and Simões da Silva, L.: Semi-analytical orthotropic model for the prediction of the post-buckling behaviour of stiffened cylindrically curved steel panels under uniaxial compression. Computers and Structures; 2018 *(in press)*

Manco, T., Martins, J.P., Rigueiro, C. and Simões da Silva, L.: Post-buckling behaviour of isotropic and orthotropic curved panels under combined in-plane and out-of-plane loading using semi-analytical methods. *(Submitted to Ocean Engineering for publication on 24 August 2018)*

Manco, T., Martins, J.P., Rigueiro, C. and *Simões da Silva, L.*: Ultimate resistance of isotropic cylindrically curved steel panels under uniaxial compression. *(Submitted to Journal of Constructional Steel Research)*

Conference papers

Manco, T., Martins, J.P., Rigueiro, C. e *Simões da Silva, L.:* Avaliação comparativa da regulamentação para estruturas *offshore* no dimensionamento de elementos tubulares circulares em aço (ISO 19902 e EC3). in Simões da Silva, L., Santos, F., Caeiro, J., Mendonça, T., Andrade, E. (eds.), III Congresso Luso-Africano de Construção Metálica Sustentável, cmm Press, 20-21 Novembro 2014, Luanda, Angola; 2014: II-5-14. (*in Portuguese*)

Manco, T., Martins, J.P., Rigueiro, C. and *Simões da Silva, L.:* Comportamento de painéis curvos reforçados sujeitos a ações de pressão de curta duração. in Simões da Silva, L., Vila Real, P., Rocha Almeida, J., Gonçalves, R. (eds.), X Congresso de Construção Metálica e Mista, cmm Press, Coimbra; 2015: 15-24. (*in Portuguese*)

Manco, T., Martins, J. P., Rigueiro, C. and *Simões da Silva, L.:* Comparative assessment of the design of tubular elements according to offshore design standards and Eurocode 3. in Batista, E., Vellasco, P. and Lima, L. (eds.), ISTS15 - 15th International Symposium on Tubular Structures, May 2015, Rio de Janeiro, Brazil; 2015.

Manco, T., Rigueiro, C., Martins, J. P. and *Simões da Silva, L.:* Analysis of pre-compressed steel tubular members under lateral impact: A parametric study. Dubina, D. and Ungureanu, V. (eds.), SDSS'2016 -Proceedings of the Colloquium on Stability and Ductility of Steel Structures, Wiley, May 30 –June 1 2016, Timisoara, Romania; 2016: 963-972.

Manco, T., Martins, J.P., Rigueiro, C. and *Simões da Silva, L.:* Numerical analysis of stiffened curved panels under compression. ICSAS 2016 -Eighth International Conference on Steel and Aluminium Structures, Hong Kong, China, December 7–9; 2016.

Manco, T., Martins, J.P., Rigueiro, C. e *Simões da Silva, L.:* Metodologia semi-analítica para a previsão do comportamento pós-encurvadura de painéis curvos cilíndricos sob compressão uniaxial. in Simões da Silva, L., Vila Real, P., Piloto, P. and Martins, J. P. (eds.), XI Congresso de Construção Metálica e Mista, cmm Press, Coimbra, 2017: 85-94. (*in Portuguese*)

Manco, T., Martins, J. P., Rigueiro, C. and *Simões da Silva, L.:* General semi-analytical model or the prediction of the post-buckling behaviour of unstiffened and stiffened cylindrically curved panels under uniaxial compression and out-of-plane loading. International Conference on Thin-Walled Structures (ICTWS 2018), 24-27 July 2018, Lisboa, Portugal; 2018.

Bibliography

[1] *CEN:* EN 1993-1-5:2006 - Eurocode 3: Design of steel structures, Part 1-5: Plated Structural Elements. European Committee for Standardisation, Brussels; 2006.

[2] *CEN:* EN 1993-1-6:2007 – Eurocode 3: Design of steel structures, Part 1-6: Strength and Stability of Shell Structures. European Committee for Standardisation, Brussels; 2007.

[3] *DNVGL*: RP-C202 - Buckling Strength of Shells. Recommended Practice, DNVGL; 2017.

[4] *DNVGL*: DNVGL-CG-0128. Buckling Class Guideline, DNVGL; 2015.

[5] *ABS*: Guide for Buckling and Ultimate Strength Assessment for Offshore Structures, American Bureau of Shipping; 2018.

[6] *Martins, J., Ljubinkovic, F., Simões da Silva, L.* and *Gervásio, H:* Behaviour of thin-walled curved steel plates under generalised in-plane stresses: A review. Journal of Constructional Steel Research, Vol. 140; 2018: 191-207.

[7] *Chakrabarti, S.:* Handbook of Offshore Engineering. Vol. I & II. Elsevier, Illinois, USA; 2005.

[8] *Unknown author*: Spar platform cross-section. [Online] Available from: http://images.pennwellnet.com/ogj/images/off2/0498oiraum2.jpg, n.a.. [Accessed 19th December 2017]

[9] *Taggart, R. (ed)*: Ship Design and Construction. The Society of Naval Architects and Marine Engineers, New York; 1980.

[10] *Wired*: Long Shunned, Robots Finally Infiltrate Boeing's Assembly Line. [Online] Available from: https://www.wired.com/2013/06/boeing-robots-777/, 2013. [Acessed 19th December 2017]

[11] *Massard, F.*: Pont Renault (Boulogne-Billancourt). [Online] Available from: http://www.marine-marchande.net/groupe%20mar-mar/Documents/F.Massard/Pont%20Renault/index.htm, 2009. [Accessed 19th December 2017]

[12] *Mato, F. M., Cornejo, M. O. and Ruiz, A. C.*: Design and construction of two composite tubular arches with network suspension system: Deba and Palma del Río Arch Bridges. Hormigón y Acero, Vol. 61, No. 257; 2010 :7-39.

[13] *Redshaw, S.:* The Elastic Instability of a Thin Curved Panel Subjected to an Axial Thrust, Its Axial and Circumferential Edges Being Simply Supported. British Aeronautical Research Committee. Report and Memorandum No. 1565; 1934.

[14] *Tran, K.:* Étude de la résistance et de la stabilité des tôles courbes cylindriques en acier. Application aux ouvrages d'art. PhD thesis. Université Paris-Est, Paris; 2012. (in french)

[15] *Martins, J.:* Behaviour of cylindrical curved steel panels under in-plane stresses. PhD thesis. University of Coimbra, Coimbra; 2014.

[16] *Bryan, G.*: On the Stability of a Plane Plate Under Thrusts in Its Own Plane (with Applications to the 'Buckling' of the Sides of a Ship). Proc. London Math. Soc., Vol. 22; 1891: 54–67.

[17] *Allen, H.* and *Bulson, P.*: Background to buckling. London, McGraw-Hill; 1980.

[18] *von Kármán, T., Sechler, E.* and *Donnell, L.:* The strength of thin plates in compression. Transactions of ASME, Vol. 54, No. 5; 1932: 53-57.

[19] *Marguerre, K.:* The apparent width of the plate in compression. NACA, Technical Memorandum No. 883: 1937.

[20] *Levy, S.:* Bending of rectangular plates with large deflections. National Advisory Committee for Aeronautics, Technical Notes, No. 846; 1942.

[21] *Yamaki, N.:* Postbuckling behavior of rectangular plates with small initial curvature loaded in edge compression – (continued). Journal of Applied Mechanics, Vol. 27, No. 2; 1960: 335-342.

[22] *Maquoi, R.* and *Massonnet, C.:* Théorie non linéaire de la résistance postcritique des grandes poutres en caisson raidies. IABSE Publications, Vol. 31, No. II; 1971: 91-140. (*in French*)

[23] *Prabhakara, M.* and *Chia, C.:* Post-buckling behaviour of rectangular orthotropic plates. Journal Mechanical Engineering Science, Vol. 15, No. 1; 1973: 25-33.

[24] *Jetteur, P.:* A new design method for stiffened compression flanges of box girders. Thin-Walled Structures, Vol. 1, No. 3; 1983: 189-210.

[25] *Paik, J., Thayamballi, A., Lee, K.* and *Kang, S.:* A semi-analytical method for the elastic-plastic large deflection analysis of welded steel or aluminum plating under combined in-plane and lateral pressure loads. Thin-Walled Structures, Vol. 39, No. 2; 2001: 125-152.

[26] *Paik, J., Thayamballi, A.* and *Kim, B.:* Large deflection orthotropic plate approach to develop ultimate strength formulations for stiffened panels under combined biaxial compression/tension and lateral pressure. Thin-Walled Structures, Vol. 39, No. 3; 2001: 215-246.

[27] *Paik, J.* and *Lee, M.:* A semi-analytical method for the elastic–plastic large deflection analysis of stiffened panels under combined biaxial compression/tension, biaxial in-plane bending, edge shear, and lateral pressure

loads. Thin-Walled Structures, Vol. 43, No. 3; 2005: 375-410.

[28] Paik, J., Park, J. and Kim, B.: Analysis of the Elastic Large Deflection Behavior for Metal Plates under Nonuniformly Distributed Lateral Pressure with In-Plane Loads. Journal of Applied Mathematics, Vol. 2012, Article ID 734521; 2012: 1-17.

[29] *Byklum, E.* and *Amdahl, J.*: A simplified method for elastic large deflection analysis of plates and stiffened panels due to local buckling. Thin-Walled Structures, Vol. 40; 2002: 925-953.

[30] *Ferreira, P.* and *Virtuoso, F.:* Semi-analytical models for the post-buckling analysis and ultimate strength prediction of isotropic and orthotropic plates under uniaxial compression with the unloaded edges free from stresses. Thin-Walled Structures, Vol. 77; 2014: 82-94.

[31] *Coan, P.:* Large deflection theory for plates with small initial curvature loaded in compression. Journal of Applied Mechanics, Vol. 18; 1951: 143-151.

[32] *Donnell, L.:* A new theory for the buckling of thin cylinders under axial compression and bending. Transactions of the American Society of Mechanical Engineers, Vol. 56; 1934: 795-806.

[33] *Kármán, v. K.* and *Tsien, H.-S.:* The buckling of thin cylindrical shells under axial compression. Journal of the Aeronautical Sciences, Vol. 8, No. 8; 1941: 303-312.

[34] *Southwell, R.:* On the general theory of elastic stability. Philosophical Transactions of the Royal Society of London, 1914:187-244.

[35] *Leggett, D.:* The buckling of thin cylindrical shells under axial compression. Sixth International Congress of Applied Mechanics, Paris; 1946.

[36] *Michielsen, H.:* The behavior of thin cylindrical shells after buckling. Journal of the Aeronautical Sciences, Vol. 15, No. 12; 1948: 738-744.

[37] *Almroth, B.:* Postbuckling behavior of axially compressed circular cylinders. The American Institute of Aeronautics and Astronautics Journal, Vol. 1, No. 3; 1963: 630-633.

[38] *Donnell, L.* and *Wan, C.:* Effects of imperfections on buckling of thin cylinders and columns under axial compression. Journal of Applied Mechanics, Vol. 17, No. 1; 1950: 73-83.

[39] *Hutchinson, J.:* Axial buckling of pressurized imperfect cylindrical shells. AIAA Journal, Vol. 3, No. 8; 1965.

[40] *Jones, R.:* Buckling of circular shells with multiple orthotropic layers and eccentric stiffeners. American Institute of Aeronautics and Astronautics Journal, Vol. 6, No. 12; 1968: 2031-2305.

[41] *Sheinman, I* and *Simitses, G.:* Buckling analysis of geometrically imperfect stiffened cylinders under axial compression. American Institute of Aeronautics and Astronautics Journal, Vol.15, No. 3; 1977: 374-382.

[42] *Yamada, S.* and *Croll, J.*: Buckling and Post-buckling Characteristics of Pressure-Loaded Cylinders. Journal of Applied Mechanics, Vol. 60, No. 2; 1993: 290-299.

[43] *Timoshenko, S.*: Theory of Elastic Stability. New York, McGraw-Hill; 1936.

[44] *Stowell E.:* Critical compressive stress for curved sheet supported along all edges and elastically restrained against rotation along the unloaded edges. National Advisory Committee for Aeronautics; 1943: 99–109.

[45] *Batdorf, S.:* A simplified method of elastic-stability analysis for thin cylindrical shells. National Advisory Committee for Aeronautics, Report No. 874; 1947.

[46] *Batdorf, S.* and *Schildrout, M.:* Critical axial compressive stress of a curved rectangular panel with a central chordwise stiffener. NACA. Technical note No. 1661; 1948

[47] *Schildrout, M.* and *Stein, M.*: Critical axial compressive stress of a curved rectangular panel with a central longitudinal stiffener. NACA. Technical note No. 1879; 1949.

[48] *Gerard, G.* and *Becker, H.:* Handbook of structural stability: Part III – Buckling of curved plates and shells. National Advisory Committee for Aeronautics, Technical Note 3783; 1957.

[49] *Becker, H.:* Handbook of structural stability: Part VI – Strength of stiffened curved plates and shells. National Advisory Committee for Aeronautics, Technical Note 3786; 1958.

[50] *Domb, M. and Leigh, B.:* Refined design curves for compressive buckling of curved panels using nonlinear finite element analysis. 42nd AIAA / ASME / AHS / ASC Structures, Structural Dynamics and Materials Conference, Seattle, U.S.A. Paper 1348; 2001.

[51] *Wilde, R., Zawodny, P.* and *Magnucki, K.:* Critical state of an axially compressed cylindrical panel with three edges simply supported and one free. Thin-Walled Structures, Vol. 45, No.10-11; 2007: 955-959.

[52] *Eipakchi, H.* and *Shariati, M.:* Buckling analysis of a cylindrical panel under axial stress using perturbation technique. ZAMM Journal of applied mathematics and mechanics, Vol.91, No. 2; 2011: 138–145.

[53] *Martins, J., Simões da Silva, L.* and *Reis, A:* Eigenvalue analysis of cylindrically curved panels under compressive stresses – Extension of rules from EN1993-1-5. Thin-Walled Structures, No. 68; 2013: 183–194.

[54] *Martins, J., Simões da Silva, L.* and *Silvestre, N:* Energy-based analytical model to predict the elastic critical behaviour of curved panels. Journal of Constructional Steel Research, No. 127; 2016: 165-175.

[55] *Levy, S.:* Large deflection theory of curved sheet. National Advisory Committee for Aeronautics, Technical Notes No. 895; 1943.

[56] *Volmir, A.:* A translation of flexible plates and shells. Air Force Flight Dynamics Laboratory, Technical Report No. 66-216, Wright-Patterson Air Force Base; 1967.

[57] *Tamate, O.* and *Sekine, H.:* Postbuckling Behavior of Thin Curved Panels under axial compression. Japan Society of Mechanical Engineering, Vol. 12, No. 51; 1969: 415-420.

[58] *Chia, C.:* Nonlinear vibration and postbuckling of unsymmetrical laminated imperfect shallow cylindrical panels with mixed boundary conditions resting on

elastic foundation. International Journal of Engineering Science, Vol. 25, No. 4; 1987: 427-441.

[59] *Breivik, N.:* Thermal and mechanical response of curved composite panels. PhD Thesis, Faculty of the Virginia Polytechnic Institute and State University, Blacksburg; 1997.

[60] *Magnucka-Blandzi, E.* and *Magnucki, K.:* Buckling and post-buckling behaviour of shallow – nearly flat cylindrical panels under axial compression. Bulletin of the Polish Academy of Sciences, Technical Sciences, Vol. 64, No. 3; 2016.

[61] *White, S., Raju, G.* and *Weaver, P.:* Initial post-buckling of variable-stiffeness curved panels. Journal of the Mechanics and Physics of Solids, Vol. 71; 2014: 132-155.

[62] *Koiter, W.:* On the Stability of Elastic Equilibrium. (Original in Dutch). PhD thesis, University of Delft. Delft. (Translation AFFDL-TR-70-25, Wright-Patterson Air Force Base, 1970); 1945.

[63] *Singer, J., Meer, A.* and *Baruch, M.:* Buckling of cylindrical panels under lateral pressure. TAE Report No. 85. Israel Institute of Technology – Department of Aeronautical Engineering, Israel; 1968.

[64] *Yamada, S.* and *Croll, J.:* Buckling behaviour of pressure loaded cylindrical panels. Journal of Engineering Mechanics, Vol. 115, No. 2; 1989: 327-344.

[65] *Dennis, S., Horban, B.* and *Palazotto, A.:* Instability in a cylindrical panel subjected to normal pressure: Bifurcation vs nonlinear analyses. Composites Engineering, Vol. 4, No. 6; 1994: 605-620.

[66] *van Campen, D., Bouwman, V., Zhang, G., Zhang, J.* and ter Weeme*, B.:* Semi-analytical stability analysis of doubly-curved orthotropic shallow panels – considering the effects of boundary conditions. Non-linear mechanics, Vol. 37, No. 4-5; 2002: 659-667.

[67] *Shen, H.* and *Williams, F.:* Postbuckling analysis of stiffened laminated panels loaded in compression. International Journal of Solids and Structures, Vol. 30, No. 12; 1993: 1589-1601.

[68] *Zhang, Y.* and *Matthews, F.:* Postbuckling behaviour of curved panels of generally layered composite materials. Composite Structures, Vol. 1; No. 2; 1983: 115-135.

[69] *Sheinman, I.* and *Frostig, Y.:* Postbuckling analysis of stiffened laminated curved panels. Journal of Engineering Mechanics, Vol. 116, No. 10; 1990: 2223-2236.

[70] *Kasuya, H.* and *Watamori, T.*: Postbuckling behavior of composite laminated curved plates subjected to compressive load. Transactions of the Japan Society of Mechanical Engineers, Vol. 67, No. 664; 2001: 1921-1928 (*in Japanese*)

[71] *Watamori, T.* and *Kasuya, H.:* An analysis of postbuckling behavior of composite laminated curved plates under uniaxial compression with initial imperfections. Transactions of the Japan Society of Mechanical Engineers, Vol. 69, No. 681; 2003: 854-860 (*in Japanese*)

[72] *Kasuya, H., Shigeo, M., Tsujimoto, M.* and *Keiichi, N.:* An analysis of postbuckling behavior of cross-ply laminated curved plates with initial imperfections under biaxial compression. Journal of the Society of Materials Science, Vol. 56, No. 11; 2007: 1055-1060 (*in Japanese*)

[73] *Simões da Silva, L.:* Modal Interactions in bending and buckling of sandwich structures. PhD thesis. Imperial College London, London; 1988.

[74] *Reddy, J.:* A simple higher-order theory for laminated composite plates. Journal of Applied Mechanics, Vol. 51, No. 4; 1984: 745-752.

[75] *Mindlin, R.:* Influence of rotary inertia and shear on flexural motions of isotropic elastic plates. Journal of Applied Mechanics, Vol. 18, No. 1; 1951: 31-38.

[76] *Chang, M.* and *Librescu, L.:* Postbuckling of shear-deformable flat and curved panels under combined loading conditions. International Journal of Mechanical Sciences, Vol. 37, No. 2; 1995: 121-143.

[77] *Shen, H.:* Postbuckling of axially loaded shear-deformable laminated cylindrical panels. Journal of Strain Analysis, Vol. 37, No. 5; 2002: 413-425.

[78] *Martins, J. P., Simões da Silva, L., Marques, L.* and *Pircher, M.:* Eigenvalue analysis of curved sandwich panels loaded in uniaxial compression. Romanian Journal of

Technical Sciences, Vol. 59, No 1-2; 2014: 87-104.

[79] D*uc, N.* and *Tung, H.:* Nonlinear analysis of stability for functionally graded cylindrical panels under axial compression. Computational Materials Science, Vol. 49, No. 4; 2010: 313-316.

[80] *Duc, N.* and *Tung, H.:* Nonlinear response of pressure-loaded functionally graded cylindrical panels with temperature effects. Composite Structures, Vol. 92, No. 7; 2010: 1664-1672.

[81] *Featherson, C.:* Imperfection sensitivity of curved panels under combined compression and shear. International Journal of Non-linear Mechanics, Vol. 38; 2003: 225-238.

[82] *CEN:* EN 1993-1-1 - Design of steel structures: General rules and rules for buildings. Brussels, European Committee for Standardisation; 2005.

[83] *Tran, K., Davaine, L., Douthe, C.* and *Sab, K.:* Stability of curved panels under uniform axial compression. Journal of Constructional Steel Research, Vol. 6; 2012: 30-38.

[84] *Tran, K., Douthe, C., Sab, K., Dallot, J.* and *Davaine, L.:* A preliminary design formula for the strength of stiffened curved panels by design of experiment method. Thin-Walled Structures, Vol. 79; 2014:129-137.

[85] *Tran, K., Douthe, C., Sab, K., Dallot, J.* and *Davaine, L.:* Buckling of stiffened curved panels under uniform axial compression. Journal of Constructional Steel Research, Vol. 103; 2014:140-147.

[86] *Martins, J., Simões da Silva, L.* and *Reis, A.:* Ultimate load of cylindrically curved panels under in-plane compression and bending – Extension of rules from EN 1993-1-5. Thin-Walled Structures, Vol. 77, 2014: 36–47.

[87] *Martins, J., Beg, D., Sinur, F., Simões da Silva, L.* and *Reis, A:* Imperfection sensitivity of cylindrically curved steel panels. Thin-Walled Structures, Vol. 89; 2015: 101–115.

[88] *Park, J., Kazushiro, I.* and *Tetsuya, Y.:* Characteristics of Buckling and Ultimate

Strength and Collapse Behaviour of Cylindrically Curved Plates Subjected to Axial Compression. Advanced Materials Research, Vol. 33-37; 2008: 1195-1200.

[89] *Park, J., Kazushiro, I.* and *Tetsuya, Y.:* Buckling/ultimate strength and progressive collapse behaviour comparison of unstiffened and stiffened curved plates subjected to axial compression. International Journal of Computer Applications in Technology, Vol. 41, No. 1-2; 2011: 60-72.

[90] *Seo, J., Song, C., Park, J. and Paik, J.:* Nonlinear structural behaviour and design formulae for calculating the ultimate strength of stiffened curved plates under axial compression. Thin Walled Structures, Vol. 107; 2016:1-17.

[91] *Ljubinkovic, F., Martins, J.P., Helena, G.*, *Simões da Silva, L.* and *Leitão, C.:* Experimental analysis of unstiffened cylindrically curved panels. in Simões da Silva, L., Vila Real, P., Piloto, P. and Martins, J. P. (eds.), XI Congresso de Construção Metálica e Mista, cmm Press, Coimbra, 2017.

[92] *Cho, S., Park, H., Kim, H.* and *Seo, J.:* Experimental and numerical investigations on the ultimate strength of curved stiffened plates. Proceeding of 10th International Symposium on Practical Design of Ships and Other Floating Structure, Huston; 2007.

[93] *Guo, H., Zeng, Z., Liu, X., Ju, X.* and *Zhao, X.:* Ultimate load of cylindrically curved panels under uniform compression at straight edge and the influence of curvature. 39th IABSE Symposium – Engineering the future, September 21-23, Vancouver, Canada; 2017.

[94] *Yang, T.* and *Guralnick, S.:* An experimental study of the buckling of open cylindrical shells. Experimental Mechanics, Vol. 15, No. 4; 1975: 121-127.

[95] *Christian, T.:* A study of rectangular plates subjected to non-uniform axial compression. PhD thesis. Georgia Institute of Technology, Georgia; 1974.

[96] *Kirchhoff, G.:* Über das Gleichgewicht und die Bewegung einer elastischen Scheibe. Journal für die reine und angewandte Mathematik, Vol.40; 1850: 51-88. (*in german*)

[97] *Love, A.:* A treatise on the mathematical theory of elasticity. Cambridge University

Press, 1892.

[98] *Yamaki, N.:* Elastic stability of circular cylindrical shells. North-Holland, Amsterdam: 1984.

[99] *Ventsel, E. and Kauthammer, T.:* Thin Plates and Shells – Theory, Analysis and Applications. Marcel Dekker, New York: 2001.

[100] *Flügge, W.:* Stresses in shells. 2nd Ed, Springer-Verlag Berlin Heidelberg, Berlin: 1973.

[101] *Donnell, L.:* Stability of thin-walled tubes under torsion. NACA, Report No. 479: 1933.

[102] *von Kármán, T. and Tsien, H.:* The buckling of thin cylindrical shells under axial compression. Journal of the Aeronautical Sciences, Vol. 8, No. 8: 1941: 303-312.

[103] *Mushtari , K.* and *Galimov, K.:* Non-linear theory of thin elastic shells. Israel Program for Scientific Translations: 1961.

[104] *Vlasov, V.:* Basic Differential Equations in General Theory of Elastic Shells. NACA, Technical Memorandum No. 1241: 1951.

[105] *Calladine, C.:* Theory of shell structures. Cambridge University Press, Cambridge: 1983.

[106] *Sanders, J.:* Nonlinear theories for thin shells. Quarterly of Applied Mathematics. Vol. 21, No.1: 1962: 21-36.

[107] *Koiter, W.:* A consistent first approximation in the general theory of thin elastic shells. Proceedings of the Symposium on the Theory of Thin Elastic Shells, North-Holland Publishing Company: 1960: 12-33.

[108] *Lamé, G.:* Leçons sur la théorie mathématique de l'élasticité des corps solides. Bachelier, Paris: 1852.

[109] *Novozhilov, V.:* Theory of thin Elastic Shells. P. Noordhoff, 2nd Ed., Groningen; 1964.

[110] *Hoff, N.:* The accuracy of Donnell's equations. Journal of Applied Mechanics, Vol.

22, No. 3; 1955: 329-334.

[111] *Kempner, J.:* Remarks on Donnell's Equation. Journal of Applied Mechanics, Vol. 77; 1955: 117-118.

[112] *Morley, N.:* An improvement on Donnell's approximation for thin walled circular cylinders. The Quarterly Journal of Mechanics and Applied Mathematics, Vol. 12, No. 1; 1959: 89-99.

[113] *Houghton, D.* and *Johns, D.:* A comparison of the characteristi equations in the theory of circular cylindrical shells. The Aeronautical Quarterly, Vol. 12, No. 3; 1961: 228-236.

[114] *Bažant, Z.* and *Cedolin, L.:* Stability of Structures – Elastic, Inelastic and Damage Theories. World Scientific Publishing, UK: 2010.

[115] *Chajes, A.:* Principles of structural stability. Prentice-Hall, New Jersey; 1974.

[116] *Wolfram Research Inc.:* Wolfram Mathematica. Version 11.0; 2016.

[117] *Dassault Systèmes Simulia Corp.*: ABAQUS - Version 6.14: 2014.

[118] *Arbocz, J.:* Recent developments in shell stability analysis. Technical University Delft; 1987.

[119] *Riks, E.:* A unified method for the computation of critical equilibrium states of non-linear elastic systems. Acta Technica Academiae Scientiarium Hungaricae, Tomus 87 (1-2); 1978.

[120] *Dassault Systèmes Simulia Corp.*: ABAQUS Documentation, version 6.14. Providence, USA: 2014.

[121] *Rotter, J. and Schmidt, H.:* Buckling of Steel Shells – European Design Recommendations. Ed. 5, ECCS Press - P125, Brussels; 2008.

[122] *DNV*: RP-C208 – Determination of structural capacity by non-linear FE analysis methods. Recommended Practice, Det Norske Veritas; 2013.

[123] *Alpsten, G.:* Thermal residual stresses in hot-rolled steel members. *Fritz Laboratory Reports*, No. 337.3; 1968.

[124] *Bjørhovde, R., Brozzetti, J., Alpsten, G.* and *Tall, L.:* Residual stresses in thick welded plates. *The Welding Journal*, Vol. 51, No. 8; 1972: 392-405.

[125] *Aguiar, J., Barbosa, G.* and *Batalha, G.:* Sheet bending theory applied to a three roll process. *Congresso Brasileiro de Engenharia de Fabricação*, 02-04 April 2001, Brazil; 2001.

[126] *Tadić, N.* and *Mišović, M.:* Residual stresses in cold rolled narrow strips: experimental measurement - FEM simulation. *Metalurgija - Journal of Metallurgy*, Vol. 3, No. 4; 2007: 251-257.

[127] *Abrantes, M.* and *Quach, W.:* Residual stresses in steel members: a review of available analytical expressions. *International Journal of Structural Integrity*, Vol. 7, No. 1; 2016: 70-94.

[128] *Zinn, W.* and *Scholtes, B.:* Residual stress formation processes during welding and joining. In: Totten, G., Howes, M. and Inoue, T (eds): *Handbook of Residual Stress and Deformation of Steel.* ASM International; 2002: 391-396.

[129] *Faulkner, D.:* Effects of residual stresses on the ductile strength of plane welded grillages and of ring stiffened cylinders. *Journal of Strain Analysis*, Vol. 12, No. 2; 1977: 130-139.

[130] *Dubas, P.* and *Gehri, E.:* Behaviour and design of steel plated structures. *ECCS*, Publication nº44; 1986.

[131] *Ravn-Jensen, K.* and *Tvergaard, V.:* Effects of residual stresses on plastic buckling of cylindrical shell structures. *International Journal of Solid Structures*, Vol. 26, No. 9/10; 1990: 993-1004.

[132] *Braun, B.:* Stability of steel plates under combined loading. PhD thesis. University of Stuttgart, Stuttgart; 2010.

[133] *Chen, B.* and *Guedes Soares, C.:* Effects of plate configurations on the weld induced deformations and strength of fillet-welded plates. *Marine Structures*, Vol. 50; 2016: 243-259.

[134] *CTICM:* EBPlate. Centre Technique Industriel de la Construction Metallique, version 2.01; 2014.

[135] *Reis, A. Pedro, J. O., Graça, A. B., Hendy, C., Romoli, P., Simões da Silva, L.* and *Martins, J. P.:* Report on the characterization of relevant parameters of curved plated bridge structures and identification of bridge cases where they can be found. RFCS Research Project OUBURST (RFCS-2015-709782): Deliverable 2.1; 2017.

[136] *Byklum, E.:* Ultimate strength analysis of stiffened steel and aluminium panels using semi-analytical methods. PhD thesis. Norwegian University of Science and Technology, Trondheim; 2002.

[137] *Byklum, E, Steen, E.* and *Amdahl, J.:* A semi-analytical mode for global buckling and postbuckling analysis of stiffened panels. Thin-Walled Structures, Vol. 42, No. 5; 2004: 701-717.

[138] *Paik, J., Thayamballi, A., Lee, S.* and *Kang, S.:* A semi-analytical method for the elastic–plastic large deflection analysis of welded steel or aluminium plating under combined in-plane and lateral pressure loads. Thin-Walled Structures, Vol. 39, No. 2; 2001: 125-152.

[139] *Paik, J.* and *Lee, M.:* A semi-analytical method for the elastic–plastic large deflection analysis of stiffened panels under combined biaxial compression/tension, biaxial in-plane bending, edge shear, and lateral pressure loads. Thin-Walled Structures, Vol. 43, No. 3; 2005: 375-410.

[140] *Brubak, L.* and *Hellesland, J.:* Semi-analytical postbuckling and strength analysis of arbitrarily stiffened plates in local and global bending. Thin-Walled Structures, Vol. 45, No. 6; 2007: 620-633.

[141] *Brubak, L.* and *Hellesland, J.:* Strength criteria in semi-analytical, large deflection analysis of stiffened plates in local and global bending. Thin-Walled Structures, Vol. 46, No. 12; 2008: 1382-1390.

[142] *Zizza, A.:* Buckling behaviour of unstiffened and stiffened steel plates under multiaxial stress states. PhD thesis. University of Stuttgart, Stuttgart; 2016.

[143] *Mohammed, E. A., Benson, S., Hirdaris, S.* and *Dow, R.:* Design safety margin of a 10,000 TEU contained ship through hull girder load combination analysis. Marine Structures, Vol. 46; 2016: 78-101.

Annexes

ANNEX A

A.1. Expressions for the local imperfection pattern given by sum of sines (from section 5.7)

$$z(x,y)=\begin{cases} e_{0L}\times\left[1.45\cos\left(\frac{2}{b}\times 1.924y\right)-\right. & \\ \left.\quad 0.5891\cos\left(\frac{2}{b}\times 3.715y\right)\right]\times\sin\left(m\left(\frac{\pi x}{a_y}+\frac{\pi}{2}\right)\right) & \text{, for } \alpha_{loc}\le 0.75 \\ e_{0L}\times\left[1.006\cos\left(\frac{2}{b}\times 1.598y\right)-\right. & \\ \quad 0.8065\cos\left(\frac{2}{b}\times 5.921y\right)- & \\ \quad 100.8\cos\left(\frac{2}{b}\times 8.062y\right)+ & \text{, for } \alpha_{loc}>0.75 \\ \left.\quad 101.4\cos\left(\frac{2}{b}\times 8.053y\right)\right]\times\sin\left(m\left(\frac{\pi x}{a_y}+\frac{\pi}{2}\right)\right) & \end{cases}$$

ANNEX B

B.1. Slenderness of the unstiffened curved panels of the parametric study

		α=0.5					α=1.0				
		a/h					a/h				
	Z	50	75	100	125	150	50	75	100	125	150
BUU	0	0.87	1.30	1.73	2.16	2.59	1.08	1.62	2.16	2.70	3.24
	10	0.84	1.26	1.67	2.09	2.51	0.99	1.48	1.98	2.47	2.96
	20	0.77	1.15	1.53	1.92	2.30	0.82	1.23	1.64	2.05	2.46
	30	0.68	1.02	1.36	1.71	2.05	0.69	1.03	1.38	1.72	2.06
	40	0.60	0.91	1.21	1.51	1.81	0.60	0.90	1.20	1.50	1.80
	50	0.54	0.81	1.08	1.34	1.61	0.53	0.80	1.07	1.34	1.61
BCU	0	0.87	1.30	1.73	2.16	2.59	1.08	1.62	2.16	2.70	3.24
	10	0.84	1.25	1.67	2.09	2.51	0.96	1.44	1.92	2.39	2.87
	20	0.76	1.14	1.52	1.91	2.29	0.77	1.15	1.53	1.92	2.30
	30	0.68	1.01	1.35	1.69	2.03	0.64	0.97	1.29	1.61	1.93
	40	0.60	0.89	1.19	1.49	1.79	0.57	0.85	1.14	1.42	1.70
	50	0.53	0.80	1.06	1.33	1.59	0.51	0.77	1.03	1.28	1.54
BCC	0	0.87	1.30	1.73	2.16	2.59	1.08	1.62	2.16	2.70	3.24
	10	0.83	1.25	1.67	2.08	2.50	0.91	1.36	1.81	2.26	2.72
	20	0.76	1.13	1.51	1.89	2.27	0.71	1.07	1.42	1.78	2.14
	30	0.67	1.00	1.33	1.67	2.00	0.62	0.93	1.23	1.54	1.85
	40	0.59	0.88	1.17	1.46	1.76	0.55	0.83	1.11	1.38	1.66
	50	0.52	0.78	1.04	1.30	1.56	0.50	0.75	1.00	1.26	1.51
		α=1.5					α=2.0				
		a/h					a/h				
	Z	50	75	100	125	150	50	75	100	125	150
BUU	0	1.04	1.56	2.08	2.60	3.11	1.08	1.62	2.16	2.70	3.24
	10	0.94	1.41	1.88	2.34	2.81	0.97	1.45	1.94	2.42	2.90
	20	0.82	1.23	1.64	2.05	2.46	0.79	1.18	1.58	1.97	2.36
	30	0.70	1.06	1.41	1.76	2.12	0.69	1.04	1.39	1.74	2.09
	40	0.61	0.92	1.23	1.54	1.85	0.62	0.93	1.24	1.55	1.87
	50	0.55	0.82	1.10	1.37	1.65	0.55	0.84	1.12	1.40	1.68
BCU	0	1.04	1.56	2.08	2.60	3.11	1.08	1.62	2.16	2.70	3.24
	10	0.93	1.40	1.86	2.33	2.79	0.96	1.43	1.91	2.39	2.87
	20	0.76	1.14	1.52	1.90	2.28	0.78	1.16	1.55	1.94	2.32
	30	0.64	0.95	1.27	1.59	1.91	0.65	0.98	1.30	1.63	1.95
	40	0.56	0.84	1.13	1.41	1.69	0.57	0.85	1.14	1.42	1.71
	50	0.51	0.76	1.02	1.27	1.53	0.51	0.77	1.02	1.28	1.53
BCC	0	1.04	1.56	2.08	2.60	3.11	1.08	1.62	2.16	2.70	3.24
	10	0.84	1.26	1.68	2.10	2.52	0.84	1.26	1.68	2.10	2.52
	20	0.71	1.07	1.42	1.78	2.13	0.70	1.05	1.40	1.75	2.10
	30	0.61	0.92	1.23	1.54	1.84	0.61	0.91	1.22	1.52	1.83
	40	0.55	0.82	1.10	1.37	1.64	0.54	0.82	1.09	1.36	1.63
	50	0.50	0.75	1.00	1.25	1.50	0.50	0.74	0.99	1.24	1.49

		α=3.0					α=5.0				
		a/h					a/h				
	Z	50	75	100	125	150	50	75	100	125	150
BUU	0	1.08	1.62	2.16	2.70	3.24	1.08	1.62	2.16	2.70	3.24
	10	0.96	1.44	1.92	2.40	2.88	0.96	1.44	1.92	2.40	2.88
	20	0.80	1.21	1.61	2.01	2.42	0.79	1.19	1.59	1.99	2.39
	30	0.68	1.03	1.37	1.72	2.06	0.68	1.02	1.37	1.71	2.05
	40	0.59	0.89	1.19	1.49	1.79	0.59	0.90	1.20	1.50	1.81
	50	0.53	0.80	1.07	1.35	1.62	0.54	0.82	1.09	1.37	1.65
BCU	0	1.08	1.62	2.16	2.70	3.24	1.08	1.62	2.16	2.70	3.24
	10	0.95	1.43	1.91	2.38	2.86	0.95	1.42	1.90	2.37	2.85
	20	0.77	1.15	1.53	1.92	2.30	0.77	1.16	1.55	1.94	2.33
	30	0.65	0.98	1.30	1.63	1.96	0.65	0.98	1.31	1.63	1.96
	40	0.57	0.86	1.15	1.43	1.72	0.57	0.86	1.15	1.44	1.73
	50	0.52	0.77	1.03	1.29	1.55	0.52	0.77	1.03	1.29	1.55
BCC	0	1.08	1.62	2.16	2.70	3.24	1.08	1.62	2.16	2.70	3.24
	10	0.81	1.22	1.62	2.02	2.43	0.78	1.17	1.56	1.95	2.34
	20	0.68	1.02	1.36	1.70	2.05	0.66	0.98	1.31	1.64	1.97
	30	0.60	0.90	1.20	1.50	1.79	0.58	0.87	1.16	1.45	1.74
	40	0.54	0.81	1.07	1.34	1.61	0.52	0.79	1.05	1.31	1.58
	50	0.49	0.74	0.98	1.23	1.47	0.48	0.72	0.96	1.21	1.45

		α=7.5				
		a/h				
	Z	50	75	100	125	150
BUU	0	1.08	1.62	2.16	2.70	3.24
	10	0.96	1.44	1.91	2.39	2.87
	20	0.79	1.19	1.59	1.99	2.39
	30	0.68	1.02	1.36	1.71	2.05
	40	0.59	0.89	1.20	1.50	1.80
	50	0.54	0.81	1.09	1.36	1.64
BCU	0	1.08	1.62	2.16	2.70	3.24
	10	0.95	1.43	1.90	2.38	2.85
	20	0.77	1.16	1.55	1.94	2.33
	30	0.65	0.98	1.31	1.64	1.97
	40	0.57	0.86	1.15	1.44	1.73
	50	0.52	0.78	1.04	1.30	1.56
BCC	0	1.08	1.62	2.16	2.70	3.24
	10	0.77	1.15	1.53	1.91	2.29
	20	0.63	0.95	1.26	1.58	1.90
	30	0.56	0.84	1.12	1.41	1.69
	40	0.51	0.77	1.02	1.28	1.54
	50	0.47	0.71	0.95	1.18	1.42

ANNEX C

C.1. Normalized ultimate load of the unstiffened curved panels under in-plane compression (cases from section 6.6 with w_0=min(a;b)/200)

		a/h=50													
		Positive eigenmode imperfection (P_EM)							*Worst imperfection*						
	Z	***α=0.5***	***α=1.0***	***α=1.5***	***α=2.0***	***α=3.0***	***α=5.0***	***α=7.5***	***α=0.5***	***α=1.0***	***α=1.5***	***α=2.0***	***α=3.0***	***α=5.0***	***α=7.5***
BUU	***0***	0.708	0.744	0.712	0.748	0.701	0.702	0.690	0.708	0.695	0.654	0.700	0.701	0.701	0.688
	10	0.717	0.672	0.811	0.712	0.623	0.646	0.639	0.717	0.587	0.595	0.633	0.623	0.634	0.625
	20	0.789	0.827	0.897	0.831	0.765	0.761	0.743	0.789	0.688	0.672	0.723	0.742	0.734	0.721
	30	0.847	0.875	0.919	0.954	0.802	0.808	0.821	0.847	0.827	0.791	0.839	0.802	0.808	0.821
	40	0.877	0.889	0.928	0.960	0.808	0.887	0.830	0.877	0.876	0.844	0.882	0.807	0.885	0.830
	50	0.895	0.901	0.933	0.963	0.815	0.908	0.889	0.895	0.901	0.878	0.909	0.815	0.908	0.889
BCU	***0***	0.771	0.759	0.736	0.759	0.712	0.713	0.705	0.771	0.711	0.684	0.712	0.712	0.712	0.703
	10	0.791	0.766	0.752	0.763	0.683	0.682	0.686	0.791	0.691	0.673	0.691	0.683	0.682	0.685
	20	0.850	0.887	0.852	0.863	0.759	0.765	0.775	0.850	0.815	0.766	0.799	0.759	0.764	0.775
	30	0.892	0.907	0.883	0.890	0.816	0.814	0.802	0.892	0.889	0.838	0.872	0.816	0.814	0.802
	40	0.914	0.919	0.924	0.904	0.831	0.827	0.817	0.914	0.919	0.876	0.904	0.831	0.827	0.817
	50	0.928	0.930	0.932	0.917	0.844	0.840	0.834	0.928	0.930	0.902	0.917	0.844	0.840	0.834
BCC	***0***	0.771	0.789	0.744	0.789	0.751	0.751	0.766	0.771	0.751	0.698	0.751	0.751	0.751	0.734
	10	0.791	0.777	0.841	0.844	0.768	0.783	0.789	0.791	0.687	0.766	0.829	0.746	0.767	0.789
	20	0.850	0.873	0.885	0.898	0.844	0.884	0.912	0.850	0.826	0.885	0.898	0.844	0.884	0.882
	30	0.892	0.900	0.909	0.919	0.871	0.916	0.954	0.892	0.887	0.909	0.919	0.871	0.901	0.901
	40	0.916	0.918	0.925	0.933	0.888	0.934	0.970	0.916	0.918	0.925	0.933	0.888	0.912	0.912
	50	0.931	0.932	0.938	0.945	0.904	0.946	0.978	0.931	0.932	0.938	0.945	0.904	0.920	0.920
		a/h=75													
		Positive eigenmode imperfection (P_EM)							*Worst imperfection*						
	Z	***α=0.5***	***α=1.0***	***α=1.5***	***α=2.0***	***α=3.0***	***α=5.0***	***α=7.5***	***α=0.5***	***α=1.0***	***α=1.5***	***α=2.0***	***α=3.0***	***α=5.0***	***α=7.5***
BUU	***0***	0.441	0.484	0.471	0.491	0.478	0.479	0.473	0.441	0.471	0.453	0.477	0.478	0.478	0.473
	10	0.422	0.390	0.456	0.412	0.397	0.404	0.405	0.422	0.386	0.388	0.407	0.397	0.404	0.400
	20	0.459	0.365	0.407	0.399	0.351	0.349	0.346	0.459	0.314	0.331	0.354	0.351	0.349	0.346
	30	0.548	0.529	0.542	0.618	0.447	0.453	0.466	0.548	0.413	0.396	0.417	0.447	0.434	0.430
	40	0.642	0.656	0.698	0.757	0.546	0.658	0.628	0.642	0.594	0.552	0.586	0.545	0.613	0.602
	50	0.706	0.712	0.761	0.818	0.803	0.728	0.701	0.706	0.700	0.656	0.700	0.718	0.718	0.698
BCU	***0***	0.562	0.536	0.527	0.536	0.523	0.523	0.519	0.562	0.523	0.508	0.523	0.523	0.523	0.518
	10	0.567	0.515	0.513	0.520	0.504	0.503	0.504	0.567	0.506	0.499	0.512	0.504	0.503	0.504
	20	0.611	0.567	0.549	0.543	0.502	0.491	0.494	0.611	0.516	0.498	0.504	0.499	0.491	0.494
	30	0.686	0.722	0.729	0.665	0.602	0.599	0.567	0.686	0.664	0.594	0.617	0.496	0.514	0.502
	40	0.752	0.773	0.773	0.717	0.642	0.637	0.634	0.752	0.767	0.681	0.717	0.642	0.637	0.634
	50	0.797	0.800	0.800	0.750	0.665	0.659	0.659	0.797	0.800	0.733	0.750	0.665	0.659	0.659
BCC	***0***	0.568	0.623	0.561	0.623	0.609	0.606	0.625	0.568	0.613	0.541	0.593	0.604	0.606	0.586
	10	0.567	0.543	0.627	0.550	0.538	0.531	0.528	0.567	0.535	0.523	0.550	0.538	0.531	0.528
	20	0.611	0.599	0.629	0.643	0.608	0.639	0.661	0.611	0.522	0.620	0.643	0.553	0.568	0.633
	30	0.684	0.717	0.723	0.734	0.676	0.708	0.738	0.684	0.683	0.723	0.734	0.676	0.708	0.738
	40	0.752	0.765	0.772	0.779	0.712	0.741	0.772	0.752	0.765	0.772	0.779	0.712	0.741	0.772
	50	0.798	0.797	0.803	0.809	0.737	0.763	0.792	0.798	0.797	0.803	0.809	0.737	0.763	0.792

		a/h=100													
		Positive eigenmode imperfection (P_EM)							Worst imperfection						
	Z	α=0.5	α=1.0	α=1.5	α=2.0	α=3.0	α=5.0	α=7.5	α=0.5	α=1.0	α=1.5	α=2.0	α=3.0	α=5.0	α=7.5
BUU	0	0.300	0.358	0.353	0.362	0.358	0.357	0.353	0.300	0.352	0.347	0.355	0.358	0.357	0.353
	10	0.265	0.299	0.320	0.307	0.303	0.304	0.306	0.265	0.298	0.298	0.306	0.303	0.304	0.306
	20	0.269	0.249	0.241	0.258	0.261	0.261	0.258	0.269	0.249	0.241	0.258	0.261	0.261	0.258
	30	0.313	0.267	0.279	0.431	0.232	0.224	0.231	0.313	0.216	0.224	0.235	0.221	0.224	0.231
	40	0.389	0.380	0.380	0.402	0.296	0.365	0.348	0.389	0.298	0.270	0.280	0.296	0.297	0.291
	50	0.476	0.482	0.499	0.506	0.545	0.469	0.456	0.476	0.432	0.390	0.396	0.387	0.423	0.412
BCU	0	0.440	0.435	0.425	0.435	0.429	0.429	0.426	0.440	0.428	0.414	0.428	0.429	0.429	0.425
	10	0.439	0.430	0.421	0.430	0.419	0.418	0.418	0.439	0.424	0.411	0.426	0.419	0.418	0.418
	20	0.462	0.438	0.424	0.430	0.411	0.418	0.422	0.462	0.435	0.416	0.426	0.411	0.415	0.415
	30	0.507	0.526	0.526	0.467	0.438	0.437	0.413	0.507	0.454	0.418	0.413	0.413	0.410	0.408
	40	0.570	0.606	0.595	0.529	0.488	0.487	0.424	0.570	0.585	0.500	0.521	0.399	0.396	0.338
	50	0.632	0.649	0.637	0.571	0.515	0.510	0.509	0.632	0.649	0.558	0.571	0.478	0.470	0.467
BCC	0	0.456	0.540	0.478	0.541	0.536	0.539	0.529	0.456	0.533	0.470	0.472	0.471	0.478	0.495
	10	0.448	0.483	0.524	0.459	0.448	0.444	0.364	0.448	0.477	0.446	0.459	0.448	0.444	0.364
	20	0.463	0.462	0.476	0.462	0.456	0.463	0.476	0.463	0.450	0.443	0.452	0.456	0.455	0.449
	30	0.506	0.538	0.536	0.548	0.525	0.547	0.566	0.506	0.478	0.534	0.548	0.484	0.487	0.529
	40	0.571	0.600	0.607	0.614	0.571	0.593	0.615	0.571	0.587	0.607	0.614	0.571	0.593	0.615
	50	0.635	0.646	0.652	0.659	0.603	0.623	0.645	0.635	0.646	0.652	0.659	0.603	0.623	0.645
		a/h=125													
		Positive eigenmode imperfection (P_EM)							Worst imperfection						
	Z	α=0.5	α=1.0	α=1.5	α=2.0	α=3.0	α=5.0	α=7.5	α=0.5	α=1.0	α=1.5	α=2.0	α=3.0	α=5.0	α=7.5
BUU	0	0.239	0.280	0.283	0.285	0.282	0.284	0.263	0.239	0.276	0.279	0.280	0.281	0.283	0.263
	10	0.197	0.239	0.248	0.246	0.244	0.246	0.246	0.197	0.238	0.243	0.246	0.244	0.238	0.245
	20	0.175	0.204	0.215	0.211	0.213	0.212	0.211	0.175	0.204	0.212	0.211	0.212	0.212	0.211
	30	0.194	0.175	0.189	0.269	0.197	0.183	0.183	0.194	0.175	0.188	0.190	0.183	0.183	0.183
	40	0.237	0.223	0.224	0.279	0.217	0.214	0.203	0.237	0.164	0.168	0.172	0.167	0.171	0.171
	50	0.299	0.299	0.299	0.303	0.351	0.275	0.267	0.299	0.243	0.211	0.216	0.222	0.231	0.221
BCU	0	0.363	0.366	0.359	0.365	0.362	0.361	0.362	0.363	0.361	0.351	0.361	0.362	0.361	0.361
	10	0.362	0.372	0.360	0.367	0.359	0.359	0.362	0.362	0.367	0.352	0.362	0.359	0.359	0.359
	20	0.376	0.383	0.369	0.369	0.356	0.359	0.362	0.376	0.376	0.359	0.364	0.356	0.355	0.354
	30	0.403	0.386	0.408	0.361	0.360	0.355	0.327	0.403	0.377	0.353	0.356	0.355	0.352	0.327
	40	0.443	0.480	0.457	0.409	0.388	0.388	0.348	0.443	0.429	0.378	0.342	0.350	0.347	0.344
	50	0.492	0.517	0.500	0.441	0.409	0.406	0.341	0.492	0.517	0.440	0.441	0.343	0.341	0.340
BCC	0	0.388	0.454	0.439	0.457	0.444	0.456	0.438	0.388	0.439	0.433	0.414	0.407	0.423	0.438
	10	0.380	0.451	0.397	0.404	0.390	0.389	0.382	0.380	0.443	0.397	0.404	0.390	0.389	0.382
	20	0.388	0.416	0.405	0.404	0.391	0.387	0.335	0.388	0.399	0.383	0.404	0.391	0.387	0.335
	30	0.409	0.423	0.419	0.430	0.420	0.429	0.439	0.409	0.395	0.389	0.385	0.390	0.389	0.380
	40	0.441	0.479	0.483	0.488	0.464	0.477	0.490	0.441	0.459	0.483	0.488	0.454	0.448	0.461
	50	0.495	0.520	0.529	0.534	0.495	0.509	0.525	0.495	0.520	0.529	0.534	0.495	0.509	0.525

		a/h=150													
		Positive eigenmode imperfection (P_EM)							Worst imperfection						
	Z	α=0.5	α=1.0	α=1.5	α=2.0	α=3.0	α=5.0	α=7.5	α=0.5	α=1.0	α=1.5	α=2.0	α=3.0	α=5.0	α=7.5
BUU	0	0.203	0.228	0.234	0.234	0.233	0.233	0.233	0.203	0.225	0.229	0.122	0.233	0.233	0.233
	10	0.170	0.197	0.203	0.204	0.205	0.205	0.204	0.170	0.196	0.201	0.204	0.205	0.205	0.202
	20	0.142	0.171	0.177	0.179	0.179	0.177	0.180	0.142	0.171	0.177	0.178	0.179	0.177	0.180
	30	0.129	0.150	0.157	0.168	0.184	0.157	0.158	0.129	0.150	0.157	0.159	0.184	0.157	0.158
	40	0.154	0.142	0.145	0.185	0.200	0.139	0.139	0.154	0.138	0.143	0.150	0.139	0.139	0.139
	50	0.194	0.193	0.194	0.197	0.313	0.176	0.170	0.194	0.147	0.142	0.133	0.134	0.138	0.133
BCU	0	0.310	0.314	0.311	0.314	0.312	0.312	0.312	0.310	0.311	0.304	0.311	0.312	0.312	0.311
	10	0.310	0.322	0.313	0.315	0.312	0.312	0.312	0.310	0.317	0.309	0.313	0.304	0.306	0.311
	20	0.319	0.336	0.320	0.318	0.315	0.308	0.311	0.319	0.331	0.311	0.311	0.310	0.308	0.306
	30	0.339	0.327	0.340	0.316	0.314	0.312	0.307	0.339	0.322	0.306	0.312	0.309	0.305	0.305
	40	0.366	0.394	0.370	0.342	0.329	0.327	0.309	0.366	0.319	0.290	0.303	0.303	0.301	0.298
	50	0.397	0.419	0.398	0.360	0.343	0.341	0.302	0.397	0.419	0.363	0.320	0.305	0.300	0.298
BCC	0	0.345	0.379	0.387	0.391	0.393	0.383	0.378	0.345	0.377	0.353	0.376	0.364	0.383	0.378
	10	0.336	0.412	0.350	0.367	0.351	0.357	0.346	0.336	0.391	0.345	0.367	0.351	0.357	0.346
	20	0.340	0.371	0.358	0.357	0.354	0.361	0.319	0.339	0.358	0.342	0.357	0.354	0.361	0.295
	30	0.355	0.366	0.408	0.354	0.353	0.315	0.330	0.355	0.345	0.337	0.346	0.347	0.315	0.330
	40	0.379	0.402	0.399	0.398	0.386	0.391	0.397	0.378	0.362	0.370	0.374	0.340	0.337	0.333
	50	0.398	0.427	0.433	0.436	0.413	0.421	0.430	0.398	0.427	0.433	0.436	0.413	0.418	0.409

C.2. Normalized ultimate load of the stiffened curved panels under in-plane compression (cases from section 6.7 with d_s/h_s=10.0)

			a_s/h=25									
			Positive imperfection					*Negative imperfection*				
		Z	*α=0.5*	*α=0.75*	*α=1.0*	*α=1.25*	*α=1.5*	*α=0.5*	*α=0.75*	*α=1.0*	*α=1.25*	*α=1.5*
n_s=1	*BCU*	***0***	0.990	0.963	0.980	0.970	0.979	0.985	0.946	0.925	0.919	0.919
		10	0.990	0.963	0.979	0.969	0.978	0.987	0.954	0.944	0.939	0.948
		20	0.991	0.966	0.980	0.970	0.978	0.991	0.966	0.969	0.966	0.972
		30	0.993	0.969	0.981	0.972	0.978	0.995	0.974	0.981	0.978	0.982
		40	0.997	0.973	0.984	0.975	0.980	1.000	0.980	0.989	0.984	0.989
		50	1.001	0.977	0.987	0.979	0.983	1.006	0.985	0.996	0.990	0.994
		100	1.011	1.004	1.006	1.011	1.015	0.988	0.999	0.997	0.998	0.999
		200	1.008	1.007	1.008	1.008	1.005	0.981	0.997	0.997	0.997	0.998
	BCC	***0***	0.990	0.964	0.982	0.971	0.981	0.985	0.946	0.925	0.920	0.926
		10	0.990	0.965	0.981	0.973	0.981	0.987	0.956	0.954	0.957	0.971
		20	0.991	0.969	0.983	0.978	0.983	0.991	0.968	0.974	0.975	0.985
		30	0.993	0.976	0.986	0.982	0.987	0.995	0.977	0.987	0.984	0.996
		40	0.997	0.983	0.990	0.987	0.991	1.001	0.986	0.999	0.993	1.007
		50	1.001	0.990	0.995	0.992	0.995	1.006	0.995	1.011	1.002	1.018
		100	1.010	1.001	1.006	1.010	1.011	0.977	0.998	0.997	0.996	0.998
		200	1.006	1.007	1.008	1.007	1.006	0.979	0.995	0.996	0.998	0.998
n_s=2	*BCU*	***0***	0.963	0.982	0.971	0.966	0.962	0.987	0.968	0.945	0.942	0.941
		10	0.963	0.982	0.970	0.966	0.961	0.943	0.912	0.884	0.876	0.870
		20	0.963	0.982	0.970	0.965	0.961	0.946	0.920	0.895	0.894	0.891
		30	0.963	0.982	0.970	0.965	0.961	0.953	0.942	0.933	0.936	0.933
		40	0.964	0.982	0.971	0.966	0.962	0.961	0.962	0.962	0.960	0.956
		50	0.965	0.982	0.972	0.968	0.964	0.967	0.974	0.974	0.971	0.967
		100	0.973	0.985	0.983	0.979	0.989	0.986	0.998	0.996	0.991	1.002
		200	0.994	1.016	1.033	1.029	1.032	0.993	0.985	0.990	0.993	0.994
	BCC	***0***	0.965	0.983	0.975	0.970	0.964	0.942	0.910	0.881	0.872	0.866
		10	0.964	0.983	0.974	0.971	0.966	0.943	0.913	0.887	0.887	0.913
		20	0.964	0.983	0.974	0.971	0.968	0.946	0.926	0.924	0.946	0.958
		30	0.964	0.983	0.973	0.972	0.970	0.953	0.950	0.956	0.969	0.975
		40	0.964	0.983	0.973	0.973	0.971	0.961	0.966	0.971	0.979	0.983
		50	0.965	0.984	0.974	0.974	0.973	0.968	0.976	0.979	0.985	0.987
		100	0.973	0.988	0.983	0.983	0.995	0.991	1.006	1.004	1.005	1.018
		200	0.995	1.017	1.039	1.019	1.034	0.994	0.984	0.990	0.992	0.996

			$a_s/h=25$									
			Positive imperfection					*Negative imperfection*				
		Z	***α=0.5***	***α=0.75***	***α=1.0***	***α=1.25***	***α=1.5***	***α=0.5***	***α=0.75***	***α=1.0***	***α=1.25***	***α=1.5***
n_s=3	BCU	**0**	0.980	0.973	0.960	0.953	0.943	0.919	0.875	0.828	0.809	0.787
		10	0.980	0.973	0.961	0.952	0.942	0.920	0.878	0.833	0.817	0.797
		20	0.980	0.973	0.961	0.952	0.942	0.923	0.884	0.845	0.834	0.821
		30	0.980	0.974	0.962	0.953	0.943	0.928	0.894	0.865	0.864	0.861
		40	0.981	0.974	0.963	0.955	0.945	0.934	0.911	0.904	0.912	0.913
		50	0.981	0.975	0.964	0.957	0.949	0.943	0.937	0.936	0.944	0.945
		100	0.984	0.978	0.973	0.971	0.968	0.980	0.982	0.982	0.983	0.983
		200	0.997	0.993	0.993	0.997	0.997	1.008	1.006	1.012	1.017	1.020
	BCC	**0**	0.981	0.974	0.965	0.957	0.946	0.919	0.875	0.829	0.812	0.793
		10	0.981	0.974	0.966	0.961	0.954	0.921	0.879	0.839	0.832	0.847
		20	0.981	0.974	0.967	0.963	0.959	0.924	0.887	0.858	0.889	0.912
		30	0.981	0.974	0.967	0.965	0.962	0.928	0.899	0.909	0.933	0.945
		40	0.981	0.975	0.967	0.966	0.965	0.935	0.926	0.941	0.956	0.964
		50	0.981	0.975	0.968	0.968	0.967	0.945	0.949	0.959	0.971	0.976
		100	0.984	0.979	0.974	0.975	0.977	0.981	0.985	0.989	0.993	0.995
		200	0.997	0.993	0.993	0.999	1.003	1.016	1.015	1.019	1.029	1.000
n_s=5	BCU	**0**	0.975	0.949	0.918	0.877	0.817	0.865	0.786	0.696	0.639	0.573
		10	0.975	0.949	0.919	0.877	0.817	0.866	0.789	0.703	0.652	0.592
		20	0.975	0.950	0.921	0.878	0.817	0.868	0.795	0.719	0.678	0.630
		30	0.975	0.952	0.924	0.883	0.821	0.870	0.803	0.742	0.716	0.685
		40	0.976	0.953	0.927	0.890	0.836	0.873	0.815	0.774	0.764	0.752
		50	0.976	0.955	0.931	0.899	0.857	0.876	0.835	0.813	0.820	0.819
		100	0.977	0.962	0.953	0.942	0.935	0.934	0.938	0.938	0.945	0.952
		200	0.983	0.974	0.974	0.974	0.985	0.984	0.984	0.985	0.985	0.992
	BCC	**0**	0.975	0.951	0.922	0.877	0.827	0.865	0.786	0.698	0.654	0.704
		10	0.975	0.952	0.927	0.884	0.816	0.866	0.790	0.712	0.706	0.735
		20	0.975	0.953	0.931	0.897	0.829	0.868	0.797	0.736	0.762	0.792
		30	0.975	0.954	0.936	0.911	0.873	0.870	0.807	0.781	0.825	0.854
		40	0.976	0.955	0.940	0.922	0.910	0.873	0.820	0.836	0.871	0.893
		50	0.976	0.956	0.943	0.932	0.930	0.876	0.851	0.873	0.899	0.916
		100	0.978	0.962	0.957	0.956	0.962	0.936	0.946	0.952	0.960	0.967
		200	0.983	0.975	0.975	0.975	0.987	0.985	0.986	0.988	0.991	0.998

			$a_s/h=25$									
			Positive imperfection					*Negative imperfection*				
		Z	***α=0.5***	***α=0.75***	***α=1.0***	***α=1.25***	***α=1.5***	***α=0.5***	***α=0.75***	***α=1.0***	***α=1.25***	***α=1.5***
$n_s=7$	***BCU***	***0***	0.963	0.917	0.829	0.712	0.600	0.808	0.686	0.557	0.472	0.401
		10	0.964	0.919	0.831	0.710	0.585	0.809	0.690	0.568	0.489	0.430
		20	0.965	0.922	0.835	0.713	0.580	0.811	0.697	0.586	0.519	0.472
		30	0.966	0.924	0.841	0.719	0.582	0.813	0.708	0.611	0.560	0.527
		40	0.966	0.927	0.849	0.733	0.601	0.816	0.721	0.644	0.612	0.591
		50	0.967	0.931	0.858	0.753	0.632	0.819	0.737	0.684	0.671	0.660
		100	0.969	0.948	0.915	0.889	0.857	0.851	0.862	0.861	0.878	0.890
		200	0.975	0.965	0.959	0.962	0.961	0.957	0.959	0.957	0.963	0.966
	BCC	***0***	0.964	0.920	0.829	0.741	0.713	0.808	0.687	0.563	0.621	0.628
		10	0.964	0.924	0.833	0.721	0.668	0.809	0.692	0.585	0.636	0.644
		20	0.965	0.927	0.842	0.709	0.639	0.811	0.700	0.633	0.663	0.679
		30	0.966	0.930	0.854	0.720	0.616	0.813	0.712	0.676	0.709	0.740
		40	0.966	0.933	0.867	0.763	0.660	0.816	0.727	0.723	0.763	0.795
		50	0.967	0.936	0.880	0.816	0.766	0.819	0.745	0.769	0.807	0.837
		100	0.969	0.949	0.927	0.926	0.932	0.943	0.955	0.959	0.968	0.973
		200	0.975	0.965	0.960	0.964	0.967	0.990	0.993	0.993	0.997	1.000

			$a_s/h=50$									
			Positive imperfection					*Negative imperfection*				
		Z	*α=0.5*	*α=0.75*	*α=1.0*	*α=1.25*	*α=1.5*	*α=0.5*	*α=0.75*	*α=1.0*	*α=1.25*	*α=1.5*
$n_s=1$	*BCU*	***0***	0.749	0.696	0.731	0.700	0.724	0.754	0.713	0.693	0.701	0.678
		10	0.752	0.691	0.723	0.693	0.713	0.753	0.712	0.721	0.721	0.731
		20	0.757	0.688	0.716	0.687	0.704	0.756	0.712	0.744	0.717	0.738
		30	0.764	0.689	0.712	0.685	0.698	0.766	0.717	0.743	0.718	0.732
		40	0.777	0.695	0.714	0.691	0.701	0.784	0.729	0.754	0.730	0.740
		50	0.797	0.709	0.730	0.708	0.719	0.814	0.751	0.783	0.756	0.768
		100	0.912	0.829	0.854	0.869	0.881	0.935	0.881	0.871	0.890	0.904
		200	0.905	0.924	0.941	0.956	0.967	0.916	0.939	0.958	0.971	0.979
	BCC	***0***	0.766	0.704	0.752	0.712	0.746	0.772	0.719	0.704	0.711	0.699
		10	0.768	0.695	0.734	0.699	0.723	0.771	0.716	0.751	0.730	0.759
		20	0.773	0.689	0.719	0.693	0.710	0.774	0.713	0.748	0.727	0.746
		30	0.779	0.687	0.709	0.701	0.714	0.782	0.720	0.748	0.746	0.762
		40	0.791	0.700	0.718	0.740	0.762	0.802	0.753	0.798	0.790	0.812
		50	0.810	0.734	0.764	0.798	0.822	0.836	0.804	0.870	0.822	0.850
		100	0.915	0.911	0.860	0.881	0.899	0.943	0.967	0.883	0.904	0.923
		200	0.908	0.927	0.944	0.960	0.971	0.921	0.943	0.962	0.975	0.983
$n_s=2$	*BCU*	***0***	0.703	0.762	0.704	0.661	0.603	0.722	0.673	0.581	0.512	0.451
		10	0.701	0.758	0.699	0.654	0.593	0.721	0.683	0.595	0.535	0.479
		20	0.699	0.754	0.696	0.652	0.593	0.719	0.698	0.620	0.576	0.534
		30	0.698	0.750	0.694	0.653	0.601	0.718	0.717	0.655	0.630	0.610
		40	0.697	0.746	0.693	0.658	0.614	0.718	0.738	0.694	0.688	0.686
		50	0.697	0.744	0.693	0.667	0.633	0.718	0.764	0.732	0.731	0.725
		100	0.709	0.748	0.722	0.721	0.790	0.739	0.788	0.770	0.767	0.845
		200	0.806	0.858	0.871	0.887	0.901	0.859	0.874	0.898	0.913	0.926
	BCC	***0***	0.708	0.780	0.719	0.684	0.665	0.726	0.675	0.589	0.532	0.568
		10	0.705	0.772	0.711	0.666	0.627	0.724	0.690	0.610	0.591	0.613
		20	0.702	0.764	0.705	0.662	0.595	0.722	0.710	0.638	0.661	0.683
		30	0.700	0.756	0.701	0.674	0.628	0.721	0.733	0.671	0.730	0.741
		40	0.698	0.751	0.699	0.690	0.676	0.719	0.762	0.732	0.748	0.752
		50	0.697	0.746	0.697	0.702	0.701	0.719	0.775	0.762	0.748	0.753
		100	0.715	0.758	0.733	0.758	0.790	0.755	0.827	0.848	0.796	0.857
		200	0.842	0.867	0.890	0.905	0.914	0.901	0.878	0.904	0.920	0.933

		$a_s/h=50$									
		Positive imperfection					*Negative imperfection*				
	Z	*α=0.5*	*α=0.75*	*α=1.0*	*α=1.25*	*α=1.5*	*α=0.5*	*α=0.75*	*α=1.0*	*α=1.25*	*α=1.5*
n_s=3	*0*	0.745	0.703	0.598	0.499	0.447	0.692	0.554	0.420	0.349	0.335
	10	0.743	0.700	0.587	0.475	0.424	0.697	0.563	0.436	0.372	0.354
	20	0.741	0.699	0.588	0.466	0.410	0.703	0.577	0.462	0.410	0.393
BCU	*30*	0.739	0.699	0.598	0.481	0.406	0.710	0.596	0.498	0.462	0.450
	40	0.737	0.699	0.615	0.511	0.428	0.719	0.619	0.541	0.524	0.516
	50	0.735	0.701	0.631	0.549	0.473	0.729	0.647	0.589	0.589	0.585
	100	0.730	0.711	0.686	0.680	0.668	0.755	0.757	0.751	0.750	0.749
	200	0.755	0.752	0.817	0.838	0.858	0.795	0.800	0.845	0.868	0.891
	0	0.754	0.713	0.624	0.590	0.603	0.691	0.554	0.444	0.480	0.495
	10	0.751	0.708	0.600	0.538	0.562	0.696	0.564	0.477	0.507	0.516
	20	0.748	0.706	0.596	0.486	0.519	0.702	0.579	0.517	0.547	0.572
BCC	*30*	0.745	0.705	0.611	0.487	0.479	0.709	0.599	0.562	0.603	0.639
	40	0.742	0.705	0.636	0.545	0.479	0.718	0.626	0.616	0.662	0.696
	50	0.740	0.707	0.659	0.614	0.587	0.728	0.654	0.665	0.707	0.735
	100	0.730	0.715	0.716	0.734	0.744	0.755	0.759	0.762	0.764	0.762
	200	0.773	0.790	0.825	0.843	0.862	0.827	0.844	0.862	0.884	0.908
n_s=5	*0*	0.703	0.475	0.352	0.313	0.297	0.539	0.351	0.265	0.258	0.256
	10	0.702	0.470	0.339	0.301	0.287	0.542	0.359	0.276	0.267	0.263
	20	0.701	0.471	0.332	0.295	0.282	0.546	0.370	0.293	0.283	0.275
BCU	*30*	0.701	0.478	0.334	0.296	0.283	0.552	0.386	0.317	0.308	0.298
	40	0.701	0.491	0.347	0.300	0.289	0.559	0.405	0.348	0.340	0.330
	50	0.702	0.507	0.370	0.302	0.291	0.566	0.429	0.383	0.376	0.366
	100	0.708	0.597	0.525	0.464	0.419	0.619	0.580	0.569	0.580	0.582
	200	0.721	0.692	0.689	0.687	0.755	0.753	0.741	0.748	0.743	0.849
	0	0.709	0.486	0.448	0.475	0.494	0.539	0.359	0.391	0.403	0.400
	10	0.708	0.476	0.418	0.447	0.470	0.542	0.377	0.401	0.413	0.413
	20	0.706	0.474	0.391	0.419	0.445	0.546	0.396	0.413	0.427	0.433
BCC	*30*	0.706	0.481	0.368	0.392	0.421	0.552	0.417	0.432	0.450	0.464
	40	0.706	0.494	0.351	0.367	0.397	0.559	0.441	0.458	0.482	0.503
	50	0.706	0.513	0.373	0.344	0.372	0.566	0.467	0.488	0.519	0.544
	100	0.711	0.624	0.575	0.527	0.518	0.619	0.615	0.631	0.677	0.709
	200	0.724	0.719	0.728	0.729	0.843	0.756	0.744	0.754	0.753	0.872

			$a_s/h=50$									
			Positive imperfection					*Negative imperfection*				
		Z	***α=0.5***	***α=0.75***	***α=1.0***	***α=1.25***	***α=1.5***	***α=0.5***	***α=0.75***	***α=1.0***	***α=1.25***	***α=1.5***
$n_s=7$	***BCU***	***0***	0.837	0.602	0.413	0.354	0.331	0.394	0.242	0.215	0.209	0.207
		10	0.549	0.310	0.250	0.232	0.227	0.397	0.248	0.220	0.213	0.211
		20	0.550	0.309	0.247	0.229	0.224	0.400	0.258	0.229	0.221	0.218
		30	0.552	0.313	0.249	0.230	0.224	0.405	0.270	0.242	0.232	0.227
		40	0.556	0.320	0.253	0.235	0.227	0.410	0.285	0.259	0.249	0.239
		50	0.561	0.330	0.260	0.241	0.233	0.417	0.302	0.279	0.269	0.258
		100	0.599	0.405	0.336	0.309	0.265	0.467	0.414	0.404	0.402	0.396
		200	0.667	0.544	0.475	0.462	0.426	0.622	0.637	0.634	0.651	0.637
	BCC	***0***	0.555	0.364	0.378	0.398	0.405	0.394	0.323	0.337	0.339	0.345
		10	0.553	0.348	0.359	0.377	0.386	0.397	0.330	0.345	0.346	0.349
		20	0.554	0.336	0.341	0.360	0.373	0.400	0.344	0.353	0.359	0.357
		30	0.556	0.327	0.325	0.344	0.358	0.405	0.354	0.364	0.371	0.370
		40	0.559	0.323	0.310	0.328	0.345	0.411	0.366	0.377	0.385	0.388
		50	0.564	0.331	0.298	0.312	0.329	0.418	0.379	0.393	0.404	0.411
		100	0.605	0.402	0.402	0.355	0.332	0.467	0.474	0.494	0.524	0.541
		200	0.681	0.646	0.571	0.536	0.537	0.624	0.641	0.653	0.688	0.720

		$a_s/h=75$									
		Positive imperfection					*Negative imperfection*				
	Z	***α=0.5***	***α=0.75***	***α=1.0***	***α=1.25***	***α=1.5***	***α=0.5***	***α=0.75***	***α=1.0***	***α=1.25***	***α=1.5***
$n_s=1$	***0***	0.578	0.519	0.528	0.489	0.475	0.581	0.544	0.504	0.543	0.403
	10	0.577	0.514	0.517	0.475	0.448	0.579	0.540	0.575	0.532	0.520
	20	0.575	0.512	0.516	0.474	0.446	0.578	0.538	0.566	0.527	0.523
	30	0.575	0.513	0.521	0.482	0.465	0.578	0.536	0.558	0.525	0.530
BCU	***40***	0.576	0.516	0.524	0.491	0.488	0.580	0.536	0.553	0.524	0.532
	50	0.579	0.519	0.527	0.499	0.502	0.584	0.537	0.549	0.524	0.530
	100	0.673	0.571	0.658	0.669	0.670	0.694	0.616	0.661	0.670	0.673
	200	0.732	0.758	0.785	0.807	0.820	0.742	0.771	0.802	0.827	0.847
	0	0.625	0.540	0.591	0.534	0.549	0.628	0.561	0.522	0.570	0.486
	10	0.621	0.531	0.569	0.513	0.520	0.624	0.554	0.608	0.558	0.577
	20	0.616	0.525	0.552	0.503	0.497	0.621	0.548	0.589	0.549	0.568
	30	0.611	0.521	0.543	0.505	0.508	0.618	0.542	0.574	0.542	0.557
BCC	***40***	0.608	0.520	0.537	0.508	0.517	0.616	0.538	0.562	0.536	0.546
	50	0.607	0.521	0.534	0.510	0.517	0.614	0.536	0.553	0.533	0.536
	100	0.695	0.634	0.672	0.689	0.701	0.723	0.726	0.684	0.698	0.708
	200	0.741	0.769	0.796	0.821	0.841	0.752	0.784	0.817	0.842	0.863
$n_s=2$	***0***	0.526	0.486	0.366	0.345	0.326	0.555	0.419	0.300	0.273	0.264
	10	0.523	0.479	0.367	0.328	0.319	0.553	0.437	0.309	0.288	0.271
	20	0.521	0.481	0.381	0.315	0.314	0.551	0.460	0.331	0.311	0.287
	30	0.521	0.490	0.406	0.307	0.311	0.549	0.504	0.364	0.354	0.334
BCU	***40***	0.520	0.503	0.434	0.326	0.306	0.548	0.548	0.408	0.416	0.393
	50	0.521	0.516	0.457	0.356	0.317	0.547	0.599	0.464	0.494	0.438
	100	0.526	0.544	0.512	0.487	0.554	0.544	0.577	0.564	0.542	0.604
	200	0.553	0.638	0.629	0.620	0.618	0.578	0.673	0.683	0.683	0.683
	0	0.539	0.532	0.435	0.432	0.413	0.566	0.430	0.340	0.370	0.396
	10	0.535	0.519	0.419	0.396	0.396	0.563	0.449	0.364	0.402	0.414
	20	0.533	0.518	0.413	0.370	0.382	0.560	0.482	0.396	0.447	0.458
	30	0.531	0.525	0.424	0.342	0.371	0.558	0.520	0.436	0.501	0.522
BCC	***40***	0.529	0.535	0.448	0.355	0.370	0.555	0.572	0.480	0.562	0.585
	50	0.528	0.543	0.474	0.407	0.364	0.553	0.615	0.524	0.572	0.578
	100	0.529	0.554	0.521	0.534	0.579	0.546	0.581	0.560	0.556	0.638
	200	0.569	0.649	0.655	0.643	0.637	0.612	0.688	0.699	0.700	0.697

			$a_s/h=75$									
			Positive imperfection					*Negative imperfection*				
		Z	*α=0.5*	*α=0.75*	*α=1.0*	*α=1.25*	*α=1.5*	*α=0.5*	*α=0.75*	*α=1.0*	*α=1.25*	*α=1.5*
$n_s=3$	*BCU*	***0***	0.512	0.347	0.280	0.265	0.255	0.489	0.283	0.229	0.229	0.224
		10	0.509	0.341	0.271	0.257	0.249	0.501	0.292	0.240	0.234	0.226
		20	0.508	0.342	0.265	0.252	0.246	0.522	0.306	0.254	0.244	0.235
		30	0.509	0.347	0.263	0.249	0.245	0.542	0.323	0.273	0.264	0.253
		40	0.512	0.357	0.265	0.250	0.245	0.599	0.344	0.298	0.290	0.278
		50	0.516	0.371	0.281	0.249	0.242	0.596	0.368	0.325	0.320	0.308
		100	0.536	0.458	0.407	0.372	0.347	0.583	0.523	0.494	0.516	0.525
		200	0.549	0.533	0.572	0.593	0.571	0.568	0.559	0.596	0.603	0.603
	BCC	***0***	0.538	0.371	0.345	0.361	0.373	0.472	0.286	0.304	0.320	0.329
		10	0.534	0.358	0.324	0.339	0.352	0.497	0.302	0.316	0.335	0.341
		20	0.532	0.356	0.308	0.319	0.333	0.500	0.324	0.335	0.356	0.364
		30	0.531	0.360	0.298	0.301	0.316	0.536	0.349	0.360	0.383	0.398
		40	0.533	0.372	0.290	0.285	0.300	0.615	0.375	0.387	0.415	0.438
		50	0.536	0.389	0.295	0.270	0.284	0.611	0.404	0.416	0.452	0.485
		100	0.549	0.488	0.460	0.438	0.464	0.593	0.537	0.555	0.593	0.579
		200	0.553	0.537	0.604	0.636	0.645	0.569	0.557	0.613	0.619	0.626
$n_s=5$	*BCU*	***0***	0.322	0.211	0.191	0.181	0.180	0.272	0.177	0.167	0.164	0.163
		10	0.321	0.207	0.187	0.177	0.177	0.275	0.181	0.171	0.166	0.165
		20	0.321	0.205	0.186	0.175	0.176	0.279	0.187	0.176	0.170	0.170
		30	0.323	0.205	0.187	0.176	0.176	0.283	0.195	0.183	0.177	0.176
		40	0.326	0.207	0.190	0.179	0.178	0.289	0.204	0.192	0.185	0.183
		50	0.330	0.212	0.194	0.183	0.181	0.296	0.216	0.203	0.194	0.191
		100	0.365	0.261	0.236	0.208	0.183	0.347	0.302	0.288	0.287	0.281
		200	0.456	0.367	0.338	0.331	0.305	0.503	0.475	0.492	0.466	0.494
	BCC	***0***	0.331	0.262	0.270	0.282	0.281	0.273	0.245	0.262	0.271	0.265
		10	0.329	0.252	0.257	0.272	0.273	0.276	0.252	0.264	0.273	0.267
		20	0.329	0.244	0.247	0.263	0.267	0.279	0.259	0.260	0.277	0.270
		30	0.331	0.238	0.236	0.252	0.260	0.284	0.267	0.273	0.283	0.277
		40	0.334	0.234	0.228	0.243	0.253	0.291	0.277	0.285	0.292	0.289
		50	0.338	0.234	0.222	0.234	0.246	0.298	0.289	0.298	0.305	0.303
		100	0.376	0.267	0.250	0.251	0.236	0.350	0.363	0.377	0.400	0.410
		200	0.478	0.406	0.418	0.401	0.384	0.521	0.508	0.514	0.552	0.523

			$a_s/h=75$									
			Positive imperfection					*Negative imperfection*				
		Z	***α=0.5***	***α=0.75***	***α=1.0***	***α=1.25***	***α=1.5***	***α=0.5***	***α=0.75***	***α=1.0***	***α=1.25***	***α=1.5***
$n_s=7$	***BCU***	***0***	0.214	0.160	0.146	0.144	0.145	0.184	0.139	0.132	0.131	0.129
		10	0.213	0.158	0.144	0.142	0.144	0.186	0.142	0.135	0.133	0.132
		20	0.213	0.158	0.144	0.142	0.143	0.188	0.145	0.138	0.137	0.137
		30	0.213	0.159	0.144	0.142	0.144	0.192	0.149	0.142	0.142	0.141
		40	0.215	0.161	0.147	0.144	0.145	0.195	0.154	0.147	0.147	0.146
		50	0.217	0.164	0.150	0.147	0.147	0.200	0.159	0.153	0.152	0.151
		100	0.237	0.191	0.182	0.156	0.151	0.233	0.204	0.194	0.188	0.183
		200	0.303	0.247	0.234	0.237	0.213	0.336	0.329	0.327	0.333	0.335
	BCC	***0***	0.228	0.217	0.223	0.221	0.219	0.204	0.219	0.223	0.217	0.211
		10	0.225	0.211	0.216	0.217	0.214	0.208	0.219	0.225	0.218	0.212
		20	0.223	0.206	0.210	0.212	0.210	0.211	0.222	0.227	0.219	0.213
		30	0.221	0.201	0.205	0.208	0.207	0.215	0.224	0.229	0.221	0.216
		40	0.221	0.198	0.200	0.203	0.204	0.219	0.223	0.233	0.225	0.220
		50	0.222	0.196	0.196	0.199	0.198	0.223	0.233	0.238	0.231	0.227
		100	0.241	0.209	0.196	0.184	0.206	0.260	0.275	0.277	0.275	0.273
		200	0.311	0.344	0.330	0.294	0.302	0.364	0.379	0.383	0.394	0.384

C.3. Ultimate load of the unstiffened curved panels under an initial out-of-plane pressure of 50 kPa followed by in-plane compression (from section 6.8)

	a/h=100											
	BUU				***BCU***				***BCC***			
Z	***α=0.5***	***α=1.0***	***α=2.0***	***α=5.0***	***α=0.5***	***α=1.0***	***α=2.0***	***α=5.0***	***α=0.5***	***α=1.0***	***α=2.0***	***α=5.0***
0	0.273	0.297	0.290	0.312	0.407	0.373	0.371	0.404	0.425	0.477	0.446	0.374
10	0.230	0.246	0.245	0.260	0.407	0.371	0.389	0.419	0.418	0.442	0.477	0.456
20	0.228	0.206	0.211	0.220	0.429	0.387	0.407	0.420	0.432	0.412	0.489	0.484
30	0.267	0.177	0.188	0.191	0.474	0.403	0.399	0.412	0.472	0.414	0.508	0.471
40	0.343	0.157	0.184	0.179	0.534	0.495	0.372	0.394	0.531	0.497	0.461	0.448
50	0.434	0.296	0.217	0.201	0.600	0.576	0.480	0.397	0.597	0.564	0.525	0.427

C.4. Ultimate load of the stiffened curved panels under an initial out-of-plane pressure of 50 kPa followed by in-plane compression (from section 6.9 with d_s/h_s=10 and BCC)

	a_s/h=25											
	n_s=1			n_s=2			n_s=3			n_s=5		
Z	***α=0.5***	***α=1.0***	***α=1.5***	***α=0.5***	***α=1.0***	***α=1.5***	***α=0.5***	***α=1.0***	***α=1.5***	***α=0.5***	***α=1.0***	***α=1.5***
0	0.988	0.978	0.974	0.964	0.966	0.941	0.977	0.947	0.887	0.965	0.860	0.693
10	0.989	0.978	0.974	0.963	0.966	0.945	0.977	0.949	0.902	0.966	0.868	0.648
30	0.992	0.982	0.981	0.962	0.965	0.952	0.978	0.952	0.922	0.967	0.885	0.646
50	1.000	0.992	0.990	0.963	0.965	0.957	0.978	0.954	0.935	0.968	0.898	0.782
100	1.007	1.001	1.021	0.971	0.977	0.976	0.982	0.963	0.956	0.970	0.924	0.895
200	0.986	1.008	1.006	0.995	1.020	1.010	0.997	0.991	0.989	0.979	0.956	0.947

	n_s=7		
Z	***α=0.5***	***α=1.0***	***α=1.5***
0	0.944	0.829	0.635
10	0.945	0.692	0.604
30	0.948	0.715	0.552
50	0.950	0.880	0.355
100	0.954	0.927	0.730
200	0.963	0.960	0.891

ANNEX D

D.1. Comparison of the equilibrium paths for stiffeners of type C (from section 7.4):

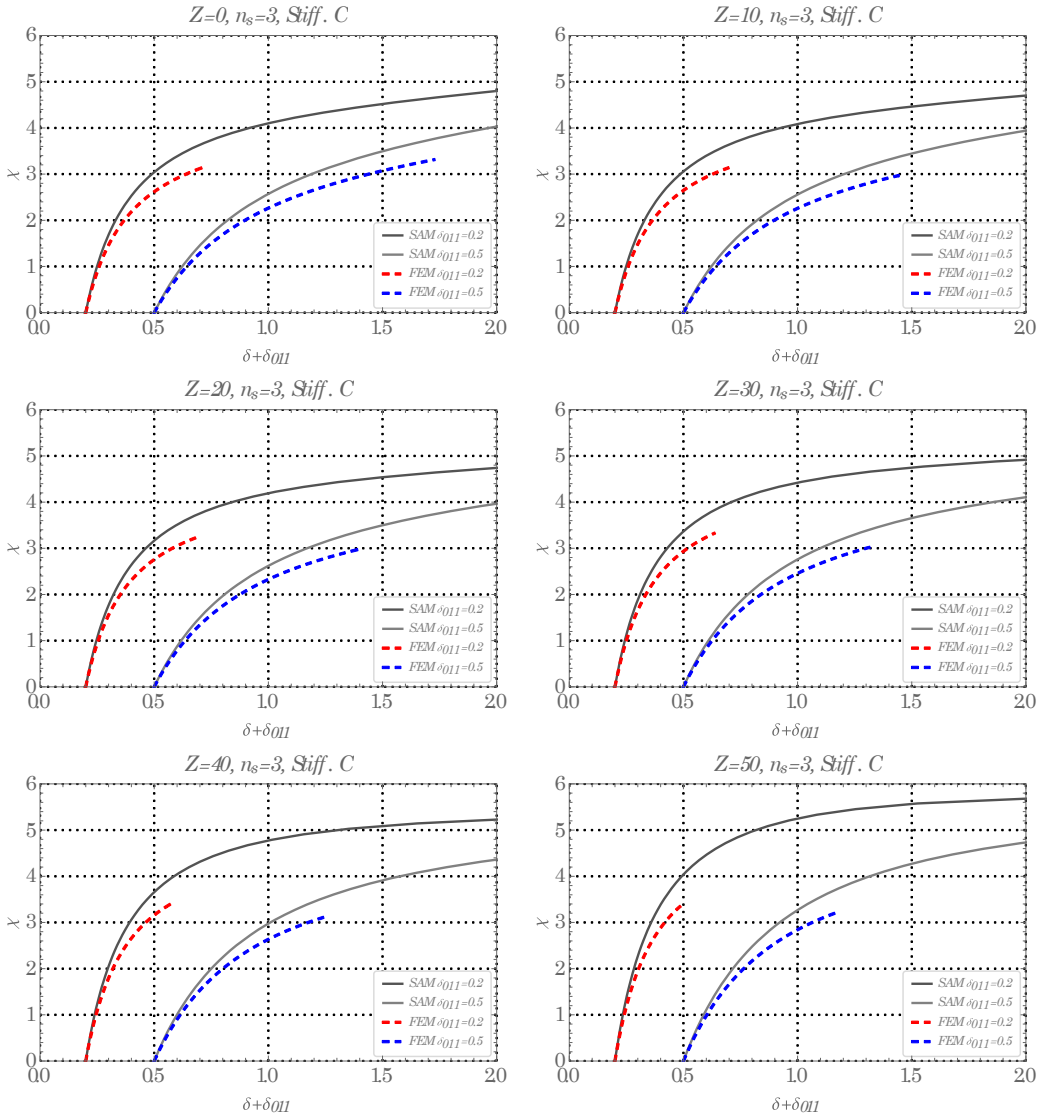

Figure AD.1: Equilibrium paths in function of the out-of-plane displacement at the centre of the panel for panels with α=1.0 and 3 stiffeners of type C

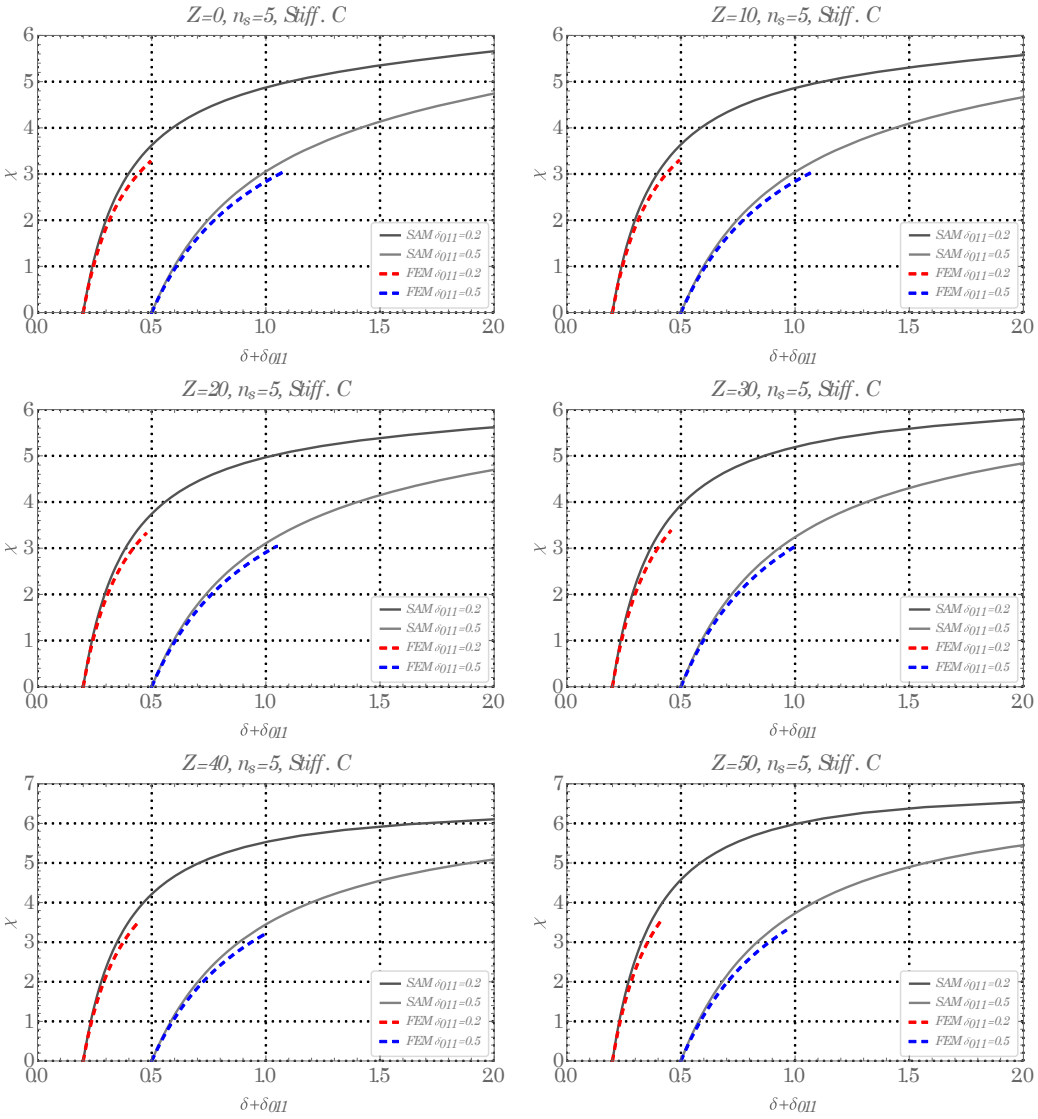

Figure AD.2: Equilibrium paths in function of the out-of-plane displacement at the centre of the panel for panels with α=1.0 and 5 stiffeners of type C

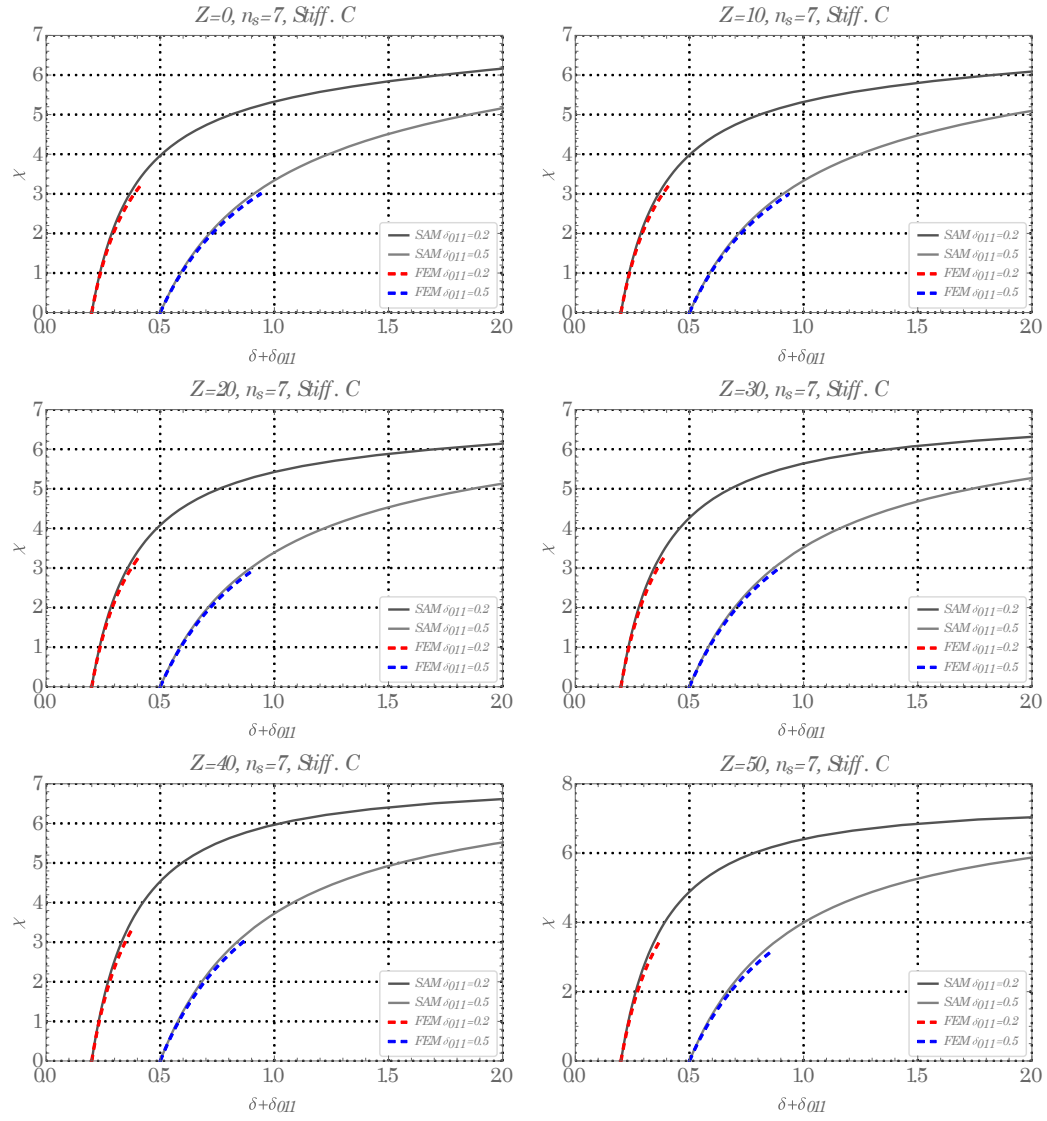

Figure AD.3: Equilibrium paths in function of the out-of-plane displacement at the centre of the panel for panels with α=1.0 and 7 stiffeners of type C